Origin of Alkaline Basalt Volcanism Inferred from Noble Gas Isotopic Systematics: Implications for Mantle Dynamics in Back Arc Region of Subduction Zone

by

Hirochika SUMINO

A dissertation submitted to the University of Tokyo for the degree of Doctor of Science, Dec. 15, 2000.

1. Introduction

1–1. Alkaline basalt from back-arc region around the Sea of Japan

Several Cenozoic alkaline basalts associated tholeiitic basalts are widely distributed in northeastern China and around the Sea of Japan (Fig. 1–1). In southwestern Japan, the Cenozoic volcanism is most voluminous in northwestern Kyushu, which is nearly half of all Cenozoic basalts hitherto erupted in Japan. Volcanism in arcs is generally believed to have some relationship with the subduction. For example, the volcanism in the northeastern Japan arc is considered to be caused by the subduction of the Pacific plate and dehydration of the slab (Tatsumi et al., 1983; Tatsumi, 1989). However, Cenozoic volcanism of the southwestern Japan arc including northwestern Kyushu is quite distinct from that of the northeastern Japan arc. First, the former is characterized by the extensive alkaline volcanism forming many monogenetic volcanic groups. Second, the southwestern Japan arc lacks a deep trench and subcrustal earthquakes. The Wadati-Benioff zones of both the Pacific and Philippine Sea plates are not observed beneath the area (Fig. 1–1). Third, northwestern Kyushu is away from the volcanic front, which across the central Kyushu, composed of active volcanoes such as Sakurajima, Kirishima, Aso, and Kuju (Fig. 1–2). Since subduction edge of Philippine Sea plate is considered to have not reached beneath the back-arc region of Japan when alkaline volcanism was ongoing, the alkaline basaltic volcanism has directly nothing to do with subduction processes but is considered to be intraplate volcanic activity.

The origin of alkaline basalt in southwestern Japan has been investigated by many researchers. Nakamura et al. (1985; 1989) and Nakada and Kamata (1991) reported that Cenozoic alkaline basalts from back-arc region of southwestern Japan show geochemical signatures (major and trace element compositions) distinct from typical island-arc volcanic rocks. For example, they are less depleted in Ta, Nb and Ti and less enriched in K, Sr, Ba and Rb compared with volcanic rocks from northeastern Japan, including alkaline basalts from Rishiri Island, back-arc region in northeastern Japan. Their Nd and Sr isotopic data suggest that they are products of interaction between a depleted mantle and an enriched mantle (Nakamura et al., 1990). From these features,

Nakamura et al. (1990) proposed a model that the alkaline basalt magma is mixture formed by an enriched mantle plume from deeper in the mantle and a depleted MORB-type upper mantle, which was weakly affected by metasomatism caused by dehydration and/or partial melting of subducted Pacific plate. In other words, they consider that alkaline volcanism in southwestern Japan was caused by similar process to continental and oceanic alkaline basalt, that is “hotspot”. Iwamori (1992) examined Cenozoic basalts in southwestern Japan and proposed a model which included the addition of fluid into the deep mantle, and melting and subsequent upwelling of the deep mantle materials enriched in incompatible elements. Kakubuchi et al. (1995) measured and compiled the trace element abundance pattern and Nd–Sr isotopic ratios of Cenozoic alkaline basalts and associated tholeiitic basalts, and suggest that mantle plumes which caused the alkaline volcanism in north Kyushu and Chugoku district are different in geochemical characteristics. Figure 1–3 is the schematic diagram of the mantle plume model from Kakubuchi et al. (1995). While mantle diapers rapidly rose from an enriched mantle plume with an EMI signature ascended from deep in the mantle in Chugoku district, mantle diapers characterized by an EMII signature rose slowly and were entrained an overlying MORB-like depleted mantle.

However, the geochemical features of alkaline basalts in southwestern Japan can be explained by passive upward injection of asthenosphere (depleted mantle) to sub continental lithosphere (enriched mantle) associated with the opening of the Sea of Japan, as in the case with volcanisms around the Japan Sea region, such as northeastern Japan (Nohda et al., 1988; Ohki et al., 1994), Yamato Basin Ridge and Ulreung and Dog islands in the Sea of Japan (Tatsumoto and Nakamura, 1991) and Shihote-Alin and Sakhalin (Okamura et al., 1998). Figure 1–4 is a schematic model after Ohki et al. (1994). In this model, passive upwelling and decompression melting of asthenosphere induced by mantle convection accompanied with retreat of Japan Trench and down going of the subducting Pacific plate play an important role in alkaline basalt volcanism.

It is difficult to show clearly which model is the case from geochemical features previously reported, because both mantle plume and sub-continental mantle are considered to have the same isotopically enriched characteristics and the source of

enriched signature in the alkaline basalts can be attributed to either shallow (sub-continental) and deep mantle (mantle plume).

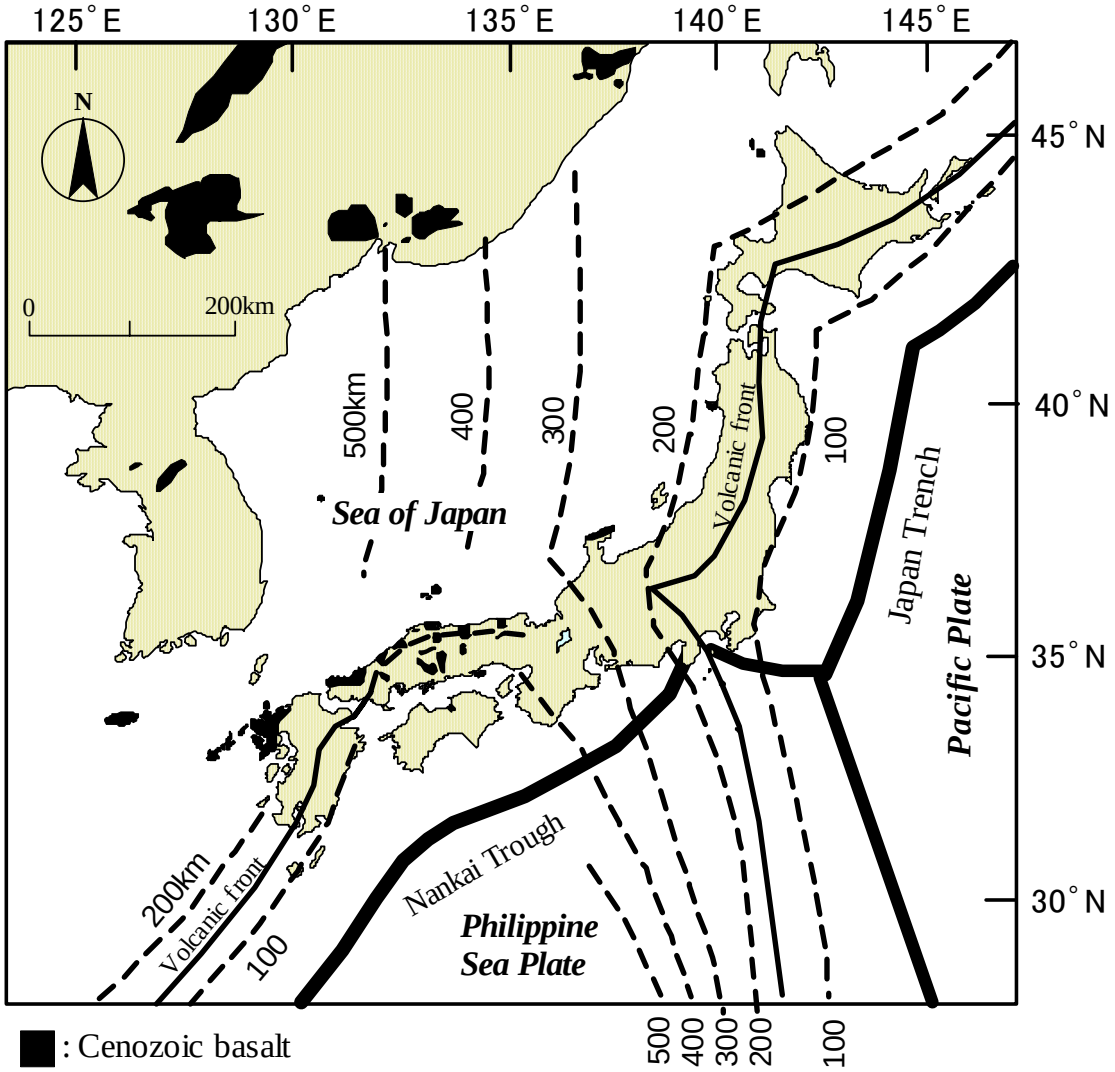

Fig. 1–1. Map showing the distribution of Cenozoic alkaline basalts and associated tholeiitic basalts after Nakamura et al. (1989). Thick solid lines and solid lines represent plate boundaries and Quaternary volcanic front, respectively (after Aramaki and Ui, 1982). Dashed lines are contours representing isobaths for deep seismic zones (Wadati-Benioff zones) after Utsu (1974). Numbers are depths in kilometers as measured the center of the seismic zone.

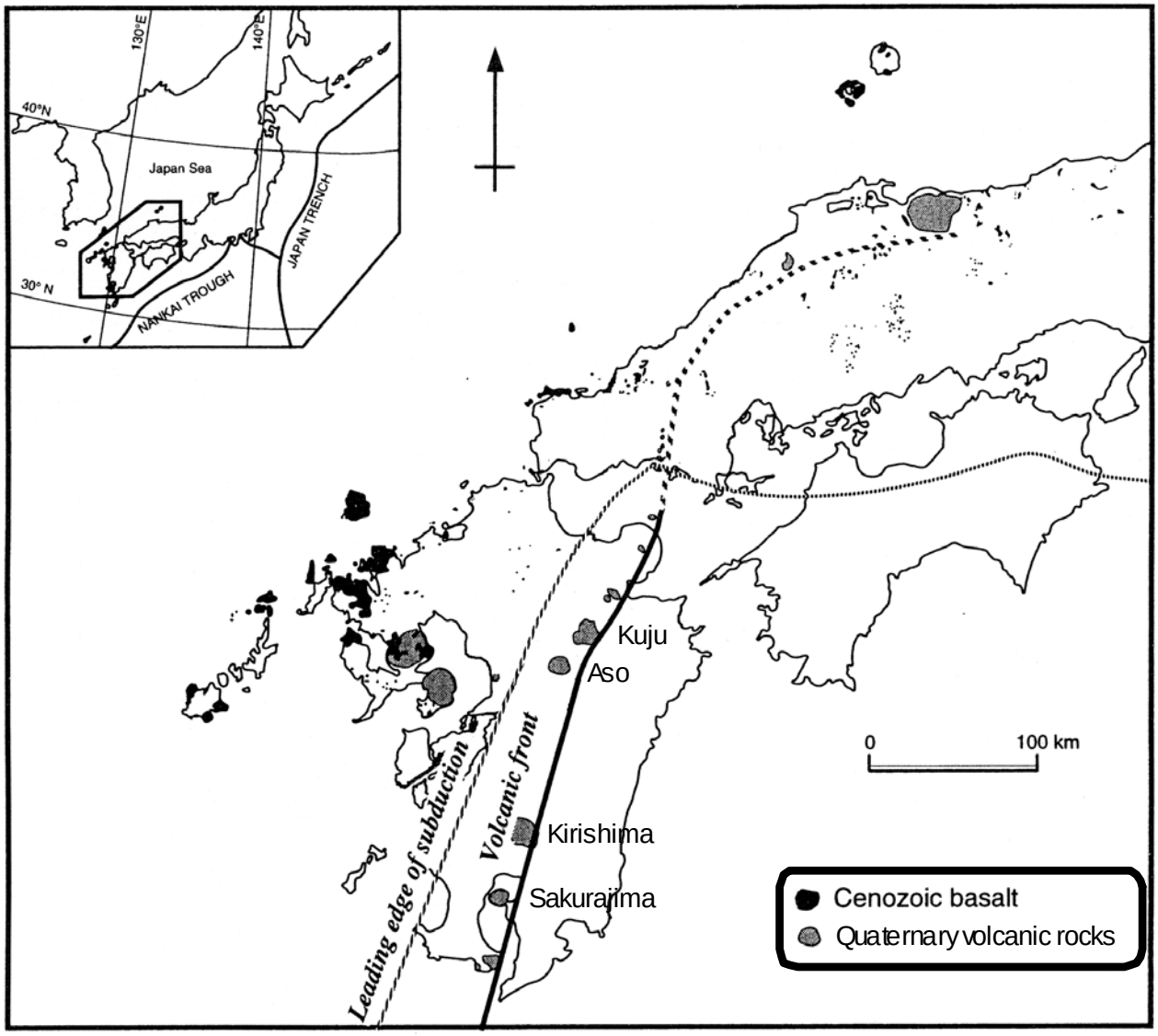

Fig. 1–2. Distribution of the late Cenozoic basalts in southwestern Japan from Kakubuch et al. (1995). The leading edge of the subducted Philippine Sea plate is from Shiono (1974). Black and Hatched area shows Cenozoic basalts and Quaternary volcanic rocks, respectively.

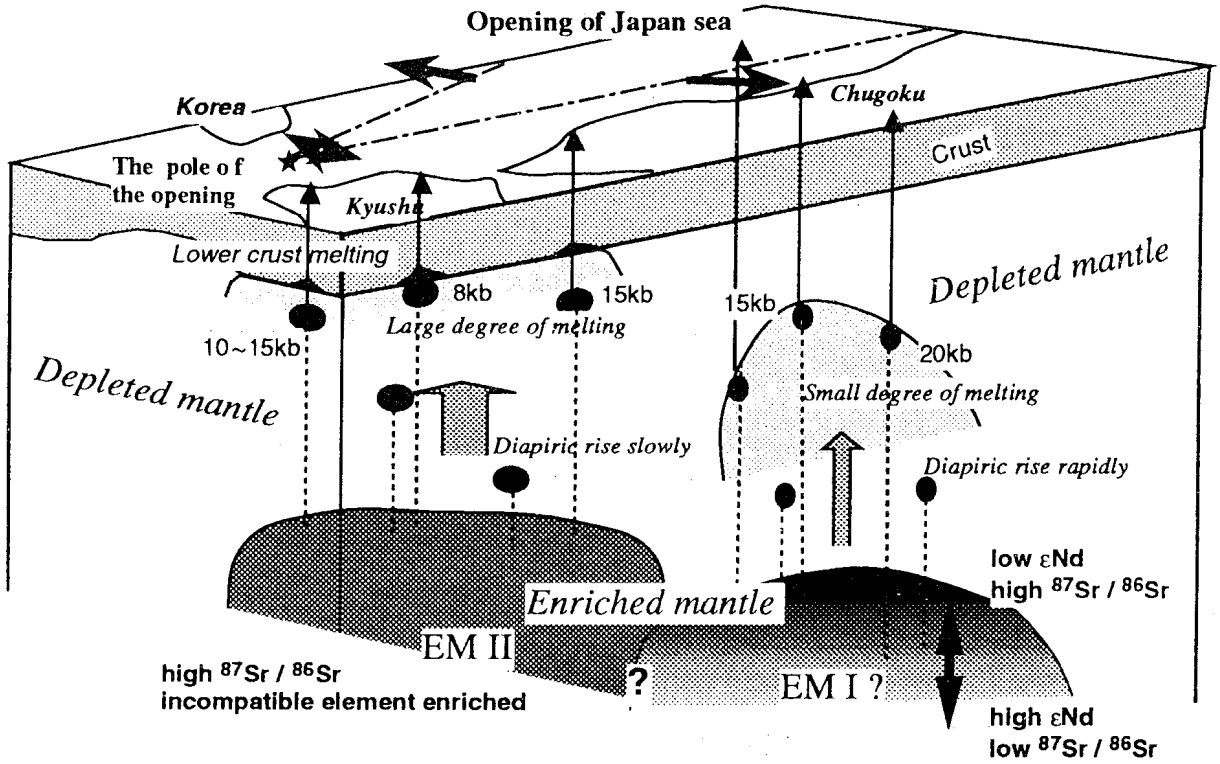

Fig. 1–3. Schematic diagram showing the origin and genesis of the late Cenozoic basaltic rocks in the southwestern Japan from Kakubuchi et al. (1995).

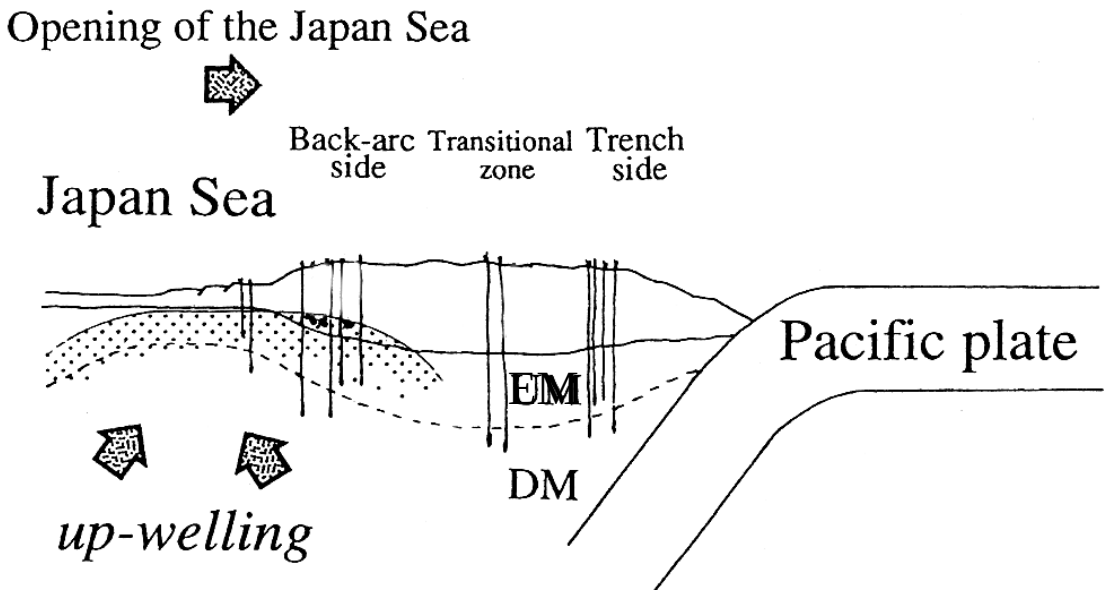

Fig. 1–4. A schematic cross section for magma genesis in the northeastern Japan arc at around 15 Ma after Ohki et al. (1994). Solid lines represent for basaltic rocks in the transitional zone to back-arc side and andesitic rocks in the trench side, respectively. EM, DM: isotopically enriched mantle, and depleted mantle. Dotted area: increased geothermal gradient due to the rise of hot asthenosphere (depleted mantle) into the overlying enriched sub-continental mantle.

1–2. Noble gas isotopes

Noble gases (He, Ne, Ar, Kr and Xe) are chemically inert resulting that their elemental and isotopic abundances are affected by physical processes. Each element has stable isotopes covering a wide mass range, so that in principle the noble gases can be sensitive tracers of mass-dependent physical processes. In addition, because each noble gas has three or more stable isotopes except for He, they are useful to identify mixing processes among several sources. Noble gas isotopes are composed of several components of different origins such as primordial, radiogenic (+ nucleogenic), cosmogenic etc. The low concentrations of noble gas isotopes in the terrestrial materials except for Ar often enable us to detect the slight addition of the isotopes produced by nuclear processes. Since noble gas isotopic ratio show clear variations among different parts of the Earth, they are quite useful to trace the processes of magma genesis in the Earth. Figure1–5 is a schematic diagram of two‐layered mantle model and $^{3}He/^{4}He$ and $^{40}Ar/^{36}Ar$ ratios of each source and tectonic setting (modified after Kaneoka, 1995). For example, He in mid-ocean ridge basalts (MORB) show worldwide uniform $^{3}He/^{4}He$ ratios of 8.18 ± 0.73 R_A (Hilton et al., 1993), where R_A is the $^{3}He/^{4}He$ ratio of the atmosphere = 1.40×10^{-6} (Ozima and Podosek, 1983), while the $^{3}He/^{4}He$ ratio of volcanic rocks from hotspots such as Hawaii, Iceland and Reunion range up to 37 R_A (e.g., Hilton et al., 1999), which indicates that hotspot volcanism taps deeper regions of the mantle enriched in primordial ^{3}He relative to the MORB reservoir, which is considered to be the upper mantle. On the other hand, some samples from continental tectonic setting show low $^{3}He/^{4}He$ ratios ($\sim10^{-8}$) owing to accumulation of radiogenic ^{4}He, produced as α particles by radioactive decay of U and Th. The isotopic ratios of the other noble gases, such as Ne, Ar, and Xe differ in each parts of the Earth.

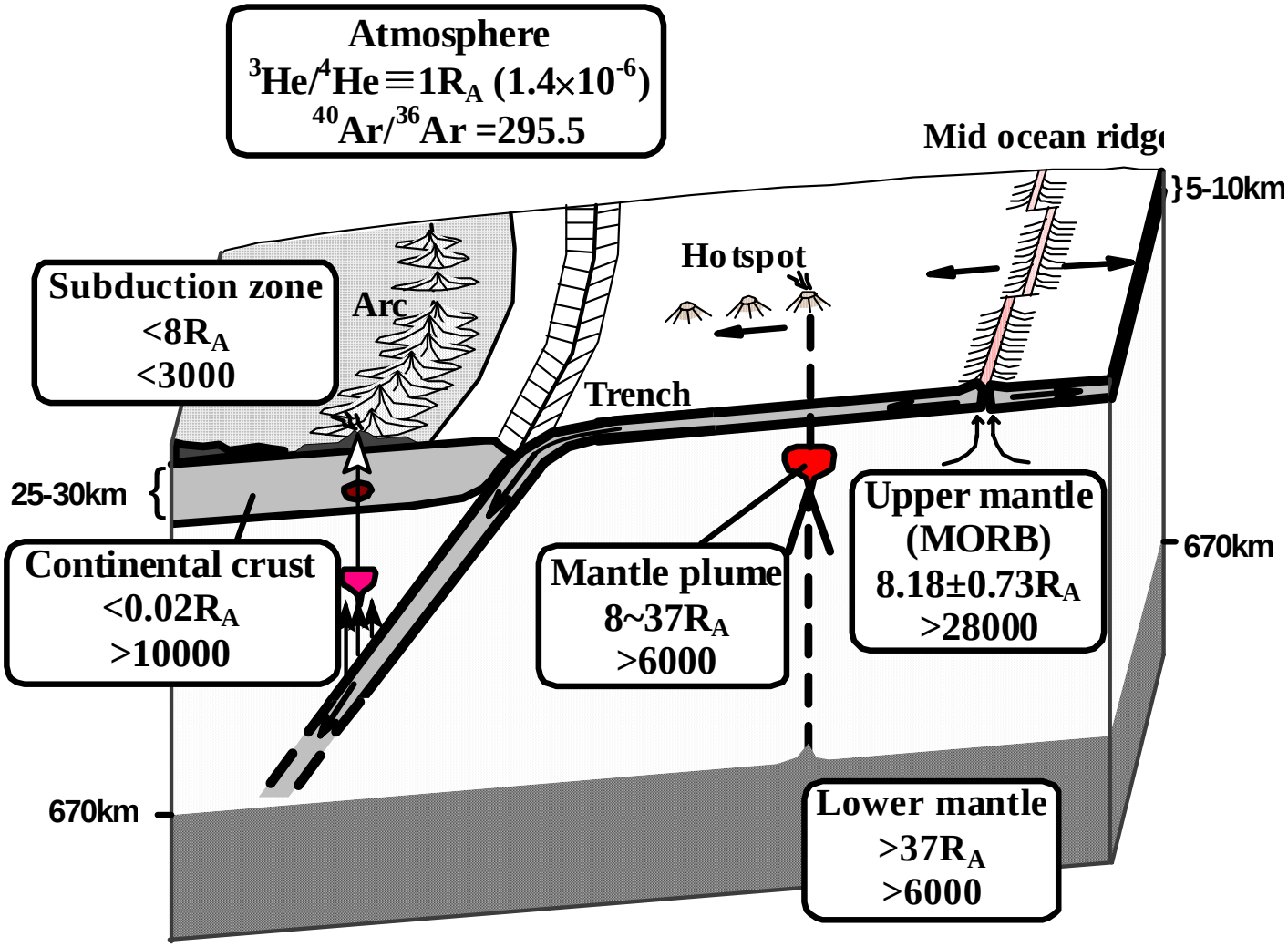

Fig. 1–5. Schematic diagram of two-layered mantle model and $^{3}He/^{4}He$ and $^{40}Ar/^{36}Ar$ ratios of each source and tectonic setting (modified after Kaneoka, 1995).

1–3. Noble gas analysis for rock samples

Mafic phenocryst (olivine and/or pyroxene) separated from igneous rocks and mantle-derived xenoliths is generally used for noble gas analysis, because groundmass lost most of the noble gases inherent from the source magma and was contaminated by the atmospheric noble gases in many cases. Even in mafic phenocryst, isotopic characteristics of noble gases dissolved in mineral lattice are changed by addition of radiogenic and/or cosmogenic component with age. Since inherent noble gases are preserved in fluid inclusions, in vacuo crushing method is effective to extract noble gases selectively from fluid inclusions (e.g., Kurz, 1986, Stuart et al., 1994). However, the concentration of He in mineral is generally very low. Especially the expected amount of He extracted by in vacuo crushing is sometimes smaller than $10^{-9}cm^3STP/g$. Therefore the previous noble gas data on volcanic rocks are limited for gas-rich and/or high $^3He/^4He$ samples except a few data (Hilton et al., 1992; 1999; Dodson et al., 1998; Dodson and Brandon, 1999).

Consequently precise measurement of noble gas isotopes including He becomes more important to investigate the source materials of volcanic rocks recently. Therefore, I first improved a noble gas mass spectrometer equipped with a double collector system for He isotopes for the purpose of determining noble gas isotopic composition with extremely low concentration in terrestrial rock samples (in chapter 2).

1–4. Aim of this study

There are no previous studies, which report noble gas data on Cenozoic alkaline basalts from the southwestern Japan arc. Previous noble gas studies on xenoliths contained in basalts from southwestern Japan are also very scarce. Only one study reported that xenoliths from the Oki-Dogo region contain He with MORB-like $^{3}He/^{4}He$ ratios (Nagao and Takahashi, 1993), however, no noble gas data have been reported for northwestern Kyushu, where Cenozoic basaltic volcanism was more widespread than in the Oki-Dogo region.

As an origin of one of the geochemical endmembers observed in oceanic island basalts, recycled material of continental origin such as subducted oceanic crust with sediments is considered (Cohen and O'Nions, 1982; Hofmann, 1997). If the mantle plume origin of the alkaline basalt is the case, the plume may be subducted material which had subducted and reached to lower mantle and was recycled back to the surface of the Earth. Alternatively, alkaline volcanism in back-arc region of subduction zone has a potential for direct occurrence of global recycling of subducted materials.

Noble gases, especially He is a powerful tracer to reveal the source materials of alkaline basalts. If higher $^{3}He/^{4}He$ ratio than MORB value is observed in this region, it will strongly support the mantle plume model. If asthenospheric upwelling is the case, each source material originally existed in upper mantle, and $^{3}He/^{4}He$ ratio will not exceed the MORB value.

Therefore, the aim of this study is that clarification of noble gas isotopic compositions of Cenozoic alkaline basalts and mantle-derived xenoliths in back-arc region of southwestern Japan, to investigate the origin of the alkaline basalt and the noble gas characteristics of the sub continental mantle around this region with respect to mantle dynamics related to subduction process.

2. Modification of a system for noble gas isotope analysis

2–1. Systems for noble gas isotope analysis used in this study

In Laboratory for Earthquake Chemistry, the University of Tokyo, there are four mass spectrometers for noble gas isotope analysis which are equipped with extraction apparatus and purification/separation line. They are named MS–I, MS–II, MS–III and MS–IV, respectively. MS–I is the oldest mass spectrometer system in our laboratory, which is specialized to He isotope measurement (Sano and Wakita, 1988). MS–II and MS–III were moved from the Institute for Study of the Earth's Interior, Okayama University to the Laboratory for Earthquake Chemistry in 1998. MS–II is the most sensitive mass spectrometer which is applied for all noble gases in extraterrestrial samples (Nagao and Abe, 1994; Nagao et al., 1999). MS–III is almost the same system as MS–II, however, MS–III is improved in evacuation system to achieve extremely low blank level and equipped with laser gas-extraction system, and only used for all noble gases in terrestrial samples and micro-gram size sample such as micrometeorite (Osawa et al., 2000; Aka et al., 2001). MS–IV is originally designed for measurement of all noble gases in gas samples, such as volcanic, hot spring and natural gases (Xu et al., 1995; Nakai et al., 1997).

Two of four systems in the Laboratory for Earthquake Chemistry were used in this study. One is MS–III. Details of the mass spectrometric techniques with MS–III are described by Aka et al. (2001). The other is MS–IV, which was mainly used in this study. A noble gas mass spectrometer in the system of MS–IV is equipped with a double collector system for He isotopes, and was improved for the purpose of determining noble gas isotopic composition with extremely low concentration in terrestrial rock samples in this study.

In this chapter, the modification of the MS–IV and experimental procedure for mineral samples are described.

2–2. Modification of MS–IV

2–2–1. Outline of MS–IV

MS–IV consists of a sector-type mass spectrometer (VG5400, VG Isotech.) and a noble gas purification and separation line for gas samples before modification. Details of the system before modification are reported by Xu et al. (1995). Several improvements have been made in this study, with an emphasis on the mass spectrometer in order to measure quite-low amount of noble gases in rock samples. Hence it is called as modified-VG5400 hereafter. A schematic drawing of the system after all modification described in this thesis is shown in Fig. 2–1. The system consists of gas extraction part, gas purification and separation part, and the modified-VG5400 mass spectrometer. Since He permeates normal glass quickly, stainless steel is used for all parts of the line. The ultra-high vacuum (10^{-8} to 10^{-10} Torr) in the system is kept by three turbo molecular pumps and two ion pumps. Since the system is originally designed for noble gas measurement of gas samples (Xu et al., 1995; Nakai et al., 1997), gas extraction apparatuses for rock samples are newly established. In addition, several modifications were made in purification and separation part, in order to achieve low blank level and high performance of the measurement.

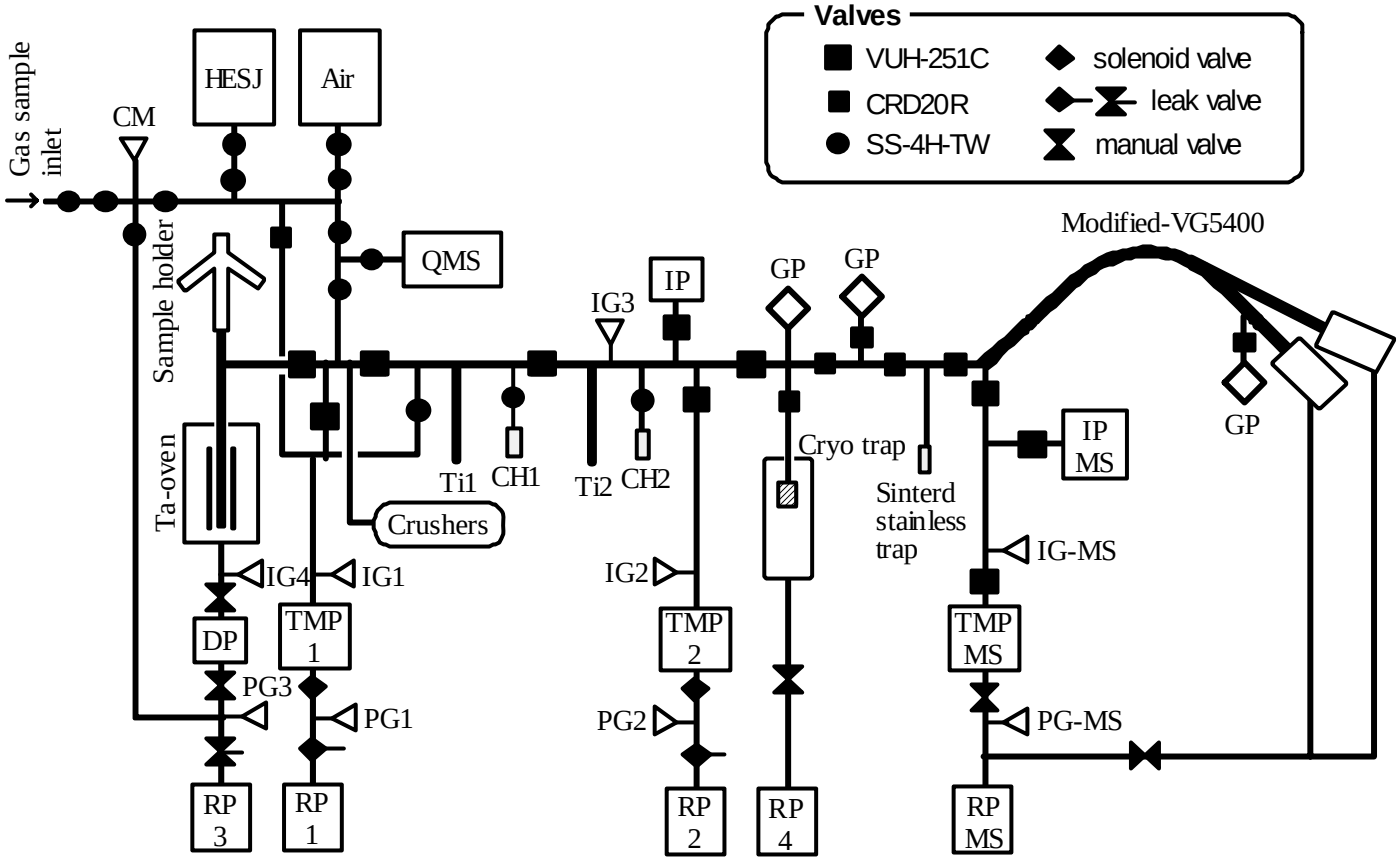

Fig. 2–1. Schematic diagram of noble gas analyzing system (MS-IV). Ta-oven: noble gas extraction furnace using Ta-heater, Crushers: crusher to mechanically crush the sample *in vacuo*, QMS: quadrupole mass spectrometer, Cryo trap: cold finger for trapping and separating noble gases, Ti1 and Ti2: Ti-Zr getter, CH1 and CH2: charcoal trap, IG1-IG4 and IG-MS: ionization gauge, PG1-PG3 and PG-MS: pirani gauge, GP: getter pump (SORB-AC), TMP1, 2 and TMP-MS: turbo molecular pump, IP and IP-MS: ion pump, RP1-RP4 and RP-MS: rotary pump, DP: oil diffusion pump, CM: capacitance manometer, Valves: VUH-251C (ULVAC Co.); CRD20R (VG Co.); SS-4H-TW (Nupro Co.).

2–2–2. Gas extraction

Two different extraction methods were used in this study; those are in vacuo heating and in vacuo crushing. For heating experiment, extraction oven (Ta-oven) is almost the same as that described in Nagao et al. (1996). MS–III is originally equipped with Ta-oven, however, a Ta-oven for MS–IV is newly established (TH-250, Horiguchi iron factory). Figure 2–2 is a schematic drawing of Ta-oven. The samples weighing ca. 0.5 g are wrapped in Al-foil 10 μm in thickness and loaded in branches of a sample holder, which is connected to the vacuum line at the extraction oven. The samples are dropped into the heating furnace, and then the furnace is heated for about 20 to 40 minutes at 400°C to 2000°C depending on the purpose. The temperature of the furnace is monitored via current applied to the Ta-heater, which is calibrated to temperature by Pt–Rh thermocouple and radiation thermometer. Total 20–50 samples can be analyzed one after another without breaking vacuum condition.

At the beginning of this study, conventional sample holders made of Pyrex-glass or lead glass were used. However, high blank level of He ($3–4\times10^{-9}$ and $3–7\times10^{-10}$ cm^3STP for Pyrex-glass and lead glass, respectively) owing to permeation of atmospheric He trough the glass wall of the holder was serious problem especially for gas-poor samples. Therefore, a sample holder made of stainless steel except a small glass window to observe sample in the furnace was newly designed (Fig. 2–3). The blank level of ^{4}He with the new stainless-steel sample holder is approximately $1–2\times10^{-11}$ cm^3STP. Dramatic decrease of blank level enables us to analyze for low amount of He, and is essential for gas-poor samples or measurement with step heating extraction method.

For crushing experiment, two kinds of crusher with different crushing methods are available in this study. One is the hydraulic-type crusher, which is newly designed by me. Up to 3g of the sample whose grain size is larger than #60 (250μm) is mechanically crushed by hydraulic pressure up to 70 MPa applied by a hand pump (Fig. 2–4A). 50–60% of the sample is crushed into powder whose grain size is less than #100 (150μm) after three times of press at 70MPa. The other is the solenoid-type crusher, which is designed by Prof. K. Nagao and Dr. F. T. Aka and is almost the same as described in Matsumoto et al. (1998), however, ours is simpler than that (Fig. 2–4B).

Solenoid coils can be separated from main body of the crusher, i.e., stainless-steel tube and nickel piston. Thus, we can connect three to six crushers to the line and prepare several samples at the same time, resulting high performance of measurement. Up to 1g of the sample can be loaded into the crushing chamber, and more than 70% of the sample is crushed into less than #100 after 1000–2000 strokes. Blank levels of He are approximately $1–2\times10^{-11}cm^3STP$ and $2\times10^{-10}cm^3STP$ with hydraulic-type crusher and solenoid-type crusher, respectively.

Extraction efficiency by the crushers was tested by stepwise crushing of a given sample and heating experiment of powder after crushing (Fig. 2–5). $^3He/^4He$ ratios of each steps are equivalent within errors, hence there is no significant secondary effect by cosmogenic and/or radiogenic component, which reside in mineral lattice. This indicates that up to three times of press at 70MPa or up to 2000 strokes can be applied without the risk of releasing He in matrix. $^3He/^4He$ ratios obtained with heating experiment for powder after crushing shows identical with that obtained with crushing method because these samples are rich in fluid inclusions. However, $^3He/^4He$ ratios obtained with heating experiment are generally different from that obtained with crushing, indicating post-eruptive addition of secondary component (see next chapter).

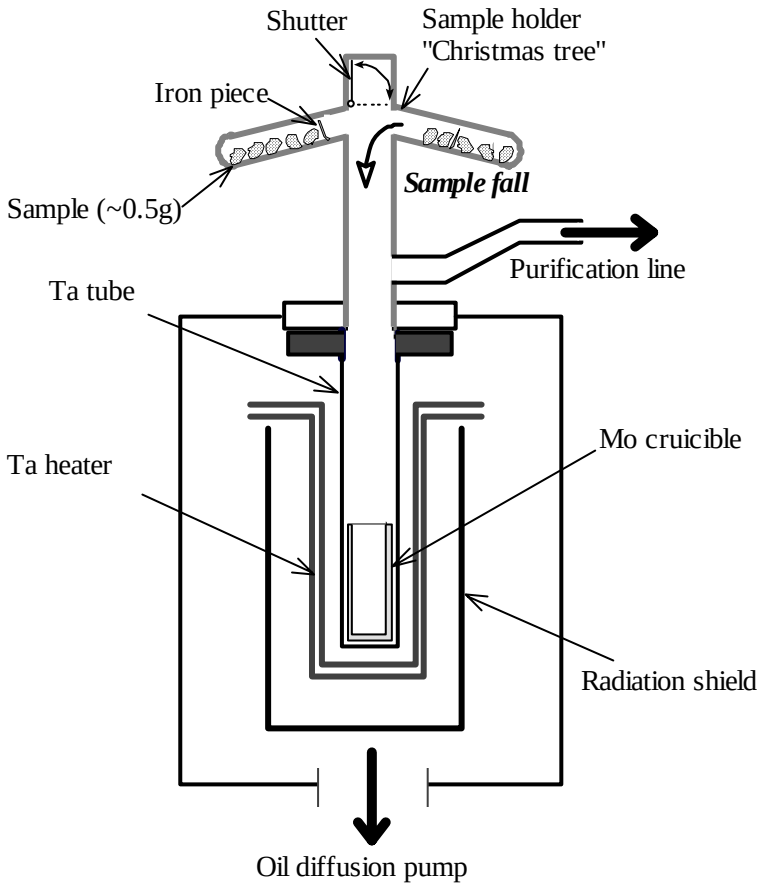

Fig. 2–2. Sample holder and Ta-oven are shown. The sample holder made of Pyrex-glass or lead glass is equipped with 10 or 4 branches, respectively. 4–5 samples weighing ca. 0.5g each can be loaded in each branch. Sample to be analyzed is dropped into the crucible by moving iron piece using hand magnet from outside the glass wall. A shutter prevents silicate from being deposited on the glass wall on the top of the holder, in order to observe the sample in the furnace.

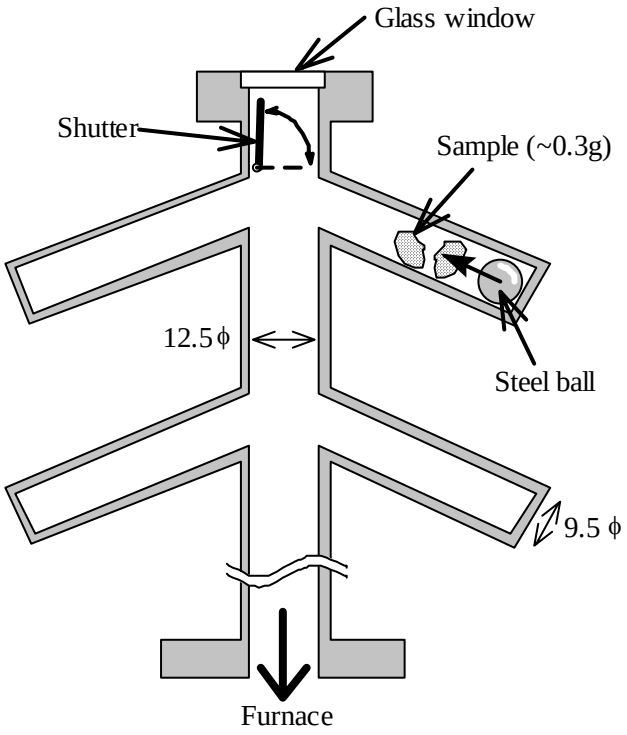

Fig. 2–3. Sample holder made of stainless-steel is shown. The sample holder is equipped with 10 branches, in which up to 3 samples weighing ca. 0.3g each can be loaded. Sample can be moved and dropped by moving a steel ball using hand magnet from outside the chamber. A shutter prevents silicate from being deposited on the glass window on the top of the holder, in order to observe the sample in the furnace.

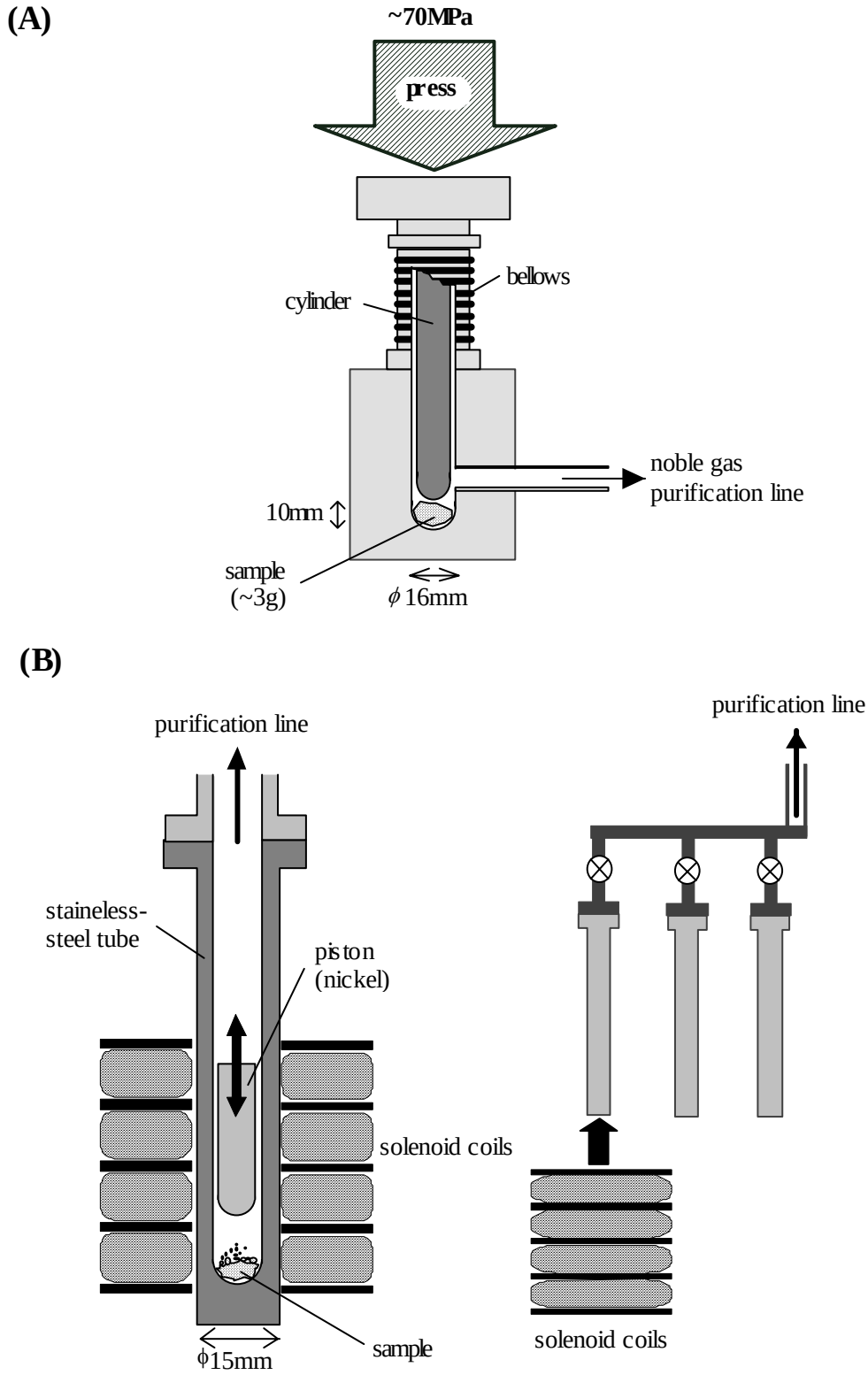

Fig. 2–4. Crushing apparatus for noble gas extraction are shown. The crushers are connected to the noble gas purification line with some valves. (A) Hydraulic-type crusher. Up to 3g of the sample can be loaded into the chamber. Crushing is performed by hydraulic pressure up to 70MPa applied by a hand pump from outside the crusher. (B) Solenoid-type crusher. A piston made from nickel is lifted upwards and accelerated downwards by an external magnetic field generated by solenoid coils. Up to 1g of the sample can be crushed after 1000–2000 strokes.

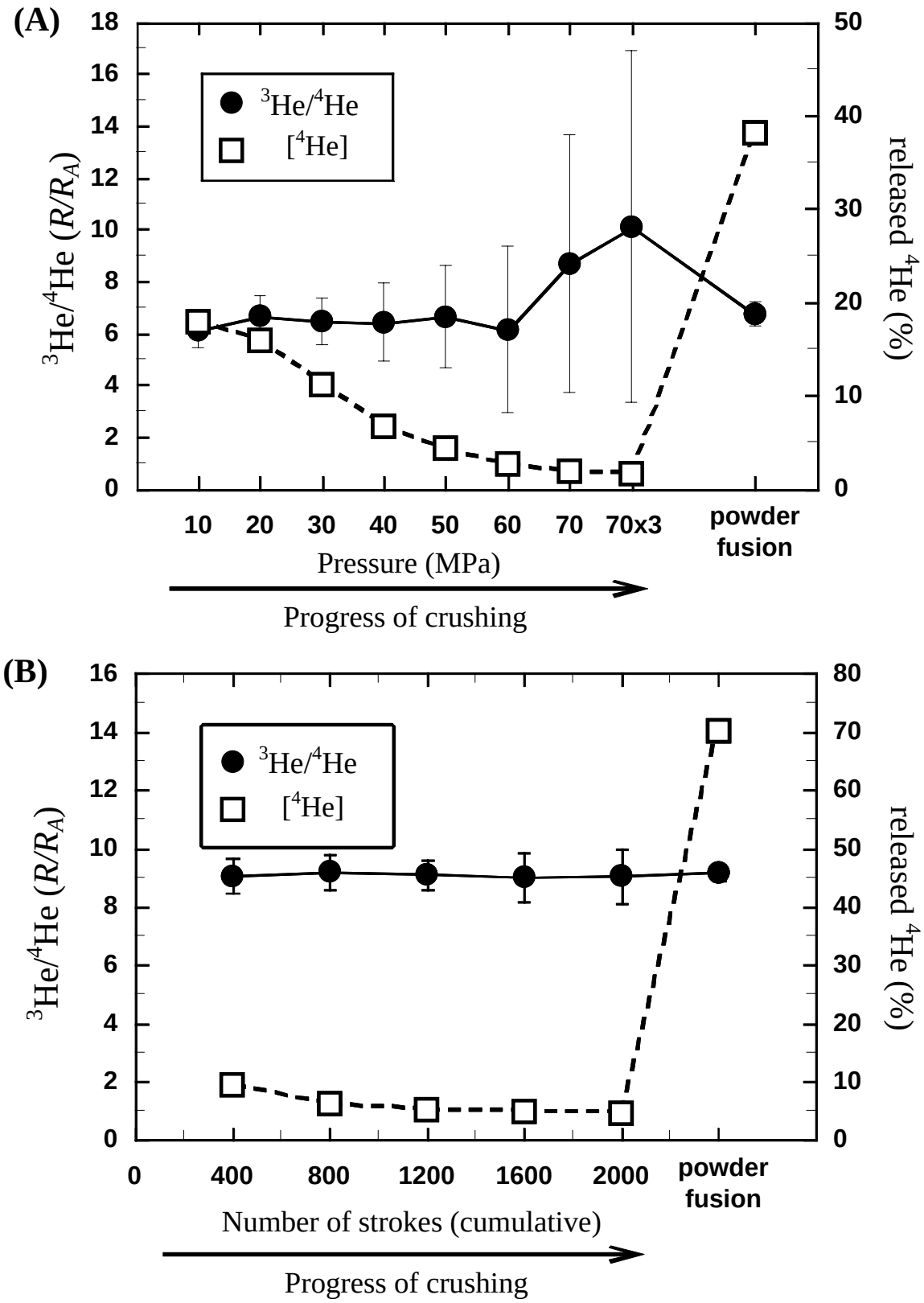

Fig. 2–5. He abundance and isotopic ratio as a function of progress of crushing with hydraulic -type crusher (A) and solenoid-type crusher (B). Progress of crushing is indicated as hydraulic pressure or number of strokes. “70x3” means 3 times of press at 70Ma. Results obtained with heating experiment of powder after cumulative crushing are also shown.

2–2–3. Modification of noble gas purification and separation line

The original design of gas purification and separation part of the system was for measurement of gas samples. Thus, the several improvements were made to achieve the ultra-high vacuum because low blank level is required for rock samples, and to increase efficiency of measurement by reducing the time for each analysis. The improvements were carried out by (1) addition of an evacuation system, including a turbo molecular pump and a rotary pump (TMP2 and RP2 in Fig. 2–1), (2) addition of a SORB-AC getter pump to further reduce background (GP in Fig. 2–1), (3) reduction of the volume of line including changing Ti-Zr getters and charcoal traps to smaller ones to avoid dilution of the noble gas with small abundance, and (4) installation of the Cryo trap which can separate each noble gas effectively and can be heated more than 100°C to release adsorbed gas. It takes about five hours for the full measurement of He, Ne, Ar, Kr and Xe described below, whereas it needed ten hours before modification.
The purification system was originally equipped with a Cryo trap containing sintered stainless filter element (Nupro Co.) connected to commercially manufactured double-stage He expansion refrigerator (Model S030, Iwatani industrial gases Co.). The old Cryo trap can be cooled down to 26K; sometimes it was inadequately cool to trap Ne for separation from He. In addition, the old Cryo trap could not be heated over room temperature, thus blank level was so high ($>3\times10^{-10}$cm^{3}STP) that it was impossible to measure Ne for mineral samples. Therefore, a new Cryo trap was made and used in this study. The new one is almost the same equipped with MS–II and MS–III (Nagao et al., 1999; Osawa et al., 2000; Aka et al., 2001), which consists of trap containing the same material as old one, and high-performance double-stage He expansion refrigerator (Model D510, Iwatani industrial gases Co.). The new Cryo trap can be routinely cooled to a temperature around 13K. At this temperature all noble gases are adsorbed on the trap. The temperature can be incrementally increased by the heater coil attached to the trap, each of the five noble gases sequentially desorbed for analysis. Figure 2–6 shows the relationship between noble gas release and trap temperature utilizing the mass spectrometer for the measurements. Helium and Ne are effectively separated from Ne and Ar at approximately 24K and 50K, respectively. For Ar, Kr, and Xe, there is

overlap in the release. Partial separation temperatures for Kr from Ar and Xe from Kr that are used are 100K and 130K, respectively. To release Xe, the trap is heated to 220K. The trap can be heated up to 100°C for baking out, reducing blank level to $<3\times10^{-12}$ cm^3STP for Ne.

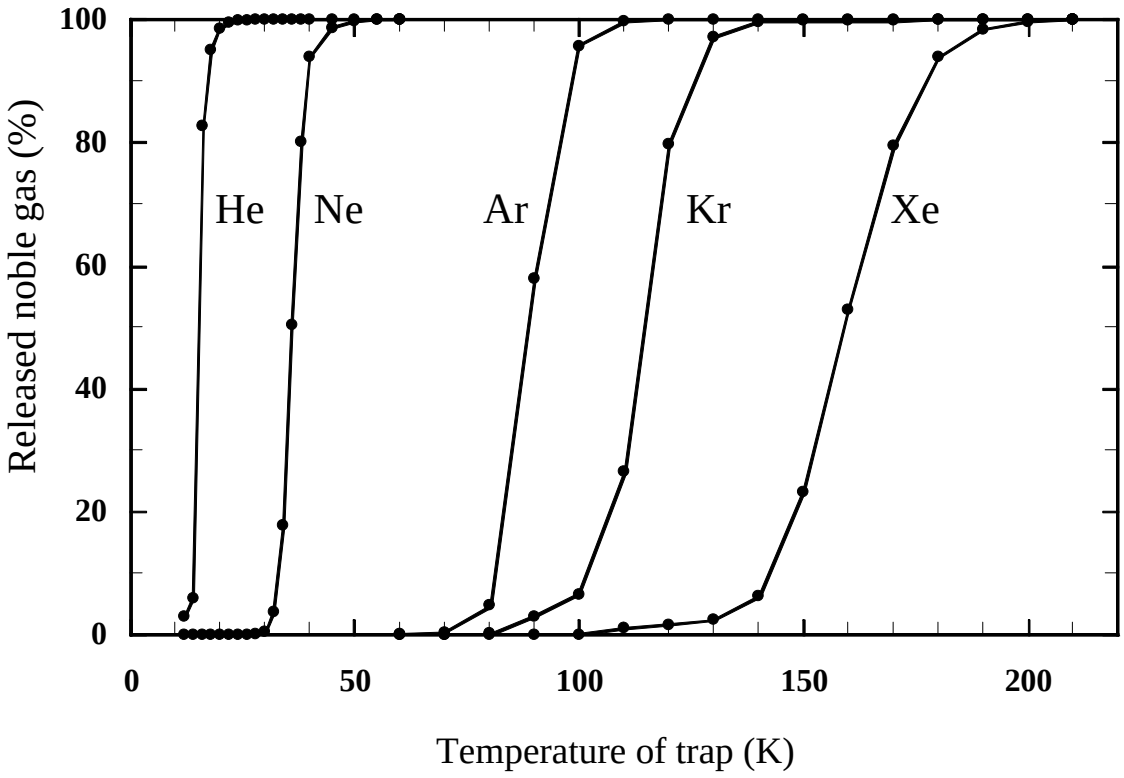

Fig. 2–6. Profiles of noble gas release from the Cryo trap.

2–2–4. Modification of the Mass spectrometer

The mass spectrometer is a catalogue model, VG5400 (VG Isotech), with split flight tubes (Fig. 2–7) for simultaneous detection of ^{3}He and ^{4}He ion beams (Sano and Wakita, 1988). The VG5400 had initially two conventional Faraday-cup systems, namely Axial-Faraday and High-Faraday, and one Daly multiplier collector consisting of a Daly-knob, a scintillator and a photoelectron multiplier. The ^{3}He beam was measured by the Daly multiplier collector, and the ^{4}He beam by the High-Faraday simultaneously. In 1999, an ion-counting system was equipped after removing the Axial-Faraday system. The ion-counting system consists of a SEM (secondary electron multiplier: SEV217, Balzers Co.), a pre-amplifier, a discriminator and a counter (ORTEC Co.), and a high voltage supply for SEM (HSX-3R5-5, Matsusada Precision Inc.). Since the noise level was decreased dramatically and the detection limit was improved compared with those of the Daly multiplier collector, which was the most sensitive among three collectors of the original VG5400, ^{3}He beam is measured using the ion-counting system thereafter. Exchange a photo multiplier to R1044 (Hamamatsu Photonics K. K.), an operational amplifier to OPA104CM (Burr-Brown Co.) and a feedback register to RHA 2B (Hydragin Co.) from original design of the Daly multiplier collector by VG Isotech have also done after Nagao et al. (1996), and greatly reduced dark current and noise levels. Overall multiplier gain of the Daly multiplier collector with operating the Daly knob and the photo multiplier at -10kV and -600V is about 1,500 after modification. Noise level of the ion-counting is less than 1×10^{-22}A corresponds to 6×10^{-4}cps, and those of the Daly multiplier collector and the High-Faraday are less than 4×10^{-14}A (-600V) and 2×10^{-15}A, respectively, in the condition of usual ^{3}He/^{4}He measurement. The extremely low noise level of ion-counting achieves very low detection limit ca. 6×10^{-16}cm^{3}STP or 1.6×10^{4} atoms of He, which is two orders of magnitude lower than that with Daly multiplier collector before modification, 4×10^{-14}cm^{3}STP. In addition, very low detection limit makes isotope analysis of Ne, Kr and Xe possible, which was impossible before modification because of their low concentration in mineral samples. The operational conditions of the mass spectrometer during this study are: acceleration voltage of ion, 4.6kV; acceleration voltage of electron, 80V; repeller voltage, -14V

relative to the source chamber; trap current, 800μA for all noble gases. Focusing and beam centering voltages are tuned up to maximize beam intensity of ^{4}He. The resolving power on the 5% level of peak height is higher than 550 for the ion-counting and the Daly multiplier collector, 200 for the High-Faraday.

Sensitivity for each noble gas during this study is listed in Table 2–1. Correction factor $k(3/4)$ for $^{3}He/^{4}He$ ratio and mass discrimination factors for $k(x/y)$ for $^{x}M/^{y}M$ isotope ratios of Ne, Ar, Kr and Xe are listed in Table 2–2. The correction factor for He includes corrections for mass discrimination and for sensitivity ratio between the two collectors. The sensitivities for all noble gases and the mass discrimination factors for Ne, Ar, Kr and Xe are calibrated by the measurement of standard atmospheric gas. The correction factor for He is obtained with analysis of He standard gas ($^{3}He/^{4}He = 20.77\pm0.24R_A$). A detailed procedure of determination of $^{3}He/^{4}He$ ratio of the standard gas is described in the later section. Since correction factor for He and mass discrimination factor for other noble gases depend on the collector and partial pressure of noble gases, the amount of standard gas admitted to the mass spectrometer is reduced to comparable amount to those of the sample runs.

Table 2–1. Sensitivity of MS–IV for each noble gas.

DATE	Std. Air	Sensitivity* ^{4}He (10^{-5}A/Torr)	^{20}Ne (10^{-5}A/Torr)	^{40}Ar (10^{-4}A/Torr)	^{84}Kr (10^{-4}A/Torr)	^{132}Xe (10^{-4}A/Torr)
1999.7.7	A2–0	4.67	7.86	3.06	4.40	5.98
7.8	1	4.38	7.69	2.31	3.30	4.61
7.13	2	4.41	6.20	3.37	5.68	12.09
7.13	***[Ion source tuning]***					
7.16	3	5.21	7.17	3.38	4.68	6.36
7.17	***[Electricity shutdown]***					
7.22	4	5.15	7.34	3.57	4.88	6.43
7.25	5	4.92	5.58	3.10	4.34	5.85
7.27	6	5.19	7.63	3.15	4.49	6.21
8.25	7	5.06	7.76	3.71	6.07	4.94
9.12	8	5.66	7.30	4.55	2.30	2.95
9.21	9	5.49	6.99	3.71	5.43	7.98
2000.2.22	10	5.58	6.91	2.61	2.77	7.14
2.26	***[Ion source tuning]***					
3.14	A3–1	4.00	4.29	2.24	2.71	9.09
4.10	2	3.99	4.43	2.23	2.50	7.85
4.15	3	3.34	3.18	1.81	2.42	6.65
4.17	4	3.55	3.29	1.93	2.43	6.30
4.20	5	3.26	3.78	1.73	2.29	5.77
4.26	6	3.59	4.43	2.08	2.40	5.61
4.28	***[Ion source tuning]***					
5.8	7	3.18	4.04	1.78	2.36	4.79
5.12	8	4.06	3.20	1.36	1.67	2.84
5.24	9	4.18	3.60	1.56	1.84	2.81
6.1	10	3.94	4.17	1.53	1.84	2.83
6.12	12	3.89	3.58	1.38	1.73	2.59
7.3	13	3.84	3.69	1.28	1.51	2.23
7.21	14	2.98	3.00	1.49	1.30	1.82
7.23	15	4.89	5.63	1.67	1.91	3.25
9.7	19	5.19	6.15	2.16	2.55	4.36
9.18	22	4.30	5.03	2.11	2.36	3.24
10.29	***[Electricity shutdown]***					
11.1	23	4.97	7.51	2.99	3.88	9.94
11.2	24	4.85	7.05	2.76	3.23	4.32
11.24	29	5.67	8.55	3.29	4.07	6.64

* Sensitivity for High-Faraday.

Table 2–2. Correction factors and mass discrimination factors for noble gas isotope analysis using MS–IV.

Correction factor for He			
Date	Std. He	k (3/4) [*1]	(R_A) [*2]
1999.7.8	R1–37	10.99	± 0.19
7.13	38	10.86	± 0.23
7.13	***[Ion source tuning]***		
7.16	39	11.23	± 0.24
7.17	***[Electricity shutdown]***		
7.27	40	11.40	± 0.25
8.26	41	11.33	± 0.25
9.16	44	11.14	± 0.24
9.23	45	11.10	± 0.26
2000.2.26	46	12.56	± 0.32
2.26	***[Ion source tuning]***		
3.13	47	13.52	± 0.32
4.11	49	13.90	± 0.34
4.13	50	14.06	± 0.20
4.15	51	14.30	± 0.24
4.21	52	14.17	± 0.24
4.28	53	14.85	± 0.21
4.28	***[Ion source tuning]***		
5.12	54	12.99	± 0.20
5.24	55	13.15	± 0.19
6.1	56	13.16	± 0.20
6.15	57	13.11	± 0.23
7.3	58	13.18	± 0.30
7.21	59	13.51	± 0.29
7.23	60	13.38	± 0.26
9.7	61	13.73	± 0.22
9.18	62	13.91	± 0.21
10.29	***[Electricity shutdown]***		
11.2	63	14.60	± 0.31
11.24	64	14.88	± 0.30

*1. $k(3/4)=(^3He/^4He)_{raw}/(^3He/^4He)_{HESJ}$

*2. Normalized to the atmospheric ratio = 1.4×10^{-6} (Ozima and Podosek, 1983).

Mass discrimination factor [*3]											
Date	Std. Air	k (20/22)		k (21/22)		Coll. [*4]	k (38/36)		k (40/36)	
1999.7.7	A2–0	0.9576	± 0.0018	0.974	± 0.013	DM	1.0102	± 0.0034	1.0336	± 0.0010
7.8	1	0.9598	± 0.0025	0.973	± 0.030	DM	1.0323	± 0.0030	1.0354	± 0.0013
7.13	2	0.9989	± 0.0033	0.997	± 0.025	IC	1.0173	± 0.0028	1.0386	± 0.0003
7.13	***[Ion source tuning]***									
7.16	3	1.0050	± 0.0037	0.996	± 0.012	IC	1.0103	± 0.0052	1.0403	± 0.0006
7.17	***[Electricity shutdown]***									
7.22	4	0.9520	± 0.0015	0.970	± 0.010	DM	1.0154	± 0.0042	1.0404	± 0.0010
7.25	5	0.9963	± 0.0014	0.990	± 0.011	IC	1.0106	± 0.0011	1.0400	± 0.0007
7.27	6	0.9550	± 0.0030	0.968	± 0.022	DM	1.0170	± 0.0026	1.0360	± 0.0008
8.25	7	0.9563	± 0.0030	0.975	± 0.013	DM	1.0117	± 0.0008	1.0355	± 0.0020
9.12	8	0.9673	± 0.0027	0.975	± 0.019	DM	1.0138	± 0.0013	1.0396	± 0.0011
9.21	9	1.0087	± 0.0024	0.991	± 0.015	IC	1.0143	± 0.0023	1.0398	± 0.0015
2000.2.22	10	0.9469	± 0.0021	0.980	± 0.013	IC	1.0151	± 0.0022	1.0535	± 0.0010
2.26	***[Ion source tuning]***									
3.14	A3–1	0.9658	± 0.0048	1.002	± 0.034	IC	1.0211	± 0.0012	1.0668	± 0.0010
4.10	2	0.9360	± 0.0033	0.970	± 0.016	DM	1.0239	± 0.0023	1.0670	± 0.0008
4.15	3	0.9338	± 0.0018	0.977	± 0.009	DM	1.0244	± 0.0012	1.0661	± 0.0003
4.17	4	0.9306	± 0.0021	0.977	± 0.007	DM	1.0230	± 0.0013	1.0668	± 0.0006
4.20	5	0.9330	± 0.0019	0.975	± 0.006	DM	1.0259	± 0.0012	1.0667	± 0.0014
4.26	6	0.9313	± 0.0012	0.973	± 0.008	DM	1.0246	± 0.0009	1.0662	± 0.0004
4.28	***[Ion source tuning]***									
5.8	7	0.9338	± 0.0017	0.975	± 0.008	DM	1.0272	± 0.0012	1.0680	± 0.0008
5.12	8	0.9662	± 0.0051	0.987	± 0.022	IC	1.0338	± 0.0014	1.0697	± 0.0012
5.24	9	0.9249	± 0.0007	0.974	± 0.006	DM	1.0311	± 0.0014	1.0732	± 0.0003
6.1	10	0.9244	± 0.0010	0.970	± 0.009	DM	1.0298	± 0.0003	1.0736	± 0.0009
6.12	12	0.9753	± 0.0029	0.989	± 0.016	IC	1.0296	± 0.0020	1.0699	± 0.0012
7.3	13	0.9773	± 0.0053	0.973	± 0.022	IC	1.0303	± 0.0015	1.0693	± 0.0009
7.21	14	0.9746	± 0.0049	0.985	± 0.028	IC	1.0281	± 0.0013	1.0712	± 0.0009
7.23	15	0.9841	± 0.0030	0.987	± 0.018	IC	1.0305	± 0.0017	1.0705	± 0.0010
9.7	19	0.9817	± 0.0032	0.995	± 0.022	IC	1.0300	± 0.0020	1.0737	± 0.0005
9.18	22	0.9765	± 0.0024	0.987	± 0.016	IC	1.0299	± 0.0018	1.0727	± 0.0009
10.29	***[Electricity shutdown]***									
11.1	23	0.9884	± 0.0043	0.983	± 0.029	IC	1.0234	± 0.0012	1.0665	± 0.0007
11.2	24	0.9897	± 0.0027	0.998	± 0.015	IC	1.0279	± 0.0012	1.0665	± 0.0008
11.24	29	0.9886	± 0.0040	0.996	± 0.019	IC	1.0281	± 0.0022	1.0674	± 0.0008

*3. $k(x/y)=(^xM/^yM)raw/(^xM/^yM)air$

*4. Collector used for Ne analysis. DM: Daly multiplier collector, IC: ion-counting.

Table 2–2. (Continued.)

		Mass discrimination factor [*1]												
Date	Std. Air	*k* (78/84)	*k* (80/84)	*k* (82/84)	*k* (83/84)	*k* (84/84)	*k* (124/130)	*k* (126/130)	*k* (128/130)	*k* (129/130)	*k* (131/130)	*k* (132/130)	*k* (134/130)	*k* (136/130)
1999.8.25	A2–7	0.964	0.9742	0.9840	0.9874	1.0014	1.026	1.025	1.003	0.997	0.992	0.992	0.993	1.000
		± 0.016	± 0.0062	± 0.0052	± 0.0069	± 0.0016	± 0.032	± 0.084	± 0.032	± 0.014	± 0.005	± 0.009	± 0.011	± 0.012
9.21	9	0.979	0.9735	0.9837	0.9896	0.9993	0.972	1.034	1.007	1.001	1.000	1.001	0.992	0.999
		± 0.013	± 0.0040	± 0.0031	± 0.0037	± 0.0032	± 0.083	± 0.102	± 0.024	± 0.013	± 0.015	± 0.010	± 0.012	± 0.013
2000.2.26	***[Ion source tuning]***													
3.14	A3–1	0.976	0.9430	0.9840	0.9949	1.0036	1.001	0.999	0.987	0.997	1.000	1.003	1.003	1.008
		± 0.015	± 0.0083	± 0.0031	± 0.0057	± 0.0029	± 0.070	± 0.044	± 0.012	± 0.008	± 0.008	± 0.005	± 0.010	± 0.015
4.10	2	0.975	0.9493	0.9841	1.0008	1.0039	1.008	0.982	0.994	0.997	1.000	1.004	1.004	1.005
		± 0.013	± 0.0057	± 0.0023	± 0.0015	± 0.0053	± 0.059	± 0.086	± 0.012	± 0.007	± 0.006	± 0.007	± 0.006	± 0.010
4.28	***[Ion source tuning]***													
5.12	8	0.958	0.9181	0.9792	1.0006	1.0031	1.024	0.993	1.003	1.003	1.006	1.013	1.037	1.033
		± 0.022	± 0.0123	± 0.0051	± 0.0077	± 0.0042	± 0.076	± 0.063	± 0.027	± 0.024	± 0.023	± 0.022	± 0.016	± 0.021
6.12	12	0.960	0.9439	0.9789	0.9978	1.0079	1.052	0.931	0.988	1.004	0.994	1.010	1.011	1.015
		± 0.031	± 0.0141	± 0.0059	± 0.0064	± 0.0037	± 0.119	± 0.068	± 0.048	± 0.024	± 0.027	± 0.025	± 0.024	± 0.030
7.3	13	0.965	0.9433	0.9811	0.9990	1.0078	1.009	0.961	0.995	0.992	1.006	1.001	1.011	1.017
		± 0.016	± 0.0086	± 0.0044	± 0.0037	± 0.0034	± 0.069	± 0.057	± 0.016	± 0.015	± 0.016	± 0.012	± 0.014	± 0.013
9.7	19	0.998	0.9343	0.9750	1.0011	1.0001	1.001	0.973	0.992	0.995	1.003	1.006	1.019	1.032
		± 0.015	± 0.0047	± 0.0048	± 0.0029	± 0.0031	± 0.043	± 0.057	± 0.008	± 0.012	± 0.018	± 0.011	± 0.017	± 0.011
9.18	22	1.031	0.9987	0.9819	1.0185	1.0053	0.986	0.999	0.986	0.998	1.006	1.014	1.009	1.017
		± 0.016	± 0.0104	± 0.0094	± 0.0063	± 0.0025	± 0.091	± 0.093	± 0.019	± 0.014	± 0.010	± 0.014	± 0.016	± 0.015
10.29	***[Electricity shutdown]***													
11.24	29	0.952	0.9708	0.9803	0.9962	1.0121	1.099	0.991	0.996	1.004	1.003	1.005	1.008	1.021
		± 0.022	± 0.0059	± 0.0031	± 0.0077	± 0.0033	± 0.072	± 0.054	± 0.019	± 0.019	± 0.016	± 0.018	± 0.018	± 0.015

*1. $k\,(x/y)=(\,^{x}M/^{y}M\,)raw/(\,^{x}M/^{y}M\,)air$

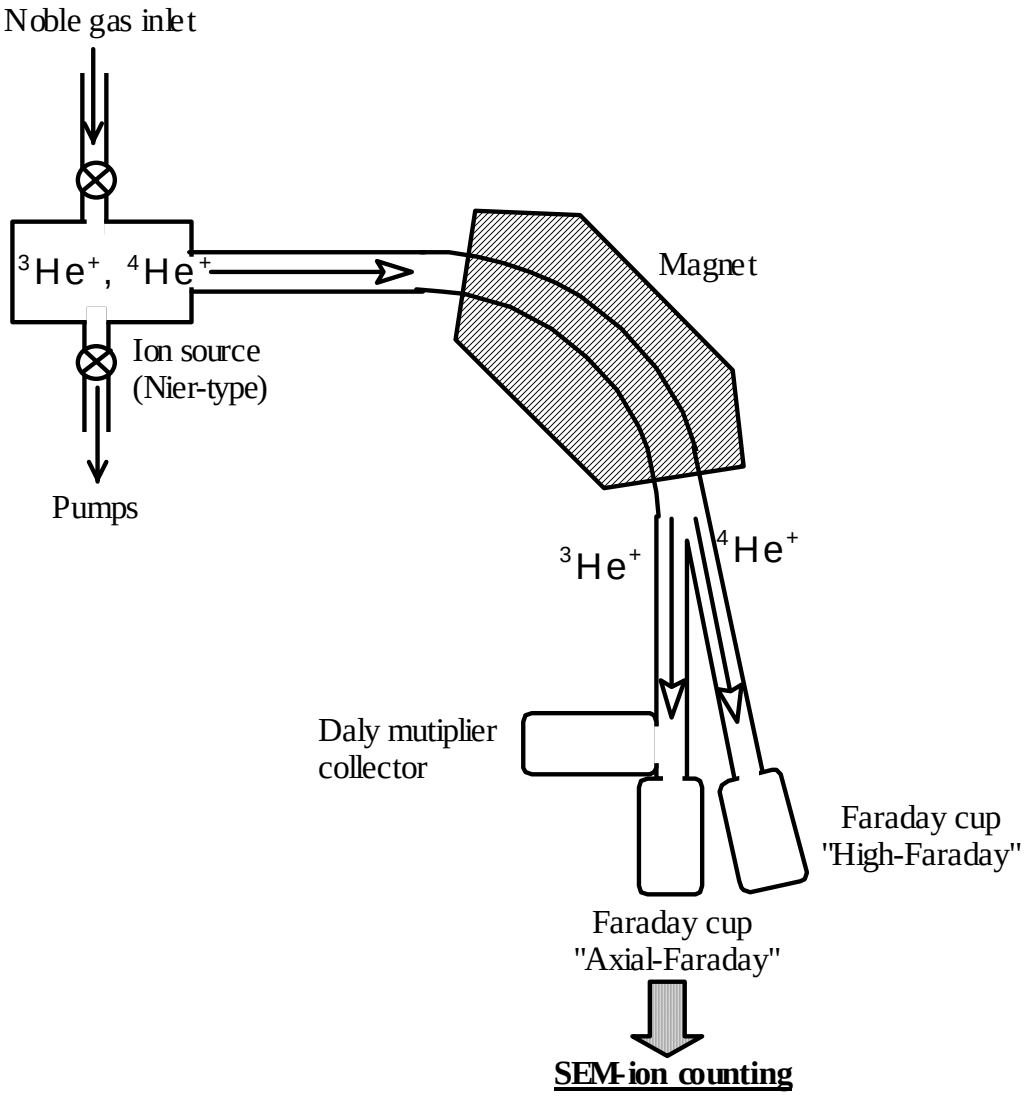

Fig. 2–7. Schematic diagram of the mass spectrometer with split flight tube for the measurement of $^3He/^4He$ isotope ratios. Ion beams of ^3He and ^4He which are generated by Nier-type electron impact ion source are measured at the same time with a Faraday cup (High-Faraday) and a Daly multiplier collector for ^4He and ^3He, respectively. After 1999, an ion-counting system equipped after removing the Axial-Faraday has been used for ^3He measurement.

2–2–5. Procedure of noble gas measurement

After loading the samples into the extraction apparatuses, the extraction and purification system are baked out over 250°C for more than one day to reduce atmospheric contamination. Samples in the sample holder and the crushers are also heated to 150–200°C to desorb the atmospheric noble gases and other gases. After finishing the baking out, noble gases in the sample are released by each extraction method, and then admitted to the purification line. First, released noble gases are purified from other major gas components by a hot Ti-Zr getter (Ti1, ~800°C). When occasion demands, an aliquot of gas is admitted to a quadrupole mass spectrometer (QMG112, Balzers Co.) to measure the major components before exposing to the Ti-Zr getter. Residual major components are purified by Ti1, and then Ar, Kr and Xe are adsorbed on a charcoal trap (CH1) cooled at the temperature of liquid nitrogen. Unadsorbed components including He and Ne are purified by the second Ti-Zr getter (Ti2, ~800°C), the second charcoal trap (CH2, liquid nitrogen temperature), and a SORB-AC getter pump (~200°C). Finally, Ne is separated from He using the Cryo trap at 24K.
Each noble gas fraction thus separated is analyzed with the modified-VG5400 successively. After introducing the He fraction into the mass spectrometer, measurement of He isotopic ratio is automatically performed by a computer controlled by a program developed in our laboratory. Details of computer-controlled He isotopic measurement are described in next section. After finishing measurement of He, adsorbed Ne on the Cryo trap is released by raising the temperature to 50K, and then admitted to the mass spectrometer and start analysis for Ne isotopes. A trap at the inlet of the mass spectrometer, containing sintered stainless which is the same material in the Cryo trap is cooled by liquid nitrogen during Ne analysis, in order to reduce interferences with ^{20}Ne and ^{22}Ne by double charges of ^{40}Ar and CO_2 (M=44). ^{40}Ar and CO_2, and ^{22}Ne-H peaks are monitored at the start and the end of each analysis. Interference of ^{20}Ne-H on ^{21}Ne estimated from ^{22}Ne-H is almost negligible. Although using the trap in the mass spectrometer, the interferences of $^{40}Ar^{++}$ and CO_2^{++} cannot be removed completely, and they are corrected using $^{40}Ar^{++}/^{40}Ar^{+}$ and CO_2^{++}/CO_2^{+} production ratios, which are measured during series of experiment. Ne analysis is

usually carried out with the ion-counting system due to generally low concentration of Ne in mineral samples. The remaining noble gases (Ar, Kr and Xe) are released from CH1 at ~250°C and then purified again by two hot Ti-Zr getters. Kr and Xe are trapped by the Cryo trap at 100K, and remaining Ar is admitted to the mass spectrometer for isotope analysis. Detail of Ar isotopic measurement by the computer program is described in Nagao et al. (1996). The Daly multiplier collector is used for Ar analysis. Multiplier gain of the Daly multiplier collector is adjusted to suitable condition for variable amounts of Ar admitted to the mass spectrometer by changing high voltage applied to photo multiplier. Finally, both Kr and Xe are released from the trap at 220K, and introduced to the mass spectrometer. Then Xe is measured first and secondly Kr, because abundance of Xe is smaller than that of Kr and important information is generally obtained with Xe in terrestrial samples. Kr and Xe analyses are usually performed using the ion-counting system.

2–2–6. Helium analysis with the double collector system

As described above, the mass spectrometer has a sub flight tube aside from a main flight tube, designed for simultaneous passing by ion beams of ^{3}He and ^{4}He (Fig. 2–7). In order to obtain coincidence of the two beams, the position of the High-Faraday is adjustable by a manipulator. Magnet scan and data acquisition are automatically carried out using HP-Basic for Windows and programs written in HP-Basic by us, which are based on the program reported in Nagao et al. (1996).

Typical mass spectra of ^{3}He and ^{4}He before and after the modification are shown in Fig. 2–8. The program automatically assigns magnetic field for ^{4}He and displays the "Peak center" assigned, and ^{3}He center estimated from mass difference between ^{3}He and HD-H_3 is also displayed as "3He center" by which an operator can confirm the coincidence of the peaks. Owing to the mass resolution over 550, $^3He^+$ and double peak of HD^+–H_3^+ are clearly separated. Base line around $^3He^+$ and HD^+–H_3^+ peaks is completely flat due to extremely low noise level of the ion-counting. Therefore, though abundance of ^{3}He admitted to the mass spectrometer was an order of magnitude smaller than in Fig. 2–8(A), the $^3He^+$ peak is clearly recognized and separated from HD^+–H_3^+ as shown in Fig. 2–8(B). Figure 2–9 demonstrates that the errors for ^{3}He/^{4}He measurements after modification are smaller than before modification, especially when He abundance introduced into mass spectrometer is small. For example, in contrast with that the error surpass 10% with ^{3}He partial pressure lower than 3×10^{-13} Torr (before modification, the error seems to remain lower than 10% around 2×10^{-14} Torr after modification. Helium extracted from mineral samples by in vacuo crushing is often lower than 3×10^{-13} Torr in ^{3}He pressure, therefore the improvement of precision has a profound effect especially on terrestrial rock samples.

If abundance of He is very small and the program cannot assign a proper center of ^{4}He as shown in Fig. 2–8(C), an operator can manually indicate a correct position of peak center estimated from the center of HD^+–H_3^+. In this case, if peak coincidence of ^{3}He and ^{4}He is not exact for some reason, it is not so critical because peak top of ^{4}He is sufficiently flat and wide. Of course ^{4}He abundance extracted from the sample is not enough to detect with High-Faraday, we can select conventional peak jumping mode

using the ion-counting as a single collector. The flexibility of the program allows us to measure $^{3}He/^{4}He$ ratio of gas-poor samples, whose He abundance is almost blank level that is in the range of 10^{-11} to $10^{-10}cm^{3}STP$ of ^{4}He.

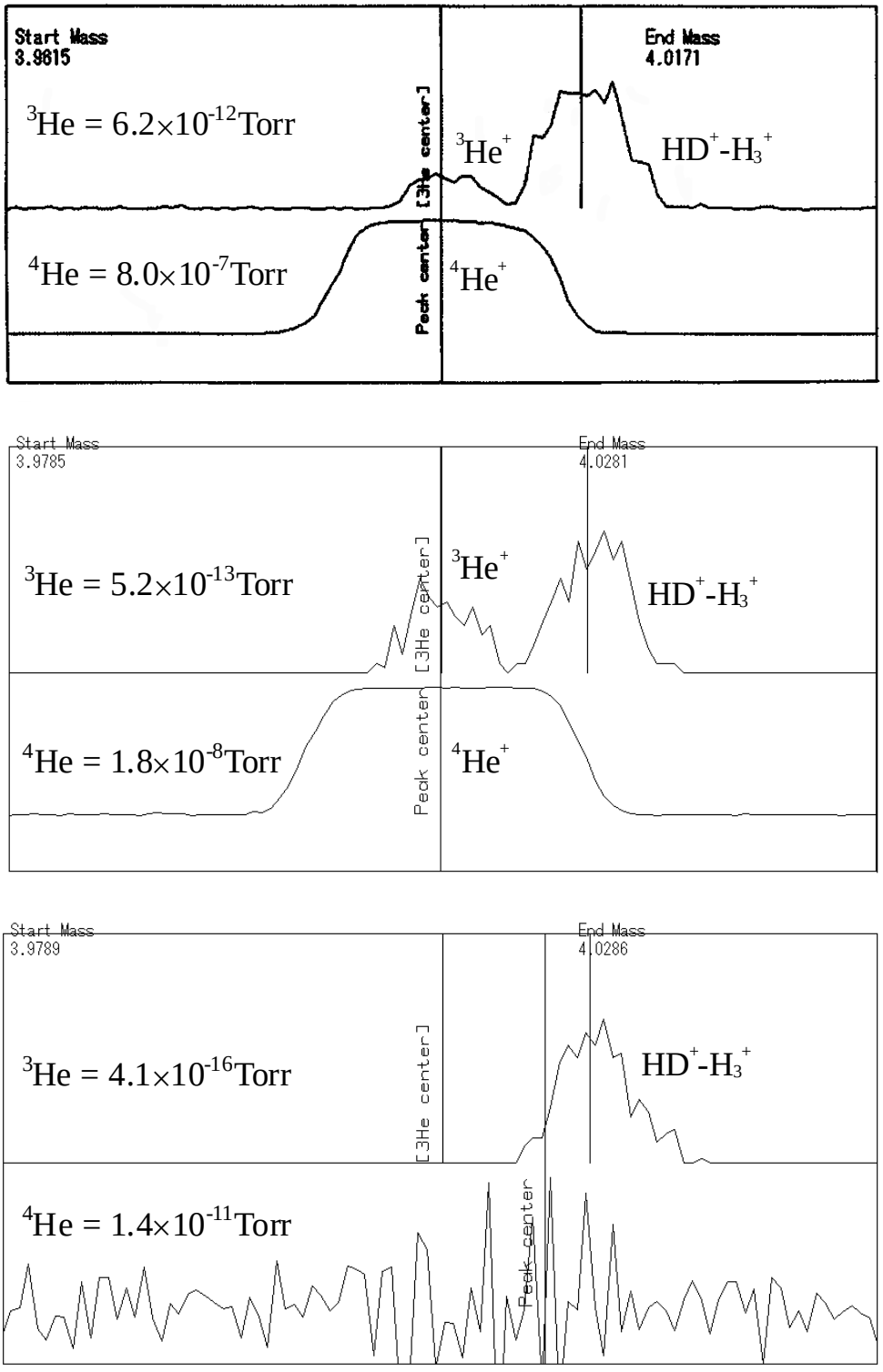

Fig. 2–8. Mass spectra of ^{3}He and ^{4}He from usual samples; (A) before modification; (B and C) after modification described in text. Samples are; (A) gas sample from Iwo-jima, Japan whose ^{3}He/^{4}He = 5.6R$_A$; (B) HESJ with ^{3}He/^{4}He = 20.8R$_A$; (C) HESJ reduced to 1/1200 of usual measurement. "Peak Center" means the peak center of ^{4}He, and "3He Center" means the peak center of ^{3}He estimated from the center of HD-H$_3$ peak determined by the computer program controlling the mass spectrometer.

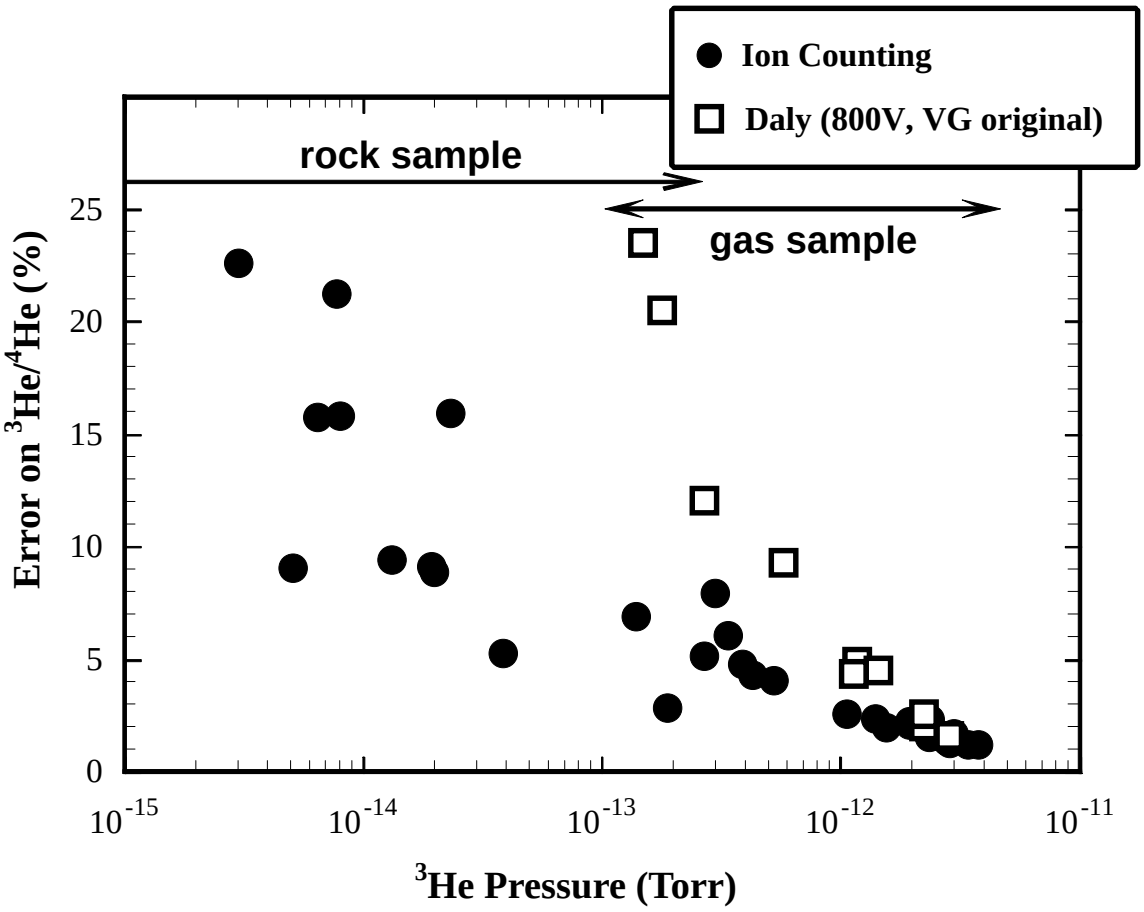

Fig. 2–9. Errors on $^3He/^4He$ ratio measurement are plotted against partial pressure of ^3He in the mass spectrometer. The errors are 1σ concurrent with raw value of $^3He/^4He$ ratio. The improved precision by modification of mass spectrometer is more effective when ^3He partial pressure is low. Arrows indicate the range of ^3He pressure in usual measurement of gas and rock samples.

2–3. Determination of $^{3}He/^{4}He$ ratio of HESJ (HElium Standard of Japan)

Since atmospheric $^{3}He/^{4}He$ ratio ($=1.40\times10^{-6}$) is globally constant (Mamyrin et al., 1970), atmospheric He has been used as a primary standard of He isotopic ratio in most laboratories in the world. However, because of a very low concentration of He (=5.24ppm) in air (Ozima and Podosek, 1983), a lot of air is necessary to be admitted to the purification line, and precise measurement of $^{3}He/^{4}He$ is not easy due to low ^{3}He intensity. Moreover, a large amount of air introduced into the purification line gives damage to some extent to the Ti-Zr getters and ultrahigh-vacuum condition. Therefore in some laboratories, He in volcanic gases or natural gases, whose $^{3}He/^{4}He$ ratio is several times of the atmospheric one and ^{4}He concentration is high, are used as a secondary standard. However, there are no common secondary standard among the laboratories, thus interlaboratory crosscheck in accuracy of $^{3}He/^{4}He$ ratio determination has not been carried out until now. A synthesized He gas with high $^{3}He/^{4}He$ ratio, which is named HESJ (HElium Standard of Japan), was selected as a working standard. The HESJ is synthesized by Nihon Sanso Kogyo Co. at a request of five noble gas laboratories in Japan, and is expected to be a common secondary standard. The HESJ consists of 99.9% of He, and its noble gas abundances measured by Prof. K. Nagao using MS–III is listed in Table 2–3.

Table 2–3. Noble gas composition of HESJ.

^{4}He	^{20}Ne	$^{36}Ar^{*}$	^{40}Ar	^{84}Kr	^{132}Xe
$\equiv 1$	1.5×10^{-5}	7.7×10^{-7}	2.3×10^{-4}	4.7×10^{-8}	4.7×10^{-9}

$^{*40}Ar/^{36}Ar = 296.0$ is assumed.

Prior to using the HESJ as the working standard for He isotopic ratio, its $^{3}He/^{4}He$ ratio was determined using atmospheric He as a primary standard. An aliquot of HESJ was stored in the well-evacuated metal reservoir (Fig. 2–1) from a distributed steel cylinder. One pipette of HESJ from the reservoir was analyzed to determine $^{3}He/^{4}He$ ratio. The amount of HESJ analyzed in this work was varied by reduction using known volumes of some parts of the purification line. Results of 17 analyses are listed in Table 2–4.

Analyses were carried out in two periods when the condition of the mass spectrometer was sufficiently stable. The error assigned to the observed $^3He/^4He$ ratios is one standard deviation, including a statistical error of an individual measurement of HESJ and an error of *k*(3/4) factor determined by repeated analysis of atmospheric He using almost constant amount (corresponds to $1–3\times10^{-6}$ Torr of He). The sensitivity and *k*(3/4) factor determined with atmospheric He is listed in Table 2–5. Trap current of ion source was adjusted to 400μA during analysis of HESJ and atmospheric He standards, because gas inlet was large enough to obtain precise data.

Table 2–4. Helium isotope ratio of HESJ.

Pipet	^4He (inlet) (10^{-7}Torr)	^4He output (V; High-Faraday)	$^3He/^4He$ R/R_A*		δ**
1st. Period (May. 31 ~ Jun.07, 1999)					
R1-21	1.28	0.031	21.15	± 0.41	+1.9
R1-22	47.93	1.145	20.23	± 0.23	-2.6
R1-23	1.26	0.030	20.94	± 0.36	+0.8
R1-24	22.97	0.549	20.36	± 0.23	-1.9
R1-25	10.95	0.262	20.52	± 0.24	-1.2
R1-27	5.20	0.124	20.77	± 0.26	+0.0
R1-28	0.61	0.015	21.16	± 0.49	+1.9
R1-29	1.23	0.029	21.01	± 0.36	+1.2
2nd. Period (Jun. 11 ~ Jul. 01, 1999)					
R1-30	1.16	0.038	20.45	± 0.33	-1.5
R1-31	0.60	0.020	20.68	± 0.36	-0.4
R1-32	0.75	0.025	20.87	± 0.45	+0.5
R1-33	2.38	0.078	20.64	± 0.32	-0.6
R1-34	2.91	0.095	20.73	± 0.30	-0.2
R1-35	16.97	0.555	20.69	± 0.26	-0.4
R1-36	4.49	0.147	20.78	± 0.29	+0.1
Average (except R1-22)			**20.77**	± **0.24**	
MS-III					
RJ-1		0.065	20.66	0.11	
RJ-2		0.068	20.61	0.16	
Average			20.64	0.04	

* Normalized to the atmospheric ratio = 1.4×10^{-6} (Ozima and Podosek, 1983)

**$\delta=\{(^3He/^4He)measured/(^3He/^4He)average-1\}\times100$

Table 2–5. Correction factors for measurement of HESJ using MS–IV.

Date	Sensitivity (10^{-5}A/Torr)	^{3}He/^{4}He (raw)	$k\,(3/4)^*$ (R/R_A)**
1st. Period (May. 31 ~ Jun.07, 1999)			
Jun. 01, 1999	1.28	0.0968 ± 0.0016	10.34
Jun. 04	1.40	0.0987 ± 0.0017	10.13
Jun. 07	1.33	0.0986 ± 0.0012	10.15
Average	1.34	0.0980 ± 0.0011	10.21 ± 0.23
2nd. Period (Jun. 11 ~ Jul. 01, 1999)			
Jun. 11, 1999	1.72	0.0904 ± 0.0001	11.06
Jun. 14	1.75	0.0909 ± 0.0011	11.00
Jun. 24	1.78	0.0928 ± 0.0024	10.77
Jun. 28	2.06	0.0901 ± 0.0021	11.10
Jun. 29	1.84	0.0900 ± 0.0020	11.11
Jul. 01	1.85	0.0915 ± 0.0019	10.93
Average	1.83	0.0910 ± 0.0011	10.99 ± 0.25

$^*k\,(3/4)=(^3\mathrm{He}/^4\mathrm{He})_{raw}/(^3\mathrm{He}/^4\mathrm{He})_{air}$

** Normalized to the atmospheric ratio = 1.4×10^{-6} (Ozima and Podosek, 1983).

Since the dependence of mass discrimination on gas pressure in the mass spectrometer is reported (Sano and Wakita, 1988; Honda et al., 1993), we measured ^{3}He/^{4}He ratio of HESJ with varying the amount of He admitted into the mass spectrometer. The pressure effects more than 5% of the ^{3}He/^{4}He ratio were reported at the pressure higher than 1.5×10^{-6}Torr (Sano and Wakita, 1988) and 5×10^{-7}Torr (Honda et al., 1993). Figure 2–10 demonstrates the relationship of ^{3}He/^{4}He of HESJ with He pressure in the mass spectrometer. Observed ^{3}He/^{4}He ratios in our study seem to decrease down to 2.4% at the highest pressure of 4.8×10^{-6}Torr. If the decrease of ^{3}He/^{4}He ratio is result from decrease of ^{3}He sensitivity of ion-counting caused by dead time of SEM, the dead time is calculated to be 2.40×10^{-6}sec for counting rate of 1.42×10^4cps, which is much larger than 8.0×10^{-8}sec estimated from sensitivity of ion-counting calibrated by known amount of atmospheric noble gases. Thus, the observed trend of ^{3}He/^{4}He ratio with partial pressure of He is caused by pressure effect on mass discrimination showed by previous studies (Sano and Wakita, 1988, Honda et al., 1993). Because Ne was completely separated from He by the Cryo-trap, Ne interference with the He isotopic ratio pointed out by Sano and Wakita (1988) is left out of consideration. In spite of the highest

pressure in our data surpass the critical pressures in previous cases, the pressure effect on discrimination is much smaller, only –2.4% at the highest pressure, than the previously reported ones. Therefore, although the pressure effect is also observed, it is not so prominent in the case of MS–IV.

An average value of $^{3}He/^{4}He$ ratios of HESJ is 20.77 ± 0.24 R_A or (2.908 ± 0.034) × 10^{-5}, excluding R1-22 (Table 2–3) whose $^{3}He/^{4}He$ ratio is significantly lower than the others beyond the analytical error due to the pressure effect. $^{3}He/^{4}He$ ratios of HESJ analyzed by Prof. K. Nagao using MS–III is also listed in Table 2–3. In the case of MS–III, correction factor *k*(3/4) was calibrated by analysis of synthesized He standard prepared by Prof. K. Nagao. The $^{3}He/^{4}He$ ratio of the standard is 1.71×10^{-4}, 120 times enriched in ^{3}He than atmospheric He, thus the errors for $^{3}He/^{4}He$ ratios of HESJ are smaller than those obtained with MS–IV. However, the determined $^{3}He/^{4}He$ ratios with the two mass spectrometers show very good agreement within experimental errors. Therefore, the value of 20.77 ± 0.24 R_A is currently used for the $^{3}He/^{4}He$ ratio of HESJ, which is used as working standard to determine $^{3}He/^{4}He$ ratio with MS-IV.

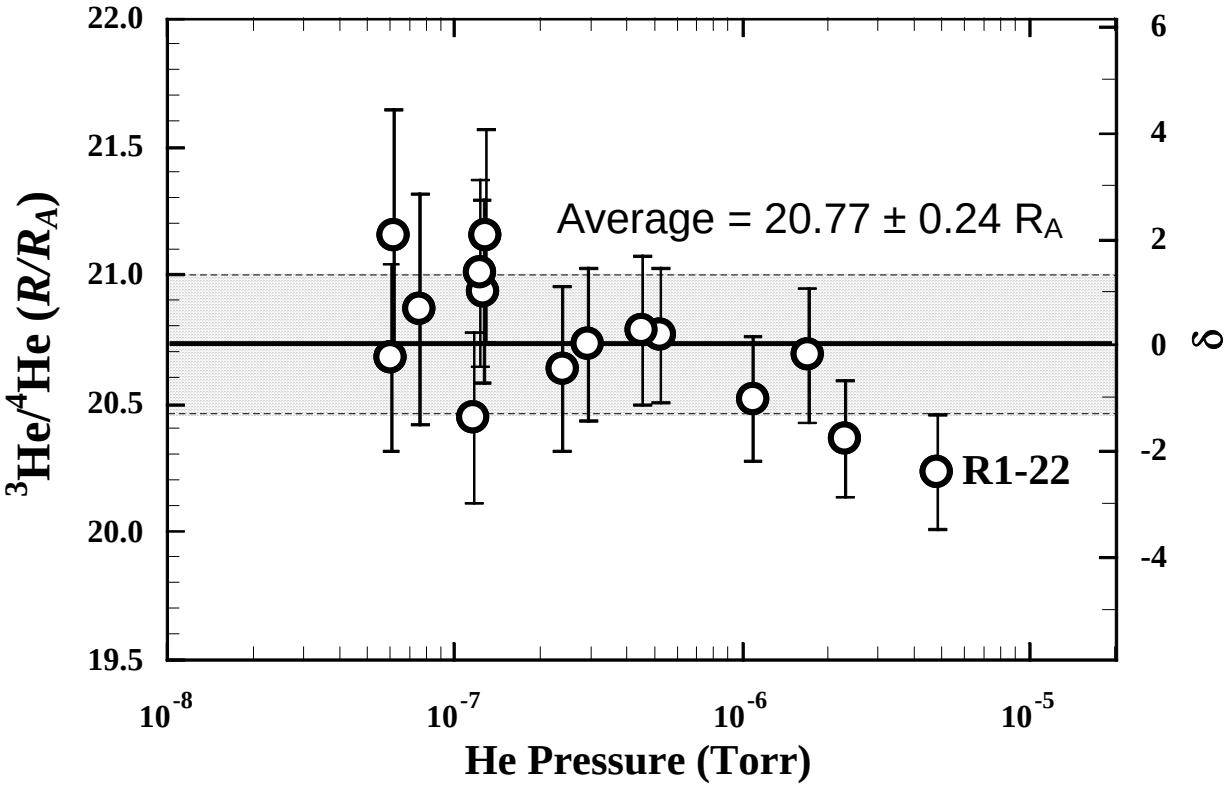

Fig. 2–10. A plot of measured ^{3}He/^{4}He ratio of HESJ against partial pressure of helium in the mass spectrometer. $\delta=\{(^3He/^4He)_{measured}/(^3He/^4He)_{average}-1\}\times100$. Averaged value is 20.77 ± 0.24 R_A, excluding one data point at the highest pressure (R1-22).

2–4. Accuracy in He isotopic ratio measurements

2–4–1. Intralaboratory crosscheck using Natural samples

To confirm the accuracy in He isotope ratio measurement with MS-IV, the $^3He/^4He$ ratios of four hot-spring and one volcanic gases collected in Izu Peninsula and Iwo-jima, Japan are measured using MS–IV, MS–III and MS–I. In addition, replicate analysis with MS–IV is also done to confirm reproducibility. Gas samples are suitable for testing accuracy and reproducibility in the measurements of $^3He/^4He$ ratio, because rock samples often show noble gas heterogeneity even in the in vacuo crushing extraction method (e.g., Hilton et al., 1993; Sumino et al., 2000; Trieloff et al., 2000).
The results are listed in Table 2–6. The He isotope standards used for the mass spectrometers MS–IV, MS–III, and MS–I are HESJ, synthesized He gas ($^3He/^4He = 1.71\times10^{-4}$), and atmospheric He, respectively. Some of the data are measured by Prof. K. Nagao and Dr. P. A. Hernandez. Because the errors for $^3He/^4He$ ratios measured by MS–IV include the uncertainty in $^3He/^4He$ determination of HESJ (=1.3%), whereas $^3He/^4He$ ratios by other two systems do not take uncertainties of $^3He/^4He$ standards into consideration, the errors with MS–IV seem to be larger than those with other two systems. The results obtained with MS–IV and MS–III show good agreement. The results obtained with MS–I are slightly higher than those with MS–IV and MS–III except one sample, however, the differences are at most 5% and within the experimental errors (1σ). Only one exception is the sample Izu–E. This may be due to the pressure effect in analysis of standard gas in measurement with MS–I, because constant amount of atmospheric He was used as He standard irrespective of He pressure of the sample. The results of replicate analyses with MS–IV assure an adequate reproducibility in $^3He/^4He$ determination. These show that any systematic errors would not occur in our modified noble gas analysis system, MS–IV.

Table 2–6. Replicate analysis and comparison of $^{3}He/^{4}He$ ratio among MS–IV, MS–III and MS–I.

Sample (Locality)	MS	$^{3}He/^{4}He$ $(R/R_A)^{*1}$
Izu Peninsula, Japan		
Izu-A	IV	6.32 ± 0.16
(Hirono)	IV	6.33 ± 0.12
	IV	6.35 ± 0.13
	III*2	6.31 ± 0.05
	I	6.52 ± 0.15
Izu-B	IV	7.16 ± 0.19
(Aakazawa)	IV	7.15 ± 0.13
	III*2	7.17 ± 0.06
	I	7.34 ± 0.17
Izu-C	IV	7.98 ± 0.21
(Atagawa)	IV	7.82 ± 0.15
	III*2	7.74 ± 0.04
Izu-D	IV	6.13 ± 0.16
(Hirono)	IV	6.30 ± 0.14
	I*3	6.63 ± 0.14
Izu-E	IV	5.02 ± 0.37
(Atami)	IV	4.94 ± 0.39
	I*3	4.04 ± 0.26
Iwo-jima, Japan		
Iwo-A	IV	1.229 ± 0.048
(Suribachiyama)	I	1.280 ± 0.025

*1. Normalized to the atmospheric ratio = 1.4×10^{-6} (Ozima and Podosek, 1983).
*2. Measured by Prof. K. Nagao.
*3. Measured by Dr. P. A. Hernandez.

2–4–2. Interlaboratory crosscheck using HESJ

The HESJ is expected to be interlaboratory standard for He isotopic analysis, and distributed to five noble gas laboratories in Japan; Osaka Univ., Hiroshima Univ., the Institute for Study of the Earth's Interior, Okayama Univ., Earthquake Research Institute, Univ. of Tokyo, and Laboratory for Earthquake Chemistry, the Univ. of Tokyo. $^3He/^4He$ ratio of HESJ obtained by Osaka Univ. and Earthquake Research Institute are listed in Table 2–7 with our data (Matsuda, personal communication; Yamamoto, personal communication). The two values obtained by both two laboratories are determined using atmospheric He as a primary standard, as well as the value obtained with MS–IV. The all values show good agreement within analytical errors, indicating that there is no systematic error in $^3He/^4He$ ratio determination among three laboratories. Weighted average in proportion to the inverse number of the square of each error is calculated to be 20.66 ± 0.19 R_A, except the data obtained with MS–III from the calculation because it is determined using the other synthesized high $^3He/^4He$ gas as a primary standard. The true $^3He/^4He$ ratio of the HESJ is not known, however, accumulation and compilation of data obtained by several laboratories are needed to determine the recommended value of $^3He/^4He$ ratio of HESJ, which will be used as an interlaboratory standard of $^3He/^4He$ ratio in the future.

Table 2–7. $^3He/^4He$ ratio of HESJ determined by several laboratories.

Laboratory		$^3He/^4He$ $(R/R_A)^*$
Osaka Univ.		20.44 ± 0.35
Earthquake Research Institute, Univ. of Tokyo		20.63 ± 0.70
Laboratory for Earthquake Chemistry, Univ. of Tokyo	(MS–IV)	20.77 ± 0.24
	(MS–III)	20.64 ± 0.04
Weighted average**		20.66 ± 0.19

* Normalized to the atmospheric ratio = 1.4×10^{-6} (Ozima and Podosek, 1983).

** Average weighted in proportion to $1/(error)^2$ except data obtained with MS–III.

3. Noble gas in alkaline basalt from northwestern Kyushu

3–1. Geological and geochemical background

A back arc volcanic belt produced by Miocene to Pleistocene basaltic volcanism extends from northwest Kyushu to Chugoku district along the Sea of Japan coast of southwest Japan (Fig. 1–2). The basalt province in northwestern Kyushu consists of two discrete areas, the Higashi-matsuura and Kita-matsuura districts. The geological history of volcanic activity and related events in northwestern Kyushu is reviewed in Yanagi and Maeda (1998). Figure 3–1 is a compilation map on eruption age of volcanic rocks in northwestern Kyushu after Yanagi and Maeda (1998). The volcanic activity in northwestern Kyushu was preceded by the formation of shallow-water sedimentary basin in Oligocene to Miocene. Sedimentation started about 44My ago with the subsidence of the basement Cretaceous metamorphic rocks and granitic plutons. The basalt volcanism started at 11Ma immediately after the 33 My-long sedimentation. At this time, the basin had continued the gentle uplift that started at about 30Ma. Eruption of the basalt started at ca. 11Ma, and continued intermittently until 1Ma (Yanagi et al., 1992). The total volume of basalt exceed more than 200km^3, though many of alkaline basalts erupted in northwestern Kyushu were eroded away and are distributed under the sea (Nakada and Kamata, 1991). The most extensive activity occurred in Kita-matsuura of 49km^3 in total volume, which is nearly half of Cenozoic basalts presently observable in southwestern Japan (Kurasawa, 1967). The volcanic activity started first in the central part of the Kita-matsuura district at about 11Ma and continued until 6Ma. Most of basaltic magma erupted to the surface to form a thick accumulation of lava flows, 350m thick at maximum. The sites of basaltic eruption shifted to the northwest (Higashi-matsuura) and south (Tara-dake) from 4 to 1Ma. The recent activity was observed in Ojika-jima and Fukue-jima of Goto Islands, which lies to the northwest of Kyushu, and is considered to still continue. The basaltic volcanism in the Higashi-matsuura district is continued a very short period around 3Ma (Nakamura et al., 1986). The early alkaline basalts in the Higashi-matsuura district contain mantle-derived ultramafic xenoliths ranging from 1cm to 30cm in diameter and megacrysts (e.g., Kuno,

1964; Ishibashi, 1970; Kobayashi and Arai, 1981), providing evidence of direct mantle derivation. Yanagi and Maeda (1998) considered that formation of the sedimentary basin was related to the lower crust erosion by mantle upwelling, which produces basalt magma by decompression melting. And the uplifting which started at about 30Ma suggests the accumulation of basaltic magma in the magma chamber beneath the sedimentary basin. However, they did not mention what caused the mantle upwelling. The mechanism of mantle upwelling is still under discussion (Chapter 1). The alkaline basalts from southwestern Japan have trace element and Nd–Sr isotopic characteristics similar to those of oceanic island basalts. For that reason, some researchers proposed a hotspot model that the volcanism of this area was triggered by a deep mantle plume which raised from the source of intraplate volcanism, that is probably core-mantle boundary or upper-lower mantle boundary (e.g., Nakamura et al., 1985, 1989, 1990; Nakada and Kamata, 1991; Kakubuchi et al., 1995). On the contrary, such geochemical features can be explained by upward injection of asthenosphere (depleted mantle) to sub continental lithosphere (enriched mantle) associated with the opening of back-arc basin. This asthenospheric injection model has been proposed to explain the origin of volcanisms around the Sea of Japan, such as northeastern Japan (Nohda et al., 1988; Tatsumoto and Nakamura, 1991; Ohki et al., 1994), and Shihote-Alin and Sakhalin (Okamura et al., 1998).

Since geochemical features previously reported cannot determine which model is the case, upwelling of enriched mantle plume or injection of depleted asthenosphere. Noble gas isotopic compositions of Cenozoic alkaline basalts from northwestern Kyushu are measured and discussed in this chapter, because they are expected to provide some constraints on the source of the alkaline basalts.

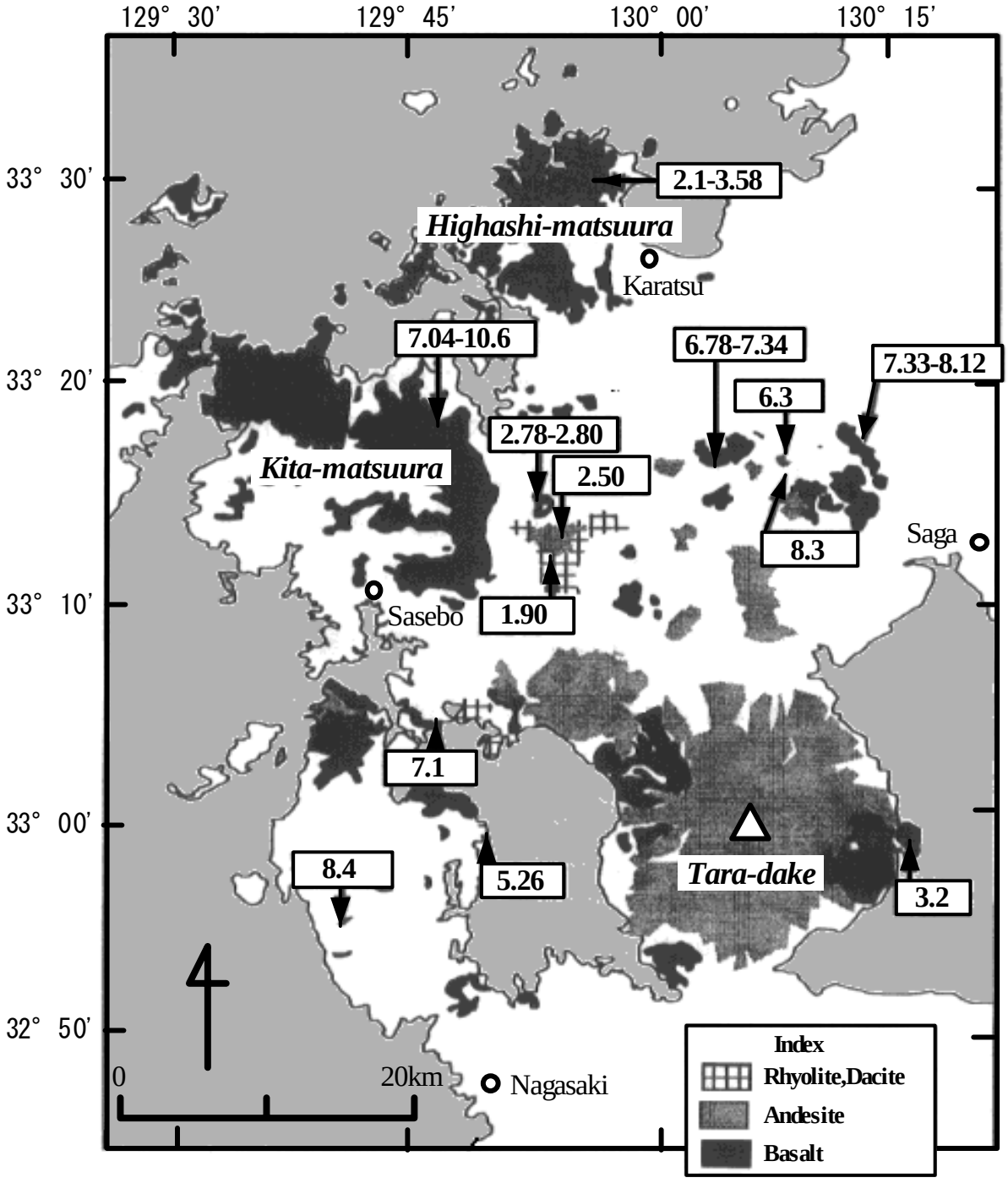

Fig. 3–1. Compilation map on radiometric dating of volcanic rocks in northwestern Kyushu from Yanagi and Maeda (1998). Numbers are eruption age (Ma).

3–2. Samples and experiments

3–2–1. Samples

Samples used in this study were collected from both Higashi-matsuura and Kita-matsuura districts in northwestern Kyushu during three filed seasons, August 1997, October 1998 (Higashi-matsuura), and March–April 2000 (Kita-matsuura). The samples are listed in Table 3–1 and sampling localities are shown on Fig. 3–2. All samples are lava chunks collected from road cut or quarry, except samples from two localities; Takashima and Oshima were collected as boulder stone. The basalt from Takashima contains large phenocrystic pyroxene (augite and bronzite) up to 3cm across. They have crystallized from the alkaline basalt magma at a pressure higher than that of the ordinary phenocryst formation, corresponding the depth little below the Moho discontinuity or near the base of the crust (Kuno, 1964; Ishibashi, 1970). An augitic megacryst was also collected and measured (TKA0940).

Table 3–1. List of samples from northwestern Kyushu

Locality name (Location No.)[*1]	Sample name	Sampling date	Sub-sample	phase[*2]	Noble gas analysis[*3]			K-Ar	XRF
					st	tf	cr		
Higashi-matsuura									
Keya	FUK9716	1997. 8. 30	FUK9716ol	ol	○		○		
(1)			FUK9716px	cpx	○		○		
			FUK9716B	wr					○
			FUK9716K	gm				○	
Takashima	TKB0001	2000. 4. 3	TKB0001ol	ol	○		○		
(2)			TKB0001px	cpx	○		○		
			TKB0001B	wr					○
			TKB0001K	gm				○	
	TKB0002	2000. 4. 3	TKB0002ol	ol			○		
			TKB0002px	cpx			○		
			TKB0002B	wr					○
			TKB0002K	gm				○	
	TKB0003	2000. 4. 3	TKB0003K	gm				○	
	TKA0940[*4]	1997. 8. 29	TKA0940px	cpx		○	○		
Ohshima	OSM9801	1998. 10. 12	OSM9801ol	ol			○		
(3)			OSM9801B	wr					○
			OSM9801K	gm				○	
Karatsu	KR8404	1998. 10. 12	KR8404ol	ol	○		○		
(4)			KR8404px	cpx	○		○		
			KR8404B	wr					○
			KR8404K	gm				○	
Karatsu	KAR9803	1998. 10. 12	KAR9803ol	ol	○	○	○		
(5)			KAR9803px	cpx	○		○		
			KAR9803B	wr					○
			KAR9803K	gm				○	
Nanatsugama	KAR9801	1998. 10. 12	KAR9801ol	ol			○		
(6)			KAR9803B	wr					○
			KAR9803K	gm				○	
Kita-matsuura									
Myokanji	SSB0001	2000. 4. 2	SSB0001ol	ol	○		○		
(8)			SSB0001px	cpx			○		
			SSB0001B	wr					○
			SSB0001K	gm				○	
Yoshii	SSB0002	2000. 4. 2	SSB0002ol	ol	○		○		
(7)			SSB0002px	cpx			○		
			SSB0002B	wr					○
			SSB0002K	gm				○	
Hirado	HRD0001	2000. 4. 2	HRD0001ol	ol			○		
(9)			HRD0001B	wr					○
			HRD0001K	gm				○	
	HRD0002	2000. 4. 2	HRD0002K	gm				○	
Doinohana	KKZ0003	2000. 4. 1	KKZ0003px	cpx			○		
(10)			KKZ0003B	wr					○
			KKZ0003K	gm				○	
Kokuzo	KKZ0001	2000. 4. 1	KKZ0001px	cpx			○		
(11)			KKZ0001B	wr					○
			KKZ0001K	gm				○	

*1. corresponds to No. in Fig. 3–2
*2. ol: olivine, cpx: clinopyroxene, wr: whole rock, gm: groundmass
*3. st: step heating, tf: total fusion, cr: crushing
*4. clinopyroxene megacryst

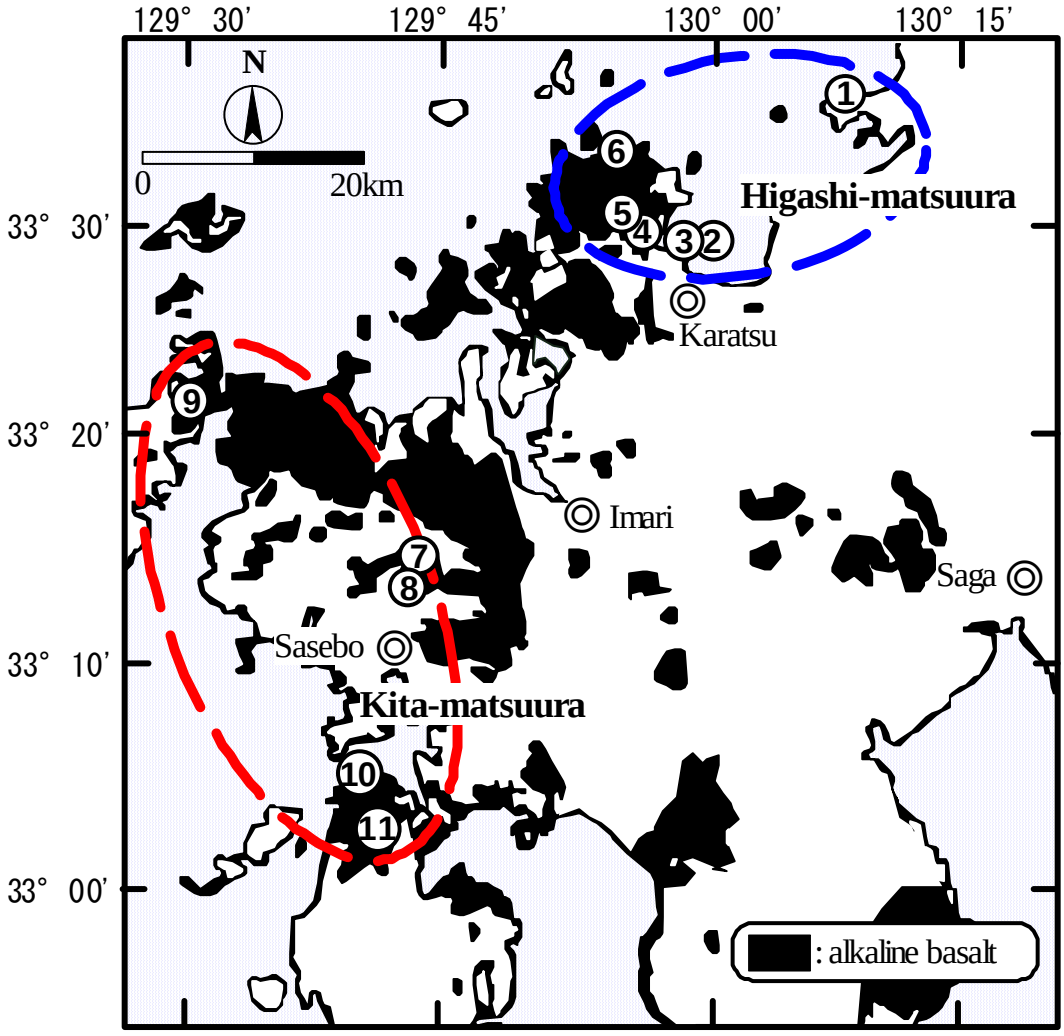

Fig. 3–2. Map showing sample localities in northwestern Kyushu. Circles with number which corresponds to that in Table 3–1 show localities of the samples. Black parts represent distribution of Cenozoic alkaline basalt (Kurasawa, 1967, Yanagi and Maeda, 1998).

3–2–2. Mineral separation

The olivine and clinopyroxene phenocrysts separated from collected basaltic rocks were used for noble gas analysis. Since the basalt from this region generally contains ultramafic xenoliths, the careful separation was necessary to avoid contamination of xenolithic fragments.

Basaltic rock (3–10kg, depending on the abundance of phenocrysts) was sliced using a diamond saw and cm-sized xenolithic fragments were removed. Then each sample was crushed to a diameter of less than 2cm by a jaw crusher and then fragments of xenolith were removed again. And then, basalt chips without xenolith are crushed into less than 2mm. An aliquot (ca. 30g) was further crushed by a steel mortar into powder < 0.1mm, which was used for determination of major and trace element compositions. Olivine and clinopyroxene phenocryst (0.25–2mm in diameter, depending on the sample) were separated using a magnetic separator (Frantz isodynamic separator in Earthquake Research Institute of the University of Tokyo), followed by handpicking under a binocular microscope. The remaining groundmass after removal of phenocrysts such as olivine, clinopyroxene, magnetite and plagioclase, etc. is used for K-Ar age determination. The 0.25–0.5mm fraction of groundmass was used for Ar analysis, and an aliquot of this fraction were further crushed into powder, and then used for K content determination.

3–2–3. Major and trace element composition

Major and trace element concentrations were determined by X-ray fluorescence spectroscopy (XRF) at the Earthquake Research Institute of the University of Tokyo. Ten major and fifteen trace elements were measured with a technique described by Tanaka and Orihashi (1997). Fused glass beads were prepared from mixture of 1.8g of rock powder (< 0.1mm), 3.6g of lithium metaborate/tetraborate flux, and 0.54g of lithium nitrate. XRF analysis was carried out using a Philips PW2400 spectrometer, with a Rh anode X-ray tube. International silicate rock and mineral reference materials provided by the Geological Survey of Japan (JA-1, JA-2, JA-3, JB-1a, JB-2, JG-1a,

JG-2, JG-3, JGb-1, JP-1, JR-1, JR-2, JF-1) and the United States Geological Survey (BIR-1, DNC-1, DTS-1, QLO-1, RGM-1, STM-1, W-2) were used to set up the calibration lines.
In order to check reproducibility, replicate analyses for two samples (JB-2 and JR-1) were carried out for each six glass beads prepared from aliquots of the same powder. A standard sample provided by the Geological Survey of Japan (JB-1a), which is basalt collected from almost the same locality of SSB0001 (Myokanji), is also analyzed to confirm accuracy of analysis.

3–2–4. Noble gas analysis

Separated olivine and clinopyroxene phenocrysts were used for noble gas analysis. After careful removal of altered mineral under a binocular, mineral samples were leached with 2N-HNO_3 in an ultrasonic bath for 1 hour, in order to remove possible contamination by groundmass which contains more abundant atmospheric noble gases than olivine and clinopyroxene. HNO_3 was used in place of HCl because $H^{35}Cl$ and $H^{37}Cl$ might superimpose the peaks of ^{36}Ar and ^{38}Ar in isotopic measurement of Ar, and it is difficult to eliminate them completely once they contaminated the mass spectrometer. The loss of weight of olivine and clinopyroxene samples by acid leaching treatment was usually less than 5% of the original weight.
Noble gas analyses were carried out with MS–IV. In vacuo crushing with a solenoid-type crusher and step heating or single step heating (total fusion) were applied for gas extraction. Details of noble gas measurement were already described in chapter 2. Concentrations of all noble gases and isotopic ratios of He, Ne and Ar were measured for all samples. Kr and Xe isotope analysis were carried out for gas rich samples or high temperature fraction of 2-step heating, because atmospheric component is dominant in low temperature fraction. Hot blanks and crushing blanks were measured in the same way as sample runs.

3–2–5. K-Ar age determination

The groundmass of the samples (0.25–0.5mm fraction) were washed in an ultrasonic bath with acetone, ethanol and distilled water. An aliquot of them were crushed into powder (<0.1mm) by a steel mortar and used for K concentrations by a XRF. Since K is major component in alkaline basalt, more diluted fused glass beads method (sample: flux =1: 5 by weight) was used to reduce the time for preparation. Other procedures were the same for major and trace element measurement. Errors on determination of K content are 2%. Ar was extracted from ca. 0.5g of remaining groundmass at 1800°C and analyzed with MS-IV following the same procedure as outlined above.

3–3. Results

3–3–1. Major and trace element compositions

Major and trace element compositions of the samples are listed in Table 3–2. Errors accompanied with analysis of major and trace elements are lower than 0.4% and 4ppm, respectively, estimated from the replicate analyses of JB-2 and JR-1. The results of JB-1a show a good agreement with recommended values (Imai et al., 1995) within analytical errors. SSB0001 and JB-1a are collected from almost the same lava flow, showing approximately consistent composition except Pb.

The samples show a continuous compositional spectrum from low alkaline tholeiitic basalt to alkaline olivine basalt across the alkaline-sub alkaline discrimination line (Miyashiro, 1978) on the Na_2O+K_2O vs. SiO_2 diagram (Fig. 3–3) and SiO_2 vs. FeO*/MgO diagram (Fig. 3–4). While all the samples from Higashi-matsuura are in the alkaline olivine basalt field, the samples from Kita-matsuura distribute across the discrimination line in Fig. 3–3. This indicates that basalts from Higashi-matsuura are derived from homogeneous magma; whereas the compositions of magmas erupted in Kita-matsuura vary due to magma mixing or fractional crystallization of magma. Yanagi and Maeda (1998) suggested that Kita-matsuura basalts are mixing products of magmas with different degrees of fractionation from a uniform primitive magma. Figure 3–5 shows SiO_2–MgO compositional distribution of basalts with data from northwestern Kyushu basalts (Yanagi and Maeda, 1998). The basalts show a crescent form of distribution. From observation of petrographic textures and chemical composition, basalts in trend of fractional crystallization make a line bottom of the crescent, and basalts plotted inside the crescent form represent compositions formed by magma mixing (Yanagi and Maeda, 1998). Basalts from Higashi-matsuura analyzed in this study are plotted on the fractionation trend near the high-MgO end, showing that they are relatively primitive. Most of the samples from Kita-matsuura lie on an upper base of the crescent form except one sample (SSB0002), indicating that they are mixing products between almost primitive magma and highly fractionated magma.

Figure 3–6 is a so-called spider diagram of incompatible elements, in which these elements are arranged in an order of increasing incompatibility and the abundances of each element is normalized to that of N-MORB (Pearce, 1982). The alkaline basalts from northwestern Kyushu show features that they are highly enriched in incompatible elements comparable to ocean-island alkaline basalt, and lack Nb-depletion which is characteristic in island-arc tholeiitic basalt. The patterns are uniform among two districts and lack time-space variation. Such characteristics of incompatible elements are almost the same as those from previous studies (Nakamura et al., 1985; 1989; Nakada and Kamata, 1991), which was consider to be an evidence that the origin of alkaline basalt volcanism in this region is not subduction-related magmatism but mantle plume as well as intraplate volcanism.

Table 3–2. Major and trace element compositions of basalts from northwestern Kyushu

Sample	*Higashi-matsuura*							*Kita-matsuura*		
	FUK9716B	KAR9801B	KAR9803B	KR8404B	OSM9801B	TKB0001B	TKB0002B	SSB0001B	SSB0002B	HRD0001B
Major element composition (%)										
SiO_2	48.69	48.75	48.09	48.19	48.38	49.35	49.17	51.61	47.75	53.34
TiO_2	1.65	1.77	1.96	1.84	1.50	1.87	1.79	1.26	3.22	1.46
Al_2O_3	14.71	16.31	15.25	15.38	14.22	16.07	15.62	14.60	16.07	16.73
Fe_2O_3	11.14	11.59	11.54	10.96	11.27	10.93	10.82	9.21	13.31	8.69
MnO	0.174	0.162	0.171	0.167	0.179	0.157	0.162	0.140	0.183	0.152
MgO	9.00	6.75	8.15	7.59	10.19	7.40	8.30	8.41	5.37	5.59
CaO	9.22	8.83	9.06	9.18	9.51	8.25	7.95	9.85	7.96	7.47
Na_2O	2.86	3.52	3.17	2.84	2.68	3.52	3.27	2.60	3.18	3.85
K_2O	1.49	1.07	1.56	1.90	1.16	1.57	1.83	1.21	1.63	1.75
P_2O_5	0.404	0.305	0.456	0.467	0.310	0.535	0.492	0.257	0.549	0.543
Trace element composition (ppm)										
Sc	27.0	24.9	24.1	24.1	29.6	21.3	22.2	31.0	23.3	18.7
V	206	184	214	201	216	173	169	216	267	128
Cr	428.7	195.1	238.8	225.5	579.3	253.5	291.8	406.6	49.9	215.8
Co	45.1	43.3	44.3	42.6	47.8	41.2	41.8	39.2	40.1	26.9
Ni	164.8	89.8	135.3	158.8	183.6	160.0	174.6	149.1	37.4	129.5
Zn	91	93	96	93	102	106	97	79	129	87
Ga	16.2	17.9	18.5	17.0	17.2	18.1	17.6	16.8	21.0	19.0
Rb	38.39	24.06	32.14	52.63	23.93	29.95	45.41	28.97	35.77	42.92
Sr	480	486	536	573	515	678	560	460	485	559
Y	21.5	27.9	24.5	23.6	24.0	23.5	23.5	23.1	32.2	27.9
Zr	135.0	122.3	175.1	166.9	127.6	176.5	182.1	128.8	240.7	253.2
Nb	29.94	18.62	37.52	39.15	17.47	35.13	37.97	24.72	44.35	38.38
Ba	565.80	346.78	536.65	624.61	377.08	542.50	547.41	519.05	522.43	722.53
Pb	11.01	3.67	14.21	10.52	7.39	36.70	14.20	12.44	22.16	15.70
Th	3.11	3.88	3.67	4.97	1.46	1.63	3.76	8.48	3.99	6.69
Sum(%)	99.56	99.22	99.63	98.74	99.63	99.89	99.63	99.38	99.42	99.80

Table 3–2. (Continued)

Sample	*Kita-matsuura*			*Standard sample*			*Replicate analysis*					
	HRD0002B	KKZ0001B	KKZ0003B	JB-1a			JB-2			JR-1		
				R.V.	Meas.	Dev.	Ave.		σ	Ave.		σ
Major element composition (%)												
SiO_2	51.97	53.32	54.27	52.41	52.73	0.32	52.76	±	0.26	76.04	±	0.35
TiO_2	1.25	1.22	1.43	1.28	1.30	0.02	1.17	±	0.01	0.06	±	0.01
Al_2O_3	15.37	17.30	15.27	14.45	14.53	0.08	14.61	±	0.06	12.73	±	0.05
Fe_2O_3	9.36	9.63	10.39	9.05	9.02	-0.04	14.23	±	0.20	0.78	±	0.01
MnO	0.156	0.139	0.140	0.148	0.146	-0.002	0.216	±	0.001	0.110	±	0.001
MgO	7.74	5.04	6.26	7.83	7.86	0.03	4.63	±	0.03	0.05	±	0.01
CaO	7.95	8.53	8.44	9.31	9.40	0.09	9.75	±	0.04	0.51	±	0.01
Na_2O	3.37	3.57	2.90	2.73	2.72	-0.01	1.99	±	0.02	4.05	±	0.10
K_2O	1.61	1.04	0.78	1.40	1.40	0.00	0.41	±	0.00	4.49	±	0.02
P_2O_5	0.428	0.240	0.183	0.260	0.257	-0.003	0.098	±	0.001	0.012	±	0.004
Trace element composition (ppm)												
Sc	20.5	23.6	23.1	27.9	28.9	1.0	50.8	±	0.4	5.26	±	1.20
V	153	144	157	205	203	-2	567	±	4	2	±	1
Cr	377.3	165.3	214.3	392.0	394.6	2.6	31.5	±	2.1	8.71	±	6.34
Co	36.6	31.3	37.7	38.6	37.5	-1.1	36.0	±	0.8	1.39	±	0.64
Ni	207.3	48.7	93.4	139.0	140.2	1.2	10.6	±	1.4	3.80	±	1.46
Zn	90	94	108	82	82	0	109	±	2	30.1	±	2.1
Ga	18.3	18.7	19.1	17.9	17.1	-0.8	17.3	±	0.5	16.3	±	0.3
Rb	39.61	26.68	20.28	39.20	39.23	0.03	5.80	±	0.98	305	±	3
Sr	505	368	289	442	445	3	175	±	1	8.1	±	0.1
Y	24.6	25.0	22.8	24.0	23.9	-0.1	24.1	±	0.4	50.4	±	0.4
Zr	226.3	120.4	101.6	144.0	139.4	-4.6	49.9	±	0.4	90.5	±	0.3
Nb	36.00	12.67	8.27	26.90	25.90	-1.00	0.83	±	0.12	17.8	±	0.1
Ba	749.54	276.70	175.39	504.00	500.98	-3.02	226.41	±	2.96	35.4	±	1.7
Pb	11.87	11.83	15.74	6.76	6.28	-0.48	6.27	±	1.35	23.0	±	0.6
Th	6.74	2.45	2.27	9.03	9.51	0.48	-0.06	±	1.08	30.5	±	0.6
Sum(%)	99.46	100.18	100.19		99.56		100.00	±	0.33	98.89	±	0.27

R. V.: recommended value of Geological Survey of Japan (Imai et al., 1995), Meas.: result of single analysis, Dev.: deviation of observed value from recommended value, Ave.: average of 6 replicate analyses, σ: standard deviation.

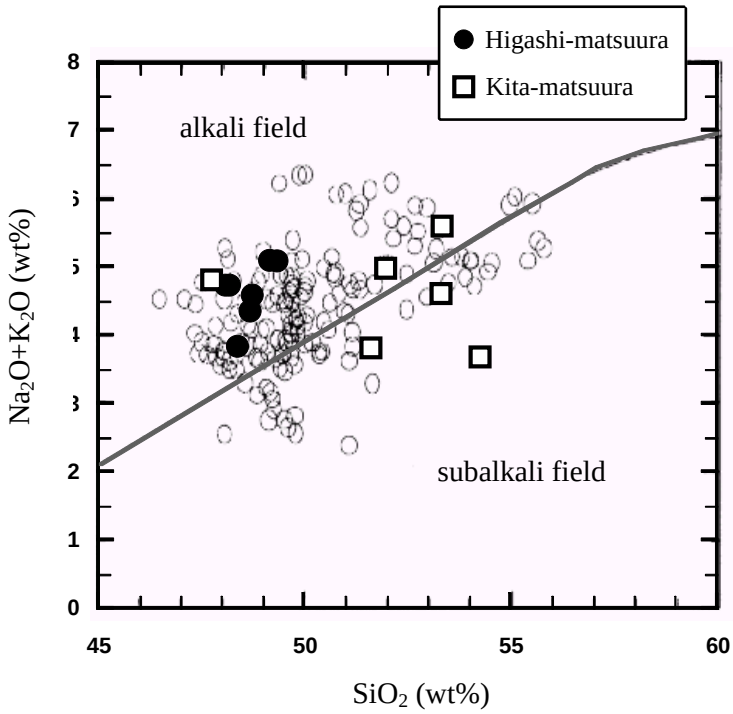

Fig. 3–3. Alkali–subalkali discrimination diagram. The discrimination line is from Miyashiro (1978). Open circles are basalts from northwestern Kyushu from Yanagi and Maeda (1998).

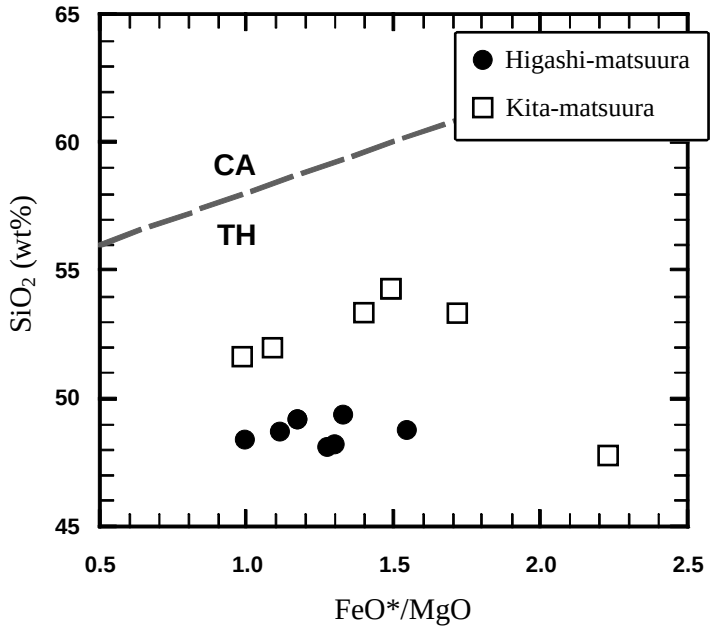

Fig. 3–4. Diagram showing relationship between SiO2 and FeO*/MgO. FeO* is total iron content assuming the composition of FeO. Dashed line is a discrimination line for classification of volcanic rocks into calc-alkalic series (CA) and tholeiitic series (TH) by differentiation trends of magma (Miyashiro, 1974).

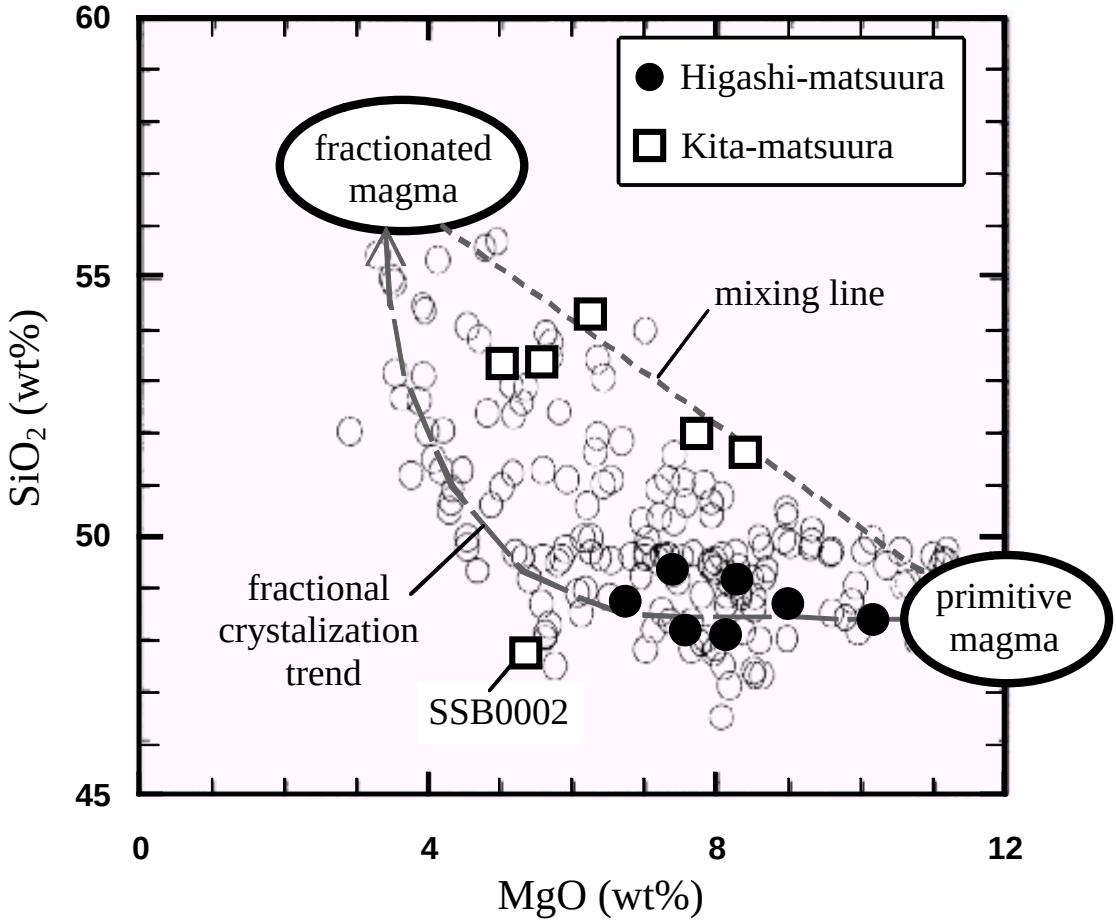

Fig. 3–5. SiO_2–MgO compositional distribution of basalts. Open circles are basalts from Kita-matsuura from Yanagi and Maeda (1998).

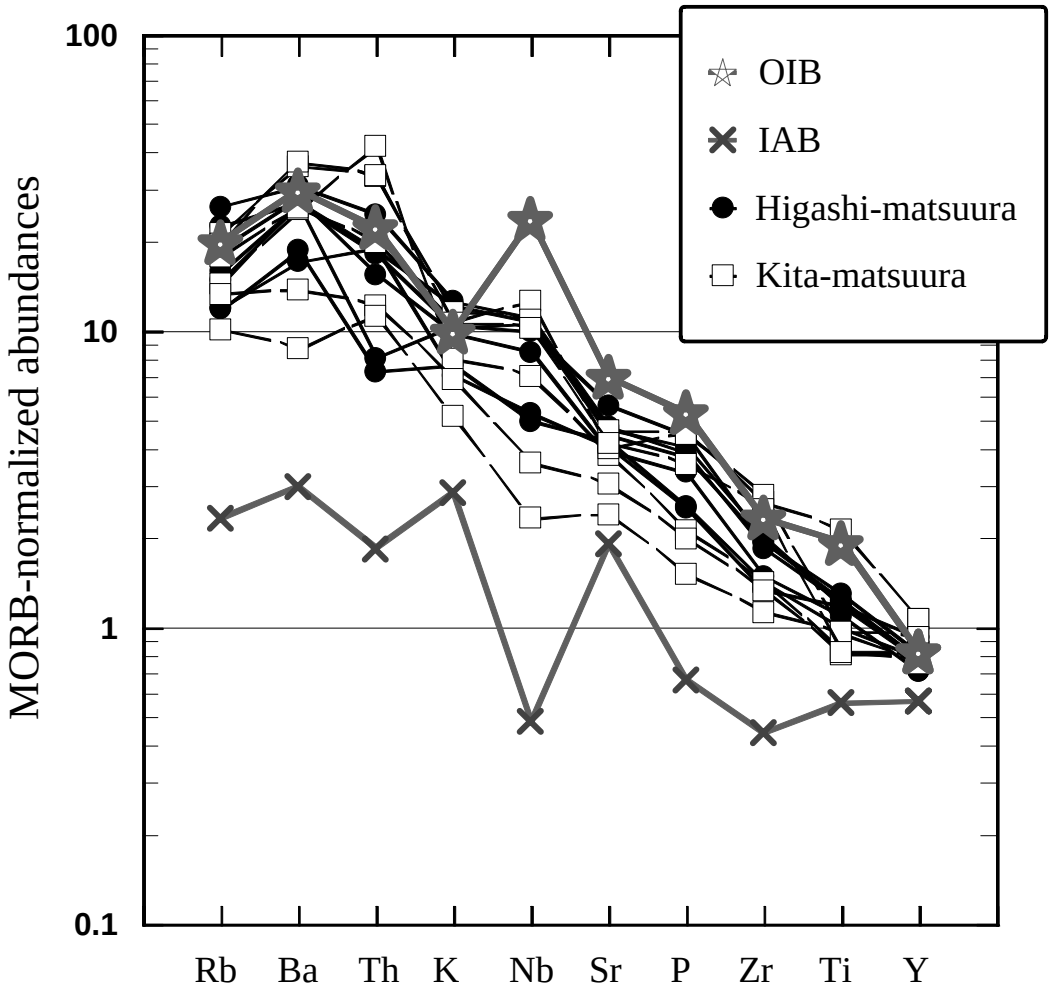

Fig.3–6. Spider diagrams of incompatible elements for basalts from northwestern Kyushu. Abundances of n-MORB are: Rb = 2.0ppm, Ba = 20ppm, Th = 0.2ppm, K_2O = 0.15%, Nb = 3.5ppm, Sr = 120ppm, P_2O_5 = 0.12%, Zr = 90ppm, TiO_2 = 1.5%, Y = 30ppm (Pearce, 1982). For comparison, the patterns of an ocean-island alkalic basalt (OIB) and an island-arc tholeiitic basalt (IAB) (Pearce, 1982) are shown.

3–3–2. K-Ar ages

Obtained K-Ar ages are listed in Table 3–3. K-Ar ages were calculated using a non-spike sensitivity method including mass fractionation correction procedure after Nagao et al. (1996). Errors on concentration of ^{36}Ar are 5%, estimated from the reproducibility of several measurements of the standard air. Errors with isotopic ratios in Table 3–3 are 1σ, including errors in blank correction and mass discrimination. K-Ar ages reported in this study were evaluated using two standard reference samples. One is YZ1, a Quaternary basalt from Zao volcano, Japan, whose reference age obtained with isotope dilution method is 0.227±0.009Ma, and the other is Baba tuff (biotite) with a reference age of 11.81±0.10Ma (Nagao et al., 1996). Two splits of YZ1 and three splits of Baba tuff were analyzed. Results listed in Table 3–3 are in good agreement with previous referenced value.

The samples from Higashi-matsuura show uniform K-Ar age, 3.04±0.13Ma. The result is in good agreement with previously reported K-Ar age (2.98±0.03Ma) of Higashi-matsuura basalt (Nakamura et al., 1986). The excellent age agreement of the samples provides strong evidence that the monogenetic alkaline basalt volcanism occurred for an extremely short period in the Higashi-matsuura district. It is consistent with major element composition of the basalts suggesting that they are derived from a uniform magma and little fractionated. Most of the samples from Kita-matsuura district show older ages than from Higashi-matsuura district, which range from 6.1 to 7.3Ma. Only one sample (KKZ0001) has exceptionally younger age, 2.99±0.05Ma, which is almost the same period eruption in Higashi-matsuura took place. Since the volcanic activity in Kita-matsuura started at about 11Ma and continued until 6Ma (Yanagi and Maeda, 1998), the samples from Kita-matsuura analyzed in this study were erupted at the latest stage of volcanism in this region.

Table 3–3. Results of K-Ar analysis

Sample	K (wt%)	Weight (g)	$[^{36}Ar]$ ($10^{-10}cm^3STP/g$)	$^{38}Ar/^{36}Ar$	$^{40}Ar/^{36}Ar$	$[^{40}Ar]_{rad}$ ($10^{-8}cm^3STP/g$)	Air-f (%)	K-Ar age (Ma)
Higashi-matsuura								
FUK9716	1.312	0.5319	18.0	0.18817 ± 0.00048	381.19 ± 0.77	15.4	77.6	3.01 ± 0.18
		0.5547	15.6	0.18841 ± 0.00045	400.69 ± 0.91	16.3	73.9	3.20 ± 0.19
		Average				15.8		3.11 ± 0.13
TKB0002	1.584	0.4285	5.32	0.18815 ± 0.00075	651.3 ± 6.2	18.9	45.4	3.07 ± 0.20
		0.4679	5.14	0.1879 ± 0.0010	665.2 ± 9.8	19.0	44.5	3.09 ± 0.22
		Average				18.9		3.08 ± 0.01
TKB0001	1.398	0.5451	5.37	0.18790 ± 0.00087	616.1 ± 6.9	17.2	48.0	3.17 ± 0.22
		0.3815	5.35	0.18808 ± 0.00073	615 ± 10	17.1	48.1	3.15 ± 0.24
		Average				17.1		3.16 ± 0.02
TKB0003	1.593	0.5935	2.33	0.18817 ± 0.00074	1120.8 ± 7.4	19.2	26.4	3.10 ± 0.20
		0.7933	1.81	0.18790 ± 0.00086	1386.3 ± 9.6	19.7	21.4	3.18 ± 0.20
		Average				19.4		3.14 ± 0.06
KR8404	1.626	0.7467	6.87	0.18788 ± 0.00051	553.3 ± 3.2	17.7	53.5	2.80 ± 0.17
		0.4060	7.62	0.18827 ± 0.00054	542.5 ± 5.1	18.8	54.6	2.98 ± 0.20
		Average				18.2		2.89 ± 0.13
KAR9801	0.960	0.4068	3.04	0.1875 ± 0.0010	644.1 ± 3.5	10.6	46.0	2.84 ± 0.18
		0.4224	2.92	0.1878 ± 0.0012	681.7 ± 4.0	11.3	43.4	3.02 ± 0.19
		Average				10.9		2.93 ± 0.13
KAR9803	1.400	0.5710	5.34	0.18828 ± 0.00067	585.2 ± 6.1	15.5	50.6	2.84 ± 0.19
		0.5247	4.28	0.18791 ± 0.00063	681 ± 11	16.5	43.4	3.03 ± 0.22
		Average				16.0		2.94 ± 0.13
OSM9801	1.053	0.4342	4.71	0.18795 ± 0.00067	555.5 ± 1.8	12.2	53.3	2.99 ± 0.18
		0.4052	3.90	0.1880 ± 0.0011	632.6 ± 2.9	13.1	46.8	3.21 ± 0.20
		Average				12.7		3.10 ± 0.16
Average (Higashi-matsuura)								3.04 ± 0.12
Kita-matsuura								
SSB0001	1.131	0.4272	8.22	0.18799 ± 0.00046	673.4 ± 6.9	31.0	44.0	7.05 ± 0.46
		0.4974	8.60	0.18853 ± 0.00061	680.2 ± 5.7	32.9	43.5	7.51 ± 0.48
		Average				32.0		7.28 ± 0.33
SSB0002	1.330	0.5736	5.96	0.18778 ± 0.00034	897 ± 11	35.8	33.0	6.93 ± 0.46
		0.6535	5.24	0.18808 ± 0.00055	1039 ± 14	38.9	28.5	7.52 ± 0.49
		Average				37.4		7.22 ± 0.42
HRD0001	1.434	0.5020	2.76	0.18898 ± 0.00074	1645 ± 13	37.3	18.0	6.69 ± 0.42
		0.4142	1.83	0.1877 ± 0.0016	2516 ± 38	40.6	11.8	7.28 ± 0.50
		Average				38.9		6.98 ± 0.42
HRD0002	1.116	0.5322	11.6	0.18841 ± 0.00056	520.42 ± 0.68	26.0	56.9	6.00 ± 0.35
		0.4537	12.5	0.18857 ± 0.00048	533.4 ± 1.4	29.6	55.5	6.81 ± 0.40
		Average				27.8		6.41 ± 0.57
KKZ0001	0.857	0.4097	3.14	0.1876 ± 0.0010	609.1 ± 3.0	9.8	48.6	2.96 ± 0.19
		0.6043	2.42	0.18824 ± 0.00080	712.6 ± 3.7	10.1	41.5	3.03 ± 0.19
		Average				10.0		2.99 ± 0.05
KKZ0003	0.650	0.4151	2.35	0.18717 ± 0.00083	945.3 ± 8.2	15.3	31.3	6.05 ± 0.39
		0.4841	2.36	0.18715 ± 0.00091	967.9 ± 7.6	15.8	30.6	6.26 ± 0.40
		Average				15.6		6.15 ± 0.15
Standard samples								
Baba tuff	6.560	0.2081	9.45	0.18819 ± 0.00066	3373 ± 117	291	8.8	11.38 ± 0.86
		0.0592	11.2	0.1883 ± 0.0014	3090 ± 58	312	9.6	12.23 ± 0.82
		0.6513	10.1	0.18832 ± 0.00081	3176 ± 39	292	9.3	11.43 ± 0.64
		Average				298		11.68 ± 0.48
		Reference values (Nagao et al., 1996)				296		11.81 ± 0.10
YZ1	1.410	0.6390	5.42	0.1814 ± 0.0022	320.7 ± 1.3	1.34	92.3	0.244 ± 0.024
		0.3836	2.81	0.1866 ± 0.0015	340.2 ± 1.1	1.24	87.0	0.227 ± 0.015
		Average				1.29		0.236 ± 0.012
		Reference values (Nagao et al., 1996)				1.240		0.227 ± 0.009

Errors on K and ^{36}Ar concentration are 2% and 5%, respectively. Errors with isotopic ratios are 1σ.

3–3–3. Noble gas isotopes

Results of noble gas analysis are summarized with conditions of gas extraction in Tables 3–4 and 3–5. Hot blanks and crushing blanks are listed in Table 3–6. Correction of blanks were carried out for all data of sample runs, however, isotopic ratios of Ne with blank which exceed 50% of total Ne, and all the isotopic ratios of Kr and Xe were not corrected because of the quite low amounts of released gases. Errors on isotopic ratios are one standard deviation, including errors with blank correction and mass discrimination. Experimental uncertainties in the concentration of each noble gas were estimated to be about 5% for He and Ar, 10% for Ne, Kr and Xe, respectively, based on the reproducibility of measurements of the standard gas.

Table 3–4. Noble gas abundances and isotopic compositions of basalts from northwestern Kyushu.

Sample (Weight) / Extraction Method[*1]	^{4}He ($\times10^{-9}$)	^{20}Ne ($\times10^{-11}$)	^{36}Ar ($\times10^{-10}$)	^{84}Kr ($\times10^{-12}$)	^{132}Xe ($\times10^{-13}$)	$^{3}He/^{4}He$ (R/R_A)[*2]	$^{20}Ne/^{22}Ne$	$^{21}Ne/^{22}Ne$	$^{38}Ar/^{36}Ar$	$^{40}Ar/^{36}Ar$
Higashi-matsuura										
Keya										
FUK9716ol (2.0219g)										
SC 1000 strokes	1.55	9.25	2.41	7.52	4.27	6.43 ± 0.61	9.68 ± 0.14	0.0295 ± 0.0019	0.18693 ± 0.00071	312.22 ± 1.34
FUK9716ol (0.7025g)										
SH 1000℃	7.79	2.19	3.48	16.2	9.30	2.40 ± 0.42			0.18855 ± 0.00067	305.18 ± 0.38
1800℃	8.43	4.33	1.56	10.7	9.68	5.59 ± 1.16	9.68 ± 0.28	0.0314 ± 0.0042	0.18783 ± 0.00119	390.31 ± 1.27
Total	16.21	6.52	5.04	27.0	18.98	4.06			0.18833	331.54
FUK9716px (0.6547g)										
SC 2000 strokes	15.7	30.5	8.41	31.8	29	4.79 ± 0.43	9.85 ± 0.09	0.0296 ± 0.0015	0.18783 ± 0.00067	334.15 ± 0.70
FUK9716px after crushing (0.5882g)										
SH 800℃	25.10	3.07	4.40	26.8	65.9	0.31 ± 0.05			0.18819 ± 0.00096	311.17 ± 0.55
1800℃	8.76	10.70	5.25	37.2	124.0	1.49 ± 0.45	9.99 ± 0.18	0.0295 ± 0.0021	0.18794 ± 0.00077	314.06 ± 0.61
Total	33.86	13.77	9.66	64.0	189.9	0.61			0.18806	312.74
Takashima										
TKB0001ol (0.5288g)										
SC 2000 strokes	22.3	5.56	4.22	18.7	21.6	7.43 ± 0.50	10.04 ± 0.18	0.0309 ± 0.0030	0.18732 ± 0.00080	372.26 ± 0.85
TKB0001ol after crushing (0.5059g)										
SH 1000℃	21.80	1.75	3.11	27.6	81.4	0.33 ± 0.14			0.18770 ± 0.00072	319.43 ± 0.57
1800℃	2.18	5.15	2.64	18.9	72.0	3.60 ± 1.09	10.29 ± 0.28	0.0341 ± 0.0034	0.18694 ± 0.00096	335.08 ± 0.57
Total	23.98	6.90	5.75	46.5	153.4	0.63			0.18735	326.63
TKB0001px (1.2622g)										
SC 2000 strokes	4.94	11.4	2.56	9.19	7.81	6.43 ± 0.87	9.88 ± 0.13	0.0287 ± 0.0018	0.18738 ± 0.00101	398.96 ± 0.73
TKB0001px after crushing (0.7663g)										
SH 800℃	22.70	2.07	3.03	21.2	59.6	0.32 ± 0.10			0.18791 ± 0.00064	316.48 ± 0.51
1800℃	9.26	8.96	5.32	43.9	161.0	1.97 ± 0.47	9.96 ± 0.18	0.0294 ± 0.0021	0.18766 ± 0.00091	330.67 ± 0.45
Total	31.96	11.03	8.36	65.1	220.6	0.80			0.18775	325.52
TKB0002ol (0.5856g)										
SC 2000 strokes	7.48	2.72	2.74	16.4	12.9	6.94 ± 0.85	9.87 ± 0.38	0.0285 ± 0.0047	0.18807 ± 0.00146	622.52 ± 6.64
TKB0002px (0.6822g)										
SC 2000 strokes	6.29	15.8	4.44	16.1	11.9	6.88 ± 0.90	9.92 ± 0.13	0.0297 ± 0.0031	0.18803 ± 0.00088	415.82 ± 1.53
TKA0940px (2.05g)										
HC 700MPa×3	22.6	116	12.0	15.2	3.88	6.80 ± 0.90	9.79 ± 0.09	0.0292 ± 0.0011	0.18812 ± 0.00049	342.40 ± 9.90
TKA0940px (0.32g)										
TF 1800℃	26.2	23.7	6.92	20.8	26.6	4.72 ± 0.65	9.62 ± 0.20	0.0288 ± 0.0027	0.18834 ± 0.00066	409.19 ± 0.39

Unit for concentrations are cm^3STP/g. Errors with isotopic ratios are 1σ.

*1. SH: Step heating, TF: Total fusion, SC: Cushing with a solenoid-type crusher, HC: Crushing with a hydraulic-type crusher.

*2. Normalized to the atmospheric ratio = 1.4×10^{-6} (Ozima and Podosek, 1983).

Table 3–4. (Continued).

Sample (Weight) / Extraction Method*1	^{4}He ($\times10^{-9}$)	^{20}Ne ($\times10^{-11}$)	^{36}Ar ($\times10^{-10}$)	^{84}Kr ($\times10^{-12}$)	^{132}Xe ($\times10^{-13}$)	$^{3}He/^{4}He$ (R/R_A)*2	$^{20}Ne/^{22}Ne$	$^{21}Ne/^{22}Ne$	$^{38}Ar/^{36}Ar$	$^{40}Ar/^{36}Ar$
Ohshima										
OSM9801ol (0.9792g)										
SC 2000 strokes	34.42	2.12	1.95	11.34	10.42	7.09 ± 0.31	9.91 ± 0.26	0.0313 ± 0.0041	0.18788 ± 0.00099	612.46 ± 4.07
SC 2000 strokes (2nd.)	0.26	0.028	0.13	0.25	0.70	10.29 ± 4.16	11.74 ± 2.45	0.0093 ± 0.0339	0.19008 ± 0.00127	422.09 ± 3.74
Karatsu										
KR8404ol (1.9482g)										
HC 700MPa×3	12.1	1.13	0.255	0.606	0.44	7.29 ± 0.56	10.50 ± 0.21	0.0344 ± 0.0030	0.18892 ± 0.00139	760.08 ± 2.21
KR8404ol after crushing (0.5258g)										
SH 1000℃	33.66	0.59	3.18	24.7	20.9	1.19 ± 0.08			0.18862 ± 0.00050	294.85 ± 0.37
1800℃	1.58	3.46	1.50	20.5	32.5	4.10 ± 1.63	9.61 ± 0.30	0.0331 ± 0.0044	0.18894 ± 0.00203	421.40 ± 10.7
Total	35.24	4.05	4.68	45.3	53.4	1.32			0.18872	335.46
KR8404ol (0.8467g)										
SH 1000℃	16.65	0.49	1.46	9.21	7.85	0.30 ± 0.11			0.18856 ± 0.00114	327.93 ± 1.41
1800℃	8.27	1.16	1.04	12.05	14.17	3.35 ± 0.51	9.97 ± 0.42	0.0348 ± 0.0040	0.18930 ± 0.00120	492.60 ± 3.37
Total	24.92	1.64	2.50	21.26	22.03	1.31			0.18887	396.49
KR8404px augite (1.8482g)										
HC 700MPa×3	4.32	13.5	3.47	7.57	28.5	6.65 ± 0.51	9.79 ± 0.09	0.0289 ± 0.0012	0.18875 ± 0.00052	357.27 ± 0.43
KR8404px augite after crushing (0.5052g)										
SH 800℃	11.2	1.03	0.50	1.91	3.81	0.81 ± 0.42			0.19066 ± 0.00137	317.42 ± 1.11
1800℃	13.5	4.56	1.43	8.52	23.40	2.63 ± 0.43	10.49 ± 0.34	0.0319 ± 0.0037	0.18691 ± 0.00185	544.28 ± 3.09
Total	24.7	5.59	1.93	10.43	27.21	1.80			0.18788	485.80
KR8404px diopside (0.6441g)										
SC 2000 strokes	2.42	21.1	5.49	10.6	5.46	4.92 ± 1.29	9.94 ± 0.09	0.0285 ± 0.0023	0.18748 ± 0.00052	324.49 ± 0.54
KR8404gm (1.5023g)										
TF 1800℃	240	7.74	4.59	22.6	73.2	0.04 ± 0.01	9.58 ± 0.10	0.0300 ± 0.0018	0.18925 ± 0.00039	520.83 ± 1.17
KAR9803ol (0.9595g)										
SC 1000 strokes	0.790	2.88	1.04	3.36	1.51	6.08 ± 1.00	10.05 ± 0.25	0.0334 ± 0.0054	0.18589 ± 0.00236	370.20 ± 14.10
KAR9803ol after crushing (0.9484g)										
TF 1800℃	12.4	6.21	2.51	13.7	35.7	4.67 ± 0.62	10.13 ± 0.15	0.0354 ± 0.0037	0.18807 ± 0.00052	422.63 ± 0.59
KAR9803ol (0.4086g)										
SH 1000℃	9.94	4.33	1.61	6.68	4.31	1.93 ± 1.56			0.18939 ± 0.00143	313.95 ± 0.65
1800℃	5.48	2.08	0.83	3.96	3.50	12.58 ± 2.24	10.10 ± 0.24	0.0348 ± 0.0051	0.18587 ± 0.00241	595.48 ± 8.51
Total	15.42	6.41	2.44	10.65	7.81	5.72			0.18819	409.59
KAR9803px (1.1714g)										
SC 2000 strokes	0.733	20.0	2.72	6.47	4.98	2.08 ± 0.89	10.18 ± 0.10	0.0295 ± 0.0016	0.18773 ± 0.00072	352.01 ± 0.60

Unit for concentrations are cm^3STP/g. Errors with isotopic ratios are 1σ.

*1. SH: Step heating, TF: Total fusion, SC: Cushing with a solenoid-type crusher, HC: Crushing with a hydraulic-type crusher.

*2. Normalized to the atmospheric ratio = 1.4×10^{-6} (Ozima and Podosek, 1983).

Table 3–4. (Continued).

Sample (Weight) / Extraction Method[*1]	^{4}He ($\times10^{-9}$)	^{20}Ne ($\times10^{-11}$)	^{36}Ar ($\times10^{-10}$)	^{84}Kr ($\times10^{-12}$)	^{132}Xe ($\times10^{-13}$)	^{3}He/^{4}He (R/R_A)[*2]	^{20}Ne/^{22}Ne	^{21}Ne/^{22}Ne	^{38}Ar/^{36}Ar	^{40}Ar/^{36}Ar
KAR9803px after crushing (0.9628g)										
SH 800℃	35.10	2.75	2.87	13.2	23.8	1.29 ± 0.11			0.18896 ± 0.00086	326.46 ± 0.64
1800℃	6.63	22.70	2.76	13.9	39.5	5.20 ± 0.53	10.10 ± 0.07	0.0299 ± 0.0012	0.18729 ± 0.00071	384.00 ± 0.73
Total	41.73	25.45	5.63	27.1	63.3	1.91			0.18814	354.66
Nanatsugama										
KAR9801ol (0.6288g)										
SC 2000 strokes	0.345	21.6	6.11	14.6	7.43	7.82 ± 4.85	9.84 ± 0.10	0.0292 ± 0.0022	0.18807 ± 0.00075	335.72 ± 0.48
Kita-matsuura										
Myokanji										
SSB0001ol (0.3949g)										
SC 2000 strokes	8.13	4.28	4.88	27.3	26.3	2.95 ± 1.02	9.53 ± 0.65	0.0300 ± 0.0059	0.18876 ± 0.00135	467.08 ± 4.44
SSB0001ol after crushing (0.3598g)										
TF 1800℃	71.9	7.53	6.98	57.5	220	0.35 ± 0.08	9.97 ± 0.18	0.0286 ± 0.0033	0.18875 ± 0.00111	309.45 ± 0.84
SSB0001px (0.3698g)										
SC 2000 strokes	11.3	17.4	3.49	18.3	21.4	0.37 ± 0.43	9.45 ± 0.12	0.0299 ± 0.0044	0.18855 ± 0.00199	475.29 ± 3.10
Yoshii										
SSB0002ol (1.0475g)										
SC 2000 strokes	1.87	1.09	1.20	6.04	5.48	3.73 ± 0.89	9.68 ± 0.32	0.0307 ± 0.0051	0.18813 ± 0.00126	323.34 ± 0.66
SSB0002ol after crushing (0.6007g)										
TF 1800℃	64.9	3.46	4.37	32.9	91.1	0.41 ± 0.04	10.19 ± 0.21	0.0302 ± 0.0029	0.18927 ± 0.00115	327.04 ± 0.50
SSB0002px (0.2668g)										
SC 2000 strokes	25.4	21.4	4.77	28.8	29.9	0.21 ± 0.38	9.68 ± 0.18	0.0277 ± 0.0049	0.18769 ± 0.00179	318.01 ± 1.24
Hirado										
HRD0001ol (0.7097g)										
SC 2000 strokes	0.192	8.95	1.79	5.35	2.83	9.89 5.82	9.70 ± 0.12	0.0289 ± 0.0038	0.18839 ± 0.00101	374.71 ± 0.62
Kokuzo										
KKZ0001px (0.9845g)										
SC 2000 strokes	0.409	19.4	5.26	13.4	6.93	10.98 3.07	9.77 ± 0.08	0.0281 ± 0.0016	0.18803 ± 0.00050	309.12 ± 0.38
Doinohana										
KKZ0003px (1.2143g)										
SC 2000 strokes	0.406	4.98	0.675	1.71	1.18	2.21 1.10	9.89 ± 0.08	0.0282 ± 0.0013	0.18697 ± 0.00120	494.99 ± 3.90
Atmosphere [*3]	5.24	16.45	31.4	0.650	0.0234	1	9.80	0.0290	0.1880	295.5

Unit for concentrations are cm^3STP/g. Errors with isotopic ratios are 1σ.

*1. SH: Step heating, TF: Total fusion, SC: Cushing with a solenoid-type crusher, HC: Crushing with a hydraulic-type crusher.

*2. Normalized to the atmospheric ratio = 1.4×10^{-6} (Ozima and Podosek, 1983).

*3. Data from Ozima and Podosek (1983).

Table 3–5. Kr and Xe isotopic compositions of basalts from northwestern Kyushu.

Sample[*1]	Weight (g) / Method[*2]	$^{78}Kr/^{84}Kr$	$^{80}Kr/^{84}Kr$	$^{82}Kr/^{84}Kr$	$^{83}Kr/^{84}Kr$	$^{86}Kr/^{84}Kr$	$^{124}Xe/^{130}Xe$	$^{126}Xe/^{130}Xe$	$^{128}Xe/^{130}Xe$	$^{129}Xe/^{130}Xe$	$^{131}Xe/^{130}Xe$	$^{132}Xe/^{130}Xe$	$^{134}Xe/^{130}Xe$	$^{136}Xe/^{130}Xe$
Higashi-matsuura														
Keya														
FUK9716ol	2.0219	0.00568	0.0402	0.2009	0.1956	0.2942	0.0276	0.0237	0.463	6.58	5.29	6.60	2.59	2.18
SC 1000 strokes		± 0.00041	± 0.0012	± 0.0034	± 0.0036	± 0.0049	± 0.0038	± 0.0021	± 0.036	± 0.49	± 0.38	± 0.47	± 0.19	± 0.16
FUK9716ol	0.7025	0.00569	0.0395	0.1970	0.1958	0.2973	0.0247	0.0213	0.466	6.44	5.13	6.54	2.52	2.17
SH 1800℃		± 0.00054	± 0.0013	± 0.0038	± 0.0060	± 0.0062	± 0.0062	± 0.0036	± 0.039	± 0.50	± 0.39	± 0.49	± 0.19	± 0.16
FUK9716cpx	0.6547	0.00596	0.0400	0.1982	0.1915	0.2919	0.0253	0.0240	0.553	6.88	5.52	6.91	2.69	2.40
SC 2000 strokes		± 0.00028	± 0.0016	± 0.0075	± 0.0065	± 0.0098	± 0.0034	± 0.0040	± 0.064	± 0.80	± 0.65	± 0.80	± 0.33	± 0.27
FUK9716cpx (pw)	0.5882	0.00611	0.0395	0.1990	0.1930	0.2908	0.0233	0.0219	0.478	6.56	5.22	6.57	2.56	2.15
SH 1800℃		± 0.00031	± 0.0009	± 0.0049	± 0.0041	± 0.0058	± 0.0020	± 0.0024	± 0.034	± 0.46	± 0.36	± 0.45	± 0.17	± 0.15
Takashima														
TKB0001ol	0.5288	0.00597	0.0390	0.1977	0.1940	0.2883	0.0274	0.0229	0.520	6.87	5.56	6.88	2.70	2.26
SC 2000 strokes		± 0.00035	± 0.0019	± 0.0087	± 0.0076	± 0.0108	± 0.0062	± 0.0052	± 0.068	± 0.79	± 0.64	± 0.80	± 0.32	± 0.26
TKB0001ol (pw)	0.5059	0.00575	0.0402	0.1976	0.1902	0.2896	0.0259	0.0217	0.473	6.52	5.22	6.58	2.55	2.14
SH 1800℃		± 0.00040	± 0.0010	± 0.0041	± 0.0048	± 0.0059	± 0.0025	± 0.0030	± 0.033	± 0.46	± 0.36	± 0.45	± 0.18	± 0.15
TKB0001cpx	1.2622	0.00622	0.0375	0.1982	0.1922	0.2871	0.0238	0.0255	0.512	7.09	5.60	7.08	2.68	2.28
SC 2000 strokes		± 0.00052	± 0.0015	± 0.0068	± 0.0066	± 0.0099	± 0.0047	± 0.0075	± 0.059	± 0.84	± 0.71	± 0.87	± 0.32	± 0.28
TKB0001cpx (pw)	0.7663	0.00628	0.0394	0.1979	0.1945	0.2919	0.0231	0.0210	0.478	6.59	5.28	6.66	2.56	2.16
SH 1800℃		± 0.00020	± 0.0010	± 0.0042	± 0.0036	± 0.0062	± 0.0022	± 0.0018	± 0.033	± 0.45	± 0.36	± 0.46	± 0.18	± 0.15
TKA0940cpx	0.32	0.00625	0.0397	0.2018	0.2004	0.3038	0.0253	0.0193	0.459	6.40	5.26	6.57	2.54	2.16
TF 1800℃		± 0.00042	± 0.0010	± 0.0038	± 0.0041	± 0.0067	± 0.0058	± 0.0037	± 0.035	± 0.37	± 0.24	± 0.32	± 0.09	± 0.07
Ohshima														
OSM9801ol	0.9792	0.00631	0.0413	0.2070	0.2004	0.3009	0.0253	0.0214	0.482	6.54	5.14	6.59	2.49	2.11
SC 2000 strokes		± 0.00034	± 0.0014	± 0.0055	± 0.0039	± 0.0089	± 0.0027	± 0.0032	± 0.025	± 0.33	± 0.29	± 0.38	± 0.14	± 0.12
Karatsu														
KR8404ol	0.5258	0.00618	0.0404	0.2016	0.2007	0.2946	0.0252	0.0225	0.470	6.51	5.25	6.58	2.54	2.15
SH 1800℃		± 0.00030	± 0.0015	± 0.0046	± 0.0042	± 0.0051	± 0.0035	± 0.0035	± 0.037	± 0.47	± 0.38	± 0.46	± 0.18	± 0.15
KR8404ol (pw)	0.8467	0.00624	0.0393	0.1993	0.1954	0.2946	0.0256	0.0216	0.476	6.52	5.17	6.55	2.54	2.14
SH 1800℃		± 0.00048	± 0.0010	± 0.0031	± 0.0051	± 0.0051	± 0.0023	± 0.0022	± 0.036	± 0.47	± 0.38	± 0.48	± 0.18	± 0.15
KR8404cpx (ag)	1.8428	0.00538	0.0397	0.2006	0.1926	0.2923	0.0265	0.0286	0.473	6.85	5.53	6.85	2.60	2.22
HC 700MPa×3		± 0.00025	± 0.0011	± 0.0063	± 0.0051	± 0.0079	± 0.0049	± 0.0103	± 0.045	± 0.58	± 0.50	± 0.62	± 0.26	± 0.22
KR8404cpx (ag)	0.5052	0.00630	0.0393	0.1978	0.1951	0.3004	0.0255	0.0220	0.491	6.65	5.30	6.79	2.58	2.18
SH 1800℃		± 0.00045	± 0.0012	± 0.0053	± 0.0085	± 0.0101	± 0.0039	± 0.0036	± 0.047	± 0.47	± 0.40	± 0.54	± 0.18	± 0.18
KR8404cpx (dp)	0.5052	0.00568	0.0389	0.1967	0.1914	0.2913	0.0233	0.0240	0.496	6.83	5.49	7.05	2.67	2.21
SC 2000 strokes		± 0.00029	± 0.0027	± 0.0069	± 0.0082	± 0.0111	± 0.0077	± 0.0085	± 0.061	± 0.87	± 0.68	± 0.84	± 0.33	± 0.29

Errors with isotopic ratios are 1σ.

*1. ol: olivine, cpx: clinopyroxene, pw: powdered sample after crushing, gm: groundmass, ag: augite, dp: diopside.

*2. SH: Step heating, TF: Total fusion, SC: Cushing with a solenoid-type crusher, HC: Crushing with a hydraulic-type crusher.

Table 3–5. (Continued)

Sample[*1]	Weight (g) / Method[*2]	$^{78}Kr/^{84}Kr$	$^{80}Kr/^{84}Kr$	$^{82}Kr/^{84}Kr$	$^{83}Kr/^{84}Kr$	$^{86}Kr/^{84}Kr$	$^{124}Xe/^{130}Xe$	$^{126}Xe/^{130}Xe$	$^{128}Xe/^{130}Xe$	$^{129}Xe/^{130}Xe$	$^{131}Xe/^{130}Xe$	$^{132}Xe/^{130}Xe$	$^{134}Xe/^{130}Xe$	$^{136}Xe/^{130}Xe$
KR8404gm	1.5023	0.00590	0.0397	0.1980	0.1949	0.2923	0.0239	0.0221	0.484	6.65	5.35	6.76	2.62	2.23
	TF 1800℃	± 0.00014	± 0.0009	± 0.0034	± 0.0033	± 0.0050	± 0.0010	± 0.0012	± 0.016	± 0.21	± 0.17	± 0.21	± 0.08	± 0.07
KAR9803ol	0.9595	0.00408	0.0397	0.2005	0.1968	0.2975	0.0245	0.0197	0.472	6.54	5.22	6.66	2.57	2.19
	SC 1000 strokes	± 0.00040	± 0.0019	± 0.0043	± 0.0059	± 0.0066	± 0.0038	± 0.0035	± 0.038	± 0.52	± 0.40	± 0.49	± 0.20	± 0.17
KAR9803ol	0.4086	0.00551	0.0389	0.1973	0.1943	0.2967	0.0285	0.0025	0.493	6.51	5.16	6.50	2.50	2.18
	SH 1800℃	± 0.00083	± 0.0021	± 0.0082	± 0.0065	± 0.0149	± 0.0079	± 0.0039	± 0.061	± 0.49	± 0.47	± 0.50	± 0.23	± 0.20
KAR9803cpx	1.1714	0.00638	0.0396	0.1981	0.1949	0.2868	0.0243	0.0206	0.490	6.58	5.37	6.74	2.62	2.13
	SC 2000 strokes	± 0.00067	± 0.0015	± 0.0058	± 0.0053	± 0.0073	± 0.0055	± 0.0052	± 0.053	± 0.54	± 0.55	± 0.53	± 0.22	± 0.19
KAR9803cpx (pw)	0.9628	0.00598	0.0396	0.1958	0.1945	0.2905	0.0241	0.0222	0.490	6.64	5.28	6.77	2.56	2.17
	SH 1800℃	± 0.00041	± 0.0008	± 0.0061	± 0.0048	± 0.0081	± 0.0035	± 0.0025	± 0.043	± 0.47	± 0.37	± 0.49	± 0.18	± 0.16
Nanatsugama														
KAR9801ol	0.6288	0.00620	0.0422	0.2049	0.2034	0.3036	0.0281	0.0240	0.497	6.67	5.24	6.57	2.48	2.05
	SC 2000 strokes	± 0.00051	± 0.0026	± 0.0056	± 0.0076	± 0.0086	± 0.0054	± 0.0040	± 0.060	± 0.48	± 0.31	± 0.44	± 0.19	± 0.13
Kita-matsuura														
Myokanji														
SSB0001ol (pw)	0.3598	0.00591	0.0387	0.1946	0.1936	0.2876	0.0250	0.0244	0.518	7.12	5.71	7.22	2.80	2.36
	SC 2000 strokes	± 0.00026	± 0.0014	± 0.0053	± 0.0048	± 0.0073	± 0.0021	± 0.0020	± 0.035	± 0.47	± 0.38	± 0.48	± 0.19	± 0.16
SSB0001cpx	0.3698	0.00632	0.0417	0.2087	0.2056	0.3076	0.0358	0.0205	0.468	6.62	5.31	6.74	2.62	2.16
	SC 2000 strokes	± 0.00100	± 0.0021	± 0.0092	± 0.0085	± 0.0128	± 0.0054	± 0.0068	± 0.060	± 0.74	± 0.62	± 0.73	± 0.31	± 0.25
Yoshii														
SSB0002ol	1.0475	0.00599	0.0410	0.2053	0.1974	0.3053	0.0246	0.0226	0.466	6.35	5.14	6.45	2.51	2.10
	SC 2000 strokes	± 0.00045	± 0.0009	± 0.0055	± 0.0038	± 0.0085	± 0.0023	± 0.0052	± 0.035	± 0.37	± 0.34	± 0.36	± 0.16	± 0.12
SSB0002ol (pw)	0.6007	0.00600	0.0388	0.1957	0.1922	0.2853	0.0252	0.0239	0.518	7.16	5.70	7.19	2.77	2.36
	TF 1800℃	± 0.00046	± 0.0012	± 0.0057	± 0.0049	± 0.0072	± 0.0025	± 0.0017	± 0.034	± 0.47	± 0.38	± 0.47	± 0.18	± 0.16
SSB0002cpx	0.2668	0.00673	0.0420	0.2119	0.2013	0.3094	0.0250	0.0171	0.475	6.45	5.02	6.40	2.52	2.06
	SC 2000 strokes	± 0.00080	± 0.0032	± 0.0067	± 0.0103	± 0.0127	± 0.0093	± 0.0075	± 0.057	± 0.89	± 0.53	± 0.66	± 0.27	± 0.23
Hirado														
HRD0001ol	,7097	0.00662	0.0426	0.2110	0.2056	0.3092	0.0275	0.0243	0.478	6.61	5.10	6.43	2.55	2.10
	SC 2000 strokes	± 0.00097	± 0.0034	± 0.0081	± 0.0106	± 0.0073	± 0.0109	± 0.0092	± 0.084	± 0.76	± 0.74	± 0.77	± 0.32	± 0.23
Kokuzo														
KKZ0001cpx	0.9845	0.00621	0.0426	0.2130	0.2079	0.3097	0.0304	0.0221	0.488	6.47	5.22	6.64	2.55	2.14
	SC 2000 strokes	± 0.00047	± 0.0014	± 0.0053	± 0.0045	± 0.0082	± 0.0054	± 0.0059	± 0.061	± 0.68	± 0.53	± 0.66	± 0.24	± 0.22
Doinohana														
KKZ0003ol	1.2143	0.00603	0.0408	0.2031	0.2015	0.3034	0.0304	0.0241	0.503	6.52	5.24	6.57	2.47	2.11
	SC 2000 strokes	± 0.00061	± 0.0021	± 0.0081	± 0.0058	± 0.0060	± 0.0086	± 0.0061	± 0.051	± 0.52	± 0.63	± 0.49	± 0.20	± 0.21
Atmosphere [*3]		0.00609	0.0396	0.2022	0.2014	0.3052	0.0234	0.0218	0.472	6.50	5.21	6.61	2.56	2.18

Errors with isotopic ratios are 1σ.

*1. ol: olivine, cpx: clinopyroxene, pw: powdered sample after crushing, gm: groundmass, ag: augite, dp: diopside.

*2. SH: Step heating, TF: Total fusion, SC: Cushing with a solenoid-type crusher, HC: Crushing with a hydraulic-type crusher.

*3. Data from Ozima and Podosek (1983).

Table 3–6. Hot blanks and crushing blanks using MS–IV.

Date	^{4}He ($\times10^{-11}$)	^{20}Ne ($\times10^{-12}$)	^{40}Ar ($\times10^{-10}$)	^{84}Kr ($\times10^{-14}$)	^{132}Xe ($\times10^{-15}$)	
Crushing						
Hydlauric-type (130℃)						
1999. 7. 6	57.40	5.15	7.89	5.90	2.58	
7. 8	11.90	13.70	9.76			
7. 11	2.58	2.97	9.08	5.74	2.47	
7. 12	2.76	3.92	10.40	6.80	2.28	
7. 15	2.81	11.22	24.10			
7. 16	1.77	4.39	6.71	5.02	2.70	
7. 21	1.89	4.11	9.97	6.82	4.46	
7. 22	2.11	2.82	8.06	4.50	7.46	
7. 25	2.27	4.80	8.68	4.50	1.64	
7. 27	2.27	4.72	11.60	8.29	3.86	
2000. 5. 16	1.28	5.04	9.60	7.81	3.30	
Solenoid-type (room temperature)						
2000. 3. 7	0.10	1.19	3.28	2.35	2.00	
5. 13	1.19	3.78	3.04	2.96	2.99	
6. 12	1.26	8.70	3.95	9.31	13.60	
7. 23	0.97	5.76	3.41	2.91	11.20	
9. 8	1.24	2.53	2.79	3.40	10.90	
9. 19	1.27	2.20	2.22	2.36	6.88	
11. 2	2.35	8.15	2.71	4.38	13.40	
Solenoid-type (blank strokes without sample)						
2000. 3. 7	0.75	11.60	73.40	32.50	41.30	1000strokes
7. 24	18.40	2.84	75.90	45.90	10.10	2000strokes
Unit for concentrations are cm^{3}STP.						

Date	^{4}He ($\times10^{-11}$)	^{20}Ne ($\times10^{-12}$)	^{40}Ar ($\times10^{-10}$)	^{84}Kr ($\times10^{-14}$)	^{132}Xe ($\times10^{-15}$)
Step heating					
(600℃)					
1999. 8. 30	42.60	3.16	2.63	1.31	0.51
9. 2	36.50	2.28	3.09	1.88	5.40
9. 17	37.10	2.66	2.83	1.27	0.69
2000. 3. 5	1.37	6.62	7.45	8.27	5.01
3. 16	0.74	4.63	4.15	2.95	1.56
6. 15	0.89	2.31	3.34	5.55	16.40
(800℃)					
2000. 3.5	1.15	7.03	5.14	5.60	4.05
3. 24	1.59	2.39	6.24	2.83	4.26
6. 15	0.85	2.20	2.61	3.33	8.60
(1000℃)					
2000. 3. 6	2.36	28.80	5.73	5.54	5.68
6. 15	1.34	2.87	3.84	4.74	8.60
6. 21	1.29	3.01	4.06	2.87	8.60
(1200℃)					
2000. 3. 6	1.19	6.49	6.26	6.73	5.47
6. 15	0.83	2.45	4.95	5.73	13.30
(1400℃)					
2000. 6.16	0.89	2.54	9.40	7.37	9.78
(1600℃)					
2000. 3. 6	1.24	6.52	8.58	7.29	4.14
3. 6	1.63	10.30	20.00	17.00	12.90
6. 16	0.88	2.79	15.90	6.84	12.10
(1800℃)					
1999. 8. 30	68.40	9.50	87.40	67.90	53.80
9. 2	63.10	3.96	19.60	19.60	22.70
9. 17	60.80	6.24	18.50	7.84	4.36
2000. 3. 16	1.15	4.81	14.60	9.79	6.24
3. 24	1.77	8.21	39.60	22.50	15.20
6. 16	1.08	3.38	24.90	13.30	23.10
6. 21	1.01	3.90	13.30	11.00	19.60
7. 6	1.08	6.36	35.50	23.30	25.80
11. 26	1.54	3.29	8.68	5.74	8.82
Al-foil					
(0.1459g, 1800℃)					
2000. 3. 6	40.2	168	1310	1240	865
Unit for concentrations are cm^{3}STP.					

Stepwise heating

The stepwise heating is a conventional method for extracting gases from rock samples. Adsorbed atmospheric, especially heavier noble gases on sample surface would not be completely removed even by heating at about 200°C in vacuum condition. The appropriate choice of stepwise temperature would make it possible to separate inherent gases of magmatic origin from gases of secondary component, such as atmospheric, radiogenic and cosmogenic. In the low temperature fraction, adsorbed gases would be removed from the sample surface while magmatic gases trapped in the matrix and/or fluid inclusions would be retained. Then, they would be degassed from the samples and analyzed at high temperature.

It is appropriate to apply multi-stage step heating method for all the samples in principle, however 2-step heating method is practicable due to limited amount of the sample available, with low noble gas concentration. Contamination by adsorbed atmospheric component is a serious problem for heavier noble gases. In this section, gas release pattern as a function of heating temperature was investigated for olivine to determine appropriate temperature, at which magmatic component will be separated from adsorptive component.

FUK9716 olivine was selected for the stepwise heating test. The noble gas elemental abundances, and He, Ne and Ar isotopic ratios were measured at each temperature step (600, 800, 1000, 1200, 1400, 1600 and 1800°C). Results are listed in Table 3–7 and shown in Fig. 3–7. No significant variations were observed for Ne isotopic ratios and $^{38}Ar/^{36}Ar$ ratios. At 600–1000°C, low $^{3}He/^{4}He$ ratios (~$1R_A$) and $^{40}Ar/^{36}Ar$ ratios with almost atmospheric value were observed. Ar released at these fractions are dominant in atmospheric component. ^{36}Ar release shows two peaks at 600°C and 1000°C, the former represents the atmospheric component adsorbed on the sample surface and the latter may be strongly adsorbed atmospheric Ar in micro cracks or altered phase. Low $^{3}He/^{4}He$ ratios at these low temperature is explained by mixing between trapped He and radiogenic ^{4}He both of which degassed from matrix via volume diffusion, because adsorbed He on the sample surface could be removed by preheating under vacuum condition.

At 1400°C, high $^{3}He/^{4}He$ and $^{40}Ar/^{36}Ar$ ratio were observed. The $^{3}He/^{4}He$ ratio of this fraction is similar to that obtained with crushing, therefore fluid inclusion might be decrepitated around this temperature. The $^{40}Ar/^{36}Ar$ ratio is the highest among all fractions, reflecting magmatic origin. On the contrary to He, $^{40}Ar/^{36}Ar$ ratio obtained with crushing is significantly lower than the highest value with step heating, probably due to adsorbed atmospheric Ar. Therefore, at least two-step heating is necessary to estimate $^{40}Ar/^{36}Ar$ ratio of magma. Thereafter in this experiment, the heating temperature in the low temperature fraction was chosen to be 1000°C for olivine to remove secondary noble gases completely. The high temperature fraction was set at 1800°C to guarantee complete melting and degassing from the sample. Since it is reported that magmatic noble gases in clinopyroxene were degassed at lower temperature than that of olivine (Hanyu et al., 1999), clinopyroxene samples were degassed at 800°C and 1800°C in this study.

Table 3–7. Stepwise heating for FUK9716 olivine.

Method (Sample weight)	Temperature (℃)	$[^4He]$ ($\times10^{-9}$)	$[^{20}Ne]$ ($\times10^{-11}$)	$[^{36}Ar]$ ($\times10^{-10}$)	$[^{84}Kr]$ ($\times10^{-12}$)	$[^{132}Xe]$ ($\times10^{-13}$)	$^3He/^4He$ $(R/R_A)^*$	$^{20}Ne/^{22}Ne$
Step heating	600	2.36	2.6	2.07	8.75	8.82	1.00 ± 0.58	10.22 ± 0.48
(0.7196g)	800	1.24	1.3	0.79	3.51	2.84	1.33 ± 1.16	9.99 ± 0.83
	1000	2.29	1.5	1.26	7.63	4.51	1.06 ± 0.72	10.46 ± 0.67
	1200	0.93	1.0	0.16	2.31	4.37	2.98 ± 1.65	10.35 ± 0.60
	1400	3.77	2.6	0.59	2.79	6.86	6.25 ± 0.93	9.92 ± 0.50
	1600	2.52	3.9	0.74	2.04	2.71	5.68 ± 1.30	10.22 ± 0.33
	1800	0.85	3.2	0.62	1.17	1.02	6.06 ± 2.13	10.13 ± 0.31
	1800 again	0.20	1.1	0.21	0.32	0.13	8.26 ± 2.73	10.31 ± 0.69
	Total	14.16	17.3	6.45	28.52	31.26	3.80	10.17
Crushing (1000 strokes)		1.55	9.25	2.41	7.52	4.27	6.43 ± 0.61	9.68 ± 0.14
(2.0219g)								

Unit for concentrations are cm^3STP/g

* Normalized to the atmospheric ratio = 1.4×10^{-6} (Ozima and Podosek, 1983).

Table 3–7. (Continued)

Method (sample weight)	Temperature (℃)	$^{21}Ne/^{22}Ne$	$^{38}Ar/^{36}Ar$	$^{40}Ar/^{36}Ar$
Step heating	600	0.0283 ± 0.0059	0.18769 ± 0.00053	298.86 ± 0.57
(0.7196g)	800	0.0286 ± 0.0051	0.18840 ± 0.00135	301.03 ± 0.89
	1000	0.0333 ± 0.0053	0.18787 ± 0.00147	306.85 ± 0.86
	1200	0.0365 ± 0.0133	0.18569 ± 0.00427	376.54 ± 4.53
	1400	0.0316 ± 0.0068	0.19189 ± 0.00239	409.72 ± 1.26
	1600	0.0279 ± 0.0028	0.18771 ± 0.00202	384.98 ± 1.24
	1800	0.0288 ± 0.0060	0.18763 ± 0.00205	356.76 ± 1.68
	1800 again	0.0322 ± 0.0093	0.18762 ± 0.00486	334.33 ± 2.89
	Total	0.0300	0.18814	329.35
Crushing (1000 strokes)		0.0295 ± 0.0019	0.18693 ± 0.00071	312.22 ± 1.34
(2.0219g)				

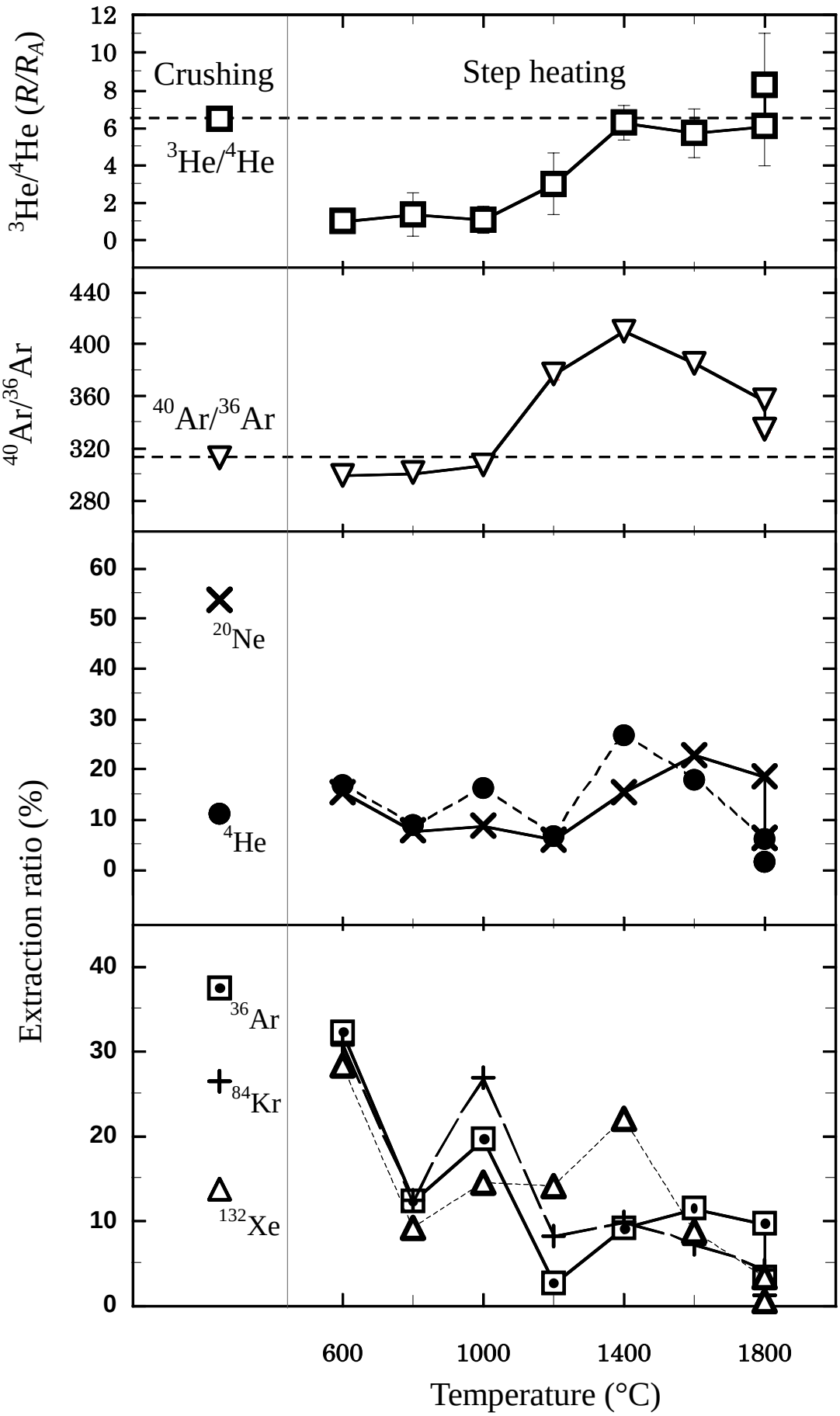

Fig. 3–7. Noble gas release pattern with stepwise heating method for the sample FUK9716 olivine. Dashed lines on He and Ar isotopic ratios represent the values obtained with crushing method.

Post-eruptive Radiogenic and Cosmogenic He

Figure 3–8 shows a comparison of the $^3He/^4He$ ratio obtained with crushing and step heating for the same sample. For the samples whose amount is limited and could not separately used for crushing and step heating, powdered sample after crushing experiment were used for heating experiment.

Most samples show lower $^3He/^4He$ ratios with heating than that with crushing. It is caused by post-eruptive addition of radiogenic ^4He except olivine and clinopyroxene separated from KAR9803. The contribution of radiogenic He is significant in low temperature fraction, because ^4He produced by radioactive decay of U and Th in matrix are extracted via volume diffusion, while fluid inclusions which contain magmatic He is not decrepitated at this temperature. Radiogenic ^4He concentration $([^4He]_{radio})_{meas}$ in phenocryst can be calculated as follows. Assuming that $^3He/^4He$ ratio obtained with crushing $(^3He/^4He)_{crush}$ is original isotopic ratio of magma, $^3He/^4He$ ratio measured by heating method is

$$(^3He/^4He)_{heat} = \frac{[^3He]_{trap} + [^3He]_{radio}}{[^4He]_{trap} + [^4He]_{radio}} = \frac{(^3He/^4He)_{crush}[^4He]_{trap} + (^3He/^4He)_{radio}[^4He]_{radio}}{[^4He]_{trap} + [^4He]_{radio}}$$

where $[^3He]_{trap}$ and $[^4He]_{trap}$ are trapped concentrations of ^3He and ^4He, respectively. $(^3He/^4He)_{radio}$ is production ratio of radiogenic component of ^3He from ^6Li and ^4He from U and Th. Assuming the Li and U contents in the phenocryst of 0.5ppm and 2ppb for olivine and 5ppm and 30ppb for clinopyroxene, respectively, and Th/U ratio of 3, $(^3He/^4He)_{radio}$ are estimated to be lower than $0.001R_A$ both for olivine and clinopyroxene (Andrews, 1985), thus negligible. Total ^4He concentration $[^4He]_{heat}$ totally released by heating is

$$[^4He]_{heat} = [^4He]_{trap} + [^4He]_{radio}$$

Thus, $[^4He]_{radio}$ is calculated from

$$[^4He]_{radio} = [^4He]_{heat} \times \left(\frac{(^3He/^4He)_{crush} - (^3He/^4He)_{heat}}{(^3He/^4He)_{crush}} \right)$$

Obtained $[^4He]_{radio}$ and $[^4He]_{trap}$ for each sample except KAR9803 are shown in Table 3–8.

On the other hand, the amount of accumulated radiogenic ^4He depends on concentrations of U and Th, and age of eruption. Therefore, the amount of radiogenic ^4He can be estimated from U and Th concentrations of the host basalt. Partition coefficients of U between phenocryst and matrix are 0.0025 and 0.04 for olivine and clinopyroxene, respectively (Henderson, 1982). Th/U ratio is assumed to be 4.9 from Kurasawa (1968). Production rates of radiogenic ^4He from 1g of U and Th are $1.15\times10^{-7}cm^3STP$ and $2.87\times10^{-8}cm^3STP$ per year (Ozima and Podosek, 1983). Estimated concentrations of radiogenic ^4He are listed in Table 3–8. While the measured concentrations of radiogenic ^4He for clinopyroxene show good agreement with those calculated ones within an order of magnitude, those for olivine are almost an order of magnitude higher than calculated value. This discrepancy might be caused by uncertainties of partition coefficient of U for olivine, and/or relatively large contribution of α-particle implantation from matrix around phenocryst. The range of a typical α-particle in basaltic lava is approximately 20–40μm. U and Th contents in basalt matrix are 400 times of those in olivine, thus surrounding matrix 20μm in thickness of 1mm spherical olivine can produce two orders magnitude more abundant radiogenic ^4He ($1–3\times10^{-9}cm^3STP$), and can cover the excess radiogenic ^4He observed ($2–8\times10^{-10}cm^3STP$ in 1mm olivine). Depletion of radiogenic ^4He of groundmass (KR8404K) is probably due to diffusive loss of He, because diffusivity of He in groundmass may be three to four orders of magnitude higher than that of olivine and clinopyroxene, respectively (Trull and Kurz, 1993).

Samples of olivine and clinopyroxene separated from KAR9803 basalt show higher $^3He/^4He$ ratios at high temperature fraction of step heating than those with crushing (Table 3–3 and Fig. 3–8), indicating cosmogenic ^3He addition. This basalt was collected along a thin road cut on a hill with possible exposure to cosmic ray. Total He concentration and $^3He/^4He$ ratio with crushing are low in this sample. Therefore, cosmogenic component can be conspicuous compared to other samples. Assuming that concentration of radiogenic He at high temperature fraction is equal to that at low temperature fraction, excess ^3He at high temperature fraction in olivine and

clinopyroxene are 5.0×10^{-14}cm^{3}STP/g and 2.9×10^{-14}cm^{3}STP/g, respectively. ^{21}Ne/^{22}Ne ratios of these samples (0.0348 and 0.0299 for olivine and clinopyroxene, Table 3–3) are also higher than atmospheric ratio (0.0290), indicating cosmogenic ^{21}Ne addition. If all excess ^{21}Ne is cosmogenic origin, ^{3}He/^{21}Ne ratios of olivine and clinopyroxene are estimated to be 4.2 and 7.4, showing good agreement with the value of 3.5 for mafic phenocryst by Staudacher and Allègre (1993) considering relatively large uncertainties in ^{21}Ne/^{22}Ne ratios of the samples.

Cosmogenic ^{3}He in other sample may be negligible, because most of the samples are collected from bottom of lava flow with ca. 20m in thickness and the ^{3}He production will decrease by 90% with 1m of shielding by rock of 3g/cm^3 (Lal, 1987). For boulder stone samples from Takashima and Ohshima, contribution of cosmogenic ^{3}He is less than 5% of total He in heating experiments, estimated from their ^{21}Ne/^{22}Ne ratio assuming all excess ^{21}Ne relative to atmospheric composition is cosmogenic origin and cosmogenic ^{3}He/^{21}Ne is 3.5 (Staudacher and Allègre, 1993).

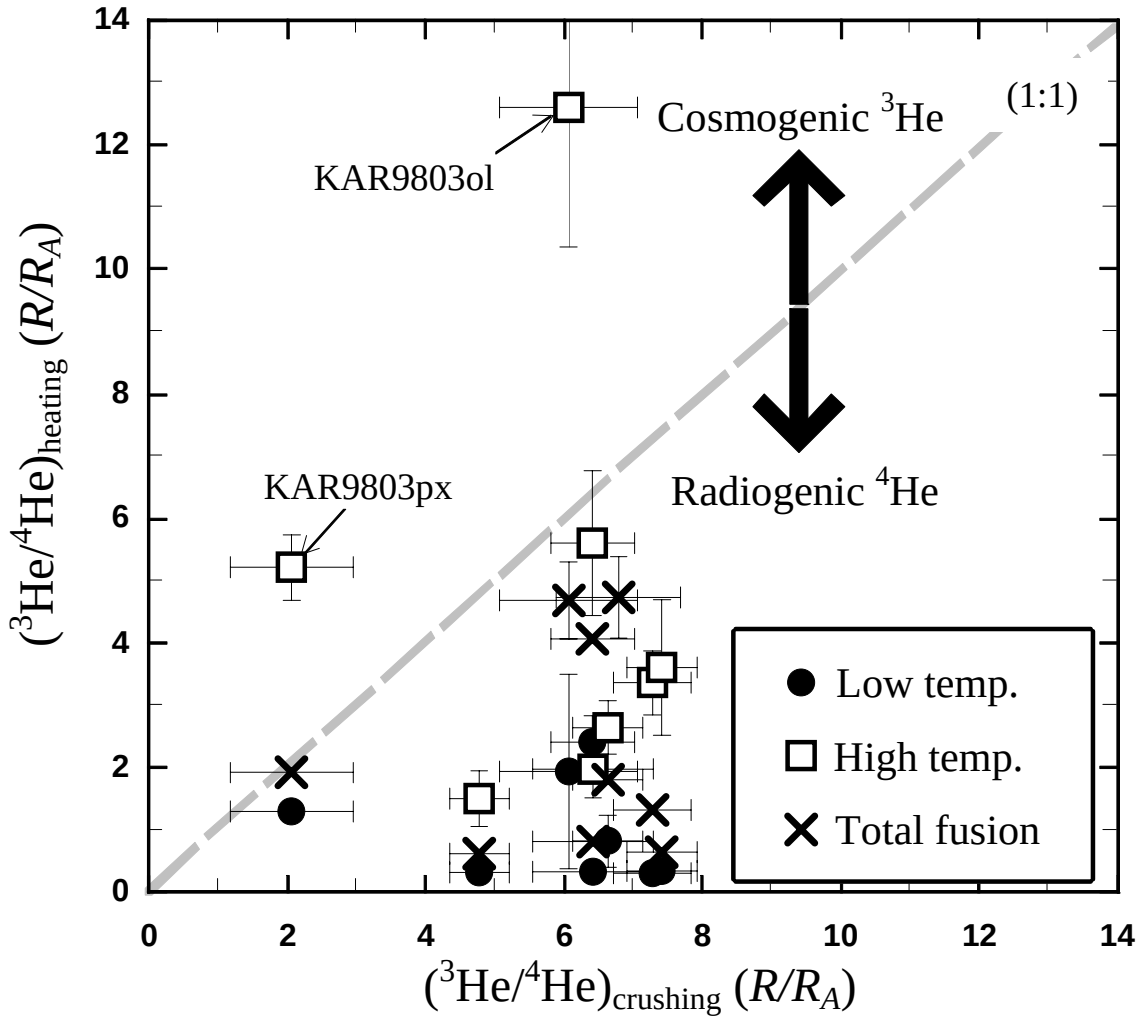

Fig. 3–8. Comparison of ^{3}He/^{4}He ratios obtained with crushing and heating for the same samples. The dashed line gives the 1:1 correlation line. Most samples are plotted below the line, indicating post-eruptive addition of radiogenic ^{4}He. Two exceptions are KAR9803 olivine and clinopyroxene, containing cosmogenic ^{3}He.

Table 3–8. Comparison of radiogenic ^4He measured and estimated.

Sample	Method	$[^4He]_{total}$ ($10^{-8}cm^3STP/g$)	$(^3He/^4He)_{total}$ (R/R_A)	$(^3He/^4He)_{crush}$ (R/R_A)	$([^4He]_{radio})_{meas}$ ($10^{-8}cm^3STP/g$)	$[^4He]_{trap}$ ($10^{-8}cm^3STP/g$)	Age (Ma)	Th (ppm)	U*1 (ppm)	$([^4He]_{radio})_{calc}$ ($10^{-8}cm^3STP/g$)	Ratio*2
KR8404ol	cr+pw	4.73	2.84	7.29	2.89	2.29	2.89	4.97	1.01	0.19	15.05
KR8404px	cr+pw	2.90	2.52	6.65	1.80	1.10	2.89	4.97	1.01	3.07	0.59
FUK9716ol	bl ht	1.62	4.06	6.43	0.60	1.02	3.11	3.11	0.63	0.13	4.63
FUK9716px	cr+pw	4.96	1.94	4.79	2.95	2.01	3.11	3.11	0.63	2.07	1.43
KAR9803ol	bl ht	1.54	5.72	6.08	0.09	0.24	2.94	3.67	0.75	0.14	0.64
KAR9803px	cr+pw	4.25	1.91	2.08	0.34	0.22	2.94	3.67	0.75	2.30	0.15
TKB0001ol	cr+pw	4.63	3.91	7.43	2.19	2.44	3.16	1.63	0.33	0.07	31.91
TKB0001px	cr+pw	3.69	1.56	6.43	2.80	0.89	3.16	1.63	0.33	1.10	2.54
SSB0001ol	cr+pw	7.30	0.689	2.95	5.60	1.71	7.28	8.48	1.73	0.82	6.79
SSB0002ol	cr+pw	7.38	0.433	3.73	6.52	0.86	7.22	3.99	0.81	0.38	16.95
KR8404K	bl ht	24.0	0.035	1.00*3	23.16		2.89	4.97	1.01	76.69	0.30

cr+pw = total result of crushing and heating of crushed powder.

bl ht = total heating of bulk sample.

*1. Th/U = 4.9 is assumed.

*2. Ratio = $([^4He]_{radio})_{meas}/([^4He]_{radio})_{calc}$

*3. Atmospheric $^3He/^4He$ ratio is assumed.

He in coexisting pairs of olivine and clinopyroxene

As described above, radiogenic and cosmogenic He would make it difficult to identify the trapped He. In vacuo crushing is one of the effective methods to obtain the magmatic information avoiding secondary components (e. g., Kurz, 1986; Stuart et al., 1994). Thus, data obtained by crushing are used in the following discussion on He isotopic ratio. Figure 3–9 is a comparison of $^{3}He/^{4}He$ ratios in the clinopyroxene with those of the coexisting olivine. Although samples with high $^{3}He/^{4}He$ ratios in also olivine show similar $^{3}He/^{4}He$ ratios in coexisting clinopyroxene, samples with low $^{3}He/^{4}He$ ratios in olivine show significantly lower $^{3}He/^{4}He$ ratios in coexisting clinopyroxene. This indicates addition of radiogenic He (not post-eruptive additional origin) after crystallization of olivine and clinopyroxene in host magma before eruption. The source material of the contaminant He with low isotopic ratio ($<0.2R_A$, estimated from lowest $^{3}He/^{4}He$ ratio) will be discussed later.

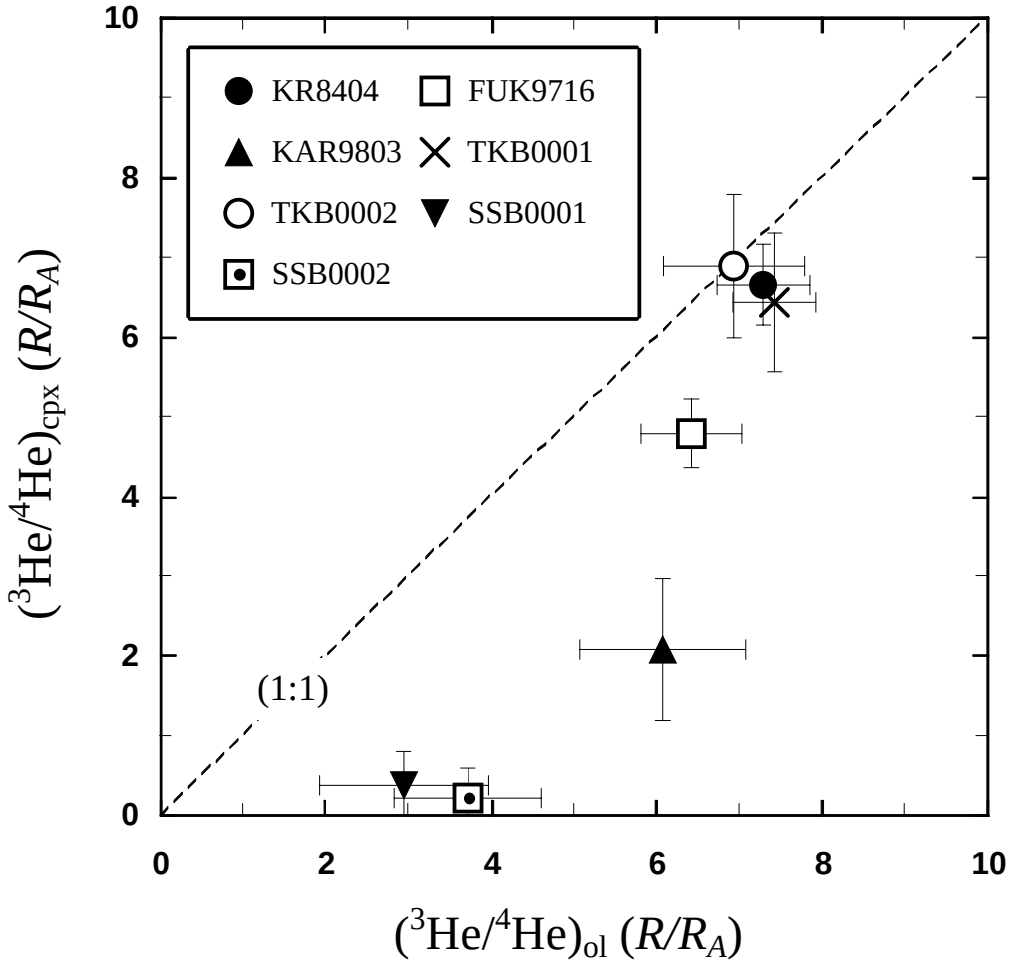

Fig. 3–9. Comparison of $^3He/^4He$ ratios in pairs of coexisting olivine (ol) and clinopyroxene (cpx) obtained with crushing method. The dashed line gives the 1:1 correlation line.

Ne, Kr and Xe isotopes

Ne three-isotope plot is shown in Fig. 3–10. Most of data obtained with both crushing and heating indicate that Ne isotope ratios are not distinct from atmospheric values. They may originally have trapped gases with atmospheric composition or they might have been contaminated by atmospheric gas due to scarcity of Ne in samples. Only five data seem to have distinguishable Ne isotopic ratios from the atmospheric values. These data are plotted on a MORB correlation line of Sarda et al. (1988), indicating the existence of Ne derived from upper mantle in the samples. Only one data seems to plot on a Loihi-Kilauea line defined by Honda et al. (1991), which is considered to be a signature of lower mantle Ne. However, large uncertainties due to scarcity of Ne in the sample preclude further discussion of Ne data. In addition, KAR9803 might shift from atmospheric ratios due to cosmogenic ^{21}Ne addition as revealed by presence of cosmogenic ^{3}He.

Kr and Xe isotopes were measured for most of the samples and shown in Table 3–4. In all cases, observed Kr and Xe isotopic ratios are indistinguishable from atmospheric composition within 1σ uncertainty, which would be due to small amounts of Kr and Xe in extracted gases, and to small anomalies in their isotopic ratios.

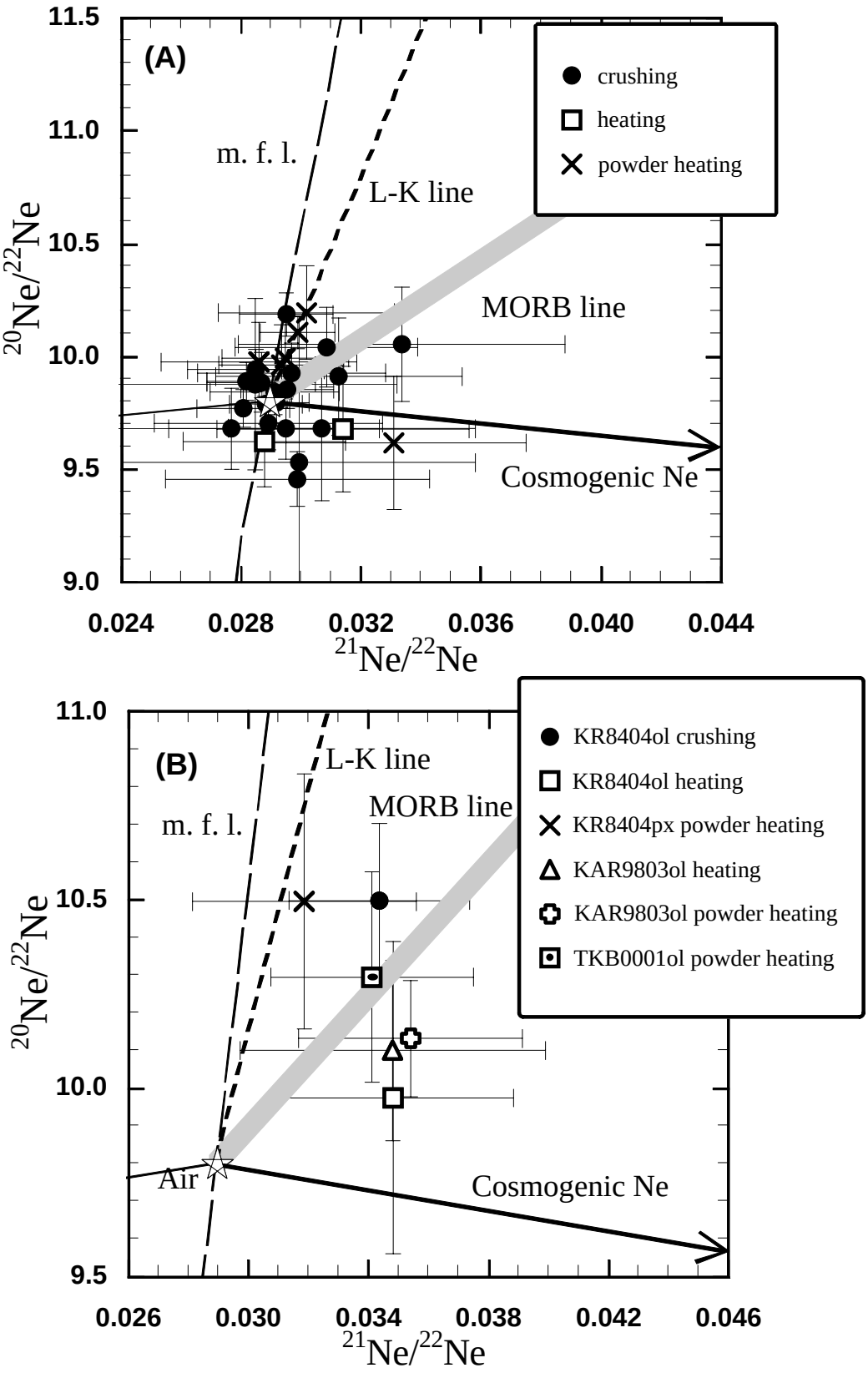

Fig. 3–10. Ne three isotope plot of (A) samples whose ratios are indistinguishable from atmospheric ratio and (B) representative samples. The correlation lines defined by MORB samples (MORB line; Sarda et al., 1988), Loihi-Kirauea line (L-K line; Honda et al.,1991), and mass fractionation line (m. f. l.) are shown for comparison.

He–Ar systematics

The $^{3}He/^{4}He$–$^{40}Ar/^{36}Ar$ diagram is shown in Fig. 3–11. $^{40}Ar/^{36}Ar$ ratios of the samples are obtained at high temperature with two-step heating or the highest ratio with multi-stage step heating to minimize contamination by adsorbed atmospheric Ar. $^{3}He/^{4}He$ ratios are obtained with crushing to remove post eruptive radiogenic and/or cosmogenic components. Arrows link olivine and clinopyroxene separated from the same host basalt. Clinopyroxene has $^{40}Ar/^{36}Ar$ ratio comparable with or lower than that of olivines as well as the case of $^{3}He/^{4}He$ ratio described before. Original isotopic characteristic of alkaline basalt magma is inferred from basalt without isotopic discrepancy between olivine and clinopyroxene, and with high $^{3}He/^{4}He$ and $^{40}Ar/^{36}Ar$ ratios. Based on the data for the samples, estimated $^{3}He/^{4}He$ and $^{40}Ar/^{36}Ar$ ratios of alkaline basalt magma are about $7R_A$ and more than 800, respectively. These ratios are distinct from MORB ($^{3}He/^{4}He \sim 8R_A$, $^{40}Ar/^{36}Ar < 28000$) and hotspot ($^{3}He/^{4}He > 8R_A$ for "high-^{3}He hotspot"), which will be discussed later.

The discrepancy between olivine and clinopyroxene in the same basalt seems to be significant for the samples from Kita-matsuura. Generally, such a discrepancy is explained by contamination of atmospheric noble gases or crustal fluids containing radiogenic ^{4}He at shallower depth (Hilton et al., 1995; Marty et al., 1994). Since this trend is apart from mixing line between the two components for magma and air, the discrepancy cannot be explained by simple contamination of atmospheric noble gases (Fig. 3–11). Diffusivity of He is so high at the magma temperature of alkaline basalt around 1300°C that He equilibrium between mm-sized phenocryst and magma is achieved during less than one month (Trull and Kurz, 1993). Therefore, the contamination by an unknown material whose $^{3}He/^{4}He$ ratio is less than $0.2R_A$ and $^{40}Ar/^{36}Ar$ ranges from 300 to 500 occurred just before an eruption. Since $^{3}He/^{4}He$ ratio of this components is lower than atmospheric value as well as that of crustal materials ($<0.02R_A$, Itoh, 1998) but $^{40}Ar/^{36}Ar$ ratio is distinct from that of crustal materials, this component is called sub-crustal He hereafter for convenience. Further discussion on the origin of the sub-crustal component will be later.

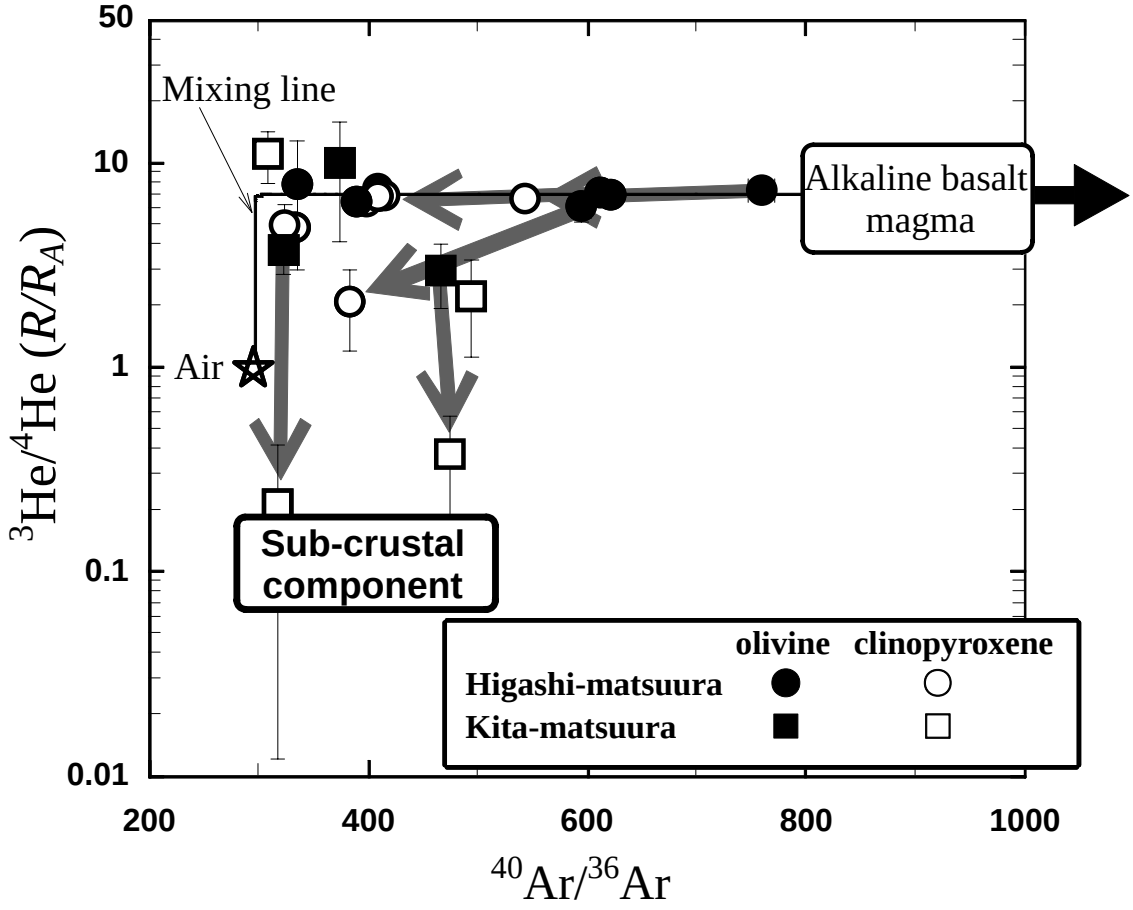

Fig. 3–11. $^3He/^4He$–$^{40}Ar/^{36}Ar$ diagram. Allows link coexisting olivine and clinopyroxene in the basalts. Calculated mixing line between air and alkaline basalts magma inferred from Higashi-matsuura basalts is shown as “Mixing line”. The trend composed by isotopic discrepancy between coexisting olivine and clinopyroxene suggests the contamination during magma ascending by low-$^3He/^4He$ (<0.2R_A) and $^{40}Ar/^{36}Ar$ (<500) component, which is called sub-crustal component hereafter.

Abundance pattern

Figure 3–12 shows the noble gas elemental abundance pattern of the samples. Relative noble gas abundances are expressed by F-values;

$$F(m)=(^{m}X/^{36}Ar)sample/(^{m}X/^{36}Ar)air$$

where ^{m}X corresponds to ^{4}He, ^{20}Ne, ^{84}Kr and ^{132}Xe, respectively. Atmospheric $^{m}X/^{36}Ar$ values are from Ozima and Podosek (1983). Results with heating extraction in Fig. 3–12 include noble gases extracted by crushing experiment when powdered sample after crushing is used. Heavy noble gases (Ar, Kr and Xe) in low temperature fractions of step heating in are subtracted in order to exclude atmospheric contamination.
It is noteworthy that all the samples are depleted in Ne and enriched in heavy noble gases. This feature is distinct from abundance patterns of MORB (Staudacher et al., 1989; Hiyagon et al., 1992) and Loihi samples (Kaneoka et al., 1983), which are representative of upper and lower mantle, respectively. In addition, the samples are less enriched in He compared to other mantle derived materials. These suggest that either noble gases of the sample do not originate from normal upper and lower mantle material or some processes to transport and extrude alkaline basalt magmas might have caused fractionation of noble gas composition. The abundance patterns of alkaline basalt are similar to the patterns of deep-sea water (Allègre et al., 1986/87), old oceanic crusts and oceanic sediments (e.g., Matsuda and Nagao, 1986; Staudacher and Allègre, 1988). Since heavy noble gases in low temperature fractions of step heating are subtracted as noted above, the enrichment in heavy noble gases may not be caused by artificial fractionation such as adsorption of atmospheric noble gases on the sample surface. On the other hand, relatively low enrichment in heavy noble gases and wide scattering of the enrichments with crushing may be result from adsorption of sample-derived heavy noble gases on the fresh surface of the sample. Clear systematics among F(20), F(84) and F(132) are found for alkaline basalt, which will be discussed later.

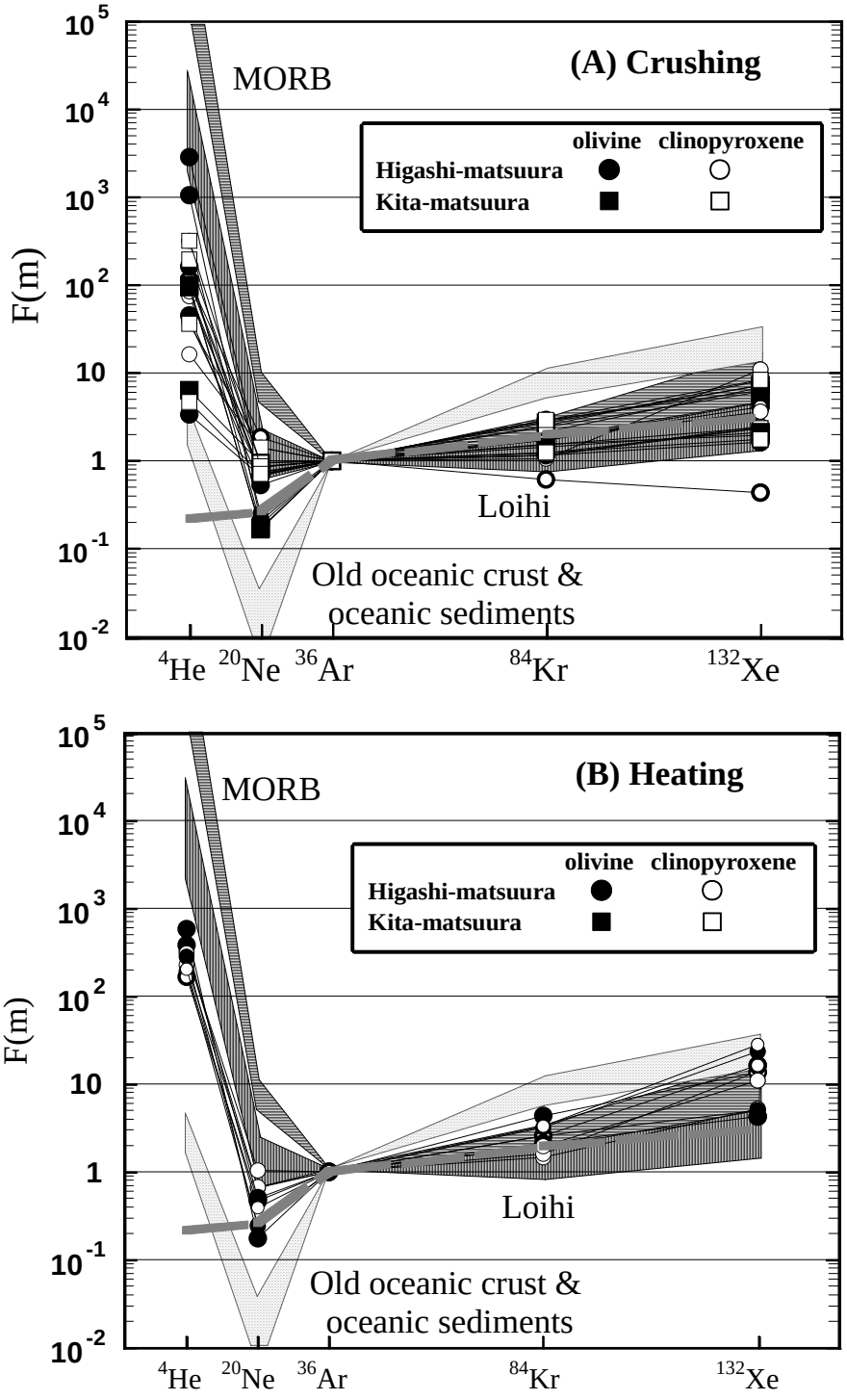

Fig. 3–12. Noble gas elemental abundance patterns for olivine and clinopyroxene separates from northwestern Kyushu basalts obtained with (A) crushing and (B) heating. The abundance pattern of deep-sea water (Allegre et al., 1986/87) is indicated by a broken line. Typical abundance patterns of MORB (Staudacher et al., 1989; Hiyagon et al., 1992), Loihi (Kaneoka et al., 1983), and old oceanic crust and oceanic sediments (Matsuda and Nagao, 1986, Staudacher and Allegre, 1988) are shown by hatches.

3–4. Discussion

3–4–1. Constraint on origin of alkaline basalt magma in northwestern Kyushu

As described above, the He and Ar in alkaline basalt magma in northwestern Kyushu is characterized by $^{3}He/^{4}He$ ratios slightly lower than MORB and $^{40}Ar/^{36}Ar$ ratio much lower than MORB. Since Nd–Sr isotopic ratios observed in Higashi-matsuura and Kita-matsuura (listed in Table 3–9, data from Nakamura et al., 1990; Notsu et al., 1991; Kakubuchi et al., 1995; Imai et al., 1995) are plotted near the depleted end of the trend composed by alkaline basalts from northwestern Kyushu (Fig. 3–13), the depleted endmember in the alkaline basalts has MORB-like but slightly modified noble gas isotopic composition. An exception is HRD0001, which is plotted near the enriched end of the trend.

The noble gas characteristics of the basalts analyzed in this study and literature data of Nd–Sr isotopic composition for the basalts are consistent with both models on the origin of alkaline volcanism previously proposed, one is a mantle plume model (e.g., Nakamura et al., 1985; Nakada and Kamata, 1991; Kakubuchi et al., 1995) and the other is MORB-like asthenospheric injection model (e.g., Nohda et al., 1988; Ohki et al., 1994; Okamura et al., 1998). In the mantle plume model, the depleted endmember in the alkaline basalts are considered to be derived from heated depleted material which surround a enriched mantle plume (Nakamura et al., 1990). Since Nd–Sr isotopes of the basalts used in this study show most depleted characteristics among the alkaline basalts from northwestern Kyushu, there is no contradiction between mantle plume model and lack of high $^{3}He/^{4}He$ ratio in the basalts analyzed in this study. On the other hand, if the alkaline basalts analyzed in this study are derived from injecting MORB-like asthenosphere, noble gas features of alkaline basalts support the idea that passive upwelling and decompression melting of asthenosphere induced by mantle convection accompanied with down going of the subducting slab (Nohda et al., 1988; Ohki et al., 1994).

There is no evidence that the source material of the alkaline basalt analyzed in this study is a mantle plume as well as in the case of Hawaii. Since $^{3}He/^{4}He$ ratio of the only one

sample (HRD0001) with enriched characteristics in Nd–Sr isotopes is 9.9±5.8R_A with large uncertainty due to low He concentration in the sample, He isotopic ratio of the enriched endmember is not constrained by the data obtained in this study. Thus, noble gas features of alkaline basalts cannot give constraints by itself which model is favorable. Further discussion will be later accompanying with noble gas data obtained for mantle-derived xenoliths from the back-arc region of southwestern Japan.

Table 3–9. Nd and Sr isotopic compositions of basalts from northwestern Kyushu.

Locality	Sample correspond	Sr (ppm)*1	$^{87}Sr/^{86}Sr$	εNd*2	Data source
Higashi-matsuura					
Keya	FUK9716	480.19	0.704097	1.93	Kakubuchi et al., 1995
Takashima	TKB0001	678.26	0.70426	1.6	Nakamura et al., 1990
	TKB0002	559.65			
Karatsu	KR8404	573.21	0.70417	2.2	Nakamura et al., 1990
	KAR9803	535.58			
Ohshima	OSM901	514.94	0.703775	1.97	Kakubuchi et al., 1995
Kita-matsuura					
Myokanji	SSB0001	460.2	0.704126	2.53	Imai et al., 1995
Yoshii	SSB0002	484.83	0.70399	3.8	Nakamura et al., 1990
Hirado	HRD0001	558.71	0.704915	1.07	Kakubuchi et al., 1995
Kokuzo	KKZ0001	368.13	0.70492–6		Notsu et al., 1991
Crustal materials *3					
Ganite		186	0.70561	0.2	Kagami et al., 1993; Imai et al., 1995
Gabbro		330	0.70640	1.0	Kagami et al., 1993; Imai et al., 1995

*1: Measured by XRF (Table 3–2).

*2: $\varepsilon Nd = [(^{143}Nd/^{144}Nd)_{sample}/(^{143}Nd/^{144}Nd)_{CHUR}-1]\times10^4$, where CHUR is chondritic uniform reservoir.

*3: Isotopic ratios are data for granitic and gabbroic xenoliths from Takashima (Kagami et al., 1993). Sr contents are data for typical granite (JG-1) and gabbro (JGb-1), respectively (Imai et al., 1995).

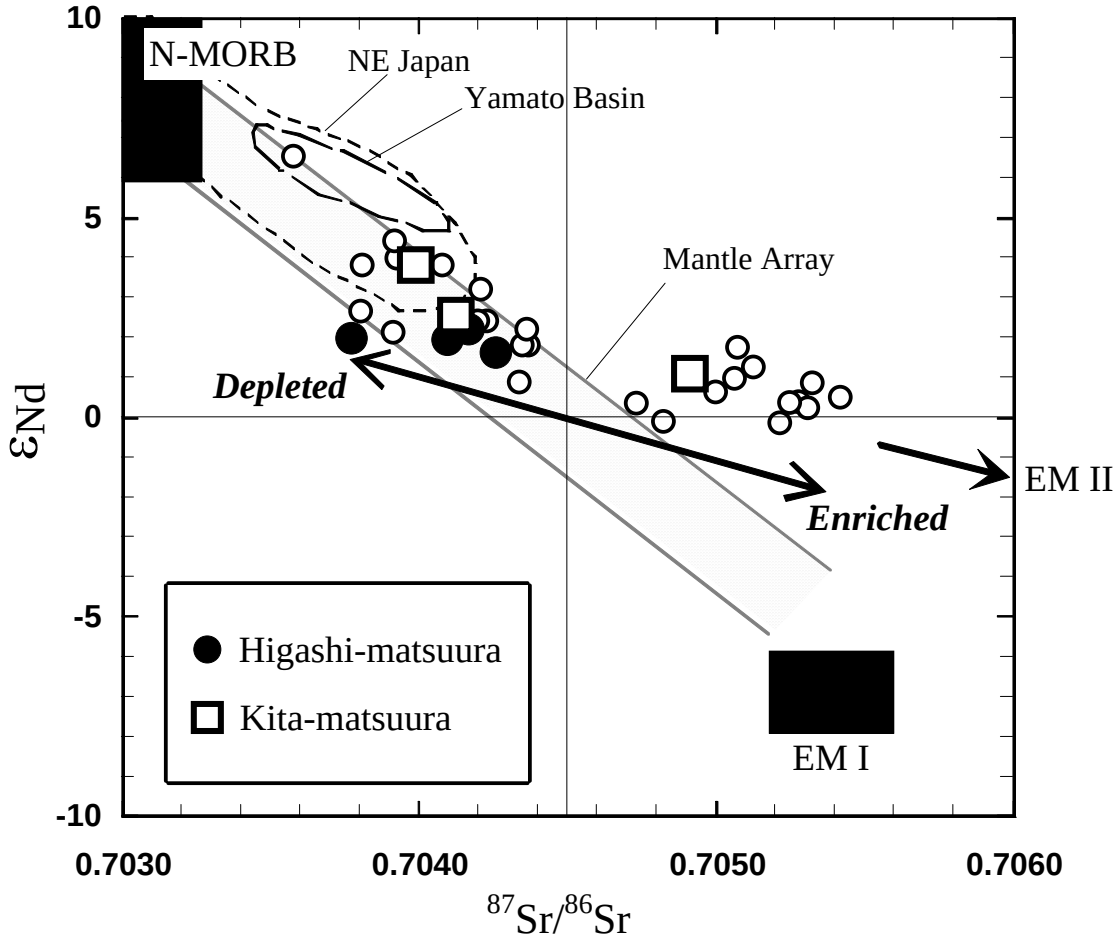

Fig. 3–14. Sr and Nd isotopic compositions of alkaline basalts from northwestern Kyushu. Open circles are alkaline basalts and tholeiites from northwestern Kyushu (Nakamura et al., 1990; Kakubuchi et al., 1995). Data of basalts from Yamato Basin, the Sea of Japan (Tatsumoto and Nakamura, 1991) and Quaternary volcanic rocks from northeast Japan (Nohda and Wasserburg, 1981) are also shown by hatches. The fields for the mantle components N-MORB, EM I and EM II (Zindler and Hart, 1986) are also shown.

3–4–2. Origin of the sub-crustal component

The suggestion that low $^{3}He/^{4}He$ ratios in some samples result from late-stage addition of low $^{3}He/^{4}He$ He is supported by the observation that clinopyroxenes have systematically lower $^{3}He/^{4}He$ ratios than coexisting olivine (Fig. 3–9). Similar isotopic disequilibrium was observed in arc samples from Etna by Marty et al. (1994), from Papua New Guinea by Patterson et al. (1997), and in oceanic intraplate basalts from Heard Island by Hilton et al. (1995). As shown in Fig. 3–9, the data obtained from alkaline basalts from northwestern Kyushu are consistent with these earlier results, and are interpreted to reflect a time dependent decrease in the He isotopic ratio of the parental magma resulting from addition of a low $^{3}He/^{4}He$ component, which is called sub-crustal component in this thesis.

Petrographic textures and major element composition of the basalts from Kita-matsuura, where the isotopic disequilibrium is more significant than that in Higashi-matsuura, indicate that olivine crystallized within magma before or at the same time of clinopyroxene crystallization (Yanagi and Maeda, 1998). In addition, since He diffusivity in clinopyroxene is higher than that in olivine (Trull and Kurz, 1993), He in clinopyroxene would be more affected by radiogenic He at a lower temperature when olivine has become closed in effect (Hilton et al., 1995; Marty et al., 1994). These are consistent with that clinopyroxene trapped He from a parental magma with a decreasing $^{3}He/^{4}He$ ratio.

Three possible sources proposed as the low $^{3}He/^{4}He$ component in previous studies which report isotopic discrepancy between olivine and clinopyroxene are; addition of atmospheric He, addition of radiogenic He from crustal materials, and evolution of $^{3}He/^{4}He$ ratio of magma (Patterson et al., 1997 and references therein).

Atmospheric contamination and diffusive loss

Because of the low He concentration in the atmosphere, addition of atmospheric He into the sample is negligible. The facts that He/Ne ratios (60–200) of low $^{3}He/^{4}He$ samples are significantly higher than atmospheric ratio (0.318) and that the data plot aside from

mixing line between magma and air in Fig. 3–11 are support negligible contamination of atmospheric He.

Helium isotope ratios could theoretically be affected by post- or syn-eruptive diffusive loss of He. Trull and Kurz (1993) experimentally determined the isotopic diffusivity ratio (D^3He/D^4He) for helium in olivine and clinopyroxene to be almost one and concluded that isotopic fractionation of residual He is unlikely to occur. Taking the value for the diffusivity ratio in clinopyroxene of 1.04 (Trull and Kurz, 1993) and assuming a Rayleigh fractionation process, a 3 order of magnitude decrease in He abundance will result in only a 24% decrease in the ^{3}He/^{4}He ratio. Such diffusive loss would lower the ^{3}He/^{4}He ratio from $7R_A$ to $5.3R_A$, much higher than the lowest observed value of about $0.3R_A$. In addition, the He abundances in clinopyroxene samples with low ^{3}He/^{4}He ratios are comparable with or only an order of magnitude smaller than those of other samples, indicating that significant diffusive loss of He is unlikely.

Crustal fluids

Contamination by crustal fluids containing radiogenic ^{4}He at shallower depth was proposed as a candidate for the low ^{3}He/^{4}He contaminant (Hilton et al., 1995). Since Oligocene to Miocene shallow-water sedimentary basin is well developed in northwestern Kyushu (Yanagi and Maeda, 1998), fossil water, which had filtered into crust enriched in radiogenic He with $0.014R_A$ (JG-1 granite Miura and Nagao, 1991), and have atmospheric Ar isotopic ratio due to its meteoric origin, can be considered as a carrier of radiogenic He and atmospheric Ar. Assuming that He concentration in groundwater is 1×10^{-5}cm^{3}STP/g (Ozima and Podosek, 1983), initial ^{3}He/^{4}He ratio of magma is $7R_A$, and partition coefficient between olivine and melt is 0.07 (Hiyagon and Ozima, 1986), required amount of water contaminated into 1g of magma to explain He data of SSB0001 olivine and clinopyroxene is 0.31g. The ^{87}Sr/^{86}Sr ratio of crustal fluids is unknown. However, the ratio of fossil shells from Tertiary to Quaternary sediment in Cheju Island ranges from 0.7088 to 0.7091 (Kim et al., 1999). If crustal fluids in sedimentary basin in northwestern Kyushu have similar Sr isotopic ratio to those of Cheju Island, quite large amount of fossil water required to decrease ^{3}He/^{4}He ratio will cause drastic increase of ^{87}Sr/^{86}Sr ratio of magma. In addition, since a magma chamber

of alkaline basalt from northwestern Kyushu is 70km deep in the mantle (Kuno, 1964) and alkaline basalt usually erupted directly from the chamber in a few days (Kushiro et al, 1976), interaction with crustal fluids (groundwater for example) as in the case of acidic magma (Hanyu, 1995) is unlikely to occur. After all, the idea that contamination of fossil water caused lowering of $^3He/^4He$ ratio of magma is precluded.

Evolution of $^3He/^4He$ ratio of magma

Considering diffusivity of He in olivine and clinopyroxene under temperature of alkaline basalt magma at around 1300°C (Trull and Kurz, 1993), isotopic equilibrium between mm-sized phenocryst and host magma would have achieved over 10–100 years (Marty et al., 1994; Hilton et al., 1995). Therefore it is unlikely that He isotopic disequilibrium between olivine and clinopyroxene could reflect the relatively slow isotopic response to magma aging except in the case of extremely high (U+Th)/He ratios. Given the He concentration in SSB0001 magma of $2.4\times10^{-7}cm^3STP/g$ estimated from $[^4He]_{trap} = 1.7\times10^{-8}cm^3STP/g$ and partition coefficient of 0.07 (Hiyagon and Ozima, 1986), Th content of SSB0001 basalt of 8.48ppm, and Th/U=5.75 (JB-1a, Imai et al., 1995), the $^3He/^4He$ ratio of magma decrease at only 0.02% during 100 years. Therefore, evolution of $^3He/^4He$ ratio of magma with age cannot explain isotopic disequilibrium between olivine and clinopyroxene.

Crustal rocks

It is possible that decrease of $^3He/^4He$ ratio is caused by assimilation of continental crustal rocks. Similar interaction with crust has been argued for a number of cases including subduction related volcanic rocks (Patterson et al., 1997 and references therein), as well as in intraplate samples from Heard Island (Hilton et al., 1995). Therefore, assimilation of lower crustal rocks during accumulation probably account for the low $^3He/^4He$ component. In Fig. 3–15, the results of mixing calculations are shown, with which the effects of crustal assimilation on the He isotopes can be compared with other chemical parameters. In the mixing calculation, concentration of He and $^3He/^4He$ ratio of crustal material are $2.9\times10^{-6}cm^3STP/g$ and $0.012R_A$, data for granodiorite xenolith from Takashima (Itoh, 1998), respectively, and SiO_2 content and K_2O/P_2O_5 are 72.3% and 40, data for typical granodiorite (JG-1, standard rock of Geological Survey

of Japan; Imai et al., 1995), respectively. In each figure, the He concentration of the alkaline basalt magma is allowed to vary from 10^{-8} to 10^{-6} cm^3STP/g. In order to explain low $^3He/^4He$ ratios of clinopyroxenes in Kita-matsuura basalts, He concentration of the magma of 10^{-8} cm^3STP/g is required for the magma. Since distribution coefficient of He between olivine and basaltic melt experimentally determined is lower than 0.07 (Hiyagon and Ozima, 1986), the required He concentration of magma, which is comparable to that of concentration of trapped He in olivines and clinopyroxene ($0.8–3.9\times10^{-8}cm^3STP/g$ from Table 3–8), is too low and thus improbable.

In addition, crustal materials are expected to have higher $^{40}Ar/^{36}Ar$ ratios than 500 as a result from accumulation of ^{40}Ar produced from ^{40}K. Figure 3–17 is He–Ar isotopic diagram for the samples and crustal xenoliths observed in northwestern Kyushu (Itoh, 1998). As representative crustal materials, the data for JG-1 (granodiorite) and JGb-1 (gabbro) are also shown in the figure (Miura and Nagao, 1995). As shown in Fig. 3–16, the trend of the sample cannot be explained by three components mixing; atmospheric component, alkaline basalt magma, and crustal materials. In conclusion, the possibility of assimilation of granotoid rocks at shallow depth is precluded, because their He–Ar isotope ratios are far away from isotopic composition of the sub-crustal component and there is no other chemical evidence of assimilation of crustal rocks.

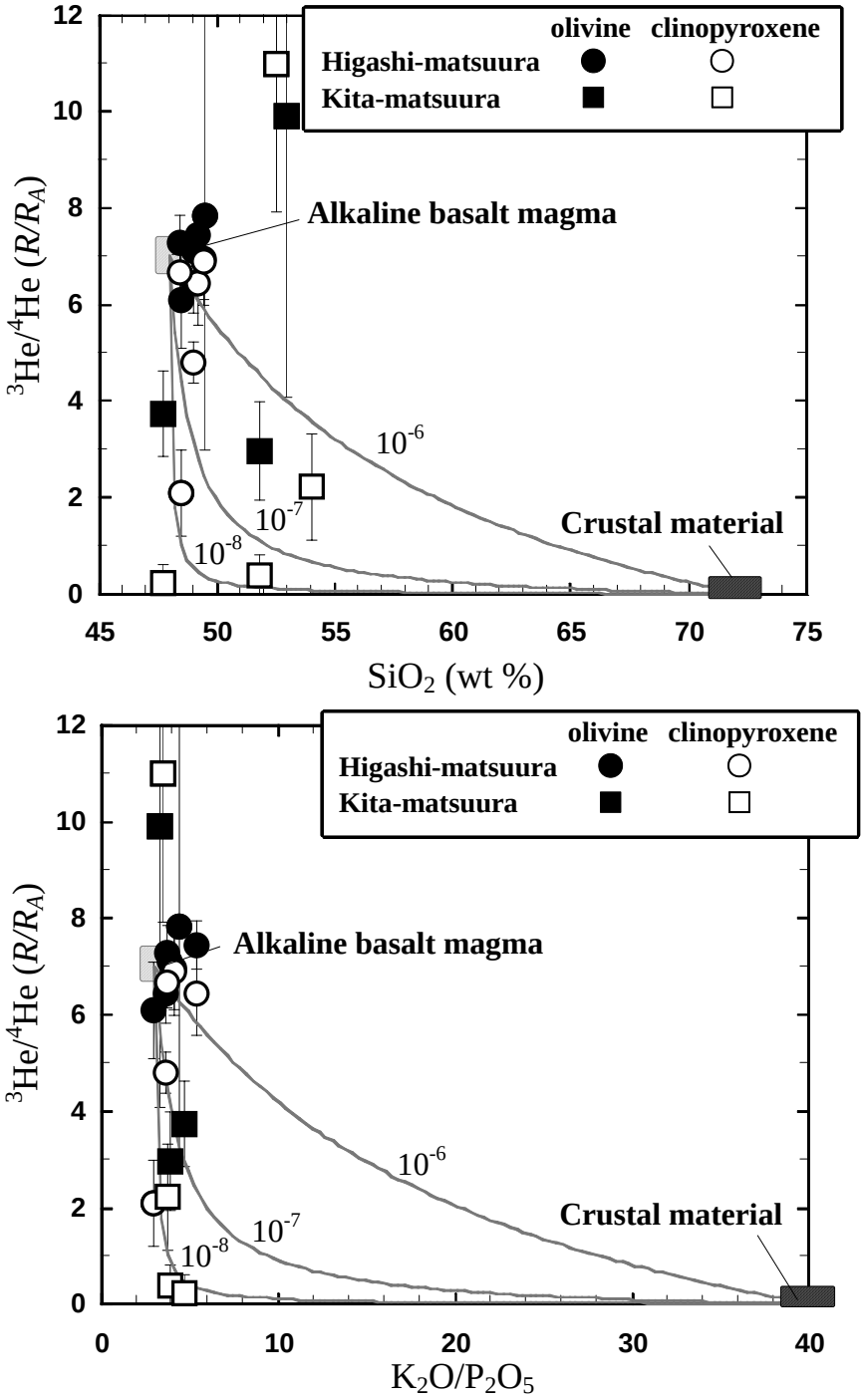

Fig. 3–15. Helium isotopic composition as a function of (A) silica content and (B) K/P ratio (plotted as K_2O/P_2O_5), often used as indexes of crustal contamination. Mixing lines are drawn assuming He concentration of magma range from 10^{-8} to 10^{-6} cm^3STP/g. Crustal material are represented by granodiorite xenoliths from Takashima for He (Itoh, 1998) and JG-1 granodiorite for silica content and K_2O/P_2O_5 (Imai et al., 1995).

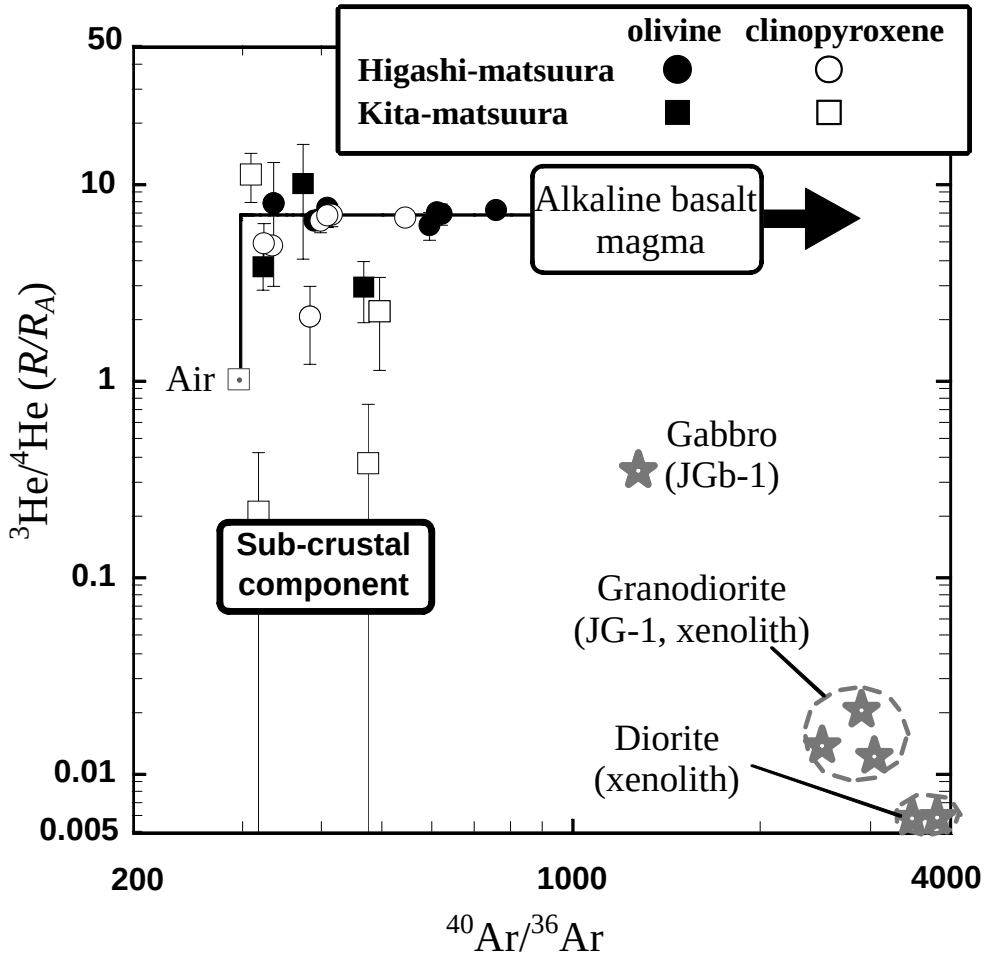

Fig. 3–16. He–Ar isotopic diagram for the basalts from northwestern Kyushu and crustal materials which are granodiorite and diorite xenolith from Takashima, northwestern Kyushu (Itoh, 1998), JG-1 granodiorite and JGb-1 gabbro (Miura and Nagao, 1995).

Accumulated magma beneath Kita-matsuura

Yanagi and Maeda (1998) show that alkaline basalts from Kita-matsuura is mixing product between primitive magma and highly fractionated magma (Fig. 3–5). The highly fractionated magma seems to have accumulated in the eroded portion of the lower crust since 30Ma. The source material of accumulated magma is almost the same composition with the source of alkaline basalt erupted in northwestern Kyushu, because the fractional crystallization trends in MgO-SiO_2 diagram (Fig. 3–6) made by basalts from Higashi-matsuura and Kita-matsuura start from the same point, suggesting that the evolution of all magma in this region starts from common primitive magma composition. This is supported by the fact that Nd and Sr isotopic compositions of basalts from Higashi-matsuura and Kita-matsuura are explained in terms of an identical mixing trend (Kakubuchi et al., 1995). Therefore, the accumulated magma beneath lower crust might have characteristics of the sub-crustal component. The possible mechanisms to decrease $^{3}He/^{4}He$ ratio of accumulated magma are, (1) assimilation of lower crustal material directly above the magma chamber, (2) evolution of $^{3}He/^{4}He$ ratio of the accumulated magma since 30Ma, and (3) assimilation of uppermost mantle surrounding the magma chamber.

Lower crustal material

Lower crust beneath northwestern Kyushu is composed of gabbro, which is found as xenolith in Takashima alkaline basalts (Kobayashi and Arai, 1981). There is no noble gas data on gabbroic xenoliths from this region, thus noble gas data of gabbro (JGb-1: standard rock of Geological Survey of Japan) from Utsushigatake, Fukushima Prefecture, Japan (Miura and Nagao, 1995) is used for mixing calculation. To reduce $^{3}He/^{4}He$ ratio from $7R_A$ to $0.2R_A$, over 90% of gabbro is required. However, the amount of crustal assimilation is limited by Sr isotopic ratio. Given Sr concentration of magma (100ppm) estimated by Kakubuchi et al. (1995) and $^{87}Sr/^{86}Sr$ isotopic ratios of the northwest Kyushu basalts ranging from 0.7037 to 0.7050 (Kakubuchi et al., 1995; Notsu et al., 1991; Imai et al., 1995), degree of assimilation greater than 10% by weight of gabbro with Sr content of 330ppm and $^{87}Sr/^{86}Sr$ ratio of 0.70524 (Imai et al., 1995) into the magma is highly unlikely. In addition, $^{40}Ar/^{36}Ar$ ratio of JGb-1 is 1280, which is a

lower limit because the ratio was obtained with single step heating probably containing contamination of adsorbed air (Miura and Nagao, 1995), but still much higher than the ratio of the contaminant. Therefore, it is difficult to explain the sample trend by three component mixing between air, alkaline basalt magma, and gabbro (JGb-1), otherwise lower crustal material beneath Kyushu have already been contaminated by atmospheric Ar (Fig. 3–16). One possible mechanism for atmospheric contamination is dragging seawater or sediment into the mantle wedge. However, the gabbro is considered to have formed in Cretaceous-Paleogene (Kagami et al., 1992) almost the same period when JGb-1 was formed in northeast Japan (103Ma, Imai et al., 1995). Thus, it is unlikely that source material of gabbroic xenolith only beneath northwestern Kyushu was contaminated by atmospheric Ar and that $^{40}Ar/^{36}Ar$ ratio has not evolved with the age. It is possible that extraction of He from a volume of crustal rocks larger than that directly assimilated will take place (so-called decoupling of noble gases and other geochemical tracers), invalidating a simple bulk-mixing model. However, selective He extraction in order to explain $^{3}He/^{4}He$ ratios and $^{87}Sr/^{86}Sr$ ratios of the samples required He/Sr atomic ratio should be 0.248, that is 700 times of that of JGb-1, thus it is not a case.

Evolution of $^{3}He/^{4}He$ ratio in the accumulated magma

Evolution of $^{3}He/^{4}He$ ratio in the accumulated magma since 30 Ma, which is the age to start to accumulate the magma beneath lower crust (Yanagi and Maeda, 1998) to 7Ma (eruption age of SSB0001 basalt) is another possible explanation for the low $^{3}He/^{4}He$ of the accumulated magma. Given the same He and U concentration in the magma estimated above, and initial $^{3}He/^{4}He$ ratio of $7R_A$ as in the case of alkaline basalt magma in Higashi-matsuura, $^{3}He/^{4}He$ ratio of the magma will reduce to $0.17R_A$, which agrees well with required $^{3}He/^{4}He$ ratio of the contaminant. However, $^{40}Ar/^{36}Ar$ ratio of magma increases concurrently with evolution of $^{3}He/^{4}He$ ratio, because ^{40}Ar produced by electron capture decay of ^{40}K accumulates in magma as well as ^{4}He. Thus, $^{40}Ar/^{36}Ar$ ratio of accumulated magma should be higher than that of the original alkaline basalt magma, because source material of accumulated magma and that of relatively primitive basalt (in Higashi-matsuura) are the same in composition. Therefore, evolution of $^{3}He/^{4}He$ ratio contradicts with the low $^{40}Ar/^{36}Ar$ ratio of the accumulated magma by itself.

Uppermost mantle beneath northwestern Kyushu

Another proposed explanation to decrease $^{3}He/^{4}He$ and $^{40}Ar/^{36}Ar$ ratio of the accumulated magma is that uppermost mantle beneath northwestern Kyushu contains noble gas with sub-crustal He and Ar. The uppermost mantle material beneath Shihote-Alin, Siberia, where subduction was active from Late Cretaceous to Late Oligocene, has similarly low isotopic compositions (Yamamoto et al., 2001). The low $^{3}He/^{4}He$ and $^{40}Ar/^{36}Ar$ ratios in the mantle of this region are explained by radioactive decay, with large-scale contamination of parental nuclides such as U, Th and K into the mantle by subducted crustal materials, and contamination by atmospheric component, which is much effective to Ar. Subduction of the Izanagi plate and the Pacific plate was active in northwestern Kyushu from Triassic to Cretaceous (Maruyama et al., 1997), as well as Shihote-Alin. Therefore, there is possibility that the uppermost mantle beneath Kyushu have noble gas isotopic features similar to Shihote-Alin. Alternatively, the uppermost mantle beneath Kyushu might have been metasomatized by ancient subduction processes, and retain vestige of the metasomatism as radiogenic He and atmospheric Ar isotopic ratios. The idea of metasomatized uppermost mantle beneath Kita-matsuura is supported by the noble gas elemental ratio (F-value), which will be discussed later combined with the results of mantle-derived xenoliths.

In conclusion, mixing with accumulated magma contaminated by metasomatized mantle during ancient subduction are plausible candidates for the sub-crustal component observed in Kita-matsuura basalts. Alternatively, the uppermost mantle beneath Kyushu might be contaminated with U, Th and atmospheric Ar from ancient subduction materials.

4. Noble gases in mantle xenoliths around the Sea of Japan

4–1. Geological and geochemical background

4–1–1. Mantle-derived xenolith around the Sea of Japan

The upper mantle materials can be sampled as massive peridotite that have been tectonically exposed to the Earth's surface, or as peridotite xenoliths entrained in alkaline magma. In the latter case, rapid transportation, probably in less than a few tens of hours, prevents the re-equilibration of mantle materials to lower pressure and temperature (Kushiro et al., 1976). Therefore, ultramafic xenoliths are believed to be fragments of the most pristine mantle. They offer a potentially important source of information about the physical and chemical properties of upper mantle and its chemical and isotopic evolution. Therefore, ultramafic xenoliths have been an important material for many mineralogical, petrological, geochemical and geothermal investigations. Peridotite xenoliths are usually brought up by alkaline basalts of intraplate type or kimberlites and related magmas and, therefore, represent the upper mantle beneath hotspots, continental rifts and continental cratons. Ultramafic xenoliths included within arc-related magmas may give us direct information of the mantle wedge. Arc magmas carrying mantle xenoliths are, however, very rare on Earth.

The back-arc side of the Southwest Japan has been a locus of intraplate volcanism activity since late Miocene (chapter 1). Several tens of volcanic centers are known to yield mantle-derived xenoliths, some of which have been studied by a number of researchers. Representative localities of mantle-derived xenoliths are shown in Fig. 4–1. (Umino and Yoshizawa, 1996; Hee, 1998). Previous studies indicate regional heterogeneity of the upper mantle chemistry and mineralogy beneath back-arc side of Japan. The upper mantle beneath Takashima and Oki-Dogo is dominated by thick cumulus mantle (Kobayashi and Arai, 1981; Takahashi, 1978), while On-yama, Kurose and Fukue-jima are underlain by residual peridotite (Arai and Muraoka, 1992; Arai and Abe, 1994; Umino and Yoshizawa, 1996). Beneath Aratoyama and Shingu both residual and cumulus peridotites are severely metasomatized through melt migration and

associated with later magmatism (Goto and Arai, 1987). Such heterogeneity is a manifestation of complex processes affecting the back-arc upper mantle, among which probably the most important is the opening of the Japan Sea. The remnant of this tectonic event is at present observed as anomalies of high heat flow and geotherm in and around the Japan Sea (Jessop, 1990; Yoshii, 1979; Umino and Yoshizawa, 1996). These features are considered to be caused by injection of the hot-asthenosphere and/or post-rifting uprise of mantle diapers which produced alkaline basalt magma in this region (Umino and Yoshizawa, 1996).

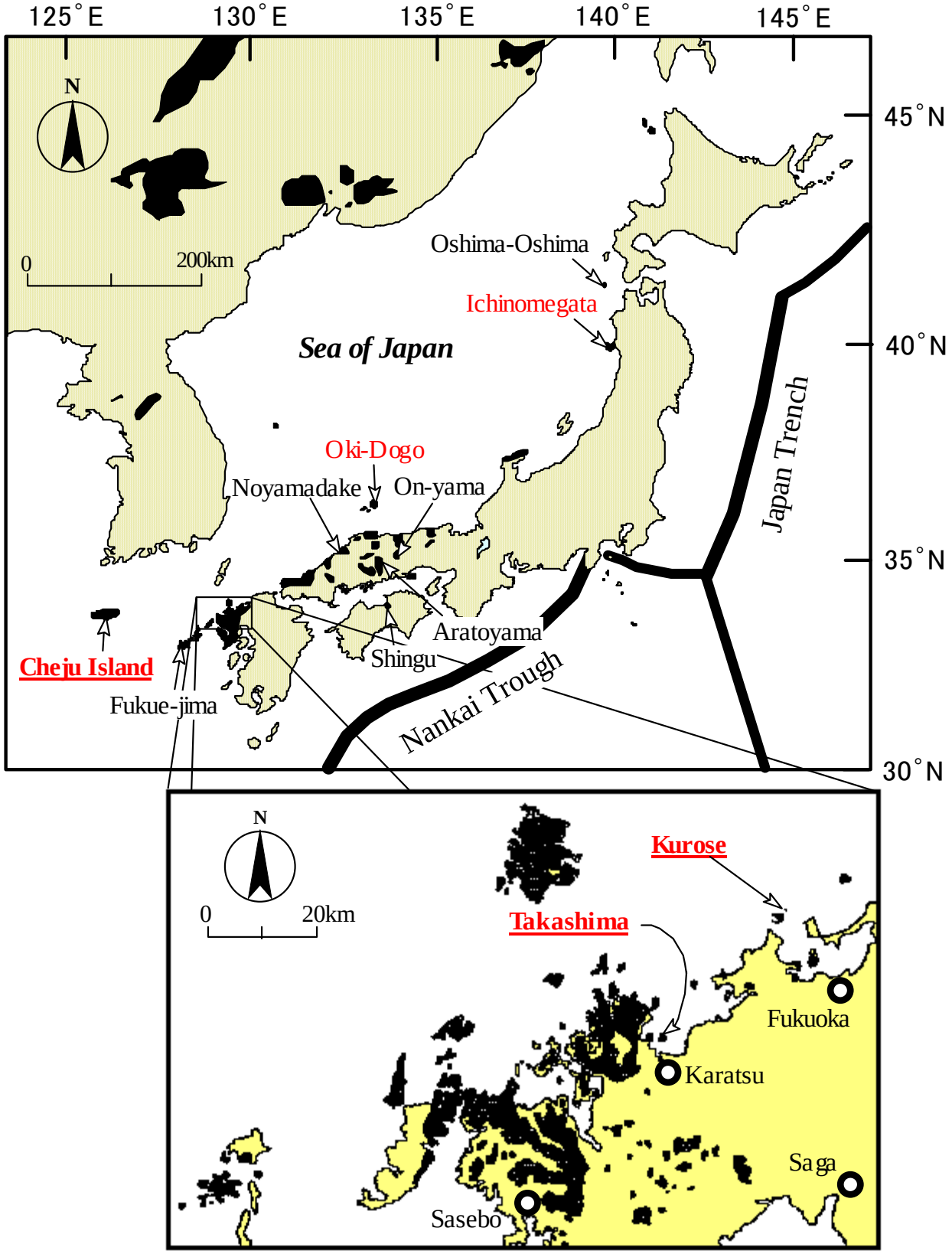

Fig. 4–1. Location map of the samples studied in this work (underlined). Other representative localities of mantle xenoliths are shown for reference (Umino and Yoshizawa, 1996; Hee, 1998). Black part are distribution of Cenozoic alkaline basalt (Kurasawa, 1967; Nakamura et al., 1990).

4–1–2. Noble gases in mantle derived xenoliths from subduction zone

Since peridotite xenoliths from arc regions are believed to represent part of the mantle wedge above the subducting slab, analysis of them may offer an important insight into the noble gas transfer from subducting material to the overlying mantle wedge. Noble gas isotopic compositions in a wedge mantle at a subduction zone indicate heavy contamination by atmospheric component probably introduced by the subducting seawater except He, which shows little difference from that in the asthenospheric mantle as represented by MORB (Miura and Nagao, 1991; Porcelli, et al., 1992; Nagao and Takahashi, 1993) in spite of He in oceanic crust dominated by radiogenic component (Staudacher and Allègre, 1988). Since He has strong preference for the fluid phase (Trull and Kurz, 1993), the lack of a distinctive He isotopic composition in subduction-derived samples is thought to indicate that He in the subducting slab is lost early in the subduction process probably with fluids, which is derived from the dehydration of subducting materials and are thought to play an important role in the generation of arc magmas (Tatsumi, 1989; Stolper and Newman, 1994), not reaching beneath mantle wedge where mantle-derived xenolith originally existed (Patterson et al., 1997). One more explanation is that the volumetric contribution from the slab-derived fluid or melt is extremely small (Eiler et al., 1998). However, Dodson and Brandon (1999) suggested that radiogenic ^{4}He-rich fluid or melt from metasomatized mantle directory above the slab has ascended and modified quite small portion of mantle represented by a few xenoliths from Simcoe, back-arc region of Cascade volcanic arc. Therefore, further investigation on noble gases in mantle-derived xenoliths from arc tectonic settings are needed.

Since minerals in mantle xenoliths such as olivine, clinopyroxene and orthopyroxene have higher retentivities of noble gas than other minerals and groundmass in volcanic rocks (Harts, 1984; Trull and Kurz, 1993), mantle xenoliths are ideal for noble gas studies. However, a key issue in interpreting noble gases especially He isotope results in xenoliths is whether the measured value reflect the nature of the mantle where xenolith originally existed, or has been overprinted by noble gases introduced from host magma. It has been reported that He in the xenoliths from Hawaii and Samoa is distinct from

host basalts, indicating that the host basalts are not a primary source of He trapped in the xenoliths (Kaneoka and Takaoka, 1978; Poreda and Farley, 1992). On the other hand, He in some parts of Hawaiian xenoliths has revealed exchange with that in the host basalt magma (Rocholl et al., 1996). Kaneoka et al. (1983) revealed that Ar in xenoliths and host basalts from Loihi Seamount, Hawaii have not reached isotopic equilibrium but He have, reflecting higher mobility of He than Ar. Dodson and Brandon, (1999) has also reported that only core part of large (ca. 10cm in diameter) xenoliths retain original He isotopic ratio, while He in other smaller xenoliths have been overprinted by He in the host basalt magma.

I measured noble gas isotopic compositions of mantle-derived xenoliths in Cenozoic alkaline basalt from northwestern Kyushu and Cheju Island, to investigate the noble gas characteristics of the sub-continental mantle around this region, together with the origin of alkaline volcanism in southwestern Japan.

4–2. Samples and experiments

4–2–1. Sample Localities

Several Cenozoic basalts containing mantle-derived xenoliths are distributed in northeastern China and around the Sea of Japan (e.g., Ishibashi, 1970; Takahashi, 1978; Umino and Yoshizawa, 1996; Hee, 1998). Thirty-two xenoliths from three Cenozoic volcanoes were collected for analysis, as shown in locality map (Fig. 4–1). Two of the volcanoes are Takashima and Kurose, monogenetic alkaline basalt volcanoes in northwestern Kyushu, and the other is Cheju Island, a shied volcanic island located in Korean straight to the southwest of the Korean Peninsula. Details of analyzed samples are listed in Table 4–1.

Takashima and Kurose

Takashima (33°28’25”N, 129°59’26’’E) is a small island in Karatsu Bay, Saga Prefecture, with about 3km in circumference. The island composed by pre-Tertiary granodiorite, granite and Pleistocene alkaline basalt flows covering the granitic rocks. The basalt flows commonly contain mantle-derived xenoliths, with diameters up to 20–30cm, gabbroic xenoliths of possible lower crustal origin, and also xenoliths of the basement rock (Kuno, 1964; Ishibashi, 1970; Kobayashi and Arai, 1981). The eruption age of the alkaline basalt is 3.00±0.04Ma (Nakamura et al., 1986). The rock type of mantle-derived xenoliths are dunite, wehrlite and pyroxenite, which were considered to be derived from cumulus mantle between mantle peridotite and Moho, through which Takashima alkaline basalt erupted, and dunite constitutes the deepest layer of the cumulus mantle (Ishibashi, 1970; Kobayashi and Arai, 1981). Residual mantle peridotites (harzburgite/ lherzolite) are almost absent in the Takashima xenolith suite; only one lherzolite xenolith has been found (Arai and Kobayashi, 1984). 14 mantle-derived xenoliths (14 dunites and 1 clinopyroxenite) were sampled from boulder stone, which have fallen down from cliff of lava flow to the east-north-west coast of the island (Table 4–1) in Aug-Sep and December 1997 and October 1998.
Kurose (33°41’42”E, 130°13’58”E), located near the Genkai-jima in the Hakata Bay, Fukuoka Prefecture, is composed of several small rocks of alkaline basalts. Uto et al.

(1993) reported the K-Ar ages for two blocks of alkaline basalts from Kurose to be 1.14±0.12 and 1.10±0.22 Ma. The activity of the Kurose is younger than other volcanics in Southwestern Japan arc which contain ultramafic xenoliths. Harzburgite and clinopyroxene-poor lherzolite are dominant among the Kurose peridotite (Arai and Abe, 1994). The xenoliths derived from the so-called cumulus mantle (Takahashi, 1978) are much less abundant (less than one twentieth in volume) than those of the residual mantle peridotite, possibly implying the very thin cumulus mantle (Arai and Abe, 1994). Eight xenoliths (lherzolite and dunite) were collected in October 1998.

Cheju Island

Cheju Island, which rises to an elevation of 1950m above sea level, is situated about 90km south of the Korean Peninsula. This island is a shield volcano formed by central eruptions in the vicinity of Mount Halla (1950m), where eruptions occurred from the upper Pliocene to the lower Pleistocene, and eruptive activity have been continuing to historical time (Lee, 1982). The island consists mainly of basaltic lava flows with minor pyroclastic rocks corresponding petorographically to the alkaline olivine basalt-trachyte association (Lee, 1982). Ultramafic xenoliths are observed in lava flow of Quaternary alkaline basalt from eastern part of the island (Yun et al., 1998, Hee, 1998). Spinel lherzolites are the major constituent of ultramafic xenoliths, and clinopyroxenite, wehrlite and websterite are also observed. All the ultramafic xenoliths are thought to be derived from the lithospheric upper mantle (Yun et al., 1998; Hee, 1998). Two spinel lherzolites were collected at Sinasanri (Yun et al., 1998; Hee, 1998) in May 1999 for this study.

Table 4–1. List of xenolith samples from back-arc region of southwestern Japan.

Sample	Rock type[*1]	Sub-sample	Phase[*2]	Noble gas analysis[*3]		
				cr	tf	sw ht
Takashima (northwestern Kyushu)						
TKS01	dun	TKS01ol	ol	○	○	○
TKY01	dun	TKY01ol	ol	○	○	○
TKD1350	dun	TKD1350ol	ol	○	○	
TKD1550	dun	TKD1550ol	ol	○	○	○
TKD1250	dun	TKD1250ol	ol	○	○	
TKD1120	dun	TKD1120ol	ol	○	○	
TKD0900	dun	TKD0900ol	ol	○		
TKD1000	dun	TKD1000ol	ol	○		
TKD1340	dun	TKD1340ol	ol	○	○	
TKD1610	dun	TKD1610ol	ol	○	○	
TKC1212	dun	TKC1212ol	ol	○	○	
TKC1422	dun	TKC1422ol	ol	○	○	
TKC0222	dun	TKC0222ol	ol	○	○	
TKC014[*4]	dun	TKC014Aol	ol	○		○
		TKC014Bol	ol	○		○
		TKC014Col	ol	○		○
TKP1040	cpx	TKP1040px	cpx			○
Kurose (northwestern Kyushu)						
KRS9803	lhz	KRS9803ol	ol	○		
		KRS9803opx	opx	○		
KRS9806	dun	KRS9806ol	ol	○		
KRS9814	lhz	KRS9814ol	ol		○	
KRS9810	lhz	KRS9810wr	wr		○	
KRS9811	lhz	KRS9811wr	wr		○	
KRS9805	lhz	KRS9805wr	wr		○	
KRS9801	lhz	KRS9801wr	wr		○	
KRS9807	lhz	KRS9807wr	wr		○	
Cheju Island						
CHJ9901	lhz	CHJ9901ol	ol	○		
		CHJ9901opx	opx	○		
CHJ9902	lhz	CHJ9902ol	ol	○		
		CHJ9902opx	opx	○		

*1. dun: dunite, cpx: clinopyroxenite, lhz: lherzolite

*2. ol: olivine, cpx: clinopyroxene, opx: orthopyroxene, wr: whole rock

*3. Noble gas analysis with cr: crushing, tf: total fusion, st ht: stepwise heating, respectively.

*4. Core sample (see text).

4–2–2. Sampling and treatment

Most samples have been exposed on the fresh surface of host alkaline basalt, and collected by chiseling. One of the sample (TKC014) was a drill core sample which was collected using a water cooled, diamond-tip rock drill (Natsuhara Giken Co. Ltd., Model N-3). The obtained drill core, which was 1 inch in diameter and 6cm in length, was separated to three parts (Fig. 4–2), in order to assess atmospheric contamination with weathering and to check heterogeneity in an individual xenolith. Collected xenolith samples were hand-crumbled into discrete minerals using a steel mortar. For noble gas analyses, olivine, clinopyroxene, and/or orthopyroxene were carefully separated under a binocular microscope, and then altered parts and impurities were carefully excluded, because secondary and atmospheric noble gas might concentrate in them. Then, samples were leached using 2N–HNO_3 in an ultrasonic bath for 1 hour, in order to remove secondary noble gases possibly adsorbed on the mineral surface or grain boundary. After washing with distilled water in ultrasonic bath, dried sample were weighed and used for noble gas analysis.

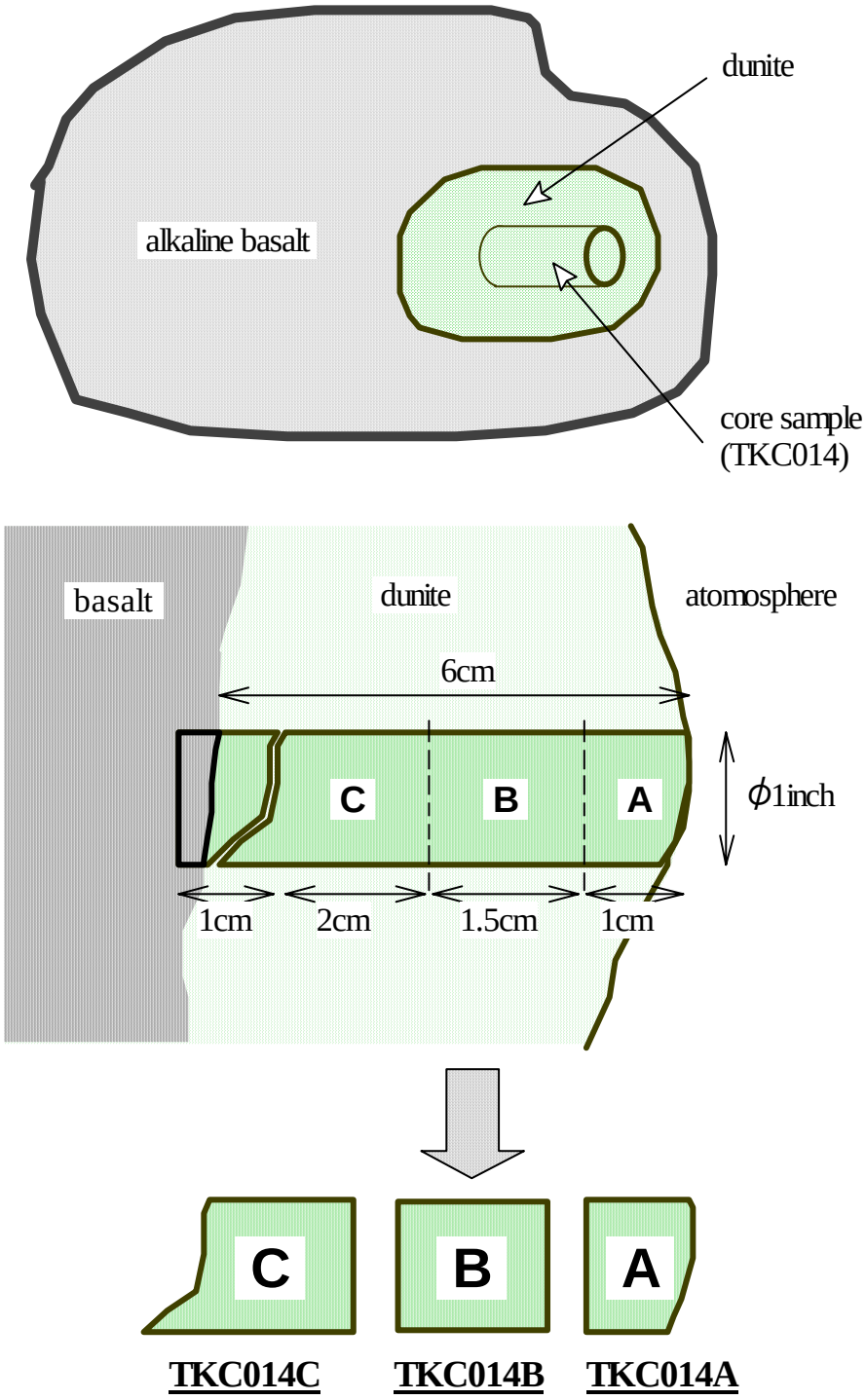

Fig. 4–2. Sampling of core sample (TKC014). TKC014 is a one of the core samples collected from dunite using a diamond-tip rock drill. The core was 1 inch in diameter and 6cm in length, and was separated into three parts (TKC014A–C). Note that TKC014A was exposed to atmosphere and that TKC014C was in contact with host basalt.

4–2–3. Major element composition

Major element compositions of olivine, pyroxene and spinel phenocrysts separated from Takashima xenolith were determined using a scanning electron microprobe equipped with energy dispersive spectrometer (SEM-EDS; JEOL JSM-5310 with Oxford ISIS EDS) at Department of Earth and Planetary Science of the Graduate School of Science, the University of Tokyo. Analyses were carried out with an accelerating voltage of 20kV and a beam current of 53μA. Integrated time for 1 spot with 50–100μm in diameter was 100 seconds. In order to remove the influences by the metasomatism caused by the host magma, electron beam was irradiated in the core part of each mineral grain. Intergrain heterogeneity in a single mineral was checked by analyzing several points in the core of each grain.

4–2–4. Noble gas analysis

Noble gas analyses were carried out with MS–IV before and after modification described in chapter 2, and partly with MS–III. In vacuo crushing with solenoid-type and hydraulic-type crushers, and step heating or single step heating (total fusion) were applied for gas extraction. Details of noble gas measurement were already described in chapter 2.

Concentrations of all noble gases and isotopic ratios of He, Ne and Ar were measured for all samples. However, the abundance and isotopic ratios of Ne could not be measured due to high blank level derived from an unbakable Cryo trap with MS–IV before modification. Kr and Xe isotope analyses were carried out for gas rich samples or high temperatures fraction of 2-step heating samples because atmospheric component is dominant in low temperature fraction. Hot blanks and crushing blanks were measured in the same way as sample runs.

4–3. Results

4–3–1. Major element composition

Results of major element composition determined by SEM-EDS for mineral separates from Takashima xenoliths are listed in Table 4–1. Data with error, which is standard deviation including reproducibility of the measurement and intergrain heterogeneity, is an average of analyses for several points in single mineral grain. Other data are results of single measurement for each mineral grain. Errors on X-ray counting with single spot analysis are approximately 1%. Fo (=Mg/(Mg+Fe)×100) of olivine within each grain of most samples are homogeneous within the statistical error with one measurement (<1%), indicating homogeneous chemical composition in olivine separated from an individual xenolith. Cr# (=Cr/(Cr+Al)) of spinels in dunites shows relatively variable values ranging from 0.56 to 0.81, while Fo of olivines are relatively uniform ranging from 86.9 to 91.5. Plots of the Cr# of spinel against Fo of coexisting olivine are plotted in Fig. 4–3. In this figure, OSMA (Olivine Spinel Mantle Array) defined by Arai (1994) is also shown, in which mantle-derived spinel peridotites are plotted. Whereas the xenoliths from Kurose make a trend coincident with OSMA (data from Arai 1994), the dunites from Takashima analyzed in this study are plotted off the OSMA. This shows definitely that the dunites are mostly not mantle restites but could be cumulates formed by fractional crystallization of relatively primitive magma. At this moment, it is uncertain that what kind of magma from which dunites are cumulated. Kagami et al. (1993) showed that pyroxenite xenoliths from Takashima have distinctive Nd–Sr isotopic characteristics from their host basalts, and suggested their cumulative origin from arc magmatism which formed granite long before alkaline volcanism, because Tertiary granite and the xenoliths have common Nd–Sr ratios with age back to 93Ma. On the other hand, Yanagi and Maeda (1998) suggested that cumulate formed by the crystallization deposits on the floor of the chamber of accumulated magma of alkaline basalts and then removed by the mantle convection. Some of alkaline basalts from northwestern Kyushu show comparable Nd–Sr ratios with those of ultramafic xenoliths (Kakubuchi et al., 1995), allowing cognate origin of xenoliths with the alkaline basalts.

Therefore, Takashima xenoliths might be cumulates from alkaline basalt magma preceding that erupted at Takashima.

Table 4–2. Major element composition (%) of minerals in xenoliths from Takashima.

Sample	Phase[*1]	NA[*2]	SiO_2	MgO	FeO	Al_2O_3	Cr_2O_3	CaO	Fo (olivine)[*3]	Cr# (spinel)[*4]
TKD0900	ol	2	34.44 ± 1.85	41.73 ± 2.63	9.52 ± 0.17				88.65	
	ol	2	37.21 ± 0.42	44.63 ± 0.95	10.11 ± 0.32				88.73	
	ol	2	38.10 ± 0.37	45.45 ± 0.09	9.54 ± 0.06				89.46	
	ol	2	38.12 ± 0.00	45.60 ± 0.08	9.94 ± 0.37				89.11	
		Average	36.96 ± 1.74	44.35 ± 1.80	9.78 ± 0.29				88.99 ± 0.37	
	sp	2		10.91 ± 0.01	21.13 ± 0.04	12.12 ± 0.19	46.93 ± 0.66			0.722
	sp	1		10.80	21.51	12.51	48.46			0.722
		Average		10.86 ± 0.08	21.32 ± 0.27	12.31 ± 0.28	47.69 ± 1.09			0.722 ± 0.000
TKD1000	ol	1	40.26	49.31	9.92				89.86	
	ol	3	36.48 ± 0.76	43.84 ± 0.41	9.95 ± 0.39				88.70	
	ol	3	38.93 ± 0.30	47.09 ± 0.70	9.64 ± 0.31				89.70	
	ol	3	39.66 ± 0.42	47.79 ± 0.33	9.61 ± 0.05				89.86	
		Average	38.83 ± 1.66	47.01 ± 2.31	9.78 ± 0.18				89.53 ± 0.56	
	sp	1		10.51	23.27	7.87	55.06			0.824
	sp	1		11.68	24.35	8.80	53.92			0.804
		Average		11.10 ± 0.83	23.81 ± 0.76	8.34 ± 0.66	54.49 ± 0.81			0.814 ± 0.014
TKD1120	ol	1	36.92	44.13	9.59				89.13	
	ol	1	36.84	44.32	9.73			0.17	89.03	
	ol	1	35.32	43.39	10.08			0.16	88.47	
	ol	1	36.44	44.27	9.62				89.13	
		Average	36.38 ± 0.74	44.03 ± 0.43	9.76 ± 0.22			0.17 ± 0.01	88.94 ± 0.32	0.782 ± 0.014
	cpx	2	50.24 ± 0.34	17.49 ± 0.22	3.01 ± 0.19	1.56 ± 0.15	1.00 ± 0.13	18.71 ± 0.21		
	cpx	2	46.56 ± 0.34	15.25 ± 0.20	3.15 ± 0.19	2.19 ± 0.15	1.32 ± 0.13	18.64 ± 0.21		
	cpx	3	50.33 ± 0.34	16.74 ± 0.22	3.43 ± 0.19	2.51 ± 0.17	1.31 ± 0.15	18.41 ± 0.21		
	cpx	2	50.08 ± 0.34	17.23 ± 0.22	3.58 ± 0.19	2.05 ± 0.15	0.74 ± 0.13	18.49 ± 0.21		
		Average	49.30 ± 1.83	16.68 ± 1.00	3.29 ± 0.26	2.08 ± 0.40	1.09 ± 0.28	18.56 ± 0.14		
	sp	1		12.02	20.63	10.44	51.11			0.767
	sp	1		9.99	18.35	8.68	50.89			0.797
	sp	1		10.66	19.83	9.83	50.25	0.15		0.774
	sp	1		10.66	19.20	9.30	52.05			0.790
		Average		10.83 ± 0.85	19.50 ± 0.97	9.56 ± 0.75	51.08 ± 0.75			0.782 ± 0.014
TKD1250	ol	3	39.04 ± 1.31	46.46 ± 2.48	10.70 ± 0.31				88.56	
	ol	3	39.27 ± 2.09	46.77 ± 2.50	10.61 ± 0.18				88.71	
	ol	3	36.22 ± 1.52	42.68 ± 1.48	10.10 ± 0.40				88.28	
		Average	38.18 ± 1.70	45.30 ± 2.28	10.47 ± 0.33				88.51 ± 0.21	

Data are averages of analyses for each single grain. Errors with single spot analysis are 1%.

*1. ol: olivine, cpx: clinopyroxene, sp: spinel, inc: included in olivine. *2. Number of analysis. *3. Fo = Mg/(Mg+Fe)×100 *4. Cr# = Cr/(Cr+Al)

Table 4–2. (Continued).

Sample	Phase*1	NA*2	SiO_2	MgO	FeO	Al_2O_3	Cr_2O_3	CaO	Fo (olivine)*3	Cr# (spinel)*4
TKD1340	ol	1	33.14	40.37	7.97				90.03	
	ol	1	38.32	47.16	7.60				91.71	
	ol	1	33.46	40.42	7.58				90.48	
	Average		34.97 ± 2.90	42.65 ± 3.91	7.72 ± 0.22				90.74 ± 0.87	
	sp(inc)	1		10.31	19.73	9.15	49.99			0.786
TKD1350	ol	3	39.35 ± 0.32	46.46 ± 0.16	10.76 ± 0.17				88.50	
	ol	3	38.52 ± 0.80	45.76 ± 1.38	10.78 ± 0.19				88.32	
	ol	3	39.43 ± 0.84	46.77 ± 1.30	10.76 ± 0.14				88.57	
	Average		39.10 ± 0.50	46.33 ± 0.52	10.77 ± 0.01				88.46 ± 0.13	
	cpx	2	48.25 ± 0.01	15.87 ± 0.53	2.88 ± 0.47		0.92 ± 0.35	21.19 ± 0.67		
	cpx	1	49.60	16.03	3.36		1.33	21.41		
	cpx	1	50.04	15.74	3.25		0.80	22.43		
	cpx(inc)	1	49.40	17.80	3.62	2.36	1.10	17.69		
	Average		49.32 ± 0.77	16.36 ± 0.97	3.28 ± 0.31		1.04 ± 0.23	20.68 ± 2.06		
	sp	1		9.77	17.47	15.88	44.69			0.654
	sp	3		11.07 ± 0.48	18.00 ± 0.37	11.86 ± 0.13	47.28 ± 3.21			0.728
	Average			10.42 ± 0.92	17.74 ± 0.37	13.87 ± 2.84	45.99 ± 1.83			0.691 ± 0.052
TKD1550	ol	3	39.58 ± 0.29	48.91 ± 0.53	7.73 ± 0.57				91.85	
	ol	3	39.94 ± 0.11	49.12 ± 0.56	8.38 ± 0.19				91.26	
	ol	3	39.91 ± 0.73	48.99 ± 0.82	8.36 ± 0.19				91.26	
	ol	3	40.66 ± 0.19	50.00 ± 0.21	8.21 ± 0.16				91.57	
	Average		40.02 ± 0.45	49.26 ± 0.50	8.17 ± 0.30				91.49 ± 0.28	
	cpx	1	47.53	16.63	2.35		0.51	19.75		
	cpx	1	47.12	15.41	2.66	4.65	1.16	18.70		
	cpx	1	49.79	16.83	2.35	1.50	0.57	20.79		
	Average		48.15 ± 1.44	16.29 ± 0.77	2.45 ± 0.18	3.08 ± 2.23	0.75 ± 0.36	19.75 ± 1.05		
	sp	2		12.66 ± 0.16	17.80 ± 1.25	10.69 ± 0.69	55.92 ± 0.47			0.778
	sp	1		8.61	26.72	12.62	49.16			0.723
	sp	1		12.40	19.17	11.30	52.25			0.756
	sp	1		12.94	17.54	9.76	55.78	0.16		0.793
	sp	1		13.28	17.35	10.29	54.22			0.779
	Average			11.98 ± 1.91	19.72 ± 3.98	10.93 ± 1.10	53.47 ± 2.83			0.766 ± 0.027

Data are averages of analyses for each single grain. Errors with single spot analysis are 1%.

*1. ol: olivine, cpx: clinopyroxene, sp: spinel, inc: included in olivine. *2. Number of analysis. *3. Fo = Mg/(Mg+Fe)×100 *4. Cr# = Cr/(Cr+Al)

Table 4–2. (Continued).

Sample	Phase[*1]	NA[*2]	SiO_2	MgO	FeO	Al_2O_3	Cr_2O_3	CaO	Fo (olivine)[*3]	Cr# (spinel)[*4]
TKD1610	ol	1	39.40	47.50	10.46			0.26	89.00	
	ol	1	43.08	51.45	10.39				89.82	
	ol	1	43.98	53.11	10.43			0.28	90.08	
	ol	1	40.72	49.03	10.74				89.06	
	ol	1	37.16	44.08	10.11				88.60	
		Average	41.80 ± 2.76	50.27 ± 3.51	10.51 ± 0.22				89.31 ± 0.62	
	cpx(inc)	1	43.04	13.73	3.71	1.85	1.65	18.30		
	sp	1	0.49	13.24	21.24	15.13	49.78			0.688
	sp	1		12.99	20.28	14.48	50.42			0.700
	sp	1		10.35	19.14	13.33	46.41			0.700
	sp	1		12.56	21.03	12.99	50.15			0.721
		Average		12.29 ± 1.32	20.42 ± 0.95	13.98 ± 1.00	49.19 ± 1.87			0.703 ± 0.014
TKS01	ol	2	38.67 ± 0.61	46.39 ± 1.03	9.86 ± 0.23			0.18 ± 0.04	89.35	
	ol	2	36.42 ± 1.90	43.84 ± 2.59	9.86 ± 0.17			0.21 ± 0.01	88.80	
	ol	2	40.07 ± 2.36	48.20 ± 2.41	10.36 ± 0.19			0.18 ± 0.07	89.24	
		Average	38.39 ± 1.84	46.14 ± 2.19	10.02 ± 0.29			0.19 ± 0.02	89.13 ± 0.29	
TKY01	ol	3	40.24 ± 0.16	46.96 ± 0.31	12.80 ± 0.42				86.73	
	ol	3	39.81 ± 1.19	46.19 ± 1.19	12.21 ± 0.61			0.24 ± 0.04	87.08	
	ol	3	37.96 ± 0.33	45.02 ± 0.37	10.81 ± 0.22				88.13	
		Average	39.34 ± 1.21	46.06 ± 0.98	11.94 ± 1.03				87.32 ± 0.73	
	cpx	1	48.92	15.98	3.32	1.64	0.92	20.47		
	cpx(inc)	2	48.07 ± 0.34	16.29 ± 0.22	4.53 ± 0.22	4.64 ± 0.19	1.84 ± 0.15	17.72 ± 0.21		
		Average	48.50 ± 0.60	16.14 ± 0.22	3.93 ± 0.86	3.14 ± 2.12	1.38 ± 0.65	19.10 ± 1.94		
	sp	2		12.65 ± 0.18	21.02 ± 0.13	20.44 ± 0.30	40.26 ± 1.48			0.569
	sp	2		13.51 ± 0.28	19.66 ± 0.27	21.34 ± 0.68	38.92 ± 0.30			0.550
	sp	2		12.83 ± 0.34	19.58 ± 0.01	21.12 ± 0.11	39.01 ± 0.18			0.553
		Average		13.00 ± 0.46	20.08 ± 0.81	20.96 ± 0.47	39.40 ± 0.75			0.558 ± 0.010
TKC0222	ol	3	36.88 ± 1.47	43.76 ± 1.72	9.62 ± 0.21			0.23 ± 0.00	89.02	
	ol	3	38.11 ± 0.83	44.90 ± 1.51	10.02 ± 0.32				88.87	
	ol	3	37.66 ± 1.22	45.01 ± 1.30	9.94 ± 0.19			0.19 ± 0.04	88.98	
		Average	37.55 ± 0.62	44.56 ± 0.69	9.86 ± 0.21			0.21 ± 0.03	88.95 ± 0.08	
TKC1212	ol	3	39.87 ± 0.23	47.66 ± 0.38	9.20 ± 0.44				90.22	
	ol	4	37.30 ± 2.54	44.99 ± 2.75	9.46 ± 0.14				89.45	
	ol	2	41.59 ± 4.53	50.99 ± 6.22	9.44 ± 0.04				90.60	
		Average	39.59 ± 2.16	47.88 ± 3.01	9.37 ± 0.14				90.09 ± 0.59	
	sp	3		11.01 ± 0.36	24.10 ± 0.36	12.02 ± 0.31	47.62 ± 0.57			0.727
	sp	3		11.48 ± 0.16	24.59 ± 0.24	11.67 ± 0.06	49.45 ± 0.08			0.740
		Average		11.25 ± 0.33	24.34 ± 0.35	11.85 ± 0.24	48.54 ± 1.29			0.733 ± 0.009

Data are averages of analyses for each single grain. Errors with single spot analysis are 1%.

*1. ol: olivine, cpx: clinopyroxene, sp: spinel, inc: included in olivine. *2. Number of analysis. *3. Fo = Mg/(Mg+Fe)×100 *4. Cr# = Cr/(Cr+Al)

Table 4–2. (Continued).

Sample	Phase[*1]	NA[*2]	SiO_2	MgO	FeO	Al_2O_3	Cr_2O_3	CaO	Fo (olivine)[*3]	Cr# (spinel)[*4]
TKC1422	ol	2	39.20 ± 0.42	45.93 ± 0.47	10.96 ± 0.23				88.20	
	ol	2	39.16 ± 0.54	45.61 ± 0.75	12.14 ± 0.42				87.01	
	ol	2	38.89 ± 0.63	44.83 ± 0.18	12.43 ± 0.13				86.54	
	ol	2	38.21 ± 0.42	44.00 ± 0.24	13.04 ± 0.14			0.17 ± 0.01	85.74	
	Average		38.86 ± 0.46	45.09 ± 0.86	12.14 ± 0.88				86.87 ± 1.03	
	sp	2	0.38 ± 0.04	11.57 ± 0.09	22.36 ± 0.35	18.21 ± 0.12	42.52 ± 0.68			0.610
TKC014A	ol	2	41.12 ± 0.34	51.07 ± 0.32	8.59 ± 0.27				91.38	
	ol	2	36.13 ± 2.43	44.05 ± 3.80	8.61 ± 0.32				90.12	
	ol	2	37.51 ± 1.08	45.26 ± 1.22	8.67 ± 0.23				90.30	
	Average		38.25 ± 2.58	46.79 ± 3.76	8.62 ± 0.04				90.60 ± 0.68	
TKC014B	ol	3	39.75 ± 1.15	48.08 ± 1.27	8.94 ± 0.09				90.55	
	ol	3	39.38 ± 1.77	47.89 ± 2.19	9.14 ± 0.36				90.32	
	ol	3	39.98 ± 0.33	48.87 ± 0.20	9.02 ± 0.17				90.62	
	Average		39.71 ± 0.30	48.28 ± 0.52	9.04 ± 0.10				90.50 ± 0.15	
TKC014B	cpx(inc)	2	57.32 ± 0.38	33.66 ± 0.27	5.54 ± 0.23	1.51 ± 0.17	1.16 ± 0.13	1.78 ± 0.10		
	cpx(inc)	2	50.11 ± 0.34	17.08 ± 0.22	2.94 ± 0.19	1.40 ± 0.15	1.71 ± 0.15	18.26 ± 0.22		
	Average		53.72 ± 5.10	25.37 ± 11.72	4.24 ± 1.84	1.46 ± 0.08	1.44 ± 0.39	10.02 ± 11.65		
	sp	2		13.57 ± 0.20	17.10 ± 0.48	12.13 ± 0.29	56.19 ± 0.01			0.757
	sp	2		10.08 ± 0.03	16.12 ± 0.08	9.50 ± 0.17	53.45 ± 1.17			0.791
	sp	3		12.97 ± 0.15	17.27 ± 0.15	10.90 ± 0.20	54.50 ± 0.88			0.770
	sp	2		11.67 ± 0.91	16.91 ± 0.33	10.14 ± 1.27	53.83 ± 0.14			0.781
	Average			12.07 ± 1.55	16.85 ± 0.51	10.67 ± 1.13	54.49 ± 1.21			0.775 ± 0.015
TKC014C	ol	3	40.04 ± 1.56	48.84 ± 1.87	8.75 ± 0.15				90.87	
	ol	2	37.34 ± 0.46	45.42 ± 0.87	8.55 ± 0.25				90.45	
	ol	2	37.85 ± 0.30	46.25 ± 0.06	8.56 ± 0.09			0.18 ± 0.01	90.60	
	Average		38.41 ± 1.44	46.83 ± 1.78	8.62 ± 0.11				90.64 ± 0.21	
	sp(inc)	1	0.31	12.18	17.48	12.01	51.88			0.743

Data are averages of analyses for each single grain. Errors with single spot analysis are 1%.

*1. ol: olivine, cpx: clinopyroxene, sp: spinel, inc: included in olivine. *2. Number of analysis. *3. Fo = Mg/(Mg+Fe)×100 *4. Cr# = Cr/(Cr+Al)

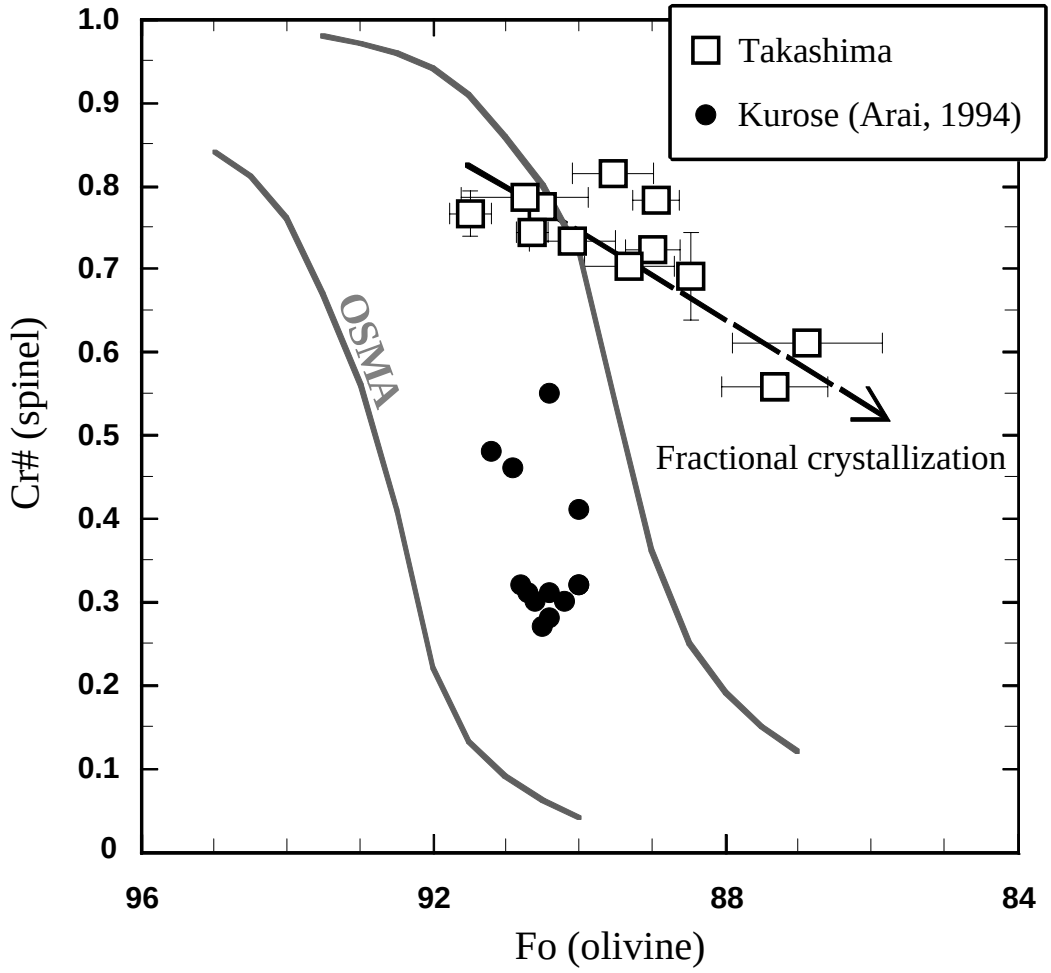

Fig. 4–3. Relationships between Fo (= Mg/(Mg+Fe)×100) content of olivine and Cr# (= Cr/(Cr+Al)) of spinel in dunite xenoliths from Takashima. Dash-outlined area represents the OSMA, olivine-spinel mantle array, which was proposed by Arai (1994) as a trend of upper-mantle derived peridotites. The data for lherzolite from Kurose (Arai, 1994) are plotted for comparison.

4–3–2. Noble gas isotopes

Results of noble gas analysis are summarized with conditions of gas extraction in Table 4–4 and 4–4. Hot blanks and crushing blanks have been already listed in Table 3–6. Correction of blanks were carried out for all data of sample runs, however, isotopic ratios of Ne with blank exceeding 50% of total Ne, and all the isotopic ratios of Kr and Xe were not corrected because of quite low amount of released these noble gases from the samples. Errors on isotopic ratio are one standard deviation, including errors with blank correction and mass discrimination. Experimental uncertainties in the concentration of each noble gas were estimated to be about 5% for He and Ar, 10% for Ne, Kr and Xe, respectively, based on the reproducibility of measurements of the standard gas.

Table 4–3. Noble gas abundances and isotopic compositions of xenoliths from back-arc region of southwestern Japan.

Sample (Weight) / Extraction Method[*1]	MS	^{4}He ($\times10^{-9}$)	^{20}Ne ($\times10^{-11}$)	^{36}Ar ($\times10^{-10}$)	^{84}Kr ($\times10^{-12}$)	^{132}Xe ($\times10^{-13}$)	$^{3}He/^{4}He$ (R/R_A)[*2]	$^{20}Ne/^{22}Ne$	$^{21}Ne/^{22}Ne$	$^{38}Ar/^{36}Ar$	$^{40}Ar/^{36}Ar$
Takashima (northwest Kyushu)											
TKY01 olivine (1.89g)											
HC 70MPa×3	IV*	48.0	b.b.	1.74	0.0980	0.0640	7.58 ± 0.52	n. m.	n. m.	0.18848 ± 0.00044	378.9 ± 6.6
TKY01 olivine (1.50g)											
HC 70MPa×3	IV*	20.0	b.b.	2.51	72.2	32.9	7.58 ± 0.61	n. m.	n. m.	0.18861 ± 0.00045	445.4 ± 19.7
TKD0900 olivine (3.57g)											
HC 70MPa×3	IV*	0.369	b.b.	0.183	0.370	0.0690	9.8 ± 3.0	n. m.	n. m.	0.19042 ± 0.00062	397.1 ± 1.4
TKD1000 olivine (2.56g)											
HC 70MPa×3	IV*	0.107	b.b.	0.644	2.40	0.460	n. m.	n. m.	n. m.	0.1891 ± 0.0040	326.12 ± 0.47
TKD1120 olivine (2.90g)											
HC 70MPa×3	IV*	27.3	13.1	2.84	7.42	2.26	6.82 ± 0.53	9.48 ± 0.11	0.0284 ± 0.0010	0.19060 ± 0.00033	536 ± 15
TKD1120 olivine (3.57g)											
HC 70MPa×3	IV*	33.5	17.1	6.65	26.7	16.7	7.14 ± 0.31	9.822 ± 0.072	0.02919 ± 0.00075	0.19059 ± 0.00076	470.8 ± 2.0
TKD1120 olivine(1.4443g)											
HC 70MPa×3	IV	38.2	14.3	7.64	23.1	15.9	6.87 ± 0.37	10.37 ± 0.17	0.0340 ± 0.0091	0.19297 ± 0.00092	503.85 ± 0.97
TKD1120 olivine (0.51g)											
TF 1800℃	III	21.7	9.10	4.17	16.2	19.7	7.47 ± 0.61	9.61 ± 0.12	0.0277 ± 0.0023	0.18832 ± 0.00063	498.84 ± 0.32
TKD1120 olivine after crushing (0.55g)											
TF 1800℃	III	4.79	13.6	5.20	23.0	41.2	7.1 ± 1.0	9.61 ± 0.12	0.0277 ± 0.0023	0.18777 ± 0.00081	363.17 ± 0.55
TKD1120 olivine after crushing (0.7222g)											
TF 1800℃	IV	9.93	6.72	3.56	14.6	24.0	6.75 ± 0.47	9.94 ± 0.18	0.03036 ± 0.0017	0.18801 ± 0.00051	457.27 ± 0.46
TKD1250 olivine (1.97g)											
HC 70MPa×3	IV*	0.281	22.7	0.950	1.26	0.351	n. m.	8.85 ± 0.15	0.0266 ± 0.0032	0.18707 ± 0.00044	294.6 ± 1.0
TKD1250 olivine (0.47g)											
TF 1800℃	III	0.145	2.94	1.12	3.59	4.12	n. m.	10.20 ± 0.41	0.0315 ± 0.0081	0.1871 ± 0.0013	301.36 ± 0.67
TKD1340 olivine (3.24g)											
HC 70MPa×3	IV*	0.174	51.8	9.74	14.6	4.34	n. m.	9.829 ± 0.069	0.02876 ± 0.00071	0.18931 ± 0.00063	296.7 ± 7.7
TKD1350 olivine (2.26g)											
HC 70MPa×3	IV*	1.50	5.00	0.901	1.20	0.289	n. m.	9.578 ± 0.065	0.0305 ± 0.0030	0.18751 ± 0.00039	374 ± 12
TKD1350 olivine (2.16g)											
HC 70MPa×3	IV*	2.78	6.20	1.04	1.39	0.441	17.9 ± 6.0	7.84 ± 0.14	0.0267 ± 0.0035	0.18789 ± 0.00092	382 ± 12
TKD1350 olivine (3.46g)											
HC 70MPa×3	III	4.98	5.21	1.68	5.30	3.54	6.37 ± 0.43	9.45 ± 0.23	0.02829 ± 0.00093	0.18833 ± 0.00087	506.29 ± 0.42
TKD1350 olivine (2.16g)											
HC 70MPa×3	III	0.671	5.04	0.995	b.b.	b.b.	5.9 ± 3.1	9.43 ± 0.16	0.0255 ± 0.0038	0.1887 ± 0.0022	384.0 ± 1.1

Unit for concentrations are cm^3STP/g. Errors with isotopic ratios are 1σ. b.b.=below blank, n. m. = not measu *MS–IV before modification.

*1. SH: Step heating, TF: Total fusion, SC: Cushing with a solenoid-type crusher, HC: Crushing with a hydraulic-type crusher.

*2. Normalized to the atmospheric ratio = 1.4×10^{-6} (Ozima and Podosek, 1983).

Table 4–3. (Continued)

Sample (Weight) / Extraction Method[*1]	MS	^{4}He ($\times10^{-9}$)	^{20}Ne ($\times10^{-11}$)	^{36}Ar ($\times10^{-10}$)	^{84}Kr ($\times10^{-12}$)	^{132}Xe ($\times10^{-13}$)	$^{3}He/^{4}He$ (R/R_A)[*2]	$^{20}Ne/^{22}Ne$	$^{21}Ne/^{22}Ne$	$^{38}Ar/^{36}Ar$	$^{40}Ar/^{36}Ar$
TKD1350 olivine (0.49g)											
TF 1800℃	III	1.36	2.37	0.945	2.61	2.81	18.0 ± 6.5	10.12 ± 0.56	0.0343 ± 0.0062	0.1881 ± 0.0013	364.05 ± 0.49
TKD1550 olivine (3.54g)											
HC 70MPa×3	IV*	0.962	0.384	0.503	1.35	0.569	15.9 ± 4.6	9.68 ± 0.12	0.0313 ± 0.0030	0.18996 ± 0.00066	419.4 ± 1.8
TKD1550 olivine (3.30g)											
HC 70MPa×3	IV*	2.13	1.83	0.393	1.09	0.460	12 ± 10	9.08 ± 0.14	0.0271 ± 0.0016	0.19092 ± 0.00086	407.0 ± 1.7
TKD1550 olivine (2.97g)											
HC 70MPa×3	III	2.01	99.9	10.8	19.4	9.84	5.1 ± 2.6	10.098 ± 0.063	0.0290 ± 0.0012	0.18570 ± 0.00046	301.16 ± 0.23
TKD1550 olivine (4.78g)											
HC 70MPa×3	III	0.938	2.24	0.453	b.b.	b.b.	6.7 ± 1.0	9.47 ± 0.20	0.0307 ± 0.0044	0.18931 ± 0.00079	567.8 ± 1.7
TKD1550 olivine (0.59g)											
TF 1800℃		28.9	2.05	1.39	10.8	57.0	16.6 ± 1.4	9.89 ± 0.24	0.0331 ± 0.0054	0.1890 ± 0.0011	329.55 ± 0.46
TKD1550 olivine (1.92g)											
SH 600℃	III	0.31	0.88	0.40	2.46	3.77	n. m.	n. m.	n. m.	0.18810 ± 0.00138	301.24 ± 0.63
1800℃		2.84	5.59	2.99	8.88	10.80	13.2 ± 2.7	9.77 ± 0.19	0.0311 ± 0.0018	0.18796 ± 0.00094	405.63 ± 0.76
Total		3.15	6.47	3.39	11.34	14.57				0.18798	393.21
TKD1610 olivine (1.97g)											
HC 70MPa×3	III	0.351	0.665	0.44	b.b.	b.b.	9 ± 10	9.94 ± 0.39	0.029 ± 0.016	0.18810 ± 0.00280	419.0 ± 1.5
TKD1610 olivine (0.50g)											
TF 1800℃	III	0.267	13.7	4.47	16.8	26.4	14.5 ± 2.8	9.55 ± 0.23	0.0278 ± 0.0025	0.18796 ± 0.00070	301.94 ± 0.33
TKD1610 olivine (1.99g)											
SH 600℃	III	0.11	1.01	0.83	3.56	5.73	n. m.	n. m.	n. m.	0.18870 ± 0.00134	295.95 ± 0.62
1800℃		1.46	4.16	2.26	10.10	15.10	38 ± 13	9.48 ± 0.31	0.0329 ± 0.0029	0.18891 ± 0.00078	357.84 ± 0.56
Total		1.57	5.17	3.09	13.66	20.83				0.18885	341.14
TKS01 olivine (2.00g)											
HC 70MPa×3	IV*	100	n. m.	n. m.	n. m.	n. m.	9.22 ± 0.64	n. m.	n. m.	n. m.	n. m.
TKS01 olivine (2.00g)											
HC 70MPa×3	IV*	100	n. m.	n. m.	n. m.	n. m.	8.92 ± 0.56	n. m.	n. m.	n. m.	n. m.
TKS01 olivine (1.99g)											
HC 70MPa×3	IV*	160	n. m.	n. m.	n. m.	n. m.	9.40 ± 0.21	n. m.	n. m.	n. m.	n. m.
TKS01 olivine (1.90g)											
HC 70MPa×3	IV*	122	b.b.	0.725	1.38	0.745	9.93 ± 0.30	n. m.	n. m.	0.18987 ± 0.00055	1109 ± 58
TKS01 olivine (1.8667g)											
HC 70MPa×3	IV	105	6.58	1.05	3.02	1.88	9.15 ± 0.51	9.47 ± 0.10	0.0311 ± 0.0026	0.1881 ± 0.0024	1126.1 ± 3.5
TKS01 olivine (0.54g)											
TF 1800℃	III	131	16.1	3.62	9.26	7.35	8.96 ± 0.33	9.60 ± 0.22	0.0284 ± 0.0011	0.18800 ± 0.00059	687.1 ± 1.1

Unit for concentrations are cm^3STP/g. Errors with isotopic ratios are 1σ. b.b.=below blank, n. m. = not measu *MS–IV before modification.

*1. SH: Step heating, TF: Total fusion, SC: Cushing with a solenoid-type crusher, HC: Crushing with a hydraulic-type crusher.

*2. Normalized to the atmospheric ratio = 1.4×10^{-6} (Ozima and Podosek, 1983).

Table 4–3. (Continued)

Sample (Weight) / Extraction Method*1	MS	^{4}He ($\times10^{-9}$)	^{20}Ne ($\times10^{-11}$)	^{36}Ar ($\times10^{-10}$)	^{84}Kr ($\times10^{-12}$)	^{132}Xe ($\times10^{-13}$)	$^{3}He/^{4}He$ (R/R_A)*2	$^{20}Ne/^{22}Ne$	$^{21}Ne/^{22}Ne$	$^{38}Ar/^{36}Ar$	$^{40}Ar/^{36}Ar$
TKS01 olivine after crushing (1.4095g)											
TF 1800℃	III	46.0	34.7	8.11	29.6	37.0	9.34 ± 0.30	n. m.	n. m.	0.18576 ± 0.00036	373.70 ± 0.30
TKS01 olivine after crushing (0.7733g)											
TF 1800℃	IV	80.4	5.46	1.80	7.38	17.8	9.16 ± 0.26	10.16 ± 0.20	0.0312 ± 0.0030	0.18810 ± 0.00060	687.18 ± 0.87
TKC1212 olivine (3.33g)											
HC 70MPa×3	IV*	0.0346	b.b.	0.261	0.630	0.140	n. m.	n. m.	n. m.	0.19013 0.00081	336.8 1.3
TKC1422 olivine (3.36g)											
HC 70MPa×3	IV*	0.517	b.b.	0.228	0.830	0.230	7.1 ± 1.7	n. m.	n. m.	0.19138 ± 0.00070	740.4 ± 1.7
TKC1422 olivine (1.89g)											
Total fusion 1800℃	III	0.390	0.561	0.650	7.35	33.9	4.31 ± 0.47	9.80 ± 0.25	0.0308 ± 0.0037	0.18793 ± 0.00044	359.76 ± 0.47
TKP 1040 clinopyroxene (1.0226g)											
SH 600℃	IV	3.91	0.22	3.53	10.10	8.71	0.51 ± 0.44	10.05 ± 0.34	0.0303 ± 0.0069	0.18834 ± 0.00093	300.4 ± 1.9
1800℃		28.40	23.10	4.57	9.22	17.60	1.03 ± 0.24	9.74 ± 0.07	0.0300 ± 0.0012	0.18886 ± 0.00035	542.9 ± 1.5
Total		32.31	23.32	8.10	19.32	26.31	0.97	9.75	0.0300	0.18863	437.2
Kurose (northwest Kyushu)											
KRS9801 whole (1.5882g)											
SH 600℃	IV	0.640	1.64	0.17	1.40	0.35	1.3 ± 1.5	10.47 ± 0.36	0.0316 ± 0.0067	0.1886 ± 0.0014	308.15 ± 0.67
1800℃		0.967	2.22	0.29	2.27	4.03	14.8 ± 2.7	10.07 ± 0.25	0.0350 ± 0.0055	0.1883 ± 0.0013	348.95 ± 0.99
Total		1.607	3.86	0.46	3.67	4.38	9.4	10.23	0.0336	0.1884	334.03
KRS9803 olivine (2.1037g)											
HC 70MPa×3	IV	0.0175	1.54	0.243	0.627	0.611	21 ± 50	10.28 ± 0.25	0.0299 ± 0.0051	0.1879 ± 0.0011	309.3 ± 1.2
KRS9803 orthopyroxene (1.4837g)											
HC 70MPa×3	IV	0.0655	6.88	0.0920	0.949	1.04	22 ± 22	10.24 ± 0.19	0.0325 ± 0.0042	0.1869 ± 0.0023	363.1 ± 1.4
KRS9805 whole rock (0.97g)											
SH 600℃	IV	0.028	1.22	0.85	1.13	0.37	19 ± 68	11.36 ± 0.91	0.0349 ± 0.0087	0.18711 ± 0.00080	296.85 ± 0.83
1800℃		0.388	4.64	35.54	237.00	287.00	26 ± 10	10.04 ± 0.21	0.0289 ± 0.0018	0.18905 ± 0.00055	298.29 ± 0.44
Total		0.416	5.86	36.39	238.13	287.37	26	10.29	0.0300	0.18901	298.25
KRS9806 olivine (2.1175g)											
HC 70MPa×3	IV	0.020	1.68	0.2363	0.502	0.419	14 ± 18	10.29 ± 0.28	0.0296 ± 0.0034	0.19048 ± 0.00216	321.3 ± 1.2
KRS98707 whole rock (0.7825g)											
SH 600℃	IV	0.258	3.50	0.36	1.74	5.38	6.7 ± 2.8	10.08 ± 0.19	0.0314 ± 0.0035	0.18770 ± 0.00233	308.62 ± 1.08
1800℃		0.609	8.04	0.93	1.79	2.71	13.2 ± 6.0	10.06 ± 0.25	0.0294 ± 0.0025	0.18752 ± 0.00098	326.44 ± 0.66
Total		0.867	11.54	1.29	3.53	8.09	11.3	10.07	0.0300	0.18757	321.51

Unit for concentrations are cm^3STP/g. Errors with isotopic ratios are 1σ. b.b.=below blank, n. m. = not measu *MS–IV before modification.

*1. SH: Step heating, TF: Total fusion, SC: Cushing with a solenoid-type crusher, HC: Crushing with a hydraulic-type crusher.

*2. Normalized to the atmospheric ratio = 1.4×10^{-6} (Ozima and Podosek, 1983).

Table 4–3. (Continued)

Sample (Weight) / Extraction Method[*1]	MS	^{4}He ($\times10^{-9}$)	^{20}Ne ($\times10^{-11}$)	^{36}Ar ($\times10^{-10}$)	^{84}Kr ($\times10^{-12}$)	^{132}Xe ($\times10^{-13}$)	$^{3}He/^{4}He$ (R/R_A)[*2]	$^{20}Ne/^{22}Ne$	$^{21}Ne/^{22}Ne$	$^{38}Ar/^{36}Ar$	$^{40}Ar/^{36}Ar$
KRS9810 whole rock (1.6535g)											
SH 600℃	IV	3.38	1.34	0.263	0.94	1.35	3.8 ± 1.9	10.28 ± 0.16	0.0292 ± 0.0033	0.18778 ± 0.00098	308.30 ± 0.82
1800℃		0.88	5.22	0.668	1.65	1.60	6.7 ± 2.1	9.91 ± 0.06	0.0291 ± 0.0016	0.18761 ± 0.00071	321.96 ± 0.70
Total		4.26	6.56	0.931	2.59	2.95	4.4	9.98	0.0291	0.18766	318.11
KRS9811 whole rock (1.1101g)											
SH 600℃	IV	0.24	4.97	0.203	0.295	0.247	0.2 ± 5.9	12.19 ± 1.32	0.0383 ± 0.0103	0.1893 ± 0.0021	305.7 ± 1.0
1800℃		1.11	1.25	0.259	0.453	0.565	4.4 ± 2.1	10.05 ± 0.41	0.0306 ± 0.0045	0.1899 ± 0.0019	618.6 ± 5.5
Total		1.35	6.22	0.461	0.748	0.812	3.6	11.69	0.0365	0.1897	481.1
KRS9814 olivine (1.1837g)											
HC 70MPa×3	IV	0.0452	2.66	0.794	n. m.	n. m.	11.18 ± 34.41	10.31 ± 0.21	0.0312 ± 0.0037	0.1873 ± 0.0013	314.94 ± 0.78
Cheju Island											
CHJ9901 olivine (2.1862g)											
HC 70MPa×3	IV	127	2.95	0.264	0.752	0.583	6.51 ± 0.22	10.95 ± 0.25	0.0354 ± 0.0047	0.1818 ± 0.0053	4426 ± 50
CHJ9901 orthopyroxene (1.7264g)											
HC 70MPa×3	IV	95.3	38.1	5.70	8.69	2.91	6.44 ± 0.33	10.27 ± 0.12	0.0306 ± 0.0019	0.18721 ± 0.00085	651.1 ± 1.3
CHJ9902 olivine (2.1670g)											
HC 70MPa×3	IV	0.878	1.53	0.306	0.719	0.790	9.7 ± 4.3	10.62 ± 0.25	0.0328 ± 0.0039	0.1879 ± 0.0029	1105 ± 16
CHJ9902 orthopyroxene (1.4837g)											
HC 70MPa×3	IV	4.46	1.34	0.193	0.43	0.545	6.5 ± 1.1	10.49 ± 0.45	0.0362 ± 0.0054	0.1897 ± 0.0021	1319 ± 18
Atmosphere[*3]		5.24	16.45	31.4	0.650	0.0234	1	9.80	0.0290	0.1880	295.5

Unit for concentrations are cm^3STP/g. Errors with isotopic ratios are 1σ. b.b.=below blank, n. m. = not measu *MS–IV before modification.

*1. SH: Step heating, TF: Total fusion, SC: Cushing with a solenoid-type crusher, HC: Crushing with a hydraulic-type crusher.

*2. Normalized to the atmospheric ratio = 1.4×10^{-6} (Ozima and Podosek, 1983).

*3. Data from Ozima and Podosek (1983).

Table 4–4. Kr and Xe isotopic compositions of xenolith from back-arc region of southwestern Japan.

Sample (Weight) / Extraction Method[*1]	MS	$^{78}Kr/^{84}Kr$	$^{80}Kr/^{84}Kr$	$^{82}Kr/^{84}Kr$	$^{83}Kr/^{84}Kr$	$^{86}Kr/^{84}Kr$	$^{124}Xe/^{130}Xe$	$^{126}Xe/^{130}Xe$	$^{128}Xe/^{130}Xe$	$^{129}Xe/^{130}Xe$	$^{131}Xe/^{130}Xe$	$^{132}Xe/^{130}Xe$	$^{134}Xe/^{130}Xe$	$^{136}Xe/^{130}Xe$
Takashima (northwest Kyushu)														
TKD1120 olivine (0.51g)		0.00619	0.03971	0.2031	0.2010	0.3069	0.0247	0.0203	0.476	6.68	5.24	6.71	2.566	2.168
TF 1800℃	III	± 0.00032	± 0.00093	± 0.0038	± 0.0051	± 0.0035	± 0.0041	± 0.0029	± 0.033	± 0.31	± 0.20	± 0.22	± 0.083	± 0.061
TKD1120 olivine after crushing (0.55g)		0.00622	0.03959	0.2011	0.1996	0.3033	0.0252	0.0213	0.471	6.55	5.18	6.67	2.571	2.150
TF 1800℃	III	± 0.00029	± 0.00118	± 0.0035	± 0.0045	± 0.0029	± 0.0038	± 0.0029	± 0.021	± 0.17	± 0.09	± 0.17	± 0.054	± 0.044
TKD1120 olivine after crushing (0.7222g)		0.00582	0.03849	0.1958	0.1925	0.2897	0.0270	0.0239	0.525	7.20	5.73	7.28	2.835	2.381
TF 1800℃	IV	± 0.00060	± 0.00133	± 0.0054	± 0.0064	± 0.0071	± 0.0058	± 0.0036	± 0.040	± 0.50	± 0.40	± 0.48	± 0.189	± 0.163
TKD1250 olivine (0.47g)		0.00616	0.04130	0.2004	0.2069	0.3101	0.0354	0.0264	0.491	6.61	5.39	6.65	2.534	2.237
TF 1800℃	III	± 0.00062	± 0.00184	± 0.0081	± 0.0045	± 0.0050	± 0.0145	± 0.0069	± 0.032	± 0.20	± 0.24	± 0.33	± 0.145	± 0.161
TKD1350 olivine (3.46g)		0.00622	0.04056	0.2031	0.2057	0.3085	0.0312	0.0174	0.473	6.62	5.28	6.62	2.566	2.149
HC 70MPa×3	III	± 0.00045	± 0.00207	± 0.0065	± 0.0054	± 0.0085	± 0.0124	± 0.0026	± 0.031	± 0.25	± 0.31	± 0.31	± 0.126	± 0.088
TKD1350 olivine (0.49g)		0.00529	0.03991	0.2055	0.1995	0.3030	0.0310	0.0247	0.466	6.78	5.75	7.29	2.751	2.340
TF 1800℃	III	± 0.00097	± 0.00265	± 0.0128	± 0.0109	± 0.0104	± 0.0140	± 0.0097	± 0.097	± 0.44	± 0.28	± 0.50	± 0.213	± 0.094
TKD1550 olivine (2.97g)		0.00624	0.04025	0.2034	0.2027	0.3038	0.0259	0.0183	0.464	6.46	5.12	6.63	2.500	2.096
HC 70MPa×3	III	± 0.00034	± 0.00077	± 0.0025	± 0.0030	± 0.0049	± 0.0074	± 0.0025	± 0.027	± 0.29	± 0.29	± 0.26	± 0.107	± 0.050
TKD1550 olivine (0.59g)		0.00572	0.03891	0.2040	0.1976	0.3033	0.0253	0.0223	0.469	6.58	5.24	6.68	2.578	2.178
TF 1800℃	III	± 0.00049	± 0.00112	± 0.0064	± 0.0066	± 0.0060	± 0.0044	± 0.0034	± 0.020	± 0.13	± 0.11	± 0.14	± 0.073	± 0.048
TKD1610 olivine (0.50g)		0.00644	0.03847	0.2026	0.1999	0.3055	0.0224	0.0194	0.464	6.45	5.23	6.72	2.549	2.176
TF 1800℃	III	± 0.00047	± 0.00123	± 0.0054	± 0.0050	± 0.0062	± 0.0033	± 0.0032	± 0.016	± 0.22	± 0.17	± 0.17	± 0.088	± 0.037
TKS01 olivine (0.54g)		0.00612	0.03916	0.2018	0.2025	0.3039	0.0221	0.0224	0.465	6.65	5.32	6.72	2.588	2.186
TF 1800℃	III	± 0.00025	± 0.00228	± 0.0034	± 0.0039	± 0.0077	± 0.0049	± 0.0054	± 0.042	0.45	± 0.34	± 0.45	± 0.146	± 0.122
TKS01 olivine after crushing (0.7733g)		0.00607	0.03918	0.1964	0.1930	0.2881	0.0247	0.0263	0.510	7.17	5.72	7.24	2.756	2.364
TF 1800℃	IV	± 0.00031	± 0.00153	± 0.0061	± 0.0050	± 0.0095	± 0.0043	± 0.0033	± 0.042	± 0.55	± 0.40	± 0.50	± 0.200	± 0.164
TKP 1040 clinopyroxene (1.0226g)		0.00583	0.03981	0.1980	0.1947	0.2924	0.0245	0.0235	0.487	6.68	5.35	6.80	2.641	2.222
SH 1800℃	IV	± 0.00020	± 0.00100	± 0.0036	± 0.0032	± 0.0050	± 0.0019	± 0.0030	± 0.021	± 0.29	± 0.20	± 0.29	± 0.092	± 0.081
Kurose (northwest Kyushu)														
KRS98707 whole rock (0.7825g)		0.00604	0.04042	0.2013	0.1945	0.2999	0.0289	0.0219	0.450	6.20	5.02	6.43	2.492	2.080
SH 1800℃	IV	± 0.00075	± 0.00316	± 0.0064	± 0.0067	± 0.0086	± 0.0090	± 0.0043	± 0.056	± 0.61	± 0.57	± 0.65	± 0.249	± 0.214
KRS9810 whole rock (1.6535g)		0.00648	0.03868	0.1955	0.1946	0.2918	0.0321	0.0231	0.490	6.70	5.39	6.92	2.637	2.239
SH 1800℃	IV	± 0.00053	± 0.00154	± 0.0038	± 0.0074	± 0.0063	± 0.0068	± 0.0037	± 0.045	± 0.42	± 0.35	± 0.34	± 0.192	± 0.178
Atmosphere [*2]		0.00609	0.03960	0.2022	0.2014	0.3052	0.0234	0.0218	0.472	6.50	5.21	6.61	2.563	2.176

Errors with isotopic ratios are 1s.

*1. SH: Step heating, TF: Total fusion, SC: Cushing with a solenoid-type crusher, HC: Crushing with a hydraulic-type crusher.

*2. Data from Ozima and Podosek (1983).

Helium

Figure 4–4 displays $^{3}He/^{4}He$ ratios versus ^{4}He concentrations of minerals separated from xenoliths. Previous data on mantle xenoliths from Oki-Dogo and Ichinomegata, in the back-arc region of Japan (Fig. 4–1) are also plotted for comparison (Porcelli et al., 1992; Nagao and Takahashi, 1993). Some samples from Takashima were analyzed several times to check their homogeneity of He distribution using different aliquots of olivine separated from the same xenolith, and the results of replicate analyses are also listed in Table 4–3 and Fig. 4–4. In addition, analyzed noble gases of some samples were extracted using both crushing and heating methods.

Helium concentrations vary by about three orders of magnitude among the samples from Takashima and Cheju Island. The xenolith from Kurose contains very small amount of He, precluding further discussion on $^{3}He/^{4}He$ ratios obtained with crushing due to too large uncertainty. The most interesting result in Fig. 4–4 is that, although most samples contain He with $^{3}He/^{4}He$ ratios similar to MORB-value (8.18 ± 0.73 R_A; Hilton et al., 1993) as well as xenoliths from Ichinomegata (Porcelli, et al., 1992; Nagao and Takahashi, 1993), some samples from Takashima show significantly higher $^{3}He/^{4}He$ ratios than that of MORB. Some $^{3}He/^{4}He$ ratios obtained from Kurose xenoliths using heating method is also higher than MORB-value. This is the first case that $^{3}He/^{4}He$ ratios higher than MORB-value are observed in a subduction zone. The remarkably low $^{3}He/^{4}He$ ratio of TKP1040, which is only one clinopyroxenite xenolith among all samples, is probably caused by post-eruptive accumulation of radiogenic He as in the case with Oki-Dogo xenoliths (Nagao and Takahashi, 1993). In contrast with Takashima xenoliths, the samples from Cheju Island show relatively uniform $^{3}He/^{4}He$ ratios which are slightly lower than that of MORB.

Figure 4–5 shows dispersion of He abundance in replicate analysis of some samples from Takashima. The facts that the He concentration is not uniform even in an individual xenolith, and that extraction by crushing shows He concentrations comparable to those by heating in spite of low extraction efficiency of crushing method, indicate that the noble gases are heterogeneously trapped mostly in fluid inclusions. Replicate analyses indicate that the $^{3}He/^{4}He$ ratio is not also uniform even in an individual xenolith, particularly in gas-poor one (Fig. 4–6). These suggest that fluid

inclusions with different $^3He/^4He$ components are contained in xenoliths from Takashima.

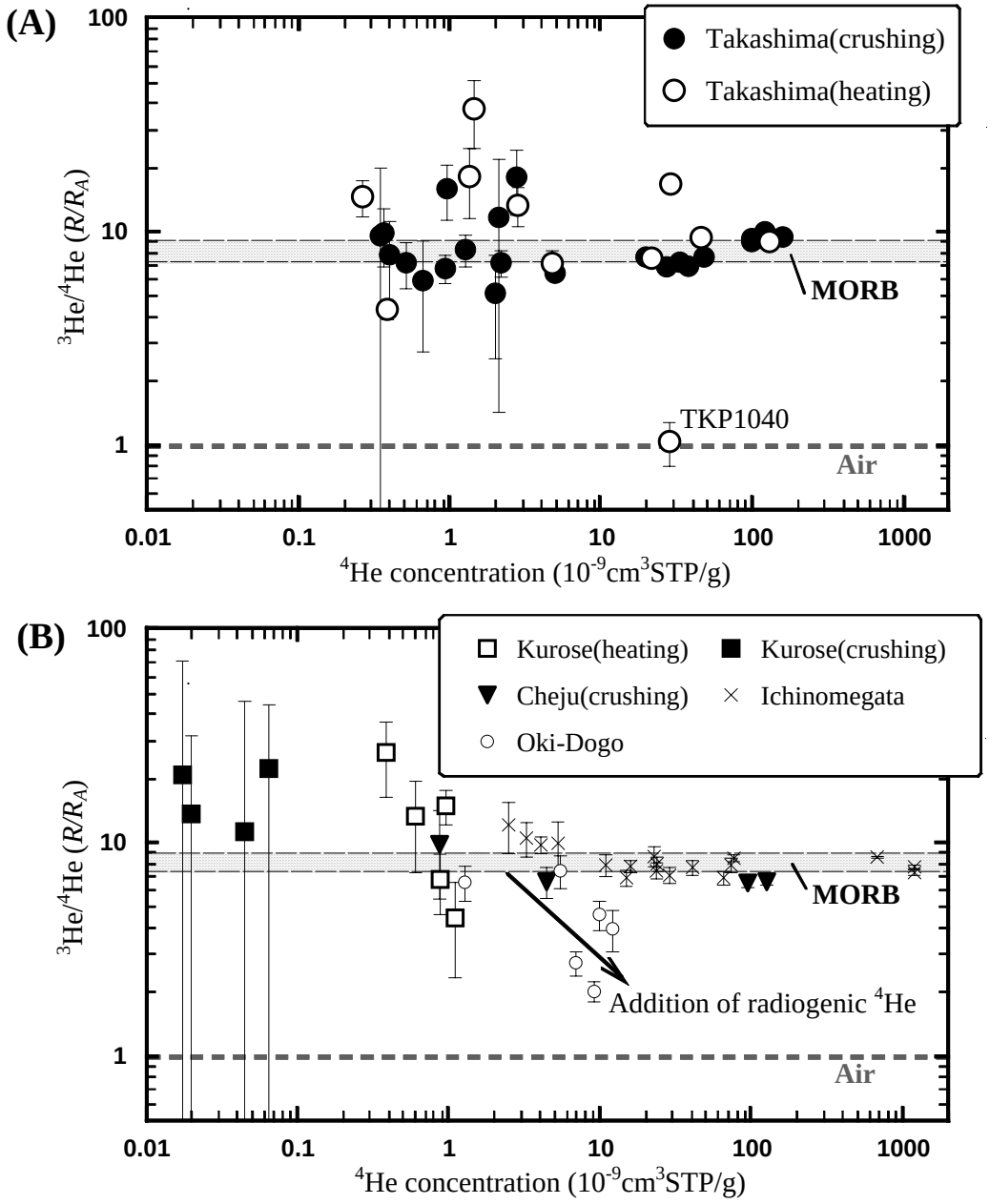

Fig. 4–4. He isotopic ratios (relative to air) and ^4He abundances for xenoliths from (A) Takashima and (B) Kurose and Cheju Island. Errors are 1σ. The results obtained with heating method are high temperature fraction when two-step heating was applied. Previous data on mantle xenoliths from back-arc region of Japan (Porcelli et al., 1992; Nagao and Takahashi, 1993) are also shown for comparison. Hatched area indicates the range of $^3He/^4He$ ratio of MORB ($8.18\pm0.73R_A$; Hilton et al., 1993).

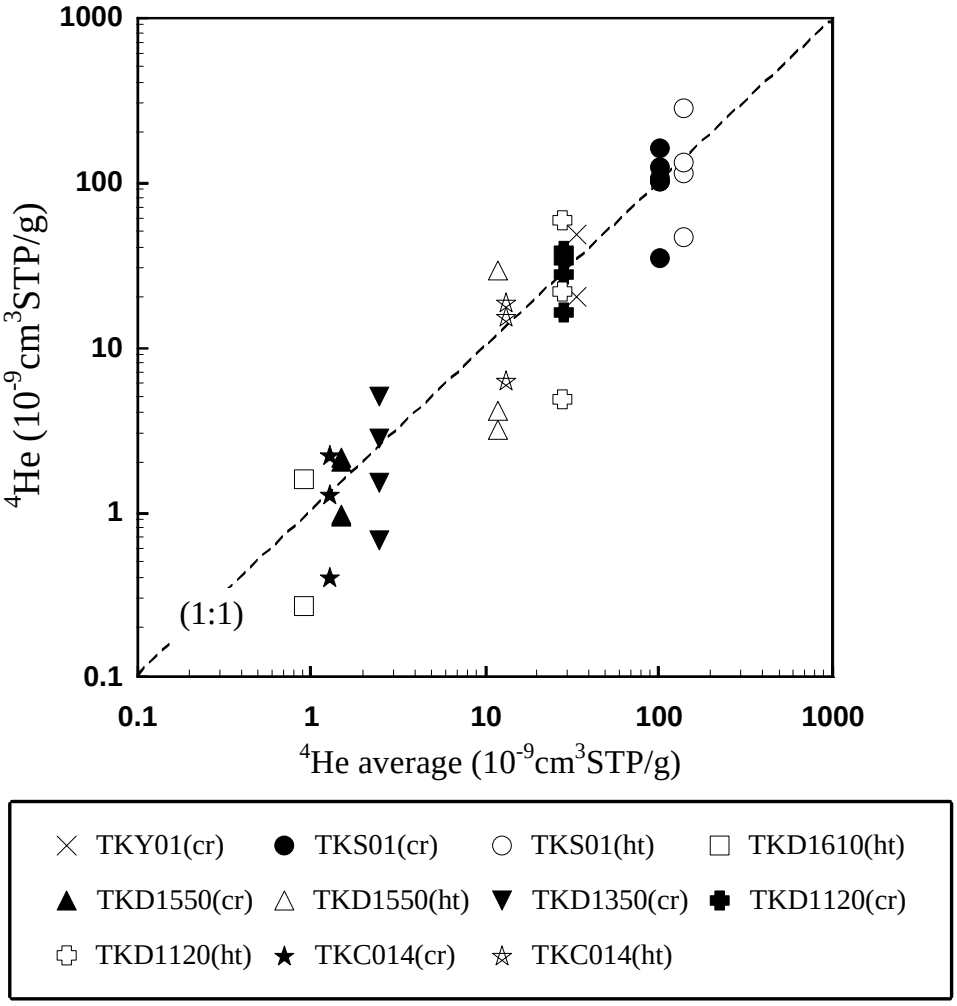

Fig. 4–5. Comparison of ^{4}He abundances of replicate analysis of xenoliths from Takashima with both crushing and heating. "^{4}He average" are averages of ^{4}He concentrations of the samples extracted from each extraction method. The dashed line gives 1:1 correlation line. "cr" and "ht" means crushing and hating extraction method, respectively.

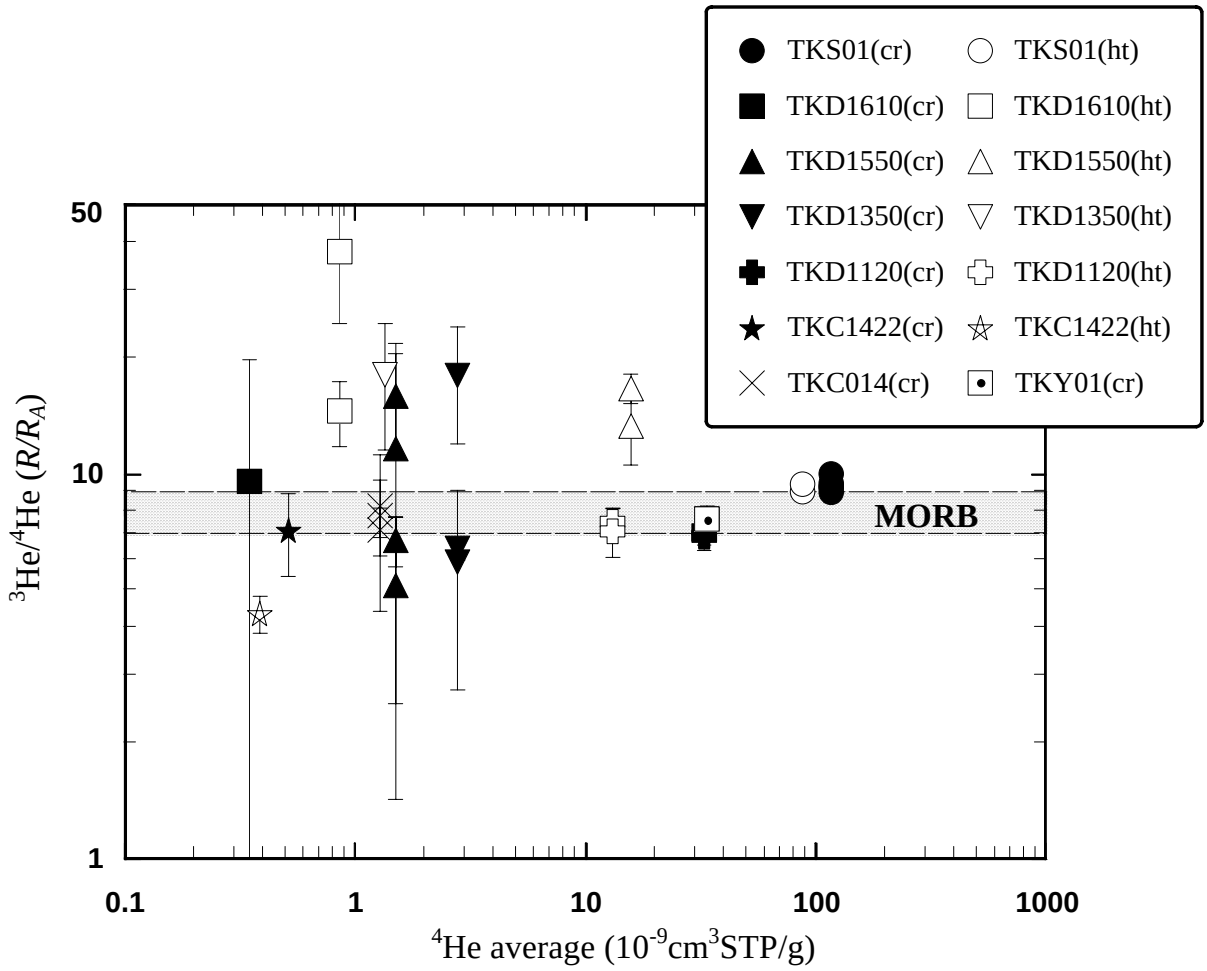

Fig. 4–6. Replicate analysis with both crushing and heating for the samples from Takashima. ^{4}He concentrations are average of replicate analysis. “cr” and “ht” means crushing and hating extraction method, respectively.

Cosmogenic and radiogenic He

The $^{3}He/^{4}He$ ratios higher than MORB-value strongly support the presence of lower mantle component, however, the possibility that these high $^{3}He/^{4}He$ ratios are due to addition of in-situ produced ^{3}He must be considered. Since it has been revealed that the crushing method can selectively extract noble gases from fluid inclusions which are enriched in volatiles, possibility of contribution of cosmogenic ^{3}He to high $^{3}He/^{4}He$ ratio obtained with crushing can be excluded (e.g., Kurz et al., 1986; Stuart et al., 1994). However, contribution of matrix-supported component including cosmogenic ^{3}He is significant in He extracted by heating method as well as magmatic component. On the other hand, radiogenic He is also produced in matrix with age and will reduce $^{3}He/^{4}He$ ratio of He extracted by heating. Therefore it is necessary to evaluate the contribution of in-situ produced cosmogenic and radiogenic He to the $^{3}He/^{4}He$ ratios obtained with heating method.

The curve in solid line shown in Fig. 4–7 indicate the change of $^{3}He/^{4}He$ ratio assuming that only production of cosmogenic ^{3}He is influencing the assumed original $^{3}He/^{4}He$ ratio of MORB value ($8.18R_A$), with the production rate of 4.1×10^{-18} $cm^3STP/g/year$ on the surface (Nagao and Takahashi, 1993). The production rate is not corrected for the effects of overburden shielding, and should be regarded as the maximum possible value, as the ^{3}He production will decrease by 90% with 1m of shielding by rock of $3g/cm^3$ (Lal, 1987). Numbers of the curves represent the assumed duration of the exposure to cosmic rays. Some high $^{3}He/^{4}He$ ratios observed in samples from Takashima and all of those from Kurose in the gas released by heating methods plot within the field where the effect of cosmogenic ^{3}He production during 500–10000 years of exposure becomes significant, suggesting high $^{3}He/^{4}He$ ratios than MORB can be attributed to addition of cosmic-ray produced ^{3}He in them. Meanwhile, to explain the highest $^{3}He/^{4}He$ ratio ($16.6\pm1.4R_A$) of all results, which was obtained from sample TKD1550 by the heating extraction method, the exposure age is estimated to be 0.1Ma, which is smaller than eruption age of host basalt (Table 3–3). This age is the minimum possible value, as the cosmogenic ^{3}He production will decrease by an order of magnitude at the depth of 1m from the surface. Judging from field occurrence of the samples in alkaline basalts, which was fallen down from the cliff probably in recent 10–100 years, they has been

buried by host basalt layer for a long time. Moreover, the $^{21}Ne/^{22}Ne$ ratio of the sample (0.033±0.005) was almost atmospheric (0.0290), indicating negligible contribution of cosmogenic ^{21}Ne. If all excess ^{21}Ne in this sample is cosmogenic origin, assuming a cosmogenic $^{3}He/^{21}Ne$ ratio of 3.5 (Staudacher and Allègre, 1993), the cosmogenic ^{3}He concentration is calculated to be 5.5×10^{-15} cm^3STP/g in maximum, which constitutes less than 1% of total ^{3}He measured in the high-$^{3}He/^{4}He$ results of TKD1550, indicating that it is negligible. Another possible in-situ component is nucleogenic ^{3}He produced from the reaction of $^{6}Li(n, \alpha)T(\beta^-)^{3}He$. Assuming the Li and U contents in the dunites are 0.5ppm and 2ppb respectively and Th/U=3, nucleogenic ^{3}He concentration accumulated during 3.0Ma is estimated to be 1.3×10^{-18} cm^3STP/g (Andrews, 1985), which shows negligible contribution of nucleogenic ^{3}He.

The changes of $^{3}He/^{4}He$ ratios of the sample caused by addition of radiogenic ^{4}He are also shown in Fig. 4–7 as the dashed lines A, B and C. The production rate of ^{4}He is $1.41\times10^{-9}cm^3STP/g$ from 1g of U assuming Th/U=4 (Ozima and Podosek, 1983). Given that U concentrations of dunites from Takashima and lherzolites from Kurose are 5ppb and 40ppb, respectively, calculated changes of $^{3}He/^{4}He$ ratios agree with the data lower than MORB value, with the eruption ages of 3.1Ma for Takashima (average of K-Ar age of basalts from Takashima, Table 3–3) and 1.1Ma for Kurose (Uto et al., 1993), respectively. TKP1040 is an only one clinopyroxenite xenolith from Takashima, and has low $^{3}He/^{4}He$ ratio indicating significant contribution of radiogenic component than in the case with dunite xenoliths. The estimated U content in the clinopyroxenite of 3ppm (Fig. 4–7) is 600 times that in dunite, which is consistent with that partition coefficient of U in clinopyroxene is larger than that in olivine (Henderson, 1982), and cumulative origin of these xenoliths from the same magmatism (Kobayashi and Arai, 1981; Kagami et al., 1993).

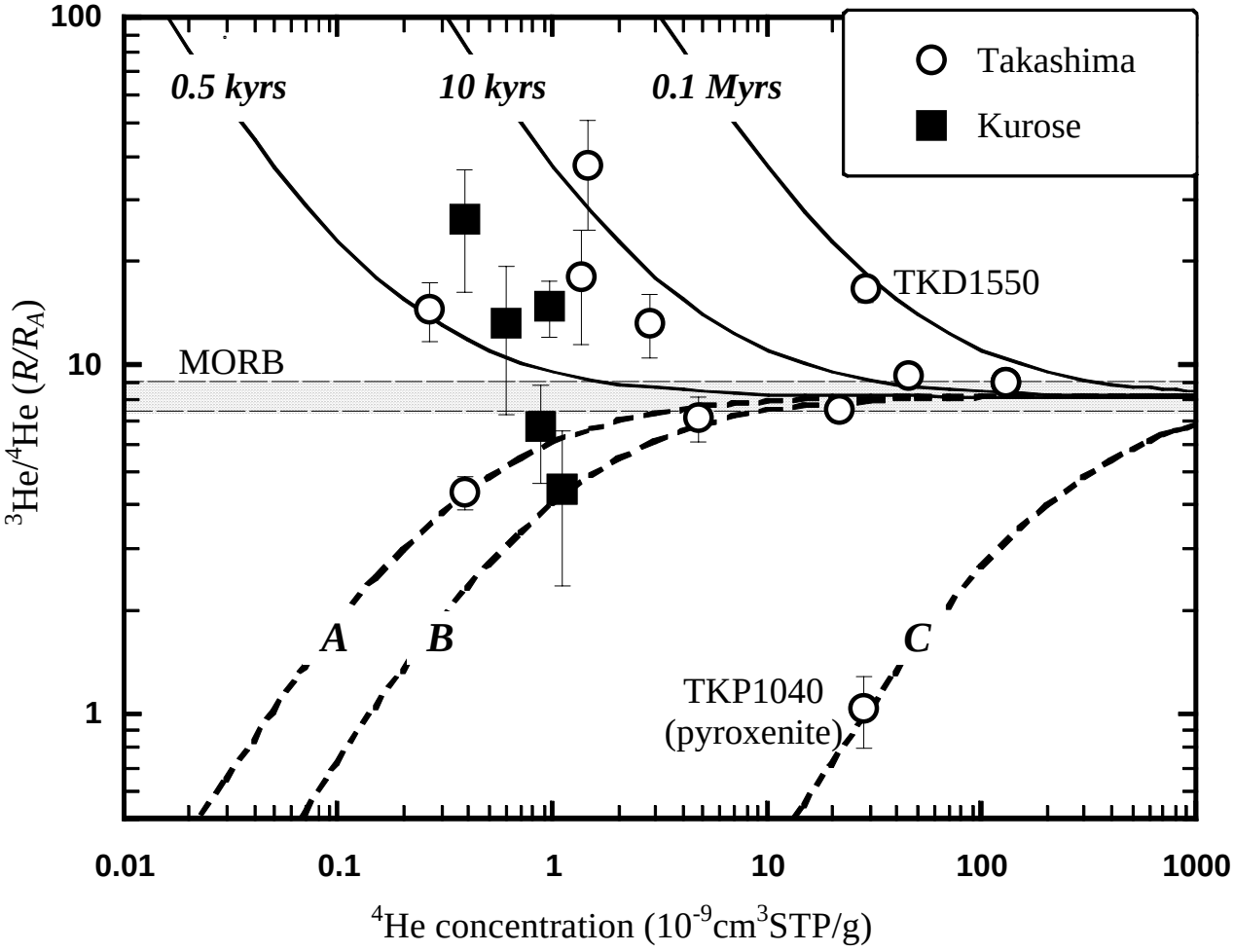

Fig. 4–7. $^3He/^4He$ ratios vs. ^4He concentration of xenoliths from Takashima and Kurose obtained with heating extraction method. The curves shown in solid indicate the change of the $^3He/^4He$ ratios by addition of cosmogenic ^3He, with the production rate of $4.1\times10^{-18}cm^3STP/g/yr$ (Nagao and Takahashi, 1993). Numbers on the curves represents the assumed duration of the exposure to cosmic rays. The changes of $^3He/^4He$ ratios of the sample caused by post-eruptive addition of radiogenic ^4He is also shown as the dashed lines (A) for Takashima dunites with U = 5ppb, (B) for Kurose lherzolites with U=40ppb, and (C) for Takashima pyroxenite with 3ppm, respectively. Eruption age are 3.1 Ma for Takashima (Table 3–3) and 1.1 Ma for Kurose (Uto et al., 1993).

Ne, Kr and Xe isotopes

Figure 4–8 presents the Ne isotopic ratios except the data including more than 50% of blank in total Ne extracted from the sample. All data obtained with MS–IV before modification are not presented due to extremely high blank level of Ne. In case that the stepwise heating was applied for gas extraction, the data with high temperature fraction are used for discussion because adsorbed atmospheric Ne might be dominant in low temperature fraction. The samples from Takashima cluster around atmospheric ratio independent of gas extraction method. Because the Ne isotope ratios with high temperature fraction of step heating eliminating contamination of adsorbed atmospheric component also show the atmospheric ratio, the samples from Takashima may contain Ne with similar atmospheric isotopic ratios. Some exceptional data are plotted near the MORB-line, indicating presence of mantle-derived Ne in the samples. The xenoliths from Kurose and Cheju Island are enriched in ^{20}Ne and ^{21}Ne with respect to atmospheric isotopic composition. Since ^{38}Ar/^{36}Ar ratios of the samples are identical with atmospheric ratio within analytical error (Table 4–3), the deviation of Ne isotope ratios from atmospheric value is not caused by mass fractionation. Whether the data plot on MORB line (Sarda et al., 1988) or Loihi-Kilauea line (Honda et al., 1991) is not clear due to large uncertainties resulting from quite low amount of extracted Ne. Therefore, it is only mentioned that Ne in upper mantle beneath Kurose and Cheju Island may contain mantle Ne, as well as other tectonic settings such as mid-ocean ridge or hotspot, whereas Ne in upper mantle beneath Takashima probably have atmospheric isotopic ratio. It may suggest that mantle beneath northwestern Kyushu have been contaminated by atmospheric Ne probably brought by ancient subduction (will be discussed later).
Kr and Xe isotopes were measured for most of the samples and shown in Table 4–4. In all cases, observed Kr and Xe isotopic ratios are indistinguishable from atmospheric composition within 1σ uncertainty due to less amounts of Kr and Xe in extracted gases.

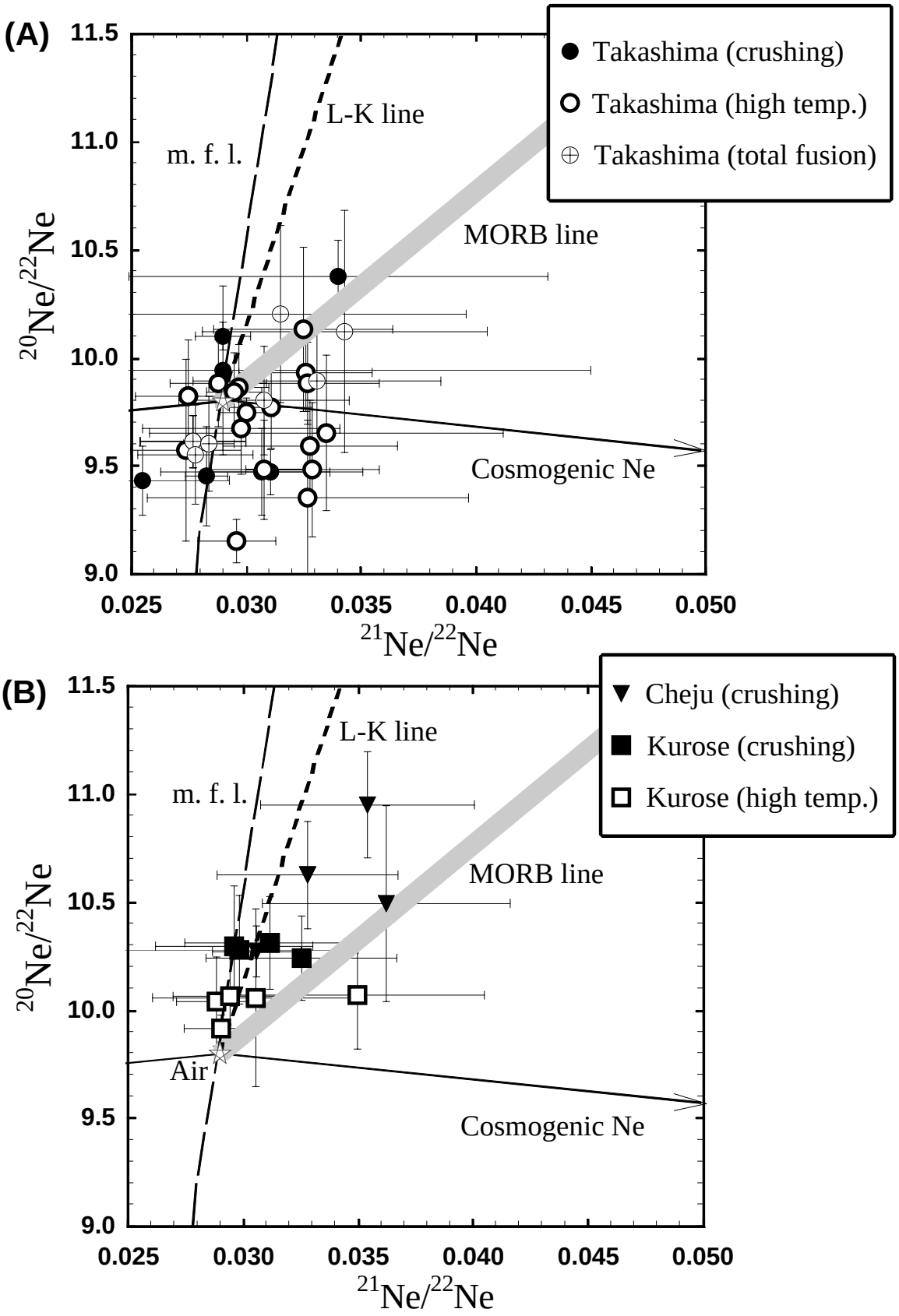

Fig. 4–8. Ne three isotope plot of xenoliths from (A) Takashima, (B) Kurose and Cheju Island The correlation lines defined by MORB samples (MORB line; Sarda et al., 1988), Loihi-Kilauea line (L-K line; Honda et al.,1991), and mass fractionation line (m. f. l.) are shown for comparison.

He–Ar systematics

The $^{3}He/^{4}He$–$^{40}Ar/^{36}Ar$ diagram is shown in Fig. 4–9. When the stepwise heating method was applied for the samples, $^{40}Ar/^{36}Ar$ ratios obtained with high temperature fraction of two-step heating or the highest ratio with multi-stage step heating are used for discussion to minimize contamination by adsorbed atmospheric Ar. $^{3}He/^{4}He$ ratios are total isotopic ratio in case of two-step heating. The data, whose $^{3}He/^{4}He$ ratios are obtained with heating and apparently disturbed by cosmogenic or radiogenic He judging from Fig. 4–7, are excluded. In addition, the data obtained with crushing experiment for Kurose xenoliths are not used because of large uncertainties with $^{3}He/^{4}He$ ratios owing to extremely low concentration of He in the samples. He and Ar in xenoliths from Cheju Island can be explained by two components mixing between atmosphere and upper mantle beneath Cheju Island. Meantime, He–Ar isotopic compositions of xenoliths from Takashima can be explained as products of three components mixing among the atmospheric component and other two components. One of the two components is characterized by MORB-like (or slightly lower) $^{3}He/^{4}He$ ratio and $^{40}Ar/^{36}Ar$ ratio over 1500, which is called MORB-type component in this thesis. The other component has higher $^{3}He/^{4}He$ ratio than $17R_A$ and relatively low $^{40}Ar/^{36}Ar$ ratio ca. 400. Higher $^{3}He/^{4}He$ ratios than MORB-values are observed in tectonic settings related to mantle plume, such as hotspots, hence the latter is called plume-type component hereafter. Using isotopic parameters in Table 4–5, all the samples from Takashima plot in the field defined by mixing lines among the three components in Fig. 4–9. $^{4}He/^{36}Ar$ ratios of these endmembers are unable to be determined uniquely, thus the highest value among all samples (1700 and 4800 for Takashima and Cheju, respectively) can be assumed for MORB-type component, and $^{4}He/^{36}Ar$ ratio for plume-type component is estimated to accord with distribution of the samples. The MORB-type component in Takashima xenoliths is almost similar to mantle beneath Cheju Island in $^{3}He/^{4}He$ ratio, however $^{40}Ar/^{36}Ar$ ratio of 2000 is lower than that of Cheju mantle (up to 3000 with crushing) despite not yet to apply step heating for Cheju samples.

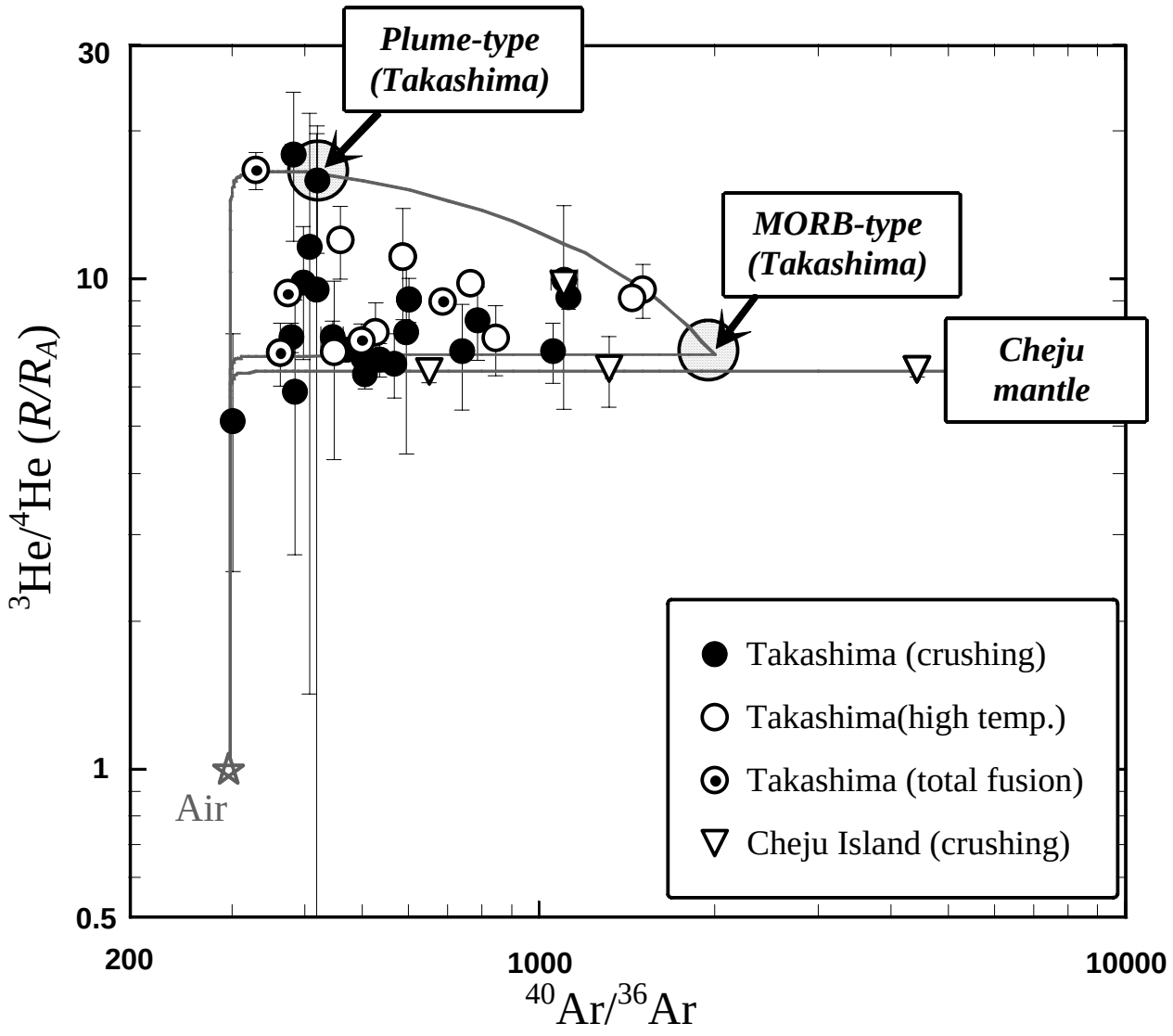

Fig. 4–9. Diagram of $^{3}He/^{4}He$ vs. $^{40}Ar/^{36}Ar$ ratios. The solid lines are mixing line among atmosphere and each endmembers in Table 4–5.

Table 4–5. He and Ar isotopic parameters for mixing calculation.

	Plume-type (Takashima)	MORB-type (Takashima)	Cheju mantle	Atmosphere*
$^{3}He/^{4}He\ (R/R_A)$	16.6	7.0	6.5	1
$^{40}Ar/^{36}Ar$	400	2000	5000	295.5
$^{4}He/^{36}Ar$	1400	1700	4800	0.165

*Data from Ozima and Podosek (1983).

Abundance pattern

Figure 4–10 shows the noble gas abundance patterns of the xenoliths. The definition of F-values has already described in chapter 3. The patterns obtained with high temperature fraction of step heating show the relatively uniform feature of depletion in light noble gases and enrichment in heavy noble gases, however, those with crushing vary widely in feature. When noble gases are extracted with crushing method, the heavier noble gases may adsorb on the fresh surface of crushed minerals, resulting F-value are shifted upward in light noble gases and downward in heavy noble gases. Therefore, the original patterns similar to those with heating are changed by artifact in crushing experiment despite heating the crusher during analysis to avoid adsorption of heavy noble gases. The abundance patterns obtained with heating for Takashima and Kurose xenoliths are distinct from mantle-derived materials such as MORB and mantle xenoliths from hotspot region, and similar to the patterns of deep-seawater (Allègre et al., 1986/87), old oceanic crust and oceanic sediments (Matsuda and Nagao, 1986; Staudacher and Allègre, 1988). This feature suggests that the upper mantle beneath northwest Kyushu contains noble gases probably released from the subducting slab. It is coincident with that $^{40}Ar/^{36}Ar$ ratios of all the samples show heavy contamination by atmospheric component in spite of their mantle origin. Further discussion will be later accompanied with the results on alkaline basalts from northwestern Kyushu.

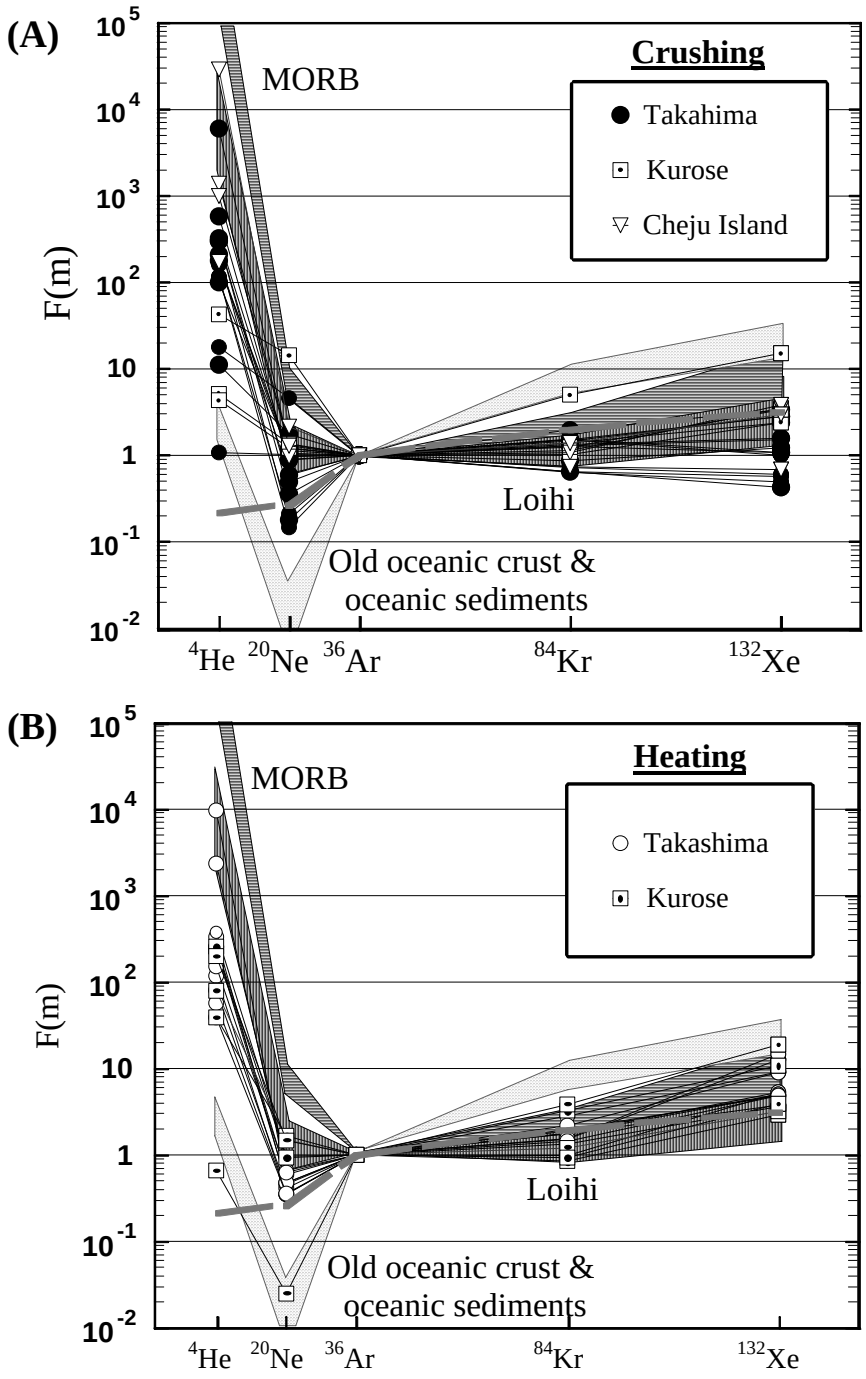

Fig. 4–10. Noble gas abundance patterns for xenoliths obtained with (A) crushing and (B) heating. Low temperature fraction of step heating in heavy noble gases (Ar, Kr and Xe) are subtracted in order to exclude atmospheric contamination on the sample surface. Typical abundance patterns of deep-sea water (Allegre et al, 1986/87), MORB (Staudacher et al., 1989; Hiyagon et al., 1992), Loihi (Kaneoka et al., 1983), and old oceanic crust and sediment (Matsuda and Nagao, 1986, Staudacher and Allegre, 1988) are shown by hatches.

4–4. Discussion

4–4–1. Origin of two kinds of noble gases in xenolith from Takashima

Stepwise heating and crushing

As mentioned above, some $^{3}He/^{4}He$ ratios of Takashima xenoliths obtained with both crushing and heating show the presence of plume-type He certainly. However, plume-type He distribute in the samples heterogeneously, and concurrently with MORB-type He, because results of replicate analyses of the sample TKD1550 show both plume-type and MORB-type $^{3}He/^{4}He$ ratios with He concentration varying by an order of magnitude.

To assess the He heterogeneity in individual xenoliths, stepwise heating and crushing were applied for two characteristic samples, TKS01 and TKD1120. Both samples show relatively constant $^{3}He/^{4}He$ ratio and He concentration irrespective of extraction method, indicating rich in fluid inclusions. While TKS01 shows higher $^{3}He/^{4}He$ ratio ranging from 8.92 to 9.93R_A, replicate analyses for TKD1120 give slightly lower $^{3}He/^{4}He$ ratio of 7.02 R_A in average.

The results obtained with stepwise heating are listed in Table 4–6 and He isotopic compositions at each temperature are shown in Fig. 4–11. Stepwise heating was also applied to TKY01 and TKD1550, and results are also listed in Table 4–6 too. TKS01 shows extremely high $^{3}He/^{4}He$ ratio at 600°C fraction, while the other samples show lower $^{3}He/^{4}He$ ratios than that obtained with crushing method due to relatively large contribution of He radiogenically produced in mineral lattice. Such a high $^{3}He/^{4}He$ ratio ($72\pm18R_A$) can be caused by addition of cosmogenic ^{3}He, however, $^{21}Ne/^{22}Ne$ ratio (0.0281 ± 0.0030) of this fraction is almost atmospheric, rejecting possibility of their cosmogenic origin. Because the amount of He extracted at this temperature is only 0.1% of total He in the sample, the high $^{3}He/^{4}He$ ratio is probably resulted from fractionation due to higher mobility of ^{3}He than that of ^{4}He. Even if difference in permeability of He and Ne cause decoupling of release temperature, $^{21}Ne/^{22}Ne$ ratio obtained with next heating step was also atmospheric, suggesting negligible contribution of cosmogenic component. Comparing ^{4}He release pattern of TKS01 and the other three samples, while

He in TKS01 concentrated in high temperature (1400–1800°C) fractions, He in the other samples start to release at low temperature, at around 1000°C. This indicate that He in TKS01 are trapped in hardier cite than that in the other samples. It suggests that low $^3He/^4He$ component is trapped in a weak structure, such as micro fracture or healed crack.

The procedure of the stepwise crushing was the same as described in chapter 2. In case that hydraulic-type crusher was used, with increasing pressure by 10MPa step and each pressure was kept for 1 minute, the noble gases released at each pressure were analyzed separately. The results are listed in Table 4–7. Figure 4–12 shows the amount and the isotopic ratio of He released at each crushing step with hydraulic-type crusher. While TKD1120 shows constant $^3He/^4He$ ratio equivalent to average of replicate analysis independent of proceeding of crushing, $^3He/^4He$ ratios of TKS01 observed in different steps are variable. The highest amount of He is released in the second crushing step with the lowest $^3He/^4He$ ratio of $8.5\pm0.3R_A$, which is in the range of MORB-He. Amounts of He released in subsequent crushing steps decreased but the $^3He/^4He$ ratios were variable. If in-situ produced components were released in our crushing experiment, the contribution of such components would become larger at higher-pressure steps as was observed by Stuart et al. (1994). However, no relationship between the $^3He/^4He$ ratio and the pressure was observed. Thus it is unlikely that our crushing technique released considerable amounts of in-situ produced components which reside in the mineral lattice, and the variation may result from isotopic heterogeneity in fluid inclusions in the olivines. Such variable $^3He/^4He$ ratios are not observed when crushing using a solenoid-type crusher was applied for the sample TKS01, probably due to wildly crushing and well mixing of the sample during crushing in the chamber. The results suggest that whereas TKD1120 contain low $^3He/^4He$ component (MORB-type), several or at least two types of fluid inclusions different in $^3He/^4He$ ratio are trapped in TKS01.

Another important point is that the $^3He/^4He$ ratio ($11.8\pm0.7R_A$) obtained at the fourth step is the highest among $^3He/^4He$ ratios with crushing method and significantly higher than MORB-value, certainly indicating that He derived from lower mantle is contained in TKS01 xenolith.

Table 4–6. Stepwise heating for selected xenolith from Takashima.

Sample (Weight) / Temp. (℃)	MS	^{4}He ($\times10^{-9}$)	^{20}Ne ($\times10^{-11}$)	^{36}Ar ($\times10^{-10}$)	^{84}Kr ($\times10^{-12}$)	^{132}Xe ($\times10^{-13}$)	$^{3}He/^{4}He$ (R/R_A)*	$^{20}Ne/^{22}Ne$	$^{21}Ne/^{22}Ne$	$^{38}Ar/^{36}Ar$	$^{40}Ar/^{36}Ar$
TKY01 olivine (2.06g)											
600	III	1.11	0.32	3.36	13.40	7.88	2.53 ± 1.50	9.90 ± 0.49	0.0337 ± 0.0090	0.18874 ± 0.00078	296.45 ± 0.52
1000		3.79	1.67	2.23	16.50	16.40	3.42 ± 0.83	9.32 ± 0.26	0.0341 ± 0.0055	0.18979 ± 0.00079	306.51 ± 0.48
1400		2.31	1.85	0.60	5.47	10.50	11.98 ± 2.03	9.65 ± 0.36	0.0335 ± 0.0077	0.18858 ± 0.00107	459.17 ± 1.06
1800		3.06	5.02	1.81	5.14	4.49	6.07 ± 1.44	9.82 ± 0.26	0.0275 ± 0.0023	0.18941 ± 0.00076	460.46 ± 1.04
Total		10.27	8.86	8.00	40.51	39.27	6.04	9.69	0.0303	0.18917	348.49
TKD1120 olivine (1.93g)											
600	III	1.58	2.97	1.72	5.93	3.89	5.53 ± 1.53	9.94 ± 0.26	0.0278 ± 0.0027	0.18826 ± 0.00089	328.10 ± 0.55
1000		14.90	14.30	3.15	11.70	8.70	6.07 ± 0.50	9.85 ± 0.24	0.0281 ± 0.0026	0.18910 ± 0.00079	406.90 ± 1.50
1400		6.83	6.20	1.41	5.85	6.35	7.77 ± 1.15	9.93 ± 0.18	0.0326 ± 0.0029	0.18853 ± 0.00091	527.51 ± 0.90
1800		34.90	20.70	8.77	31.20	22.00	6.80 ± 0.33	9.86 ± 0.20	0.0297 ± 0.0013	0.18896 ± 0.00082	514.14 ± 0.76
Total		58.21	44.17	15.04	54.68	40.94	6.69	9.87	0.0295	0.18887	471.74
TKD1550 olivine (1.90g)											
600	III	0.57	b.b	0.45	3.08	3.95	3.58 ± 3.78	10.21 ± 0.71	0.0317 ± 0.0056	0.18873 ± 0.00138	307.53 ± 0.74
1000		1.57	0.50	0.63	3.06	3.06	10.54 ± 3.45	10.12 ± 0.42	(no data)	0.18847 ± 0.00139	301.58 ± 0.69
1400		0.77	1.44	0.51	2.19	3.23	11.82 ± 6.05	9.35 ± 0.36	0.0327 ± 0.0070	0.18743 ± 0.00084	418.48 ± 0.87
1800		1.16	3.76	1.49	4.37	3.43	7.07 ± 2.80	9.67 ± 0.21	0.0298 ± 0.0043	0.18893 ± 0.00086	448.10 ± 0.90
Total		4.07	5.70	3.09	12.70	13.67	8.82	9.62	0.0281	0.18856	392.53
TKS01 olivine (2.26g)											
600	III	0.29	5.29	1.39	4.24	2.49	71.80 ± 18.32	9.84 ± 0.30	0.0281 ± 0.0030	0.18860 ± 0.00095	296.35 ± 0.75
1000		3.82	4.32	0.35	0.53	0.87	16.57 ± 1.99	9.82 ± 0.27	0.0303 ± 0.0034	0.18559 ± 0.00043	364.40 ± 1.43
1400		80.70	2.51	0.83	2.32	2.77	9.75 ± 0.34	10.13 ± 0.38	0.0325 ± 0.0039	0.18832 ± 0.00094	767.00 ± 2.10
1800		193.00	17.70	5.94	16.90	15.70	9.02 ± 0.17	9.84 ± 0.18	0.0295 ± 0.0012	0.18538 ± 0.00051	735.40 ± 1.30
Total		277.81	29.82	8.51	23.99	21.83	9.40	9.86	0.0296	0.18620	651.28
TKS01 olivine (1.0817g)											
600	IV	0.11	3.13	0.81	2.08	0.83	71.68 ± 22.87	n. m.	n. m.	0.1878 ± 0.0011	298.73 ± 0.65
800		0.31	1.01	0.06	0.26	evac	31.40 ± 8.08	n. m.	n. m.	0.1880 assumed	295.5 assumed
1000		0.39	0.00	0.11	0.13	0.11	24.08 ± 11.12	n. m.	n. m.	0.1866 ± 0.0031	338.08 ± 4.70
1200		2.05	0.52	0.05	0.15	0.14	11.98 ± 1.58	n. m.	n. m.	0.1768 ± 0.0093	709.70 ± 34.11
1400		14.70	0.45	0.16	0.65	0.56	9.29 ± 0.53	n. m.	n. m.	0.1846 ± 0.0035	911.69 ± 16.93
1600		56.70	0.74	0.25	1.04	0.88	9.12 ± 0.41	n. m.	n. m.	0.1805 ± 0.0021	1446.39 ± 18.77
1800		32.80	b.b.	0.11	0.66	0.63	8.73 ± 0.38	n. m.	n. m.	0.1739 ± 0.0055	2575.90 ± 130.39
1800 again		4.80	b.b.	0.01	0.19	0.17	8.77 ± 0.90	n. m.	n. m.	0.1333 ± 0.0682	5511.31 ± 2996.92
Total		111.87	5.85	1.56	5.15	3.31	9.25			0.1845	759.88

Unit for concentrations are cm^3STP/g. Errors with isotopic ratios are 1σ. n. m. = not measured. evac: evacuated by mistake in measurement. assumed: atmospheric ratio is assumed.

* Normalized to the atmospheric ratio = 1.4×10^{-6} (Ozima and Podosek, 1983).

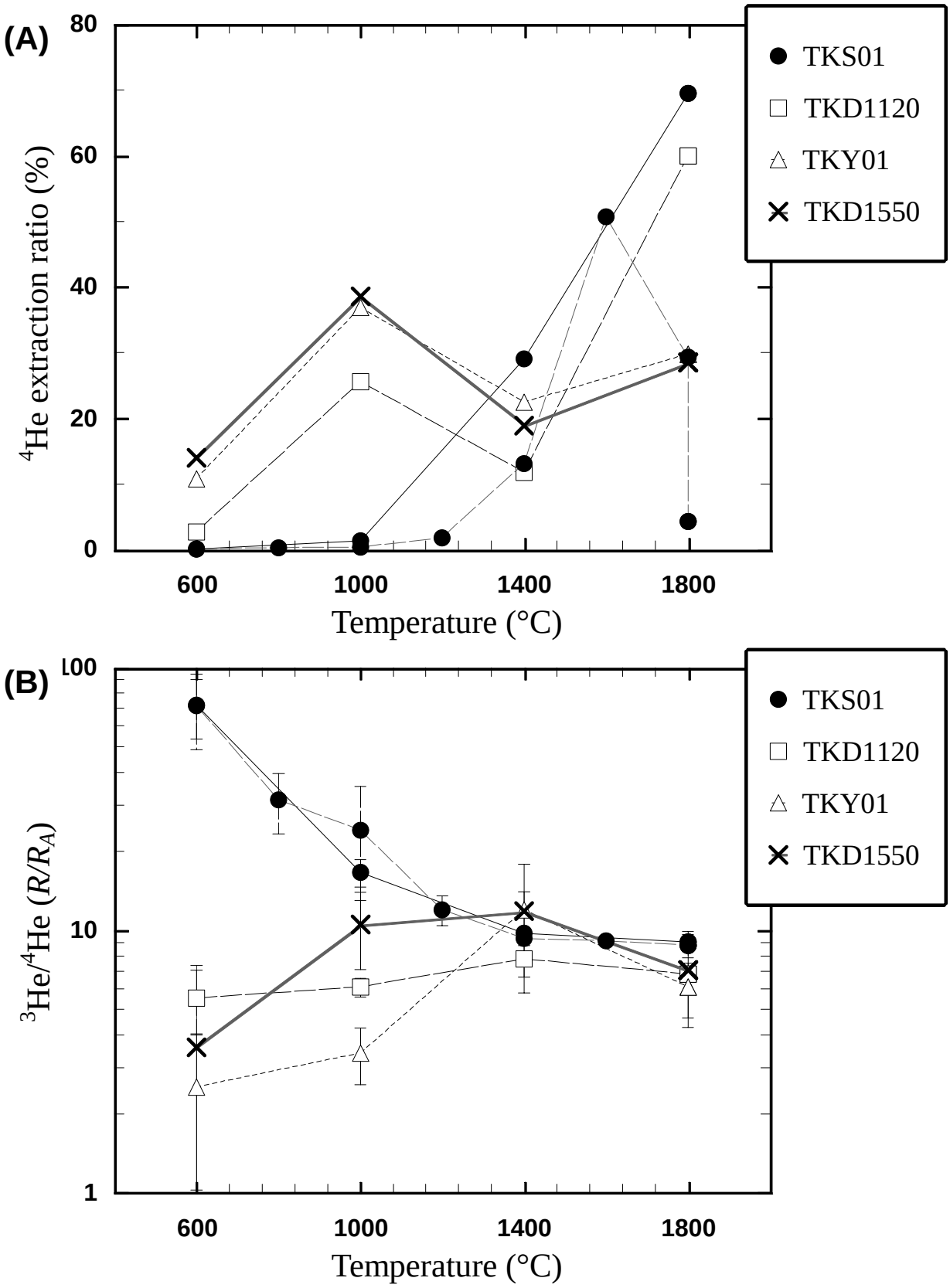

Fig. 4–11. Results of stepwise heating tests for selected xenoliths from Takashima. ^{4}He release patterns (A) and ^{3}He/^{4}He ratios (B) in each temperature step are shown. Extraction ratio means a proportion of ^{4}He released at the temperature step compared to the total released ^{4}He. TKS01 is tested twice in different division of steps.

Table 4–7. Stepwise crushing for selected xenolith from Takashima.

Sample (Weight) / Method[*1]	MS	^{4}He ($\times10^{-9}$)	^{20}Ne ($\times10^{-11}$)	^{36}Ar ($\times10^{-10}$)	^{84}Kr ($\times10^{-12}$)	^{132}Xe ($\times10^{-13}$)	$^{3}He/^{4}He$ (R/R_A)[*2]	$^{20}Ne/^{22}Ne$	$^{21}Ne/^{22}Ne$	$^{38}Ar/^{36}Ar$	$^{40}Ar/^{36}Ar$
TKD1120 olivine (2.604g)											
HC 10MPa	IV	4.65	1.79	0.40	1.21	0.95	6.11 ± 0.69	9.84 ± 0.22	0.0318 ± 0.0045	0.18847 ± 0.00054	535.51 ± 1.18
20MPa		4.14	2.50	0.46	1.41	1.12	6.66 ± 0.77	9.93 ± 0.17	0.0287 ± 0.0039	0.18797 ± 0.00073	500.93 ± 0.87
30MPa		2.90	1.96	0.34	1.08	0.86	6.45 ± 0.90	9.39 ± 0.24	0.0308 ± 0.0031	0.18820 ± 0.00066	504.69 ± 0.82
40MPa		1.73	1.00	0.17	0.61	0.51	6.42 ± 1.51	9.47 ± 0.49	0.0274 ± 0.0044	0.18818 ± 0.00118	575.13 ± 1.21
50MPa		1.12	0.43	0.12	0.44	0.36	6.63 ± 1.97	9.62 ± 0.56	0.0255 ± 0.0089	0.18758 ± 0.00127	563.73 ± 1.32
60MPa		0.68	0.51	0.10	0.35	0.28	6.14 ± 3.22	8.52 ± 0.69	0.0318 ± 0.0100	0.18474 ± 0.00070	531.13 ± 1.50
70MPa		0.49	0.20	0.07	0.22	0.15	8.67 ± 4.98	10.62 ± 0.73	n. m.	0.18725 ± 0.00140	561.82 ± 1.81
70MPa×3		0.42	b.b	0.06	0.18	0.14	10.11 ± 6.78	n. m.	n. m.	0.18825 ± 0.00275	564.27 ± 3.32
Total		16.13	8.39	1.70	5.49	4.36	6.56			0.18792	527.67
TKS01 olivine (1.7701g)											
SC 400strokes	IV	10.70	3.92	1.05	2.22	1.18	9.04 ± 0.58	n. m.	n. m.	0.18813 ± 0.00089	428.25 ± 0.62
800strokes		7.06	1.40	0.32	0.73	0.50	9.20 ± 0.60	n. m.	n. m.	0.18921 ± 0.00127	580.73 ± 2.22
1200strokes		5.87	1.12	0.25	0.51	0.38	9.10 ± 0.52	n. m.	n. m.	0.19045 ± 0.00182	563.48 ± 2.38
1600strokes		5.49	1.34	0.34	0.63	0.44	9.01 ± 0.81	n. m.	n. m.	0.19024 ± 0.00140	498.04 ± 1.63
2000strokes		5.19	0.81	0.21	0.38	0.31	9.05 ± 0.94	n. m.	n. m.	0.19096 ± 0.00147	601.63 ± 3.51
Total		34.31	8.59	2.16	4.47	2.81	9.08			0.18916	493.73
TKS01 olivine (3.18g)											
HC 10MPa	IV*	5.57	n. m.	n. m.	n. m.	n. m.	10.33 ± 0.52	n. m.	n. m.	n. m.	n. m.
20MPa		8.05	n. m.	n. m.	n. m.	n. m.	8.53 ± 0.34	n. m.	n. m.	n. m.	n. m.
30MPa		5.02	n. m.	n. m.	n. m.	n. m.	9.55 ± 0.67	n. m.	n. m.	n. m.	n. m.
40MPa		3.44	n. m.	n. m.	n. m.	n. m.	11.78 ± 0.72	n. m.	n. m.	n. m.	n. m.
50MPa		2.48	n. m.	n. m.	n. m.	n. m.	9.48 ± 1.09	n. m.	n. m.	n. m.	n. m.
60MPa		2.82	n. m.	n. m.	n. m.	n. m.	9.48 ± 0.81	n. m.	n. m.	n. m.	n. m.
70MPa		2.13	n. m.	n. m.	n. m.	n. m.	11.11 ± 1.05	n. m.	n. m.	n. m.	n. m.
Total		29.50	n. m.	n. m.	n. m.	n. m.	9.78				

Unit for concentrations are cm^3STP/g. Errors with isotopic ratios are 1σ. b.b.=below blank, n. m. = not measured

*MS–IV before modification.

*1. SC: Cushing with a solenoid-type crusher, HC: Crushing with a hydraulic-type crusher.

*2. Normalized to the atmospheric ratio = 1.4×10^{-6} (Ozima and Podosek, 1983).

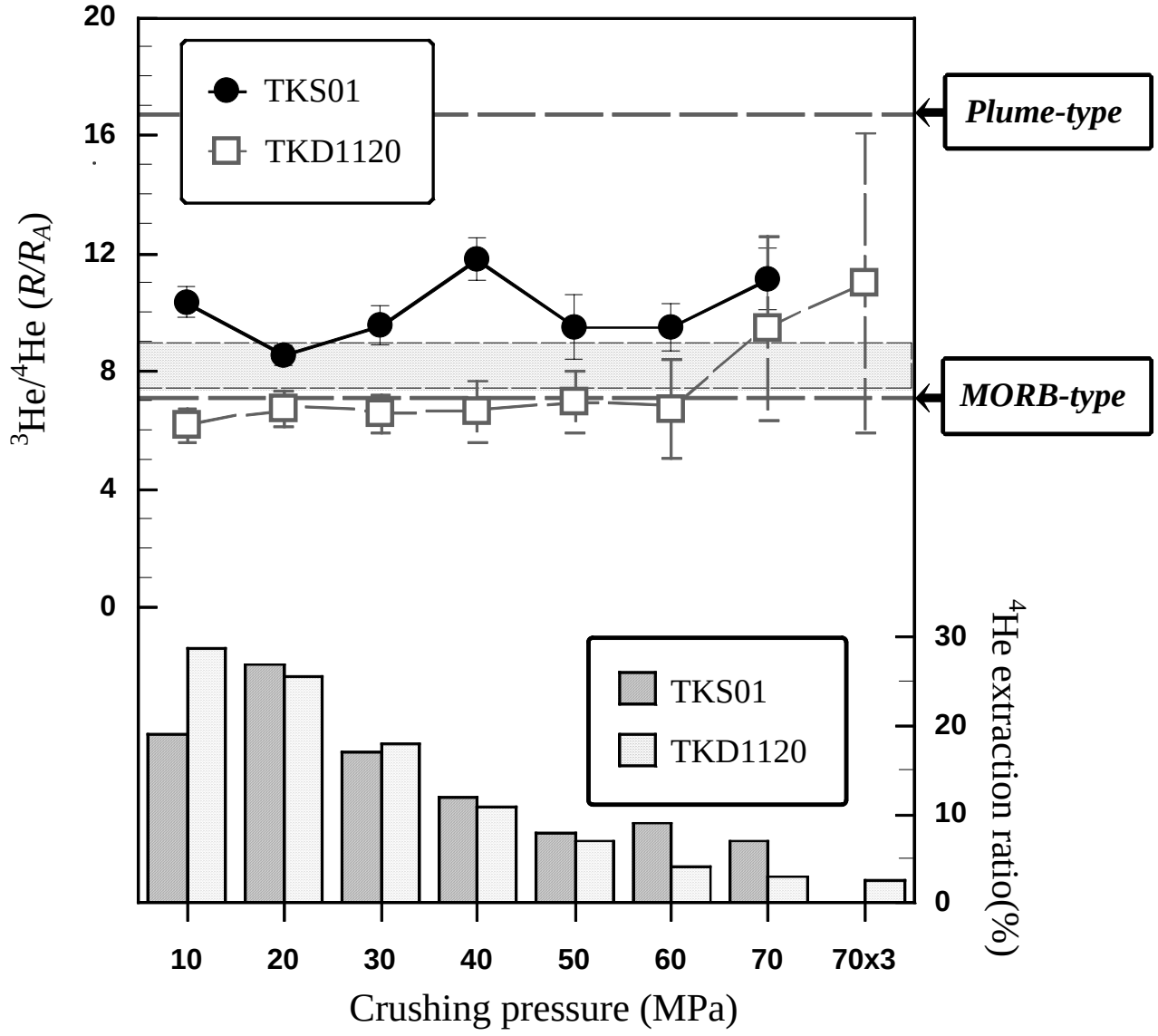

Fig. 4–12. Results of stepwise crushing test for TKS01 and TKD1120 xenoliths from Takashima. “Crushing pressure” means progressive crushing indicated as hydraulic pressure. Extraction ratio means a proportion of ^{4}He released at the temperature step compared to the total released ^{4}He. The ^{3}He/^{4}He ratios of endmembers in Takashima xenoliths are shown for comparison. Hatched area indicates the range of ^{3}He/^{4}He ratio of MORB (8.18±0.73R_A; Hilton et al., 1993).

Noble gas profile in a drill-core sample

In order to study the distribution of the different noble gas components present in xenoliths from Takashima, profile analysis of a drill-core sample, (TKC014: see Fig. 4–2) was performed. The results of noble gas analysis of separated sample with both crushing and stepwise heating method are listed in Table 4–8. Although $^{3}He/^{4}He$ ratios are uniform within analytical error, systematic variation with depth in $^{40}Ar/^{36}Ar$ and $^{4}He/^{36}Ar$ ratios are found in the results obtained with crushing (Fig. 4–13). $^{40}Ar/^{36}Ar$ ratio increase from 600 to 1100 with depth as well as $^{4}He/^{36}Ar$ ratio from 10 to 40. Since TKC014A was exposed to atmosphere, one possible explanation of these trends is atmospheric contamination via diffusion or weathering. When the diffusive exchange between Ar trapped in fluid inclusion and in atmosphere occurred, $^{4}He/^{36}Ar$ ratios will decrease due to higher diffusivity of He than that of Ar and/or depletion of He relative to Ar in the atmosphere. And $^{40}Ar/^{36}Ar$ ratio will decrease drastically in spite of retention of high $^{3}He/^{4}He$ ratio. Such prospective changes of isotopic composition of noble gases agree with the observation. However, this is not the case. According to He diffusivity experimentally determined in olivine (Hart, 1984; Trull and Kurz, 1993), He in fluid inclusion will be reserved during long time such as 0.1 million years and not exchange with those in the atmosphere. Diffusivity of Ar in olivine is larger than that of He apparently, therefore, contamination of Ar from atmosphere is improbable.
Another possible mechanism is adsorption of atmospheric Ar in altered part of mineral. Although altered olivines observable via binocular microscope were removed and samples were leached by acid prior to noble gas analysis, atmospheric noble gases might be adsorbed in fine structure, such as micro cracks. Since the atmospheric Ar intruding in micro cracks would be weakly held compared to magmatic Ar trapped in fluid inclusions, it will be released at lower temperature in step heating. However, the highest $^{40}Ar/^{36}Ar$ ratios observed in step heating analysis are almost in the same order of those with crushing (Fig. 4–14), indicating that the trend is feature of Ar trapped in fluid inclusions. In $^{40}Ar/^{36}Ar$ vs. $1/^{36}Ar$ diagram (Fig. 4–15), a suite of samples having an originally constant $^{40}Ar/^{36}Ar$ component and becoming contaminated with variable amounts of atmospheric Ar will form a positive correlation (e.g., Fisher, 1986; Staudacher et al., 1989; Farley and Craig, 1994). However, this is not the case with

TKC014 because the separated parts are arranged along to a hypothetical contamination trend, i.e. the data cannot be explained by simple addition of atmospheric Ar via contamination.

The trend in Fig. 4–15 rather seems to indicate mixing between two different mantle-derived noble gas components. As shown above, the noble gases in Takashima xenoliths can be explained by mixing among atmospheric and two mantle-derived components. Judging from $^{40}Ar/^{36}Ar$ and $^{4}He/^{36}Ar$ ratios of each endmember, the noble gas profile observed in TKC014 is produced by mixing between MORB-type component (TKC014C) and plume-type component (TKC014A), though clear variation in $^{3}He/^{4}He$ ratio is not observed due to large analytical errors. The facts that TKC014C contacts with host basalt and that TKC014A seems to be core part considering the shape of xenoliths, strongly support assign of MORB-type component to noble gases in host alkaline basalt magma.

Table 4–8. Results of noble gas analysis for separated samples from TKC014.

Sample (Depth) / Method[*1]	Weight (g)	MS	^{4}He ($\times10^{-9}$)	^{20}Ne ($\times10^{-11}$)	^{36}Ar ($\times10^{-10}$)	^{84}Kr ($\times10^{-12}$)	^{132}Xe ($\times10^{-13}$)	^{3}He/^{4}He (R/R_A)[*2]	^{20}Ne/^{22}Ne	^{21}Ne/^{22}Ne	^{38}Ar/^{36}Ar	^{40}Ar/^{36}Ar
TKC014A olivine (0–1.0cm)												
HC 70MPa×3	3.15	IV*	0.40	b.b.	0.42	1.20	0.34	7.76 ± 3.38	n. m.	n. m.	0.18972 ± 0.00050	595.76 ± 0.93
SH 600℃	1.88	III	0.07	b.b.	1.15	30.50	12.40	3.05 ± 2.19	n. m.	n. m.	0.18872 ± 0.00096	297.13 ± 0.52
1000℃			2.31	0.69	0.47	2.46	19.60	3.47 ± 1.22	9.87 ± 0.25	0.0296 ± 0.0044	0.18904 ± 0.00092	323.92 ± 0.76
1400℃			1.48	2.74	0.57	1.68	4.71	11.07 ± 2.83	9.59 ± 0.21	0.0328 ± 0.0038	0.18784 ± 0.00088	587.65 ± 1.16
1800℃			2.42	4.61	1.44	3.76	2.92	9.65 ± 2.59	9.15 ± 0.10	0.0296 ± 0.0017	0.18924 ± 0.00094	575.10 ± 1.39
Total			6.28	8.04	3.63	38.40	39.63	7.64	9.35	0.0307	0.18883	456.31
TKC014B olivine (1.0–2.5cm)												
HC 70MPa×3	3.29	IV*	1.28	0.73	0.67	2.10	0.50	8.20 ± 1.40	9.68 ± 0.09	0.0277 ± 0.0037	0.19110 ± 0.00400	786.90 ± 1.40
SH 600℃	2.14	III	0.09	0.00	0.39	1.40	1.16	17.56 ± 60.36	9.66 ± 0.87	0.0370 ± 0.0150	0.18890 ± 0.00124	299.54 ± 0.57
1000℃			6.27	2.87	1.36	6.76	6.81	3.41 ± 0.62	9.58 ± 0.18	0.0304 ± 0.0032	0.18891 ± 0.00078	342.26 ± 0.57
1400℃			3.33	2.79	0.89	3.64	5.11	7.56 ± 1.23	9.48 ± 0.23	0.0308 ± 0.0023	0.18828 ± 0.00089	844.91 ± 1.46
1800℃			8.98	5.22	2.15	5.93	5.60	7.78 ± 1.36	9.88 ± 0.20	0.0288 ± 0.0021	0.18857 ± 0.00080	838.60 ± 1.94
Total			18.67	10.88	4.80	17.73	18.68	6.32	9.70	0.0298	0.18864	654.85
TKC014C olivine (2.5–6.0cm)												
HC 70MPa×3	3.06	IV*	2.20	0.59	0.62	2.00	0.50	7.10 ± 1.00	9.72 ± 0.14	0.0296 ± 0.0020	0.19258 ± 0.00062	1058.70 ± 2.10
SC 600℃	1.90	III	0.60	0.02	0.69	11.20	51.80	3.07 ± 3.22	10.02 ± 0.79	0.0340 ± 0.0071	0.18890 ± 0.00104	321.19 ± 0.56
1000℃			2.45	1.23	0.56	2.01	5.11	5.81 ± 2.03	9.88 ± 0.44	0.0305 ± 0.0093	0.18868 ± 0.00113	381.67 ± 1.23
1400℃			3.48	1.58	0.54	2.28	15.60	9.48 ± 1.19	9.57 ± 0.42	0.0274 ± 0.0024	0.18802 ± 0.00101	1508.40 ± 4.83
1800℃			8.78	3.68	1.58	4.19	4.37	7.46 ± 0.77	9.88 ± 0.19	0.0327 ± 0.0031	0.18908 ± 0.00105	1287.29 ± 5.25
Total			15.31	6.51	3.37	19.68	76.88	7.48	9.80	0.0310	0.18881	975.05

Unit for concentrations are cm^3STP/g. Errors with isotopic ratios are 1σ. b.b.=below blank, n. m. = not measured *MS–IV before modification.

*1. SH: Step heating, HC: Crushing with a hydraulic-type crusher.

*2. Normalized to the atmospheric ratio = 1.4×10^{-6} (Ozima and Podosek, 1983).

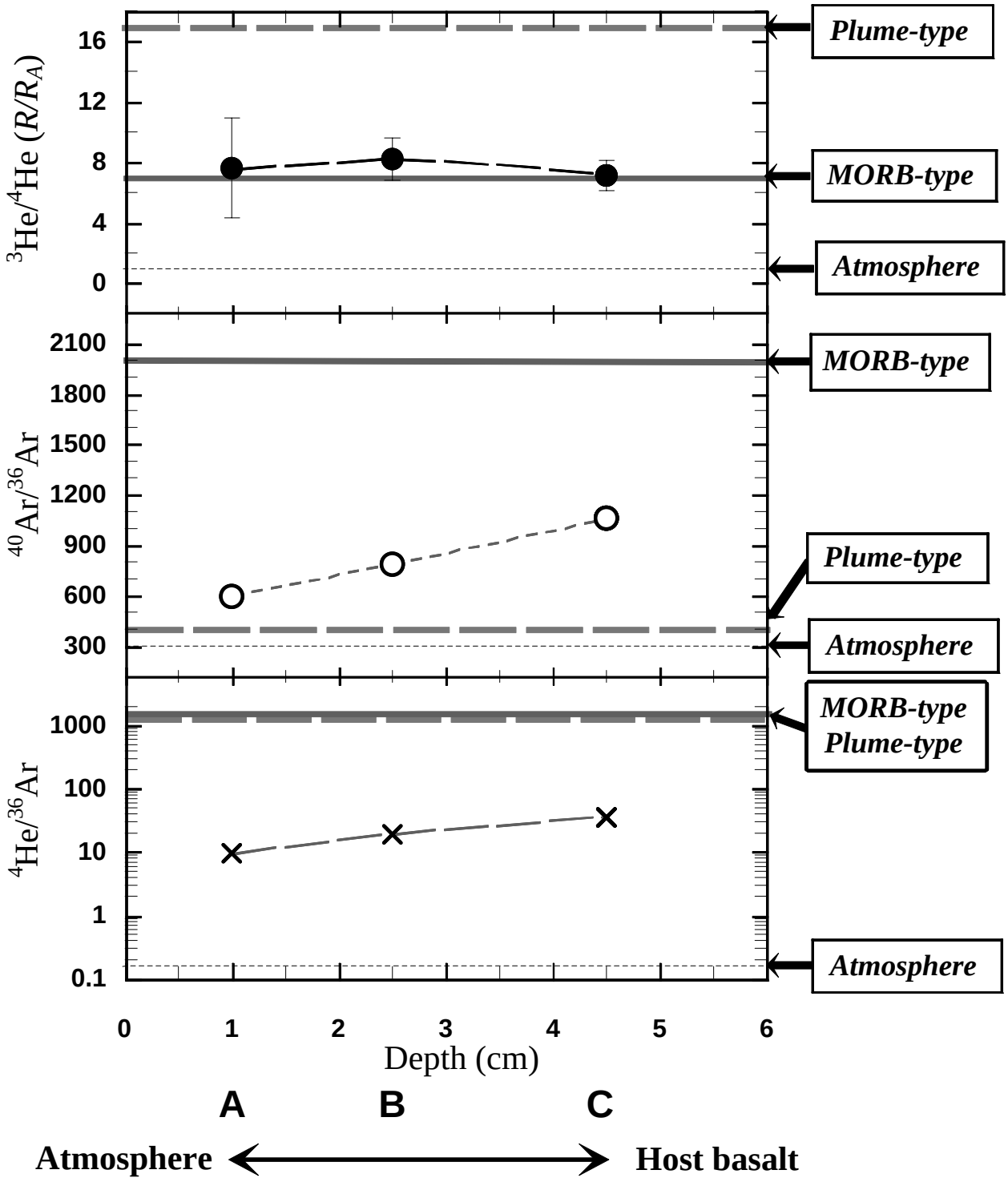

Fig. 4–13. Noble gas profile in the core sample TKC014. The isotopic compositions (Table 4–5) of each endmember observed in xenoliths from Takashima are indicated as thick dashed lines (plume-type), thick solid lines (MORB-type) and thin dotted lines (atmosphere), respectively.

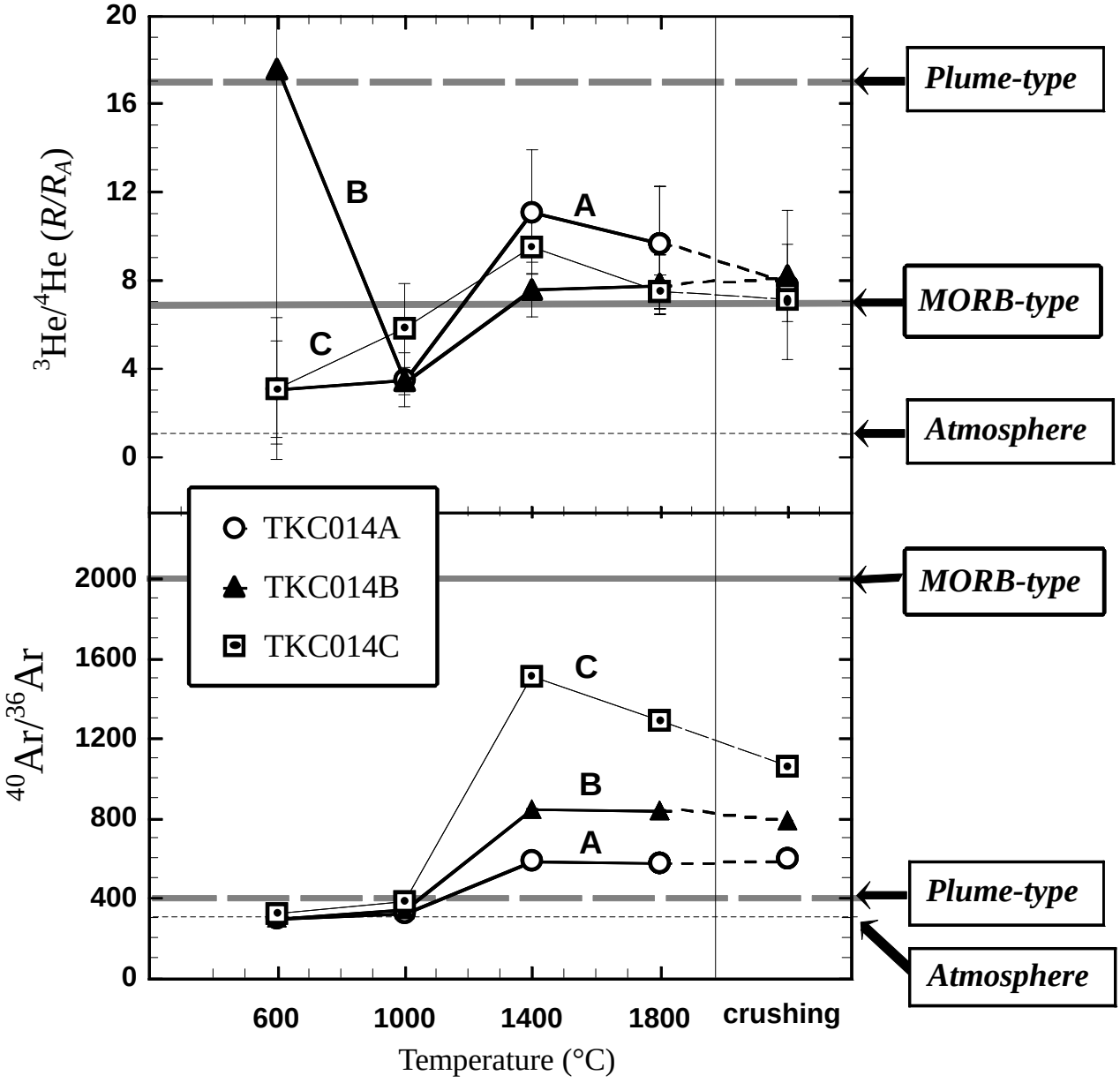

Fig. 4–14. Results of stepwise heating for splits of TKC014. The isotopic compositions (Table 4–5) of each endmember observed in xenoliths from Takashima are indicated as thick dashed lines (plume-type), thick solid lines (MORB-type) and thin dotted lines (atmosphere), respectively.

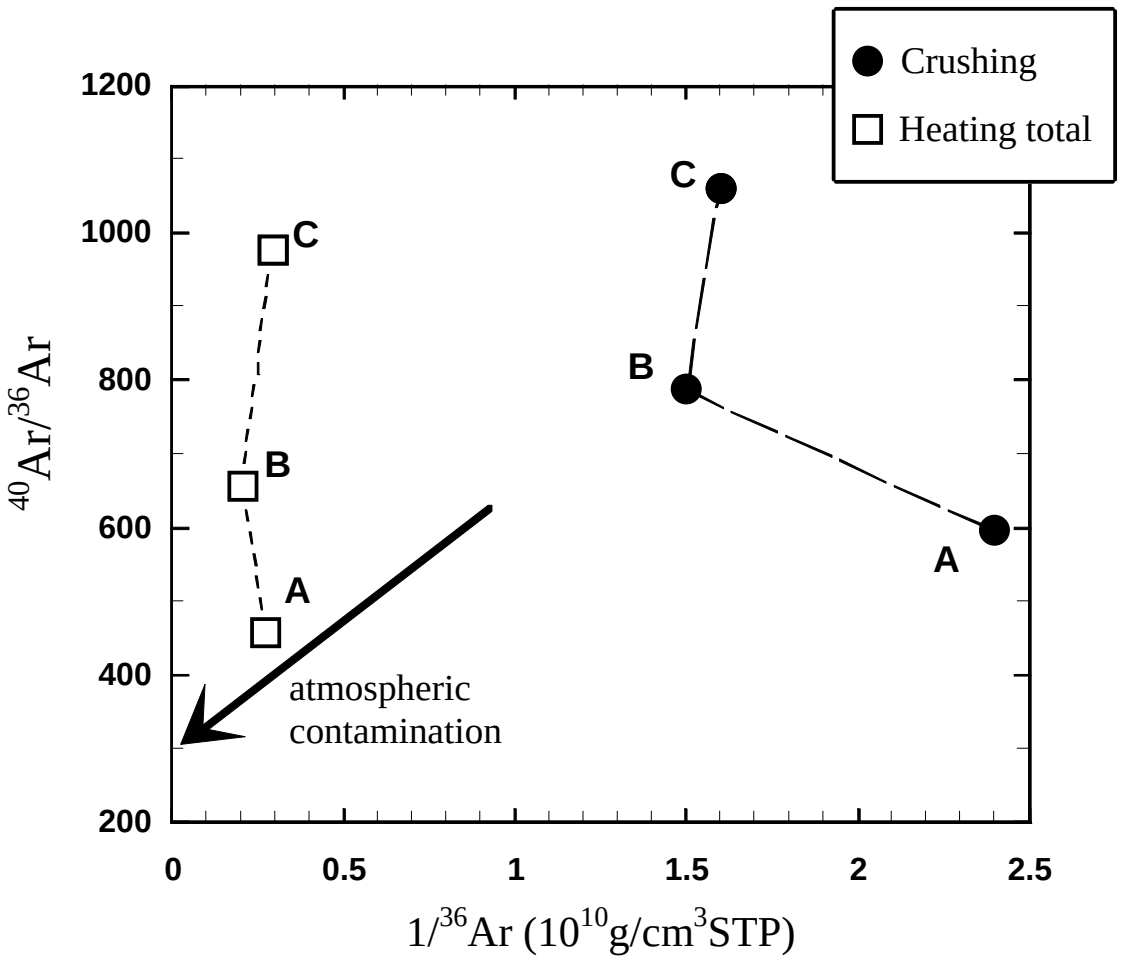

Fig. 4–15. $^{40}Ar/^{36}Ar$ vs. $1/^{36}Ar$ for the core sample (TKC014) of xenolith from Takashima. A hypothetical trend of atmospheric contamination is shown for comparison. Data for different sample splits are anti-correlated, indicating that atmospheric contamination is insignificant.

Microscopic observation of fluid inclusions

To clarify how and when the two (or more) kinds of noble gases are trapped in an individual xenolith deduced from above discussions, fluid inclusions in TKS01 and TKD1120 olivines are observed with a microscope, because stepwise crushing experiments showed that both endmember of noble gases (Fig. 4–9) are likely to be trapped in fluid inclusions. Figure 4–16 and Fig. 4–17 are photomicrographs of fluid inclusions in TKD1120 and TKS01, respectively.

Fluid inclusions which are aligned along planes of healed fractures across grain boundaries with various shapes are observed in TKD1120. Sometimes they are associated with melt inclusions. The shapes are spherical with a diameter of 5μm or elongated tubular with a diameter of 5μm and sometimes reaching to 50μm in the length. Tube-shaped inclusions are thought to change into small spherical inclusions when fractures coalesce (Wanamaker and Evans, 1989). These morphologies suggest secondary origin, which was formed during volatile penetration after accumulation of olivine in dunite xenoliths. Thus this kind of inclusions is called secondary fluid inclusion.

On the other hand, not only secondary fluid inclusions but also the other type of fluid inclusions are observed in TKS01. This type of inclusions is large (typically 20–50μm in diameter) spherical or occasionally as negative crystal, sometimes separate into two-phase (liquid and vapor), and scatter randomly. These fluid inclusions might be formed at the same time of crystallization or remelting of host olivine. Thus this kind of inclusions is called primary fluid inclusions.

Mid-infrared spectra were obtained by micro FT-IR (Fourier transform infrared) spectroscopy in order to what volatiles are dominant in primary and secondary fluid inclusions. Infrared spectra were recorded using a Perkin Elmer Spectra 2000 FT-IR spectrometer equipped with an IR microscope (Kagi and Takahashi, 1998). The samples are doubly polished thin sections with a thickness ca 500μm. The beam size of the IR incident light was 100μm and irradiated at the point indicated in Fig. 4–16 and Fig. 4–17, respectively. Obtained Mid-IR spectra are shown in Fig. 4–18. A doublet of C=O stretching of CO_2 is observed around 2350cm^{-1}. Any adsorption of other volatiles such as H_2O around 3400cm^{-1} was not observed in all spectra. It is difficult to quantitatively

estimate the amount of CO_2 and lower limit of CO_2/H_2O at present, it is revealed that at least CO_2 is trapped in both primary and secondary fluid inclusions and may be dominant.

Considering that TKD1120 indicate MORB-type $^3He/^4He$ ratio constantly and secondary fluids inclusions are dominant in it, MORB-type noble gas is trapped in secondary fluid inclusions. On the other hand, since TKS01 show both low $^3He/^4He$ ratio and high $^3He/^4He$ ratio heterogeneously and contains both primary and secondary fluid inclusions, plume-type component is trapped in primary fluid inclusions. This interpretation is consistent with that He in TKD1120 is released at relatively low temperature with step heating, because secondary inclusions may easily decreptate along healed cracks.

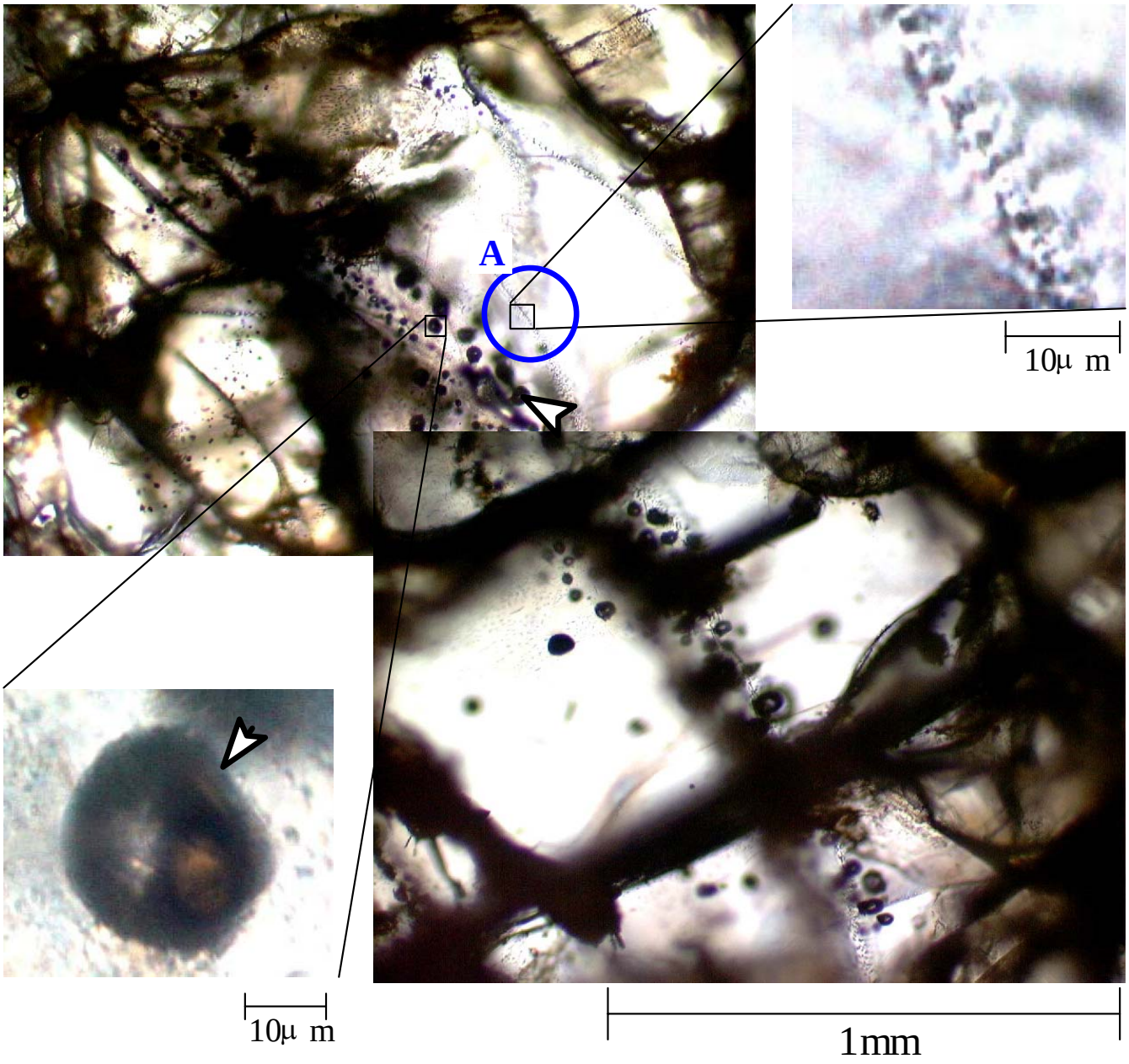

Fig. 4–16. A photomicrograph of secondary fluid inclusions in olivine in TKD1120 xenolith from Takashima, showing planar arrays of fluid inclusions across grain boundaries of olivines. Tube-shaped secondary inclusions elongated along the plane of the fracture are also shown. “A” and “B” are beam spot of micro FT-IR corresponding to spectra in Fig. 4–18. Relatively large melt inclusions associating with secondary fluid inclusions are indicated by arrows.

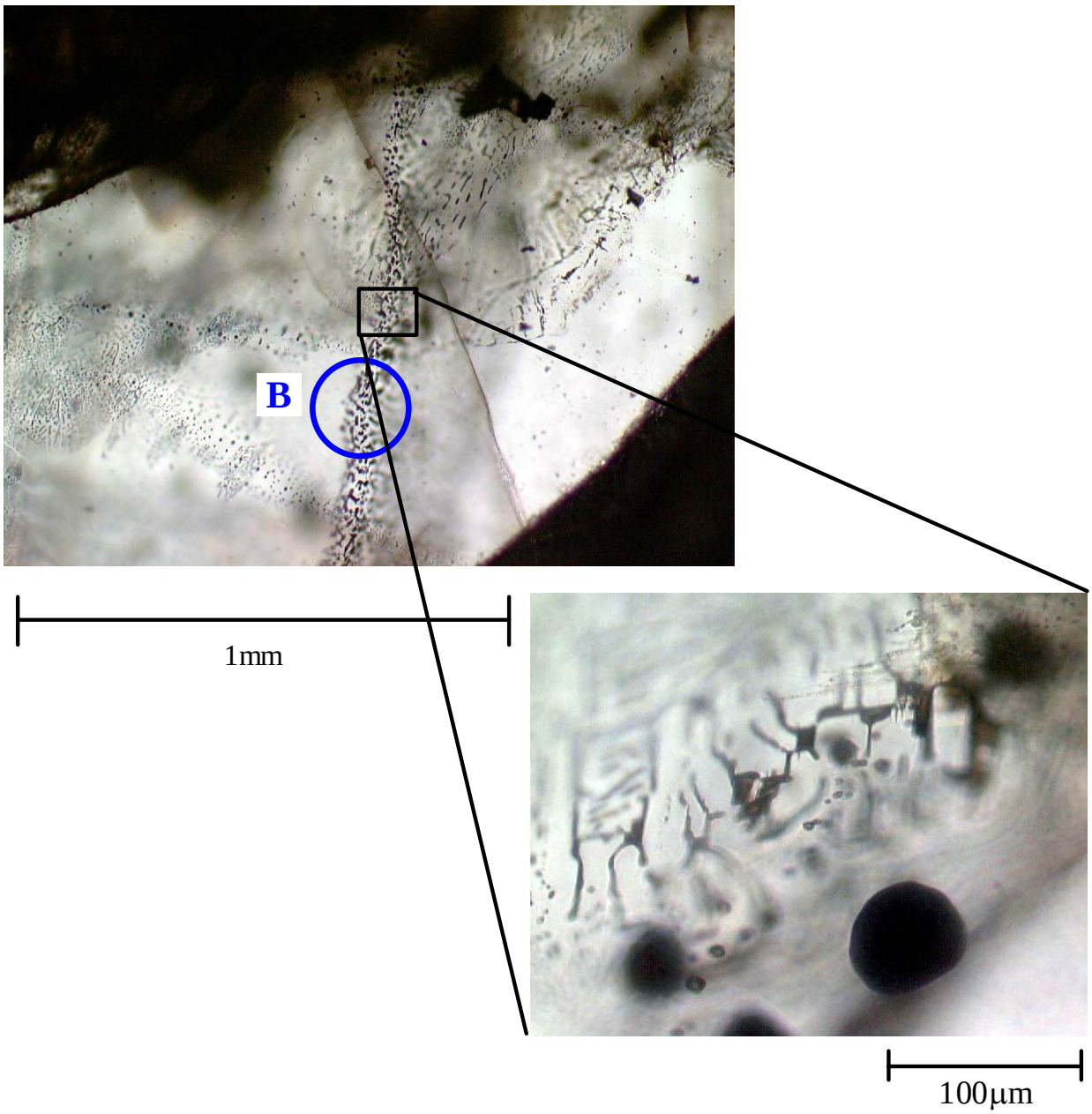

Fig. 4–16. (Continued)

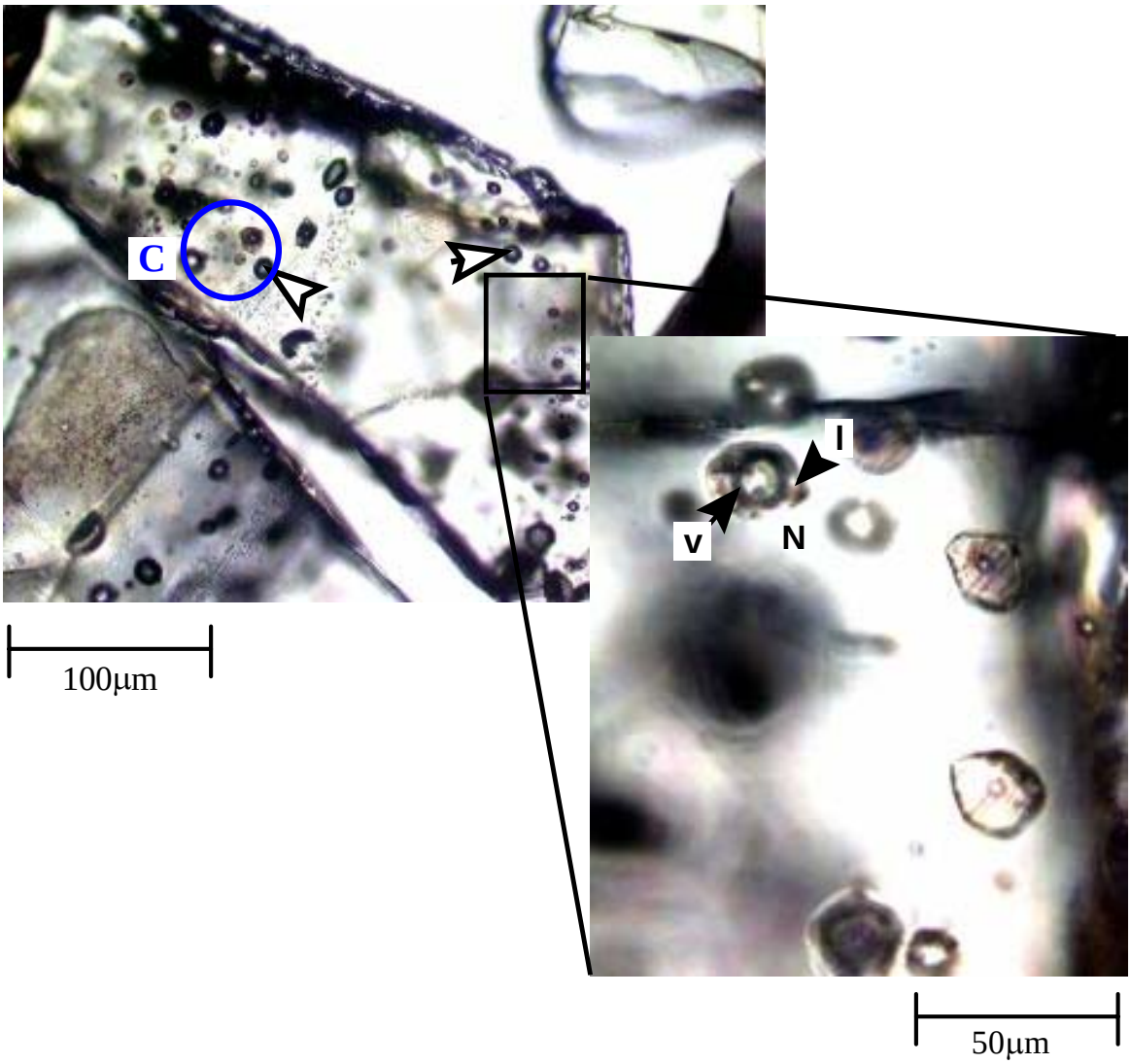

Fig. 4–17. A photomicrograph of primary fluid inclusions in TKS01 xenoliths from Takashima. Numerous two-phase spherical inclusions are arrowed and two-phase negative crystal inclusion marked (N), with indicating liquid (l) and vapor (v) phase. “C” is a beam spot of micro FT-IR corresponding to spectrum in Fig. 4–18.

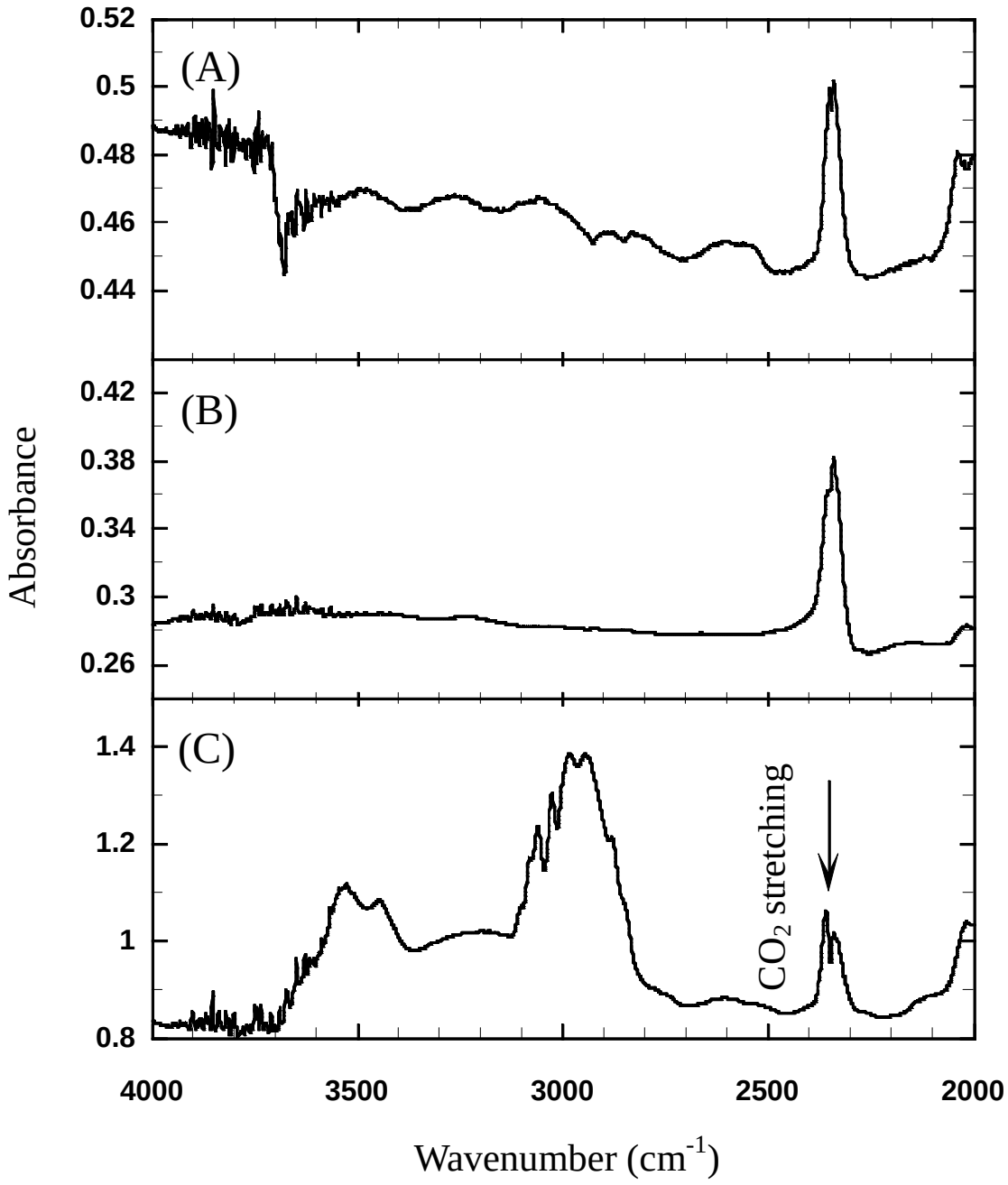

Fig. 4–18. Mid-IR absorption spectra of (A) spherical secondary fluid inclusions, and (B) tubular secondary fluid inclusions in TKD1120, and (C) primary inclusions in TKS01. Although CO_2 stretching absorption are clearly observed, H_2O which should be observed around 3400cm^{-1} with broad band, is not observed. Note that other structure in spectra are absorption of host olivine.

The origin of cognate and accidental noble gases

It is revealed that some xenolith from Takashima contain two kinds of noble gases, one is trapped in primary fluid inclusions suggesting its cognate origin with xenoliths, and the other is trapped accidentally and concurrently with formation of secondary fluid inclusions. According to Arai and Abe (1994), the last equilibration of Takashima xenoliths took place at temperatures between 1000 and 1100°C, and depths of 40-80km estimated from geotherm of xenoliths from Fukue-jima, northwestern Kyushu (Umino and Yoshizawa, 1996). At these temperatures, diffusion coefficients for He diffusion in olivine are about $3.2\times10^{-11}cm^2/s$ (Trull and Kurz, 1993) and intermineral isotopic equilibrium between mm-sized mantle phase should be achieved in less than 10 years. Since there is clear evidence for He isotopic disequilibrium in some xenoliths from Takashima, the metasomatic overprint must have occurred shortly before or concurrently with the eruption of host magma. Considering the fact that isotopic compositions of the MORB-type endmember resemble closely to that of alkaline basalt magma erupted around Takashima ($^3He/^4He\sim7R_A$, $^{40}Ar/^{36}Ar>800$), it is concluded that MORB-type noble gas in xenoliths resulted from exchange with that in host magma. It is consistent with the noble gas profile in the core sample TKC014, suggesting interaction of noble gases in the xenolith with those of host basalt magma. Alternatively, plume-type He has been trapped in cumulate beneath northwestern Kyushu, before ascending the alkaline basalt magma erupted in Takashima. This suggests that volcanism triggered by mantle plume had occurred before 7Ma, which is the eruption age the oldest basalt among those analyzed in this study. The origin of plume-type He will be further discussed in next chapter.

5. Implication for mantle dynamics deduced from noble gas isotope systematics in alkaline basalt and mantle-derived xenolith

5–1. Geochemical nature of sub-continental mantle beneath back-arc region of southwestern Japan

5–1–1. Noble gas characteristics of sub-continental mantle

Noble gas nature of sub-continental mantle beneath back-arc region of southwestern Japan is inferred from the xenoliths from Cheju Island. The noble gas in alkaline basalt magma erupted in Higashi-matsuura also represents the isotopic composition of sub-continental mantle because their noble gases and Nd–Sr isotopes lack plume-like signature (see chapter 3). Although noble gas in Takashima xenoliths have complicated characteristics resulting from interaction with host alkaline basalt magma, MORB-type endmember gives information of sub continental mantle because it is considered to be inherited from host alkaline basalt magma (chapter 4). The inferred features of noble gas isotopic composition of the sub-continental mantle are (1) lower $^{3}He/^{4}He$ ratios (6.5–7.0R_A) than that of MORB (8.18±0.73R_A), $^{40}Ar/^{36}Ar$ ratio up to 4400, which is distinctly lower than those of MORB (>28000), (3) F-values depleted in light noble gases and enriched in heavy noble gases, which is similar to the pattern of air-saturated sea water, old oceanic crust, and oceanic sediments.

5–1–2. Atmospheric Ar in the sub-continental mantle

Lower $^{40}Ar/^{36}Ar$ ratio of the sub-continental mantle than that of the MORB-source upper mantle suggests that atmospheric Ar was brought into the mantle wedge beneath northwestern Kyushu and Cheju Island by subduction process. Assuming the initial $^{40}Ar/^{36}Ar$ ratio of 28000 similar to MORB-source mantle, contributions of the

subducted Ar can be estimated. The contributions of atmospheric component are calculated to be 91% and 85% of the total ^{36}Ar for the least contaminated samples from northwestern Kyushu (1800°C fraction of TKS01ol heating) and Cheju Island (CHJ9901ol crushing), respectively. If the atmospheric Ar is derived from deep-sea water with ^{36}Ar concentration of 1.27×10^{-6}cm^{3}STP/g (Allègre et al., 1986/87), the amount of water required for the mantle beneath northwestern Kyushu and Cheju Island are 2.8 and 1.6mg for 1g xenolith, assuming ^{36}Ar concentration of upper mantle of 3.5×10^{-10}cm^{3}STP/g (Staudacher and Allègre, 1988) for xenoliths. If oceanic sediments are the source of atmospheric Ar, required amounts of sediments are more than the deep-sea water because of the lower concentrations (2.7×10^{-8}cm^{3}STP/g) of ^{36}Ar and nearly atmospheric or higher ^{40}Ar/^{36}Ar ratio in the sediments (Matsuda and Nagao, 1986; Staudacher and Allègre, 1988). Although the atmospheric Ar in CHJ9901ol may include adsorbed Ar on the surface of the sample, the contribution of atmospheric component is smaller than that in least contaminated sample from northwestern Kyushu. Therefore, degree of atmospheric contamination by subducting slab in the mantle beneath Cheju Island is smaller than that in the mantle beneath northwestern Kyushu. Nakamura et al. (1989) compared composition of major and trace element in alkaline basalt from southwestern Japan, Cheju Island and northeastern China, and considered that although upper mantle beneath southwestern Japan has been weakly affected by metasomatism caused by fluid derived from the subducted Pacific plate (not the Philippine Sea plate), the metasomatism has not affected the mantle beneath Cheju Island and northeastern China. Highly contaminated signature of the mantle beneath southwestern Japan in Ar isotopes compared to those beneath Cheju Island is consistent with the conclusion of Nakamura et al. (1989). Different degree of the contamination and the metasomatism may be due to difference in distance from trench between northwestern Kyushu and Cheju Island. The slab-derived Ar observed in sub-continental mantle beneath Cheju Island, which little metasomatized in major and trace element, may reflect higher diffusivity of noble gas in the mantle than those of the elements mentioned in Nakamura et al. (1989), because they do not chemically interact with mantle materials.

In addition, according to the petrological and geochemical observations, the mantle xenoliths from Kurose and Cheju Island have been polluted by metasomatism (Abe et al., 1998, Hee, 1998). It is reasonable that the metasomatic agent was fluid released from the subducting slab and possibly brought atmospheric Ar to the mantle beneath these regions.

5–1–3. Elemental ratio indicating slab-derived component

The idea of metasomatized sub-continental mantle by subduction-derived fluids is supported by noble gas abundance ratio (F-value). The relationships F(20) vs. F(84) and F(20) vs. F(132) are shown in Fig. 5–1. Since the results obtained with crushing seems to be disturbed by experimental effect such as contamination by adsorbed atmospheric components and adsorption of released noble gases (see 3–3 and 4–3), the data obtained with high temperature fraction of step heating and total fusion are discussed here. Noble gas compositions of the atmosphere, deep-sea water (Allègre et al., 1986/87), magma equilibrated with seawater (Patterson et al., 1990), and old oceanic crusts and sediments (Matsuda and Nagao, 1986; Staudacher and Allègre, 1988) are also shown in Fig. 5–1 for comparison.

Although the results for basalt from northwestern Kyushu are scattered, a negative correlation can be recognized. There are two possible processes to form the trends of olivines and clinopyroxenes. One is the two-component mixing and the other is the fractionation by dynamic processes in magma, such as melting, crystallization and degassing. The former requires two components. Noble gas in MORB-like upper mantle, atmosphere or magma equilibrated with seawater is one of the endmembers and the other is characterized by very low F(20) (<0.2), and very high F(84) (>3.5) and F(132) (>30), which is similar to noble gas compositions of old oceanic crust and oceanic sediments. Even if the latter accounts for the negative correlation, the compositional change starts from the source material with low F(20) and high F(84) and F(132), because prospective changes caused by the processes in the magma such as melting, crystallization and degassing are in the same direction as indicated in Fig. 5–1. In either case, noble gas elemental ratios of basalts from northwestern Kyushu suggest the existence of slab-derived component. Since some data for basalts from

Higashi-matsuura are plotted near the low-F(20) end of the trend, contribution of slab-derived material is not limited in Kita-matsuura basalt, which was affected by sub-crustal component (see section 3–4), and is the feature of source mantle of alkaline basalt which is probably sub-continental mantle beneath northwestern Kyushu.

The data for mantle-derived xenoliths from Takashima and Kurose can be explained by two component mixing between MORB-like mantle and slab-derived materials (old oceanic crust and oceanic sediments). As demonstrated in chapter 4, the noble gases in xenoliths from Takashima were contaminated by those in host basalt magma suggesting that slab-derived component is inherited from host alkaline basalt magma. However, the sample most enriched in Xe has higher F(132) value than maximum value observed in basalts, and the second enriched sample in heavy noble gases has plume-like $^{3}He/^{4}He$ ratio, contradicting contamination by host basalt.

In conclusion, existence of slab-derived component in the mantle beneath northwest Kyushu is supported by noble gas elemental ratio, as well as by much lower $^{40}Ar/^{36}Ar$ ratio than MORB source mantle.

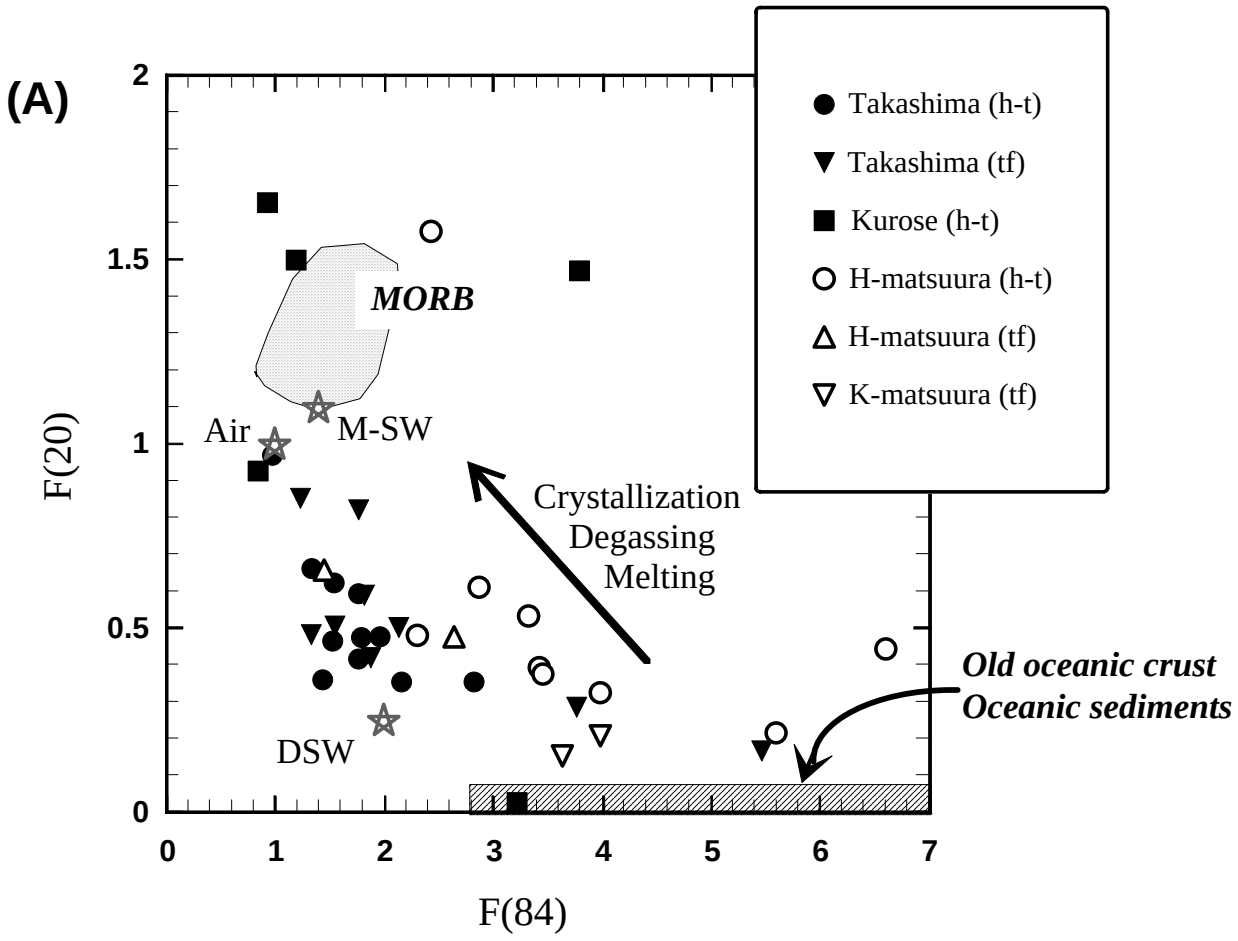

Fig. 5–1. (A) F(84) vs. F(20) and (B) F(132) vs. F(20) plot for the xenoliths from Takashima and Kurose, and basalts from Higashi-matsuura (H-matsuura) and Kita-matsuura (K-matsuura) in northwestern Kyushu. Open symbols are basalts, filled symbols are xenoliths, respectively. “h-t” and “tf” are data obtained with high temperature fraction of step heating and total fusion, respectively. The marks of “Air”, “DSW” and “M-SW” indicated the compositions of atmosphere, deep-sea water (Allegre et al., 1986/87) and magma equilibrated with seawater calculated as Patterson et al. (1990) using solubility data of alkaline olivine basalt (Lux, 1987). The range of MORB glasses (Staudacher et al, 1989; Hiyagon et al., 1992) and old oceanic crust and oceanic sediments (Matsuda and Nagao, 1986, Staudacher and Allegre, 1988) are shown. Changes of F-values by crystallization, degassing and melting are schematically illustrated by arrows.

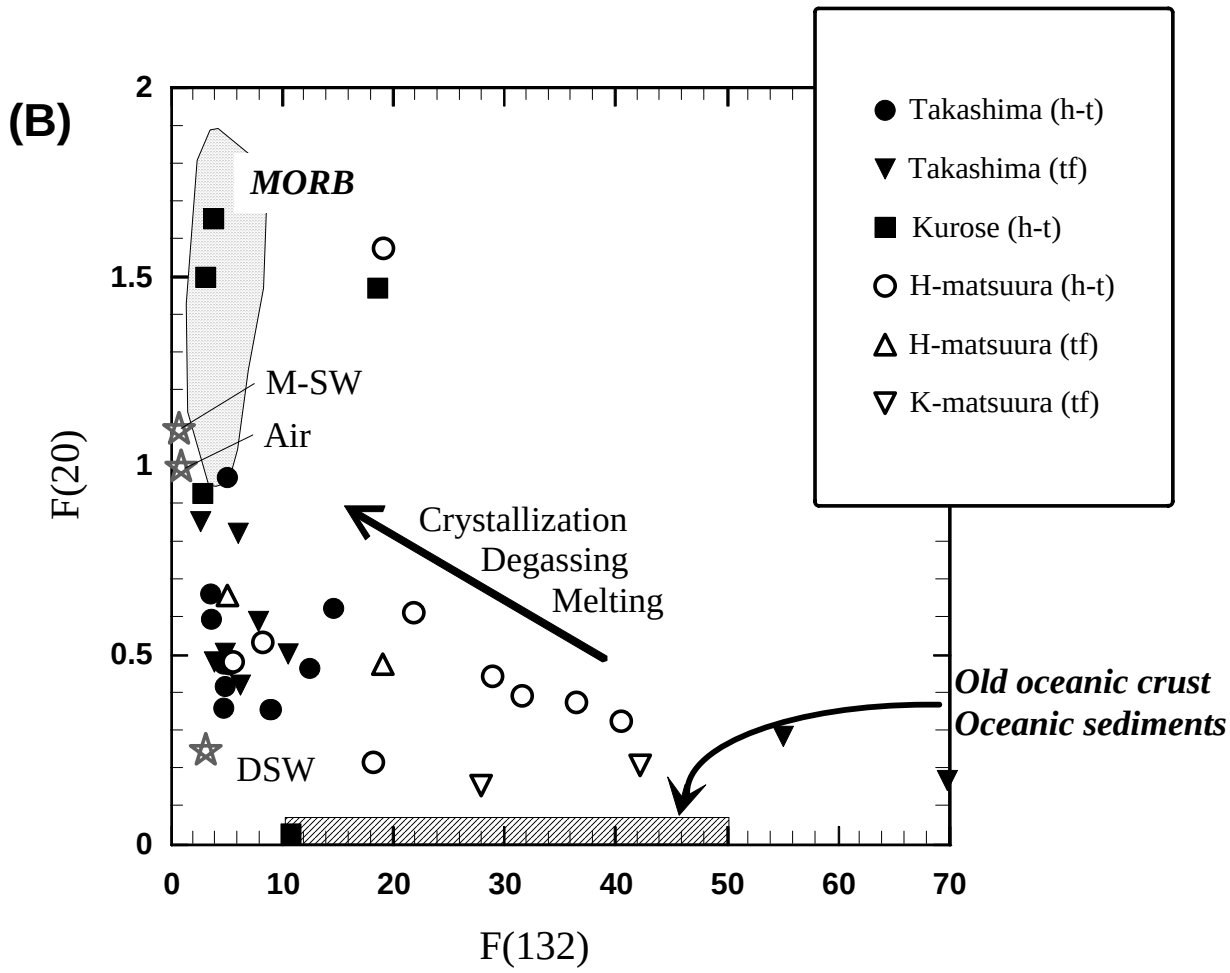

Fig. 5–1. (Continued)

5–1–4. Sources of radiogenic He in the sub-continental mantle

Low $^{3}He/^{4}He$ ratio observed in back-arc region of southwestern Japan

Ar isotopic ratio and noble gas elemental ratio of sub-continental mantle beneath back-arc region of Japan strongly suggest presence of slab-derived noble gas in the mantle wedge. Similar possibility of subduction-related metasomatism in noble gas discussed above has been argued by Nagao and Takahashi (1993) for xenolith from Ichinomegata and Oki-Dogo. However, the $^{3}He/^{4}He$ feature in the samples from Ichinomegata and Oki-Dogo is different from that observed in northwestern Kyushu in this study. In the previous study, while $^{40}Ar/^{36}Ar$ ratio and elemental ratio of noble gases indicate their subducted slab origin, $^{3}He/^{4}He$ ratio is almost the same with MORB-value, including only helium is not altered by subduction processes. Nagao and Takahashi (1993) suggested that helium originally trapped in the mantle wedge was lost by degassing, and continuous supply of helium from deeper mantle recovers helium isotopic ratio to MORB-like ratio. On the other hand in northwestern Kyushu, uppermost mantle remain helium isotopic ratio altered by radiogenic helium from slab or, enriched in U and Th resulting lowering of $^{3}He/^{4}He$ ratio. This difference might be related to different tectonic settings. Ichinomegata and Oki-Dogo are located close to the Sea of Japan, where asthenosphere upwelling concurrent with opening of the back-arc basin have occurred extensively and caused a lateral injection of asthenospheric materials into mantle wedge (Tatsumi and Kimura, 1991). In the meantime, the opening of back-arc basin did not occurred around northwest Kyushu. In addition, southwestern Japan arc rotated clockwise through 54° in association with opening the Sea of Japan, and the axis of rotation was on southwestern margin of the Sea of Japan (Otofuji and Matsuda, 1983). Therefore, although the region around the Sea of Japan was in a extensive field, northwestern Kyushu might be governed by compressive stress field, preventing asthenospheric upwelling in mantle beneath this region. In consequence, replacement of helium suffered from metasomatism did not progressed efficiently compared to around Ichinomegata and Oki-Dogo. This explanation is consistent with that relationship between contents of incompatible

elements and Nd–Sr isotopes in basalts from northwestern Kyushu indicates relatively slow uprising of mantle diapirs with mixing with surrounding mantle, although lack of such relationship in basalts from Chugoku district is considered to be resulted from quick uprise of the diapirs from the mantle plume (Kakubuchi et al., 1995).

He released directly from subducting materials

The lower $^{3}He/^{4}He$ ratio than MORB can be produced by two mechanisms. One is contamination of atmospheric or radiogenic He released by subducting materials, and the other is production of radiogenic ^{4}He in the mantle wedge.

Because of the low He concentration in deep-sea water, 5.1mg of sea water for 1g xenoliths is required to decrease $^{3}He/^{4}He$ ratio with lowest He concentration among all the samples. However, required seawater for typical low $^{3}He/^{4}He$-sample (TKD1120) with relatively high concentration of He is ca. 15% by weight. Of course, such a high concentration of water in peridotites is unrealistic. In addition, hydrous mineral is not observed in xenoliths from southwestern Japan (Takahashi, 1978). Therefore, atmospheric He derived from subducted deep-sea water cannot explain low He isotopic ratios of the samples by itself.

Since the subducting oceanic crust has a relatively high He concentration and low $^{3}He/^{4}He$ ratio (Staudacher and Allègre, 1988), it could supply radiogenic ^{4}He to the mantle wedge, resulting in a decrease of $^{3}He/^{4}He$ ratios. Although the behavior of He in the subduction environment is not well understood, much fluids is probably lost from the slab at shallow depth (Liu et al., 1996) and, since He is partitioned into fluid, almost all of He returns back into the atmosphere through subduction volcanism, limiting the ability of a slab-derived component in significant modification of the He isotopic composition of the mantle wedge.

In-situ decay of U and Th in sub-continental mantle

If the present-day $^{3}He/^{4}He$ ratio of sub-continental mantle is due to retention of radiogenic He produced by decay of U and Th in the mantle wedge, then the $(U+Th)/^{3}He$ ratio of the sub-continental mantle beneath back-arc region of southwestern Japan can be estimated. Comparison of this value with that of MORB allows us to evaluate the effect of metasomatism. The $^{3}He/^{4}He$ ratio values of the sub-continental

mantle of 6.5–7.0R_A today is determined by $^3He/^4He$ ratio at the time when the sub-continental mantle is isolated from the convecting mantle, and the $(U+Th)/^3He$ ratio, and any gain or loss of ^3He and ^4He during this time. Despite it is not well understood when arc-magmatism in the Eurasian continental margin started, Proto-Japan was located in the eastern Part of Yangtze Craton in Triassic, ca. 300Ma and the subduction of an unnamed oceanic plate, the Farallon, Izanagi or Pacific plate have continued until recently (Maruyama et al., 1997). On the other hand, 2.0Ga is the oldest geological record in Japan reported for Precambrian metamorphic rock (Shibata and Adachi, 1974), suggesting that the basement rock of the southwestern Japan had already formed at 2.0Ga and the sub-continental mantle was isolated before the time. A closed system evolution for U and He is modeled in Fig. 5–2. Initial $^3He/^4He$ ratio of the mantle at the time of isolation of sub-continental mantle is estimated using closed-system evolution from a primordial value of 100R_A at 4.5Ga to 8.18R_A today, as Reid and Graham (1996) did, resulting the initial $^3He/^4He$ ratio would higher than present MORB-value. The dashed lines indicate the range of $U/^3He$ ratios required to produce the appropriate He isotopic compositions in the sub-continental mantle beneath the back-arc region of southwestern Japan over the time since isolation from the convecting mantle at 300Ma or 2.0Ga. The $U/^3He$ ratios necessary for the sub-continental mantle are roughly four times that of MORB-source mantle today with the age of isolation of 300Ma. On the other hand, $U/^3He$ ratio required producing low $^3He/^4He$ ratio during 2.0 giga-years of isolation is about 1.5 times that of the MORB-source mantle, indicating that slightly enrichment of U relative to ^3He can account for low $^3He/^4He$ ratio.

In any case, high $U/^3He$ ratios can be produced by enrichment in U derived from subducted slab and/or effective degassing of He through arc volcanism. U concentration of sub-continental mantle beneath this region is not well constrained, however, the $^3He/^4He$ ratio suggesting U enrichment relative to MORB-source mantle is consistent with that Nd–Sr ratios of xenoliths from Kurose and Cheju Island show enriched signature in incompatible element compared to MORB (Kagami et al., 1993; Hee, 1998). In addition, source mantle of basalts from northwestern Kyushu show 8–30 times rich in large ion lithophile elements (such as K, Rb, Sr and Ba with which U and Th behave together in mantle chemistry) normalized to normal-MORB source mantle (Kakubuchi et al., 1995) even of basalts with most depleted characteristics. The composition of

metasomatic agent is still unknown, however, the sub-continental mantle beneath back-arc region of southwestern Japan is likely to be enriched in U and Th, supporting in-situ radiogenic origin of observed low $^3He/^4He$ ratio lower than MORB-value.
It is suggested that uppermost mantle beneath northwestern Kyushu contain sub-crustal He with $^3He/^4He$ ratio lower than $0.2R_A$ (chapter 3). To produce such low $^3He/^4He$ ratio with the closed-system evolution model, extremely high initial $U/^3He$ ratio of 5×10^6 and 7×10^5 are required for the lithospheric age of 300Ma and 2Ga, respectively. Such high $U/^3He$ ratios (up to 100 times that of present MORB) are incredible to result from high U concentration in the mantle by itself, suggesting effective degassing of He. If U concentration is uniform in entirely sub-continental mantle, 98.3–99.2% of He in the uppermost mantle are degassed probably though volcanism.

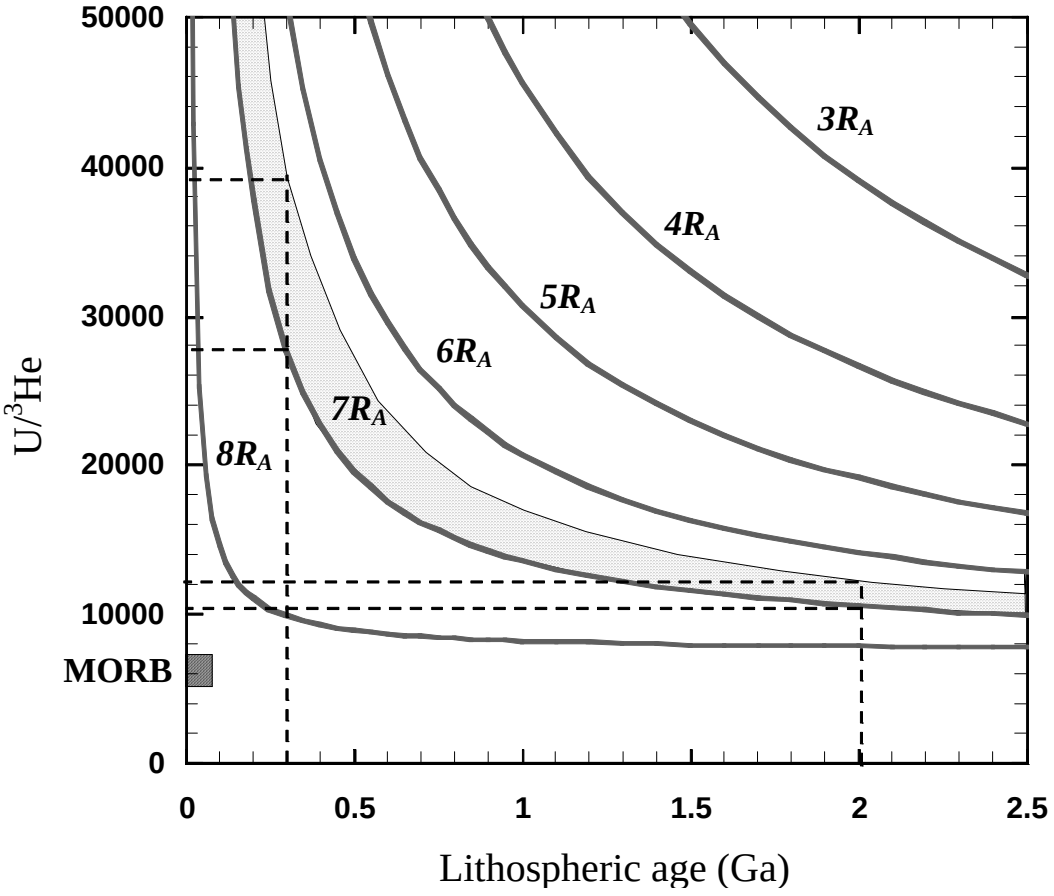

Fig. 5–2. Evolution of He isotopic ratios in lithospheric mantle regions as a function of initial $U/^3He$ (atomic ratio) and time. $U/^3He$ ratio in present-day MORB-source mantle is roughly 5200 (Zindler and Hart, 1986). Hatched area represents the observed range of $^3He/^4He$ ratio for the sub-continental mantle beneath the back-arc region of southwestern Japan. Curves are calculated assuming an initially $^3He/^4He$ ratio of the mantle estimated with closed-system evolution (Reid and Graham, 1996) from a primordial $^3He/^4He$ ratio of $100R_A$, with Th/U=3.9 and $U/^3He=7500$.

5–2. Origin of the plume source

5–2–1. Temporal change in isotopic composition of melt generated from mantle plume

As discussed in previous section (4–4–2), plume-type He had been trapped in sub-continental mantle beneath northwestern Kyushu before ascending of alkaline basalt magma analyzed in this study. This suggest that volcanism triggered by mantle plume which contained He derived from lower mantle was occurred in this region. Since arc volcanism had been active taken place by subduction of the Izanagi plate or Pacific plate before the beginning of subduction of the Philippine Sea plate at 40Ma (Maruyama et al., 1997) over several hundreds of million years, even if some plumes ascended from lower mantle, they might be arrested by the subduction of the Izanagi or Pacific plate. After the Philippine Sea plate began to subduct, sedimentary basin induced by mantle upwelling had been formed and melt produced by decompression melting had accumulated at crust-mantle boundary until alkaline basaltic volcanism came into active (Yanagi and Maeda, 1998). Therefore, it is probable that the mantle upwelling was plume containing lower mantle He, and produced early alkaline basaltic magma erupted in northwestern Kyushu before at least 7 million years ago, which is the oldest age of the sample analyzed in this study. The cumulative xenoliths observed in this region can be cumulates of the early alkaline basaltic magma and form layer of cumulus mantle beneath this region (Yanagi and Maeda, 1998). If this is the case, plume-type He in xenolith from Takashima was inherited from the early alkaline basalt magma preceding the alkaline basalts currently observable and analyzed in this study. Since the alkaline basalts erupted in recent 7 million years contain MORB-type He, the $^{3}He/^{4}He$ ratios of source material of alkaline basalt magma might change from plume-type to MORB-type with the time. The basalts analyzed in this study contain MORB-type He and show depleted Nd–Sr isotopic compositions, thus Nd–Sr isotopic ratios of the source material of alkaline basalts have shifted to depleted end of the trend of alkaline basalts in this region (Fig. 3–13).

A similar temporal change of noble gas and lithophile isotopic composition was observed in volcanic rocks from Hawaii, and a model to explain this variation was

proposed by Valbracht et al. (1996). According to the model, incipient CO_2-dominated melts, carrying noble gases with plume-like signature preceded the main body of plume and generated the initial stage of alkaline basalts in Hawaii. When the main plume, carrying the enriched lithophile signature rose and reached to partial melt zone, the main activity of alkaline tholeiites occurred. The melt of a late stage shows lower $^3He/^4He$ ratios owing to dilution by MORB-type He accompanied with entrainment by depleted mantle materials surrounding the plume.

When the model is applied to the case of northwestern Kyushu, schematic temporal change of noble gas beneath this region is illustrated in Fig. 5–3 and 5–4. First, volatiles with plume-type feature in noble gases ($^3He/^4He > 17R_A$, $^{40}Ar/^{36}Ar > 400$) separated from the plume body as the plume ascending, and generate volatile-rich silicate melt by lowering melting point of the sub-continental mantle above the plume. The early alkaline basalt melt might inherited plume-type noble gases. Iwamori (1992) suggested that alkaline volcanism in southwest Japan was caused with a plume with abundant volatile and incompatible elements rather than a plume of anomalously high temperature, supporting the existence of silicate melt which was rich in volatiles derived from the plume. Since most volume of alkaline basalts erupted in northwestern Kyushu is considered to be eroded away and distribute under the sea (Nakada and Kamata, 1991), the lost basalts may accompany with high $^3He/^4He$ ratio, or the earliest basalts observable in Kita-matsuura with age around 11Ma may have plume-like signature. If the cumulative xenoliths observed in this region are cumulate from arc volcanism, not alkaline volcanism (Kagami et al., 1993, Arai, 1994), thus the cumulates originally contained He with similar $^3He/^4He$ ratio to that of MORB or with lower ratio, probably sub-crustal type He inferred from the basalts from Kita-matsuura. When the early alkaline magma enriched in volatile passed through, a portion of cumulates are metasomatized by infiltration of fluids or melt. Since the cumulus mantle with sub-crustal type He is depleted in He due to effective degassing through arc volcanism, isotopic compositions of noble gases in the cumulate was overprinted by the plume-type component trapped in primary inclusions. If mantle-derived xenoliths from this region are cumulates from the early alkaline basaltic magma (Yanagi and Maeda, 1998), plume-type He was trapped in primary fluid inclusions coevally with formation of cumulates.

During ascending, the mantle plume was entrained by surrounding sub-continental mantle as described in Nakamura et al. (1990). When both enriched material originally contained in the plume and depleted material entrained from surrounding mantle partially melt, the migrating melts would mix in the partial melt zone. Since the volatile originally contained in the plume had fractionated into the early CO_2-dominated melt, the noble gas from depleted material is dominant in the mixed melt. The surrounding sub-continental mantle has low $^{3}He/^{4}He$ ratio (ca. $7R_A$ or lower) and $^{40}Ar/^{36}Ar$ ratio higher than that in the plume but significantly lower than that of MORB-source mantle. As a result of effective degassing of volatile from the enriched material and entrainment and concurrently melting of surrounding depleted material with enriched material, the noble gas isotopic composition of the melt separated from the plume varied from plume-type to MORB-type. Since the basalts analyzed in this study were derived from the melt in which depleted material is dominant as indicated from their depleted Nd–Sr characteristics, they show noble gas signature almost the same that of sub-continental mantle. Finding of high $^{3}He/^{4}He$ ratio in alkaline basalts which erupted in early stage of alkaline volcanism in this region strongly support the model, thus it is issue of the prospective work.

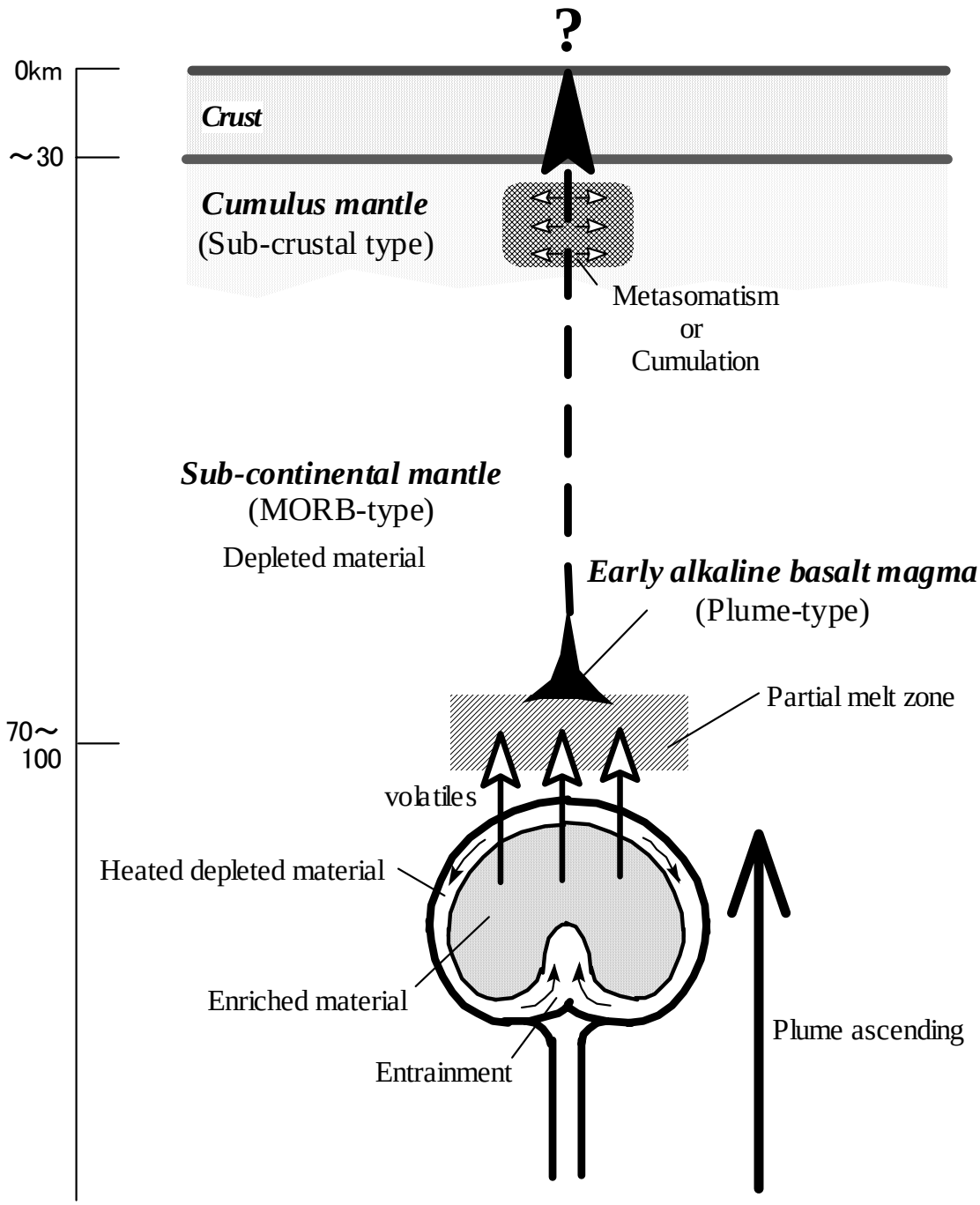

Fig. 5–3. Schematic diagram of the proposed model after retreat of Japan trench at approximately 40Ma. Volatile degassed from plume body interact with sub-continental mantle which contains MORB-type noble gases ($^{3}He/^{4}He<7R_A$, $^{40}Ar/^{36}Ar > 2600$) and generate early alkaline basaltic melt which contain plume-type noble gases ($^{3}He/^{4}He > 17R_A$, $^{40}Ar/^{36}Ar > 400$). The heated depleted material surrounding entrain into the plume according to the entrainment mixing model of Nakamura et al. (1990). Volatile-rich early alkaline basaltic melt metasomatise a portion of cumulus mantle, probably has sub-crustal type noble gases ($^{3}He/^{4}He < 0.2R_A$, $^{40}Ar/^{36}Ar < 500$).

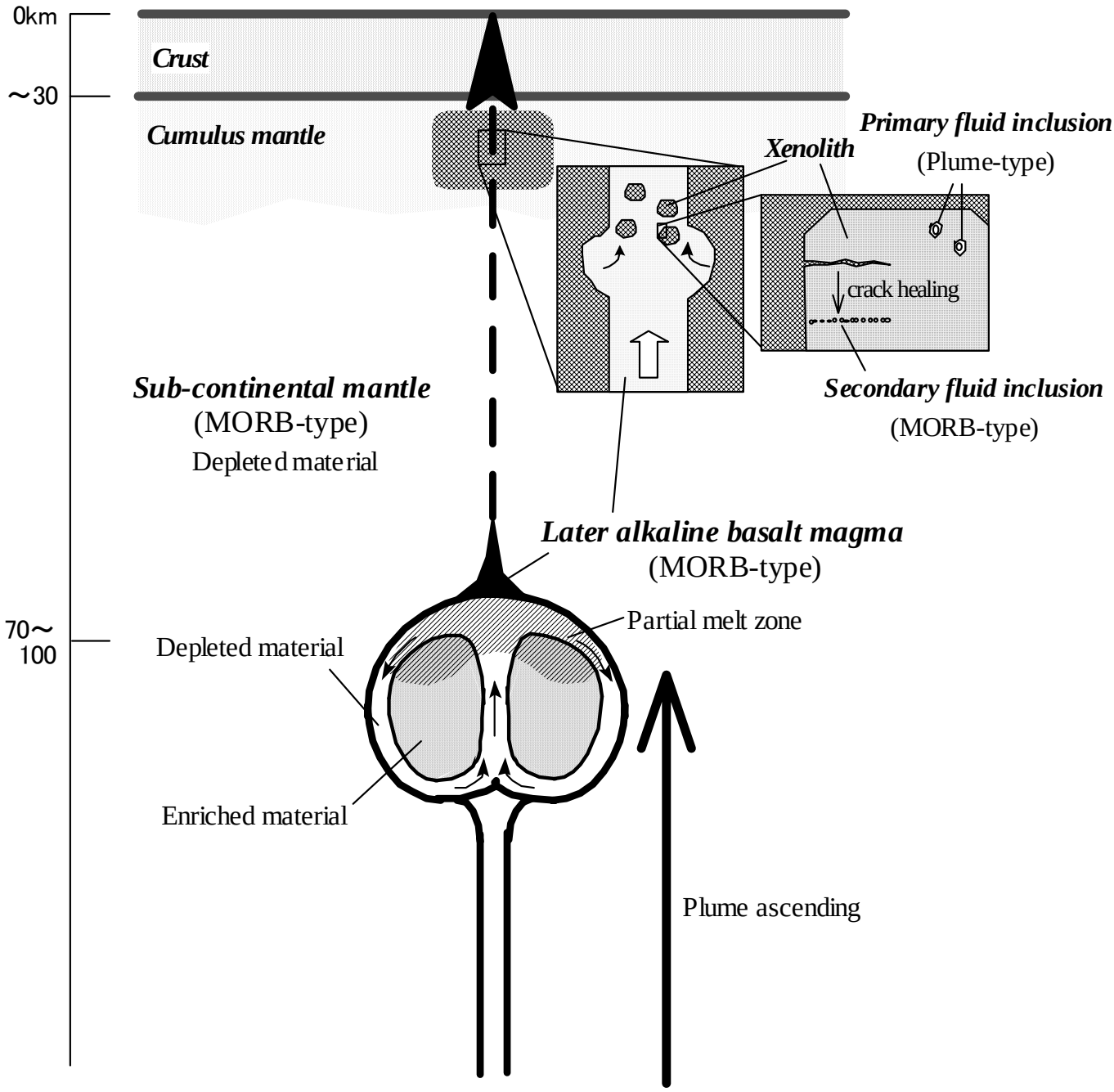

Fig. 5–4. Schematic diagram of the proposed model after 7Ma. Later alkaline basaltic melt, which is admixture of melts from enriched material and depleted material entrained into the plume, contains MORB-type noble gas. The metasomatized cumulous mantle which includes primary fluid inclusions containing plume-type noble gases, are trapped into later alkaline basalt magma, and partly exchange the noble gases with host magma as in secondary fluid inclusions.

5–2–2. Origin of the plume: recycling of subducted material

It is revealed that a mantle plume with high $^{3}He/^{4}He$ ratio indicating its origin of lower mantle have ascended to the mantle beneath the back-arc region of southwestern Japan. Combining plume models previously reported (Nakamura et al., 1990, Kakubuchi et al., 1995), the plume is considered to have EMII signature in Nd–Sr isotopes. Recycled material of continental origin such as subducted oceanic crust with sediments is considered to be responsible for the origin of EMII endmember in oceanic island basalts (Cohen and O'Nions, 1982; Hofmann, 1997). If the EMII characteristics of the plume is derived from subducted oceanic crust and sediments, the He evidence of lower mantle component suggest that the plume is subducted material which had subducted and reached to lower mantle and was recycled back to the surface of the Earth.

There is no subducted oceanic plate beneath the back-arc region of southwestern Japan above 600km in depth, revealed by the center of deep-focus earthquakes (Fig. 1–1). It is resulted from retreat of Japan Trench after opening of the Japan Sea and short space of time after beginning of the subduction of Philippine Sea plate. However, the seismic tomographic image has revealed a cold region formed at the base of the upper mantle, possibly indicating the ancient subducted slab (van der Hilst et al., 1991; Fukao et al., 1992). If this is the case, any plume ascend from deeper region such as core-mantle boundary could not go through the stagnant slab and reach to the surface of the Earth because they might be arrested by the slab. Therefore, there is a possibility that stagnant subducted materials is the origin of EMII and ascended as the plume observed in the back-arc region of southwestern Japan. The mechanism of tapping of subducted material as a plume is not clear at present, however, a speculative scenario of plume generation can be proposed (Fig. 5–5). A localized thermal anomaly, possibly generated at the core-mantle boundary, arises through the lower mantle until it reaches the 670km discontinuity. Heat transfer across the 670km boundary layer initiates upwelling of parts of stagnant slab, and only limited amount of lower mantle material including He with high $^{3}He/^{4}He$ ratio is transferred upward with recycled materials.

Alkaline volcanism in back-arc region which yield the basalts with geochemical features similar to those of volcanic rocks from hotspot are recognized in other

subduction zones such as New Zealand (Tatsumi and Tsunakawa, 1992), southern Andes (Stern et al., 1990) and Cascade arc (Fitton et al., 1991; Huang et al., 2000). Since there are no direct evidence that subducted materials are stored in some parts in Earth's interior and ascend as mantle plume, if such volcanisms in back-arc region of subduction zone are triggered by a mantle plume as well as that in southwestern Japan, the recycle of subducted material at back-arc region of subduction zone will be an important subject to understand mantle dynamics in the future.

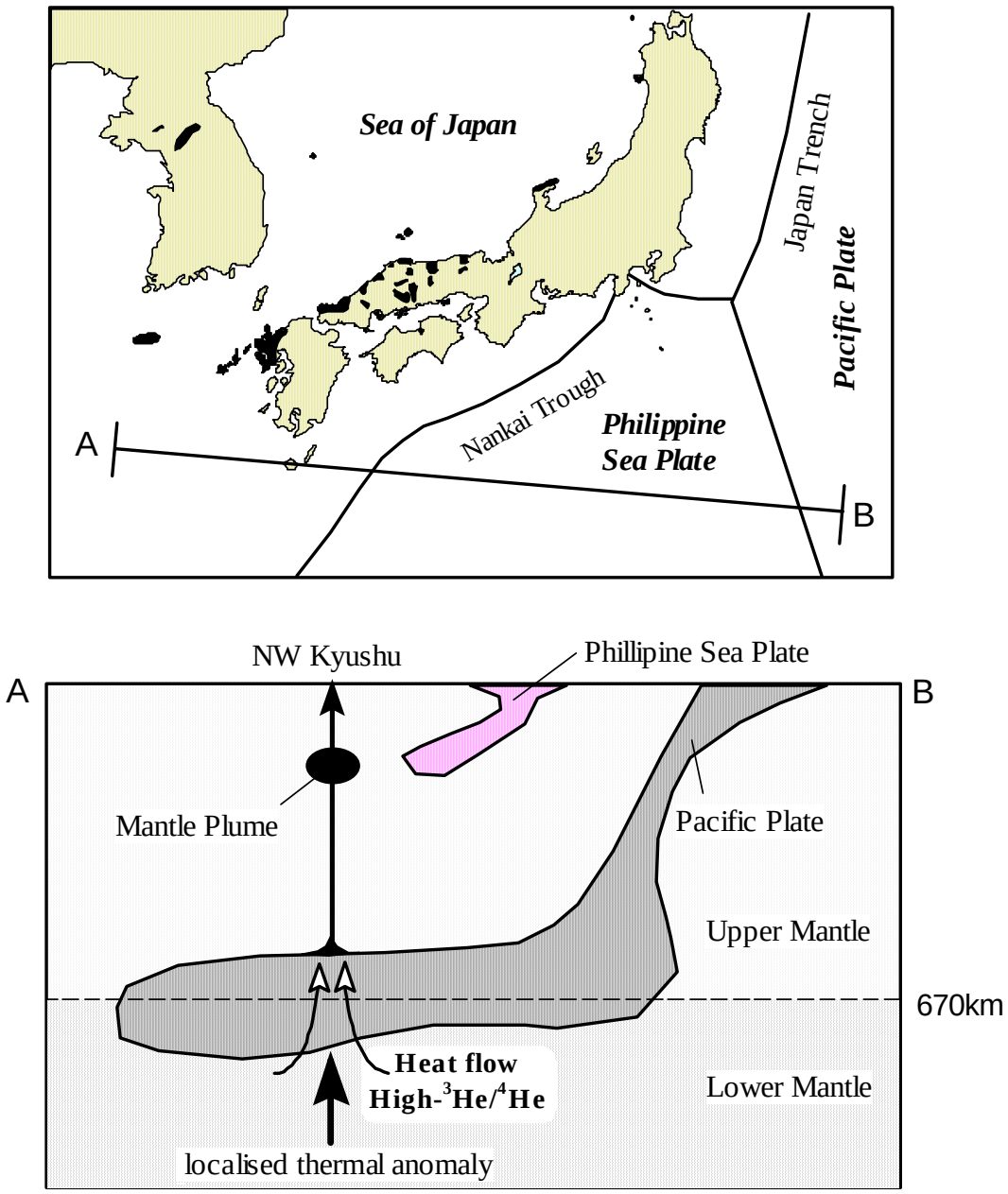

Fig. 5–5. A speculative model showing recycling of ancient subducted materials stagnant in the mantle transition zone (670km discontinuity) beneath Japan. Schematic cross section of the mantle along the profile A–B in map above is shown below. The shape of the subducted slab of the Pacific Sea Plate and the Philippine Sea Plate are modified from seismic tomographic image after Fukao et al. (1992). A localized thermal anomaly allows uprising of subducted materials and of intermixed or entrained upper mantle material. The mass contribution of the lower mantle is extremely limited, thus observable only in He isotopic ratio.

6. Summary

Noble gas isotopic composition of Cenozoic alkaline basalts and mantle-derived xenoliths from back-arc region of southwestern Japan were measured in order to investigate the origin of the alkaline basalt with respect to mantle dynamics related to subduction process. The main results are as follows.

(1) A noble gas mass spectrometer was improved in order to determine noble gas isotopic composition with extremely low concentration in the samples. As the result of modification, $^{3}He/^{4}He$ ratio can be determined with a precision of ±10% for quite small amount of He, which corresponds to 10^{-18}mol of ^{3}He. Highly improved detection limit which is 1–2 orders of magnitude lower than that before modification enables us to measure other noble gas isotopes whose abundance are generally low in mineral samples, such as Ne, Kr and Xe with the mass spectrometer specialized to He.

(2) Noble gas isotopic composition of alkaline basalt magma which erupted in northwestern Kyushu after 7Ma is characterized by $^{3}He/^{4}He$ ratio slightly lower than MORB-value and low $^{40}Ar/^{36}Ar$ ratio as mantle-derived materials. Some clinopyroxenes separated from the alkaline basalts from northwestern Kyushu show lower $^{3}He/^{4}He$ and $^{40}Ar/^{36}Ar$ ratios than coexisting olivines. This discrepancy is considered to be caused by shallow-level contamination by crustal fluids enriched in radiogenic He, and/or mixing with accumulated magma contaminated by metasomatized mantle during ancient subduction.

(3) Mantle-derived xenoliths from Takashima contain two types of noble gas which are distinguished from each other in view of He and Ar isotopes. One is plume-type component, with significantly higher $^{3}He/^{4}He$ ratio than that of MORB and relatively low $^{40}Ar/^{36}Ar$ ratio, and the other is MORB-type component, with slightly lower $^{3}He/^{4}He$ ratio than the MORB value and relatively high, but distinctly lower $^{40}Ar/^{36}Ar$ ratio than that of MORB.

(4) Microscopic observation of fluid inclusions in the xenoliths and noble gas analysis using stepwise heating and crushing extraction methods revealed that MORB-type component is trapped in secondary fluid inclusions. The fact that He and Ar isotopic ratios of MORB-like component is almost identical to that of host alkaline basalt

magma and noble gas profile observed in a core sample strongly suggests that the MORB-type noble gas in xenoliths is result from exchange with that in host magma, forming the secondary fluid inclusions.

(5) Distinctively lower $^{40}Ar/^{36}Ar$ ratios of alkaline basalt magma and xenoliths from northwestern Kyushu and Cheju Island than that of MORB suggest that atmospheric Ar derived from subducting the Pacific plate (not the Philippine Sea plate) contaminated the mantle wedge beneath these regions. Noble gas abundance patterns of these samples suggest that subducted old oceanic crust and/or oceanic sediments play an important role in recycling of atmospheric component back into the mantle wedge. Considering a closed-system evolution model of He in the sub-continental mantle, observed $^{3}He/^{4}He$ ratios lower than that of MORB source upper mantle can be explained in terms of U enrichment in metasomatized mantle by slab-derived fluids.

(6) The plume-type component trapped in primary fluid inclusions in Takashima xenolith is a clear evidence of existence of a mantle plume ascended from upper/lower mantle boundary or deeper part of the Earth. Considering that subduction had continued and blocked ascending of any mantle plume over hundreds of million years until beginning of alkaline basalt volcanism, mantle upwelling which generated alkaline basalt magma was probably the mantle plume. To explain the temporal change of He and Nd–Sr isotopes in the source material of the alkaline basalt, I propose a model that effective degassing of He from the plume took place, and followed by sequential overprint by He in surrounding sub-continental mantle.

(7) The evidence of the mantle plume containing lower mantle He and tomographic images which show the stagnant slab at the upper/lower mantle boundary suggest that ancient subducted material is recycled back to the surface of the Earth as the mantle plume. It may be a direct observation of mantle dynamics that subducted materials are stored in Earth's interior and ascend as a mantle plume, which is the source of EMII hotspot. If this is the case, alkaline volcanism in back-arc region of subduction zone may play an important role in circulation of the material in the Earth.

Acknowledgements

Sincere thanks are extended to Prof. K. Notsu for many helpful advices, critical reading of the manuscript, and many insightful suggestions. I am grateful to Prof. K. Nagao, my teacher for the experimental technique, for financial support for setting up the mass spectrometer. I am also grateful to Prof. H. Wakita for giving the opportunity to carry out this study and for supplying one of the samples used in the study. I express appreciation to Dr. S. Nakai for his guidance and encouragement.
I would like to thank Drs. G. Igarashi and H. Yurimoto for assistance in collecting the samples in Takashima, Drs. Kim K. H, J. I. Chung and J. H. Hon for that in Cheju Island. Instruction in the use of micro FT-IR by Dr. H. Kagi is gratefully acknowledged. I appreciate Dr. J. Ando and Mr. Y. Matsumura for providing with the information on microscopic observation of fluid inclusions. Drs. Y. Orihashi and S. Nakada are thanked for allowing and instructing the use of XRF machine at the Earthquake Research Institute. I am grateful to Dr. H. Hiyagon for allowing the use of SEM-EDS system at Department of Earth and Planetary Science of the Graduate School of Science, the University of Tokyo. I thank Drs. Pedro A. Hernandez and M. Ohno for allowing the use their data for gas samples from Izu Peninsula. I appreciate Dr. J. Yamamoto, Ms. R. Yokochi and Ms. A. Itoh for their help at fieldwork and useful discussions. I send my thanks to all the members of Laboratory for Earthquake Chemistry, University of Tokyo. I am indebted to all my colleagues of the noble gas group, especially Drs. Y. Miura and R. Okazaki, Ms. N. Ebisawa for their help with experiments and numerous kind services to me. I gratefully appreciate Ms. A. Shimizu for her help with processing of the data and encouragement to me. I also thank Drs. T. Matsumoto, Y. Nishio, H. Iwamori and T. Hanyu for many helpful comments and suggestions. Constructive discussions and improvement of English in my GRL paper by Drs. S. Niedermann and F. T. Aka are gratefully acknowledged.

References

Abe, N., Arai, S., and Yurimoto, H. (1998) Geochemical characteristics of the uppermost mantle beneath the Japan island arcs: implications for upper mantle evolution. *Phys. Earth. Planet. Inter.*, **107**: 233-248.

Aka, F. T., Kusakabe, M., Nagao, K., and Tanyileke, G. (2001) Noble gas isotopic compositions and water chemistry of soda springs from the islands of Bioko, Sao Tome and Annobon, along with Cameroon Volcanic Line, West Africa. *Appl. Geochem.*, **16**: 323-338.

Allègre, C. J., Staudacher, T. h., and Sarda, P. (1986/87) Rare gas systematics: formation of the atmosphere, evolution and structure of the Earth's mantle. *Earth Planet. Sci. Lett.*, **81**: 127-150.

Arai, S. (1994) Characterization of spinel peridotites by olivine-spinel compositional relationships: Review and interpretation. *Chem. Geol.*, **113**: 191-204.

Arai, S. and Abe, N. (1994) Podiform chromitite in the arc mantle: chromitite xenoliths from the Takashima alkali basalt, Southwest Japan arc. *Mineral. Deposita*, **29**: 434-438.

Arai, S. and Kobayashi, Y. (1984) Petrographical notes on deep-seated and related rocks (2) Carbonate-bearing iron-rich lherzolite xenolith in alkali basalt from Takashima, southwestern Japan. *Annual Reports, Institute of Geoscience, Univ. Tsukuba*, **10**: 119-121.

Arai, S. and Muraoka, H. (1992) Peridotite xenoliths in alkali basalts from On-yama, the Chugoku district, as a suite of fertile upper mantle peridotites beneath the Southwest Japan arc (Japanese with English abstract). *J. Min. Pet. Econ. Geol.*, **87**: 240-251.

Aramaki, S. and Ui, T. (1982) Japan. In: *Andesites: Orogenic andesites and related rocks*, edited by Thorpe, R. S. :John Wiley & Sons, p. 259-292.

Andrews, J. N. (1985) The isotopic composition of radiogenic helium and its use to study groundwater movement in confined aquifers. *Chem. Geol.*, **49**: 339-351.

Cohen, R. S. and O'Nions, R. K. (1982) Identification of recycled continental material in the mantle from Sr, Nd and Pb isotope investigations. *Earth Planet. Sci. Lett.*, **61**: 73-84.

Dodson, A. and Brandon, A. D. (1999) Radiogenic helium in xenoliths from Simcoe, Washington, USA: implications for metasomatic processes in the mantle wedge above subduction zones. *Chem. Geol.*, **160**: 371-385.

Dodson, A., DePaolo, D. J., and Kennedy, B. M. (1998) Helium isotopes in lithospheric mantle: Evidence from Tertiary basalts of the western USA. *Geochim. Cosmochim. Acta*, **62**: 3775-3787.

Eiler, J. M., McInnes, B., Valley, J. W., Graham, C. M., and Stolper, E. M. (1998) Oxygen isotope evidence for slab-derived fluids in the sub-arc mantle. *Nature*, **393**: 777-781.

Farley, K. A. and Craig, H. (1994) Atmospheric argon contamination of ocean island basalt olivine phenocrysts. *Geochim. Cosmochim. Acta*, **58**: 2509-2517.

Fisher, D. E. (1986) Rare gas abundances in MORB. *Geochim. Cosmochim. Acta*, **50**: 2531-2541.

Fitton, J. G., James, D., and Leeman, W. P. (1991) Basic magmatism associated with late Cenozoic extension in the western United States: compositional variations in space and time. *J. Geophys. Res.*, **96**: 13693-13711.

Fukao, Y., Obayashi, M., Inoue, H., and Nenbai, M. (1992) Subducting slabs stagnant in the mantle transition zone. *J. Geophys. Res.*, **97**: 4809-4822.

Hanyu, T. and Kaneoka, I. (1997) Magmatic processes revealed by noble gas signatures: the case of Unzen Volcano, Japan. *Geochem. J.*, **31**: 395-405.

Hanyu, T., Kaneoka, I., and Nagao, K. (1999) Noble gas study of HIMU and EM ocean island basalts in the Polynesian region. *Geochim. Cosmochim. Acta*, **63**: 1181-1201.

Hart, S. R. (1984) He diffusion in olivine. *Earth Planet. Sci. Lett.*, **70**: 297-302.

Hee, C. H. (1998) *Geochemical study of ultramafic xenoliths in basalts from Cheju Island, Korea*. Ph. D. thesis of Seoul National University, Korea.

Henderson, P. (1982) *Inorganic geochemistry*. Oxford: Pergamon Press.

Hilton, D. R., Barlling, J., and Wheller, G. E. (1995) Effect of shallow-level contamination on the helium isotope systematics of ocean-island lavas. *Nature* , **373**: 330-333.

Hilton, D. R., Gronvold, K., Macpherson, C. G., and Castillo, P. R. (1999) Extreme $^{3}He/^{4}He$ ratios in northwest Iceland: constraining the common component in mantle plumes. *Earth Planet. Sci. Lett.*, **173**: 53-60.

Hilton, D. R., Hammerschmidt, K., Loock, G., and Friedrichen, H. (1993) Helium and argon isotope systematics of the central Lau Basin and Valu Fa Ridge: Evidence of crust/mantle interactions in a back-arc basin. *Geochim. Cosmochim. Acta*, **57**: 2819-2841.

Hilton, D. R., Hoogewerff, J. A., Bergen, M. J., and Hammerschmidt, K. (1992) Mapping magma sources in the east Sunda-Banda arcs, Indonesia: constraints from helium isotopes. *Geochim. Cosmochim. Acta*, **56**: 851-859.

Hiyagon, H. and Ozima, M. (1986) Partition of noble gases between olivine and basalt melt. *Geochim. Cosmochim. Acta*, **50**: 2045-2057.

Hiyagon, H., Ozima, M., Marty, B., Zashu, S., and Sakai, H. (1992) Noble gases in submarine glasses from mid-oceanic ridges and Loihi seamount: Constraints on the early history of the Earth. *Geochim. Cosmochim. Acta*, **56**: 1301-1316.

Hofmann, A. W. (1997) Mantle geochemistry: the message from oceanic volcanism. *Nature*, **385**: 219-229.

Honda, M., McDougall, I., Patterson, D. B., Doulgeris, A., and Clague, D. A. (1991) Possible solar noble-gas component in Hawaiian basalts. *Nature*, **349**: 149-151.

Honda, M., McDougall, I., Patterson, D. B., Doulgeris, A., and Clague, D. A. (1993) Noble gases in submarine pillow glasses from Loihi and Kilauea, Hawaii: A solar component in the Earth. *Geochim. Cosmochim. Acta*, **57**: 859-874.

Huang, Y., Hawkesworth, C., Smith, I., van Calsteren, P., and Black, P. (2000) Geochemistry of late Cenozoic basaltic volcanism in Northland and Coromandel, New Zealand: implications for mantle enrichment processes. *Chem. Geol.*, **164**: 219-238.

Imai, N., Terashima, S., Itoh, S., and Ando, A. (1995) 1994 compilation values for GSJ reference samples, "Igneous rock series". *Geochem. J.*, **29**: 91-95.

Ishibashi, K. (1970) Petrochemical study of basic and ultrabasic inclusions in basaltic rocks from Northern Kyushu, Japan. *Mem. Fac. Sci. Kyushu Univ., ser. D. (Geol.)*, **20**: 85-146.

Itoh, A. (1998) *Installation of a system for noble gas mass spectrometry and its application on terrestrial samples – the case study of xenoliths and phenocryst from alkali basalt –* . MS thesis of Osaka City University, Japan (in Japanese).

Iwamori, H. (1992) Degree of melting and source composition of Cenozoic basalts in Southwest Japan: evidence for mantle upwelling by flux melting. *J. Geophys. Res.*, **97**: 10983-10995.

Jessop, A. M. (1990) *Thermal Geodynamics (Developments in Solid Earth Geophysics 17)* . Amsterdam: Elsevier.

Kagami, H., Iizumi, S., Iwata, M., and Nureki, T. (1993) Sr-Nd isotope systematics of xenoliths in Cenozoic volcanic rocks from SW Japan. *Proc. Japan Acad.*, **69B**: 1-6.

Kagami, H., Iizumi, S., Tainosho, Y., and Owada, M. (1992) Spatial variations of Sr and Nd isotope ratios of Cretaceous-Paleogene granotoid rocks, Southwest Japan Arc. *Contrib. Mineral. Petrol.*, **112**: 165-177.

Kagi, H. and Takahashi, K. (1998) Relationship between positive Ce anomaly and absorbed water in Antarctic lunar meteorites. *Meteoritics and Planetary Sciences*, **33**: 1033-1040.

Kakubuchi, S., Nagao, T., Kagami, H., and Hujibayashi, N. (1995) Chemical and isotopic characteristics of the source mantle for late Cenozoic basalts in southwest Japan (Japanese with English abstract). *Mem. Geol. Soc. Japan*, **44**: 321-335.

Kaneoka, I. and Takaoka, N. (1978) Excess ^{129}Xe and high ^{3}He/^{4}He ratios in olivine phenocrysts of Kapuho lava and xenolithic dunites from Hawaii. *Earth Planet. Sci. Lett.*, **39**: 382-386.

Kaneoka, I., Takaoka, N., and Clague, D. A. (1983) Noble gas systematics for coexisting glass and olivine crystals in basalts and dunite xenoliths from Loihi Seamount. *Earth Planet. Sci. Lett.*, **66**: 427-437.

Kaneoka, I. (1995) Constraints on the chemical structure and evolution of the earth based on noble gas isotopes. *J. Seismological Soc. Japan. 2nd ser.*, **48**: 187-198.

Kim, K. H., Tanaka, T., Nagao, K., and Jang, S. K. (1999) Nd and Sr isotopes and K-Ar ages of Ulreungdo alkali volcanic rocks in the East Sea, South Korea. *Geochem. J.*, **33**: 317-341.

Kurasawa, H. (1968) Isotopic composition of lead concentrations of uranium, thorium, and lead in volcanic rocks from Dogo of the Oki Islands, Japan. *Geochem. J.*, **2**: 11-28.

Kurasawa, H. (1967) Petrology of the kita-matsuura basalts in the northwest Kyushu, Southwest Japan. *Geological Survey of Japan, Report*, **217**: 1-108.

Kurz, M. D. (1986) Cosmogenic helium in a terrestrial igneous rock. *Nature*, **320**: 435-439.

Kushiro, I., Yoder Jr. H. S., and Mysen, B. O. (1976) Viscosities of basalt and andesite melts at high pressures. *J. Geophys. Res.*, **81**: 6351-6356.

Kobayashi, A. and Arai, S. (1981) Ultramafic nodules in alkali basalt from Taka-shima, Saga Prefecture, Japan (Japanese with English abstract). *Geosci. Rep. Shizuoka Univ.*, **6**: 11-24.

Lal, D. (1987) Production of ^{3}He in terrestrial rocks. *Chem. Geol.*, **66**: 89-98.

Lee, M. W. (1982) Petrology and geochemistry of Jeju volcanic island, Korea. *Sci. Rep. Tohoku Univ. ser. 3: Mineral. Petrol. Econ. Geol.*, **15**: 177-256.

Liu, J., Bohlen, S. R., and Ernst, W. G. (1996) Stability of hydrous phases in subducting oceanic crust. *Earth Planet. Sci. Lett.*, **143**: 161-171.

Lux, G. (1987) The behavior of noble gases in silicate liquids: Solution, diffusion, bubbles and surface effects, with applications to natural samples. *Geochim. Cosmochim. Acta*, **51**: 1549-1560.

Mamyrin, B. A., Anufriyev, G. S., and Kamenskiy, I. L. (1970) Determination of the isotopic composition of atmospheric helium. *Geochemistry International*, **7**: 498-505.

Marty, B., Trull, T., Lussiez, P., Basile, I., and Tanguy, J. C. (1994) He, Ar, O, Sr and Nd isotope constraints on the origin and evolution of Mount Etna magmatism. *Earth Planet. Sci. Lett.*, **126**: 23-39.

Maruyama, S., Isozaki, Y., Kimura, G., and Terabayashi, M. (1997) Paleogeographic maps of the Japanese Islands: Plate tectonic synthesis from 750Ma to the present. *The Island Arc*, **6**: 121-142.

Matsuda, J. and Nagao, K. (1986) Noble gas abundances in a deep-sea sediment core from eastern equatorial Pacific. *Geochem. J.*, **20**: 71-80.

Matsumoto, T., Honda, M., McDougall, I., and O'Reilly, S. Y. (1998) Noble gases in anhydrous lherzolites from Newer Volcanics, southern Australia: A MORB-like reservoir in the subcontinental mantle. *Geochim. Cosmochim. Acta*, **62**: 2521-2533.

Miura, Y. and Nagao, K. (1991) Noble gases in six GSJ igneous rock samples. *Geochem. J.*, **25**: 163-171.

Miyashiro, A. (1974) Volcanic rock series in island arcs and active continental margins. *Am. J. Sci.*, **274**: 321-355.

Miyashiro, A. (1978) Nature of alkalic volcanic rock series. *Contrib. Mineral. Petrol.*, **66**: 91-104.

Nagao, K. and Abe, T. (1994) Application of laser to spot analysis of noble gases in primitive meteorite. *J. Mass Spectrom. Soc. Jpn.*, **42**: 35-48.

Nagao, K., Ogata, A., Miura, Y. N., and Yamaguchi, K. (1996) Ar isotope analysis for K-Ar dating using two modified-VG5400 mass spectrometers–I: Isotope dilution method. *J. Mass Spectrom. Soc. Jpn.*, **44**: 39-61.

Nagao, K., Okazaki, R., Sawada, S., and Nakamura, N. (1999) Noble gases and K-Ar ages of five rumuruti chondorites Yamato(Y)-75302, Y-791827, Y-793575, Y-82002, and Asuka-881988. *Antarct. Meteorite Res.*, **12**: 81-93.

Nagao, K. and Takahashi, E. (1993) Noble gases in the mantle wedge and lower crust: an inference from the isotopic analyses of xenoliths from Oki-Dogo and Ichinomegata, Japan. *Geochem. J.*, **27**: 229-240.

Nakada, S. and Kamata, H. (1991) Temporal change in chemistry of magma source under Central Kyushu, Southwest Japan: progressive contamination of mantle wedge. *Bull. Volcanol.*, **53**: 182-194.

Nakai, S., Wakita, H., Nuccio, M., and Italiano, F. (1997) MORB-type neon in an enriched mantle beneath Etna, Sicily. *Earth Planet. Sci. Lett.*, **153**: 57-66.

Nakamura, E., Campbell, I. H., McCulloch, M. T., and Sun, S. (1989) Chemical geodynamics in a back arc region around the Sea of Japan: implications for the genesis of alkaline basalts in Japan, Korea, and China. *J. Geophys. Res.*, **94**: 4634-4654.

Nakamura, E., Campbell, I. H., and Sun, S. (1985) The influence of subduction processes on the geochemistry of Japanese alkaline basalts. *Nature*, **316**: 55-58.

Nakamura, E., McCulloch, M. T., and Campbell, I. H. (1990) Chemical geodynamics in the back-arc region of Japanese based on the trace element and Sr-Nd isotopic compositions. *Tectonophysics*, **174**: 207-233.

Nakamura, E., McDougall, I., and Campbell, I. H. (1986) K-Ar ages of basalts from Higashi-Matsuura district, northwestern Kyushu, Japan and regional geochronology of the Cenozoic alkaline volcanic rocks in eastern Asia. *Geochem. J.*, **20**: 91-99.

Nohda, S., Tatsumi, Y., Otofuji, Y., Matsuda, T., and Ishizaka, K. (1988) Asthenospheric injection and back-arc opening: isotopic evidence from northeast Japan. *Chem. Geol.*, **68**: 317-327.

Nohda, S. and Wasserburg, G. J. (1981) Nd and Sr isotopic study of volcanic rocks from Japan. *Earth Planet. Sci. Lett.*, **52**: 264-276.

Notsu, K., Arakawa, Y., and Kobayashi, T. (1990) Strontium isotopic characteristics of arc volcanic rocks at the initial stage of subduction in western, Japan. *J. Volcanol. Geotherm. Res.*, **40**: 181-196.

Ohki, J., Shuto, K., and Kagami, H. (1994) Middle Miocene bimodal volcanism by asthenospheric upwelling: Sr and Nd isotope evidence from the back-are region of the Northeast Japan arc. *Geochem. J.*, **28**: 473-487.

Okamura, S., Arculus, R. J., Martynov, Y. A., Kagami, H., Yoshida, T., and Kawano, Y. (1998) Multiple magma sources involved in marginal-sea formation: Pb, Sr, and Nd isotopic evidence from the Japan Sea region. *Geology*, **26**: 619-622.

Osawa, T., Nagao, K., Nakamura, T., and Takaoka, N. (2000) Noble gas measurement in individual micrometeorites using laser gas-extraction system. *Antarct. Meteorite Res.*, **13**: 322-341.

Otofuji, Y. and Matsuda, T. (1983) Paleomagnetic evidence for the clockwise rotation of Southwest Japan. *Earth Planet. Sci. Lett.*, **62**: 349-359.

Ozima, M. and Podosek, F. A. (1983) *Noble gas geochemistry*. Cambridge: Cambridge Univ. Press.

Patterson, D. B., Honda, M., and McDougall, I. (1990) Atmospheric contamination: a possible source for heavy noble gases in basalts from Loihi Seamount, Hawaii. *Geophys. Res. Lett.*, **17**: 705-708.

Patterson, D. R., Farley, K. A., and McInnes, B. I. A. (1997) Helium isotopic composition of the Tabar-Lihir-Tanga-Feni island arc, Papua New Guinea. *Geochim. Cosmochim. Acta*, **61**: 2485-2496.

Pearce, J. A. (1982) Trace element characteristics of lavas from destructive late boundaries. In: *Andesites: Orogenic andesites and related rocks*, edited by Thorpe, R. S. Chichester: John Wiley & Sons, p. 525-548.

Porcelli, D. R., O'Nions, R. K., Galer, S. J. G., Cohen, A. S., and Mattey, D. P. (1992) Isotopic relationships of volatile and lithophile trace elements in continental ultramafic xenoliths. *Contrib. Mineral. Petrol.*, **110**: 528-538.

Poreda, R. J. and Farley, K. A. (1992) Rare gases in Samoan xenoliths. *Earth Planet. Sci. Lett.*, **113**: 129-144.

Reid, M. R. and Graham, D. W. (1996) Resolving lithospheric and sub-lithospheric contributions to helium isotope variations in basalts from the southwestern US. *Earth Planet. Sci. Lett.*, **144**: 213-222.

Rocholl, A., Heusser, E., Kirsten, T., Ohem, J., and Richter, H. (1996) A noble gas profile across a Hawaiian mantle xenolith: Coexisting accidental and cognate noble gases derived from the lithospheric and asthenospheric mantle beneath Oahu. *Geochim. Cosmochim. Acta*, **60**: 4773-4783.

Sano, Y. and Wakita, H. (1988) Precise measurement of helium isotopes in terrestrial gases. *Bull. Chem. Soc. Jpn.*, **61**: 1153-1157.

Sarda, P., Staudacher, T., and Allègre, C. J. (1988) Neon isotopes in submarine basalts. *Earth Planet. Sci. Lett.*, **91**: 73-88.

Scarfe, C. M. and Brearley, M. (1987) Mantle xenoliths: melting and dissolution studies under volatile-free conditions. In: *Mantle xenoliths*, edited by Nixon, P. H. Chichester: John Wiley & Sons, p. 599-608.

Shibata, K. and Adachi, M. (1974) Rb-Sr whole rock ages of Precambrian metamorphic rocks in the Kamiaso conglomerate from central Japan. *Earth Planet. Sci. Lett.*, **21**: 277-287.

Shiono, K. (1974) Travel time analysis of relatively deep earthquakes in Southwest Japan with special reference to the underthrusting of the Philippine Sea Plate. *J. Geosci. Osaka Univ.*, **18**: 37-59.

Staudacher, T. and Allègre, C. J. (1988) Recycling of oceanic crust and sediments: the noble gas subduction barrier. *Earth Planet. Sci. Lett.*, **89**: 173-183.

Staudacher, T. and Allègre, C. J. (1993) The cosmic ray produced $^{3}He/^{21}Ne$ ratio in ultramafic rocks. *Geophys. Res. Lett.*, **20**: 1075-1078.

Staudacher, T., Sarda, P., Richardson, S. H., Allègre, C. J., Sagna, I., and Dmitriev, L. V. (1989) Noble gases in basalt glasses from a Mid-Atlantic Ridge topographic high at 14° N: geodynamic consequences. *Earth Planet. Sci. Lett.*, **96**: 119-133.

Stern, C. R., Frey, F. A., Futa, K., Zartman, R. E., Peng, Z., and Kyser, T. K. (1990) Trace-element and Sr, Nd, Pb, and O isotopic composition of Pliocene and Quaternary alkali basalts of the Patagonian Plateau lavas of southernmost South America. *Contrib. Mineral. Petrol.*, **104**: 294-308.

Stolper, E. and Newmann, S. (1994) The role of water in the petrogenesis of Mariana trough magmas. *Earth Planet. Sci. Lett.*, **121**: 293-325.

Stuart, M., Turner, G., and Taylor, R. (1994) He–Ar Isotope Systematics of Fluid Inclusions: Resolving Mantle and Crustal Contributions to Hydrothermal Fluids. In: *Noble Gas Geochemistry and Cosmochemistry*, edited by Matsuda, J. Tokyo: Terra Scientific Publishing Company (TERRAPUB), p. 261-277.

Takahashi, E. (1978) Petrologic model of the crust and upper mantle of the Japanese Island arcs. *Bull. Volcanol.*, **41**: 529-547.

Tanaka, R. and Orihashi, Y. (1997) XRF analysis of major and trace elements for silicate rocks using low dilution ratio fused glass. *Hokkaido Univ. Earth Planet. Sci. Tech. Rep.*, **2**: 1-20.

Tatsumi, Y. (1989) Migration of fluid phase and genesis of basalt magmas in subduction zone. *J. Geophys. Res.*, **94**: 4697-4707.

Tatsumi, Y. and Kimura, N. (1991) Backarc extension versus continental breakup: petrological aspects for active rifting. *Tectonophysics*, **197**: 127-137.

Tatsumi, Y., Sakuyama, M., Fukuyama, H., and Kushiro, I. (1983) Generation of arc basalt magmas and thermal structure of the mantle wedge in subduction zones. *J. Geophys. Res.*, **88**: 5815-5825.

Tatsumi, Y. and Tsunakawa, H. (1992) Cenozoic volcanism, stress gradient and back-arc opening in the North Island, New Zealand: Origin of Taupo-Rotorua Depression. *The Island Arc*, **1**: 40-50.

Tatsumoto, M. and Nakamura, Y. (1991) DUPAL anomaly in the Sea of Japan: Pb, Nd, and Sr isotopic variations at the eastern Eurasian continental margin. *Geochim. Cosmochim. Acta*, **55**: 3697-3708.

Trull, T. W. and Kurz, M. D. (1993) Experimental measurements of ^{3}He and ^{4}He mobility in olivine and clinopyroxene at magmatic temperatures. *Geochim. Cosmochim. Acta*, **57**: 1313-1324.

Umino, S. and Yoshizawa, E. (1996) Petrology of ultramafic xenoliths from Kishyuku Lava, Fukue-jima, Southwest Japan. *Contrib. Mineral. Petrol.*, **124**: 154-166.

Uto, K., Hirai, H., and Arai, S. (1993) K-Ar ages for Quaternary alkali basalts from Kurose, Fukuoka Prefecture and Kifune, Yamaguchi Prefecture, Southwest Japan (Japanese with English abstract). *Bull. Geol. Surv. Japan*, **44**: 693-698.

Utsu, T. (1974) Epicenter distribution around Japan (in Japanese). *Kagaku*, **44**: 739-746.

Valbracht, P. J., Staudigel, H., Honda, M., McDougall, I., and Davies, G. R. (1996) Isotopic tracing of volcanic source regions from Hawaii: decoupling of gaseous from lithophile magma components. *Earth Planet. Sci. Lett.*, **144**: 185-198.

Van der Hilst, R., Engdahl, R., Spakman, W., and Nolet, G. (1991) Tomographic imaging of subducted lithosphere below northwest Pacific island arcs. *Nature*, **353**: 37-43.

Wanamaker, B. J. and Evans, B. (1989) Mechanical re-equilibration of fluid inclusions in San Carlos olivine by power-law creep. *Contrib. Mineral. Petrol.*, **102**: 102-111.

Xu, S., Nakai, S., Wakita, H., and Wang, X. (1995) Mantle-derived noble gases in natural gases from Songliao Basin, China. *Geochim. Cosmochim. Acta*, **59**: 4675-4683.

Yamamoto, J., Kaneoka ,I., Nakai, S., Prikhod'ko, V. S., and Arai, S. (2001) Extremely low ^{3}He/^{4}He ratios observed in ultramafic mantle xenoliths from far eastern Siberia and the heterogeneity of subcontinental mantle. *Geophys. Res. Lett. (submitted)*.

Yanagi, T. and Maeda, S. (1998) Magma evolution observed in the Matsuura basalts in northwest Kyushu, Japan: An example of high-pressure open system fractional crystallization in a refilled magma chamber near the crust-mantle boundary. *Phys. Earth. Planet. Inter.*, **107**: 203-219.

Yoshii, T. (1979) Compilation of geophysical data around the Japanese Islands. *Bull. Earthq. Res. Inst. Univ. Tokyo*, **54**: 75-117.

Yun, S. H., Koh, J. S., and Anh, J. Y. (1998) A study on the spinel-lherzolite xenoliths in the alkali basalt from Eastern Cheju island, Korea (Korean with English abstract). *Econ. Environ. Geol.*, **31**: 447-458.

Zindler, A. and Hart, S. (1986) Chemical geodynamics. *Ann. Rev. Earth Planet. Sci.*, **14**: 493-571.